

Investigations on broadband planar monopole and slot radiators and their suitability for UWB applications

Thesis submitted to
COCHIN UNIVERSITY OF SCIENCE AND TECHNOLOGY
in partial fulfillment of the requirements
for the award of the degree of
DOCTOR OF PHILOSOPHY

DEEPTI DAS KRISHNA

Department of Electronics
Faculty of Technology
Cochin University of Science and Technology
Cochin-682022, India



September 2010

Investigations on broadband planar monopole and slot radiators and their suitability for UWB applications

Ph.D thesis in the field of Microwave Electronics

Author:

Deepti Das Krishna

Center for Research in Electromagnetics and Antennas (CREMA)

Department of Electronics

Cochin University of Science and Technology

Cochin-682022, India.

E-mail: *dasdeepti@gmail.com*

Supervisor:

Dr. C. K. Aanandan

Professor

Department of Electronics

Cochin University of Science and Technology

Cochin-682022, India.

E-mail: *anand@cusat.ac.in*

Abstract

In recent years, there is a visible trend for products/services which demand seamless integration of cellular networks, WLANs and WPANs. This is a strong indication for the inclusion of high speed short range wireless technology in future applications. In this context UWB radio has a significant role to play as an extension/complement to existing cellular/access technology.

In the present work, we have investigated two major types of wide band planar antennas: Monopole and Slot. Four novel compact broadband antennas, suitable for portable applications, are designed and characterized, namely

1. Elliptical monopole
2. Inverted cone monopole
3. Koch fractal slot
4. Wide band slot

The performance of these designs have been studied using standard simulation tools used in industry/academia and they have been experimentally verified. Antenna design guidelines are also deduced by accounting the resonances in each structure.

In addition to having compact sized, high efficiency and broad bandwidth antennas, one of the major criterion in the design of impulse-UWB systems have been the transmission of narrow band pulses with minimum distortion. The key challenge is not only to design a broad band antenna with constant and stable gain but to maintain a flat group delay or linear phase response in the frequency domain or excellent transient response in time domain. One of the major contributions of the thesis lies in the analysis of the frequency and time-domain response of the designed UWB antennas to confirm their suitability for portable pulsed-UWB systems. Techniques to avoid narrow-band interference by engraving narrow slot resonators on the antenna is also proposed and their effect on a nano-second pulse have been investigated.

Declaration

I hereby declare that the work presented in the thesis entitled *Investigations on broadband planar monopole and slot radiators and their suitability for UWB applications* is a bonafide record of the research work done by me under the supervision of Prof.C.K.Aanandan, Department of Electronics, Cochin University of Science and Technology, India and that no part thereof has been presented for the award of any other degree.

Deepti Das Krishna

Dept. of Electronics

Cochin University of Science and Technology

Cochin, India-682022

Certificate

Certified that this thesis entitled *Investigations on broadband planar monopole and slot radiators and their suitability for UWB applications* is a bonafide record of the research work carried by Ms. Deepti Das Krishna under my supervision in the Centre for Research in Electromagnetics and Antennas, Department of Electronics, Cochin University of Science and Technology. The results presented in this thesis or part of it has not been presented for the award of any other degree.

Prof.C.K.Aanandan

Dept. of Electronics

Cochin University of Science and Technology

Cochin, India-682022

Acknowledgments

It is my pleasure and privilege to thank the many individuals who made this thesis possible. First and foremost I offer my sincere gratitude towards my supervisor, Prof.C.K.Aanandan, who has guided me through this work with his patience. A gentleman personified, in true form and spirit, I consider it to be my good fortune to have been associated with him.

I thank from the bottom of my heart Prof.P.Mohanan and Prof.K. Vasudevan for their support and good will through all my years at the department. I thank Prof.P.R.S.Pillai, Head, Dept. of Electronics, CUSAT, for his support during the process of writing this dissertation. I take this opportunity to thank Prof.K.G.Nair for his vision in setting up Center for Research in Electromagnetics and Antennas (CREMA) at CUSAT.

I thank all the other teaching faculty of Department of Electronics, CUSAT for their support. I thank all the non-teaching staff and technical staff at the Department of Electronics especially Mr.Mohanan, Mr.Siraj, Mr.Rajeev, Mr.Nouruddin, Mr.Ibrahim Kutty, Mr.Pradeep, Ms.Bindu and Ms.Sudha and the staff at the Administrative Section of CUSAT for their cooperation.

Mere words are not enough to thank Gopikrishna M., who had been my work associate at the Department for almost the entire period of my research here. We have been complimentary to each other in more ways than one and this enabled us to work together productively.

I take this opportunity to thank Anju P. Mathews, Sarin V.P., Sujith R., Shameena V.A., Nishamol M.S., Dinesh R., Nijas M., Sarah Jacob, D.Laila, Jitha B., Tony D., Cyriac M.O., Jaimon Yohanan, Deepa Shankar, Prajas John, Jaison Peter, Adrine Correya, Sreenath S., Ashkar Ali at the Department of Electronics for all their support and for being such a fun to work with. Special thanks to Ananthakrishnan, Paulbert Thomas, Lindo A.O., Ullas G.K. for being at the beck and call to sort out all my hardware and software problems.

I thank the Department of Science and Technology (DST), Govt. of India for supporting my research work financially under the DST Women Scientist scheme and Dr.H.B.Singh, Scientist at DST, for facilitating the same.

I express my gratitude towards Dr.K.P.Ray at SAMEER, Mumbai for encouraging me to take up research in this field.

I thank Prof.A.K.Verma and Prof.E.K.Sharma at the Department of Electronic Science, Delhi University South Campus for introducing me to the joy of learning antennas, microwaves and electromagnetic theory during my days at Delhi University.

My deepest gratitude goes to my family for their unflagging love and support throughout my life. I cannot ask for more from my parents for they have been an epitome of unconditional love and encouragement towards my academic pursuits. My father, P.P.Menon, had spared no effort to provide the best possible environment for me and my brother to grow up and study. Although he is no longer with us in person but we can feel him sharing our joy and happiness. As for my mother, Geetha, I owe a lot to her integrity and dedication in taking care of us, especially after I became a mother myself. Dinakar, my brother, thanks for being a supportive and caring sibling. Ratnam, my grandmother, I thank her for her boundless love. I take this opportunity to remember my grandfather, M.R.K.Menon and father-in-law M.K.K.Menon, with gratitude, for inspiring me with their simple yet righteous lives. Above all, I thank my husband, Murali, for his persistent confidence in me and for inspiring me with his pursuit of learning. Hrishikesh, my son, thank you for being so patient with his mother.

Finally, I would like to thank everybody who was important to the successful realization of the thesis, as well as expressing my apology that I could not mention personally one by one.

Deepti Das Krishna

List of Figures

1.1	Global growth in mobile and fixed subscribers [Kim 2003]	2
1.2	Evolution of wireless communication technologies	3
1.3	Coverage, capacity and power spectral density comparisons	4
1.4	FCC allocated spectral mask for UWB communications	7
1.5	Comparison of (a) Impulse and (b) Multi carrier UWB spectrums.	8
1.6	Progress in antenna designs for mobile systems	10
1.7	(a) Wire dipole, (b) Twin Alpine horn, (c) Bicone, and (d) Discone antennas	12
1.8	The desired antenna response for (a) Multi-band/Multi-carrier and (b) Impulse UWB applications.	17
1.9	Arbitrarily shaped antenna with surface currents $\mathbf{J}(r',t)$	19
1.10	Representation of a system with input $x(t)$ and output $y(t)$	21
1.11	Antenna prototypes (i) elliptical monopole, (ii) band notched elliptical monopole, (iii) inverted cone monopole, (iv) band notched inverted cone monopole, (v) Koch fractal slot, (vi) dual band Koch fractal slot, (vii) wide band slot, (vii) band notched wide band slot antennas	30
2.1	CAD of the antenna in CST Microwave Studio [®]	32
2.2	Transmission model	33
2.3	(a) Antenna reception model and (b) its equivalent circuit	34
2.4	(a) Antenna transmission model and (b) its equivalent circuit	35
2.5	Ideal UWB receiving antenna response (a) impulse response and (b) transfer function	37
2.6	Gaussian pulse and its derivatives (a) waveforms in the time domain and (b) their power spectral densities	39
2.7	Time domain simulation in CST Microwave Studio [®]	41
2.8	Antenna measurement setup	47

2.9	Measured characteristics of the standard wide band horn antenna (a) transfer function amplitudes, (b) receive impulse response and (c) transmit impulse response	52
2.10	Transmit-receive antenna orientations (a) face to face and (b) side by side	53
3.1	Different modifications on planar monopole antenna for wide band characteristics	58
3.2	Geometry of the elliptical monopole antenna	62
3.3	Simulated return loss curve of an elliptical monopole antenna	63
3.4	Simulated input impedance curve of an elliptical monopole antenna	63
3.5	Simulated surface currents and E-field distribution on an elliptical monopole antenna along with its simulated radiation patterns at (a) 3.1GHz, (b) 4.2GHz, (c) 6.2GHz, and (d) 10.2GHz.	65
3.6	Simulated return loss curves for different values of (a) b_r , (b) a_r , (c) b_g , (d) a_g , and (e) g with the rest of the parameters as in Table 3.1	67
3.7	Simulated return loss curves for antenna with and without feed tapering	68
3.8	Simulated return loss curves for the elliptical monopole antennas designed on different substrates	69
3.9	Simulated and calculated f_{r1} plotted for different b_r , b_g and g values	70
3.10	Measured return loss of the elliptical monopole antenna	72
3.11	Measured radiation patterns of the elliptical monopole antenna at (a) 3.5GHz, (b) 6.5GHz and (c) 9.5GHz	73
3.12	Measured peak gain and radiation efficiency of the elliptical monopole antenna	74
3.13	Geometry of the inverted cone monopole antenna (a) ground plane with dimensions	75
3.14	Simulated return loss curves of the inverted cone monopole antenna	76
3.15	Simulated surface current and E-field distributions on the inverted cone monopole antenna along with its simulated radiation patterns at (a) 3.3GHz, (b) 6.3GHz, (c) 9GHz, and (d) 10.6GHz.	77
3.16	Measured return loss of the inverted cone monopole antenna	78

3.17 Measured radiation patterns of the inverted cone monopole antenna at (a) 3.3GHz, (b) 6.3GHz and (c) 9.5GHz	79
3.18 Measured peak gain and radiation efficiency of the inverted cone monopole antenna	80
3.19 Geometry of a notched elliptical monopole antenna	82
3.20 VSWR variations of a notched elliptical monopole antenna for different (a) slot lengths s_l with $w_l = 2.17\text{mm}$ and $t = 0.1\text{mm}$, (b) slot positions w_l with $s_l = 20.2\text{mm}$ and $t = 0.1\text{mm}$, (c) slit widths t with $s_l = 20.2\text{mm}$ and $w_l = 2.17$, (d) slit lengths s_l and slit position w_l with $d = 0.2\text{mm}$ and $t = 0.1\text{mm}$	83
3.21 Simulated return loss and VSWR curves of a notched elliptical monopole antenna with and without the slot	83
3.22 Simulated radiation patterns of a notched elliptical monopole antenna at (a) 3.1GHz, (b) 5.45GHz, (c) 7.0GHz, and (d) 10.2GHz and (e) the current distribution at 5.45GHz.	84
3.23 Simulated impedance and return loss of a notched elliptical monopole antenna	85
3.24 Measured VSWR curves of a notched elliptical monopole antenna	86
3.25 Measured radiation patterns of a notched elliptical monopole antenna	87
3.26 Measured peak gain and radiation efficiency of a notched elliptical monopole antenna	87
3.27 Geometry of a notched PIC monopole antenna	88
3.28 Simulated VSWR curves of a notched PIC monopole antenna	89
3.29 Surface current distribution at 5.5GHz of a notched PIC monopole antenna	90
3.30 Measured return loss and VSWR curves of a notched pic monopole antenna	90
3.31 Measured radiation patterns of a notched PIC monopole antenna	91
3.32 Measured peak gain of a notched pic monopole antenna	91
3.33 Geometry and simulated return loss of a dual-notched elliptical monopole antenna (a) Design 1 (b) Design 2	92

3.34	Surface current distribution on a dual-notched elliptical monopole antenna; Design 1 at (a) 3GHz, (b) 4.6GHz and Design 2 at (c) 3GHz and (d) 4.8GHz	93
3.35	Measured VSWR of a dual-notched elliptical monopole antenna (a) Design 1 (b) Design 2	93
4.1	Geometry of the Koch fractal slot antenna	103
4.2	Koch snowflake geometry in its different iteration stages (a) basic geometry, (b) 1 st iteration, (c) 2 nd iteration, and (d) 3 rd iteration. . .	104
4.3	Simulated return loss of the Koch fractal slot antenna for different iterations of the slot	105
4.4	Simulated return loss of the Koch fractal slot antenna for different sizes of the Koch slot	106
4.5	Current distribution on (a) antenna II at 3.9GHz, (b) antenna I at 2.33GHz, and (c) antenna III at 1.5GHz	106
4.6	Dimensions of the Koch slot antenna in terms of slot size 'a'	106
4.7	The simulated return loss of the second iteration Koch slot (antenna I) for various ground widths W with rest of the parameters remaining same as in Table 4.1	107
4.8	The simulated return loss of second iteration Koch slot (antenna I) with ($\alpha=90^0$) and without ($\alpha=0^0$) the flaring in the tuning stub . . .	108
4.9	Electric field in the antenna aperture and their surface current distributions at (a) 2.4GHz, (b) 3GHz, (c) 4.95GHz and (d) 6GHz	109
4.10	Simulated return loss of the antennas in Table 4.2	112
4.11	Measured return loss of the Koch slot antenna	112
4.12	Measured radiation pattern of the Koch slot antenna at (a) 2.45GHz (b) 3.2GHz and (c) 5.4GHz	113
4.13	Measured peak gain and radiation efficiency of Koch slot antenna . .	114
4.14	Geometry of the CPW-fed modified Koch fractal slot antenna	115
4.15	Evolution from (a) the 2 nd iteration Koch slot to (b) the modified 2 nd iteration Koch slot	115
4.16	Simulated return loss of the CPW-fed Koch slot antenna and the CPW-fed modified Koch slot antenna	116

4.17 Simulated return loss of the antenna for different slot resonator lengths (t_l) with $t_w=4\text{mm}$ and $t_s=0.5\text{mm}$ and rest of the parameters as in Table. 4.3	117
4.18 Measured return loss of the antenna with and without the slot with $t_l=8.8\text{mm}$, $t_w=4\text{mm}$, $t_s=0.5\text{mm}$ and rest of the parameters as in Table. 4.3	117
4.19 Geometry of the CPW-fed UWB slot antenna	118
4.20 Simulated return loss of the antenna with the parameters as in Table. 4.4	119
4.21 Surface current distribution and aperture electric field of the slot antenna at (a) 3.35GHz, (b) 6.6GHz and (c) 9.9GHz	120
4.22 The UWB slot antenna integrated with the system ground plane of USB dongles	121
4.23 The return loss of the UWB slot antenna for different ground lengths L'	121
4.24 The surface current intensity distribution on UWB slot antenna with $L'=75\text{mm}$ at (a) 3.3GHz, (b) 6.5GHz, (c) 10GHz	122
4.25 The UWB slot antenna with a slot resonator inscribed with $t_s = 0.3\text{mm}$, $t_d = 1.4\text{mm}$, $t_w = 1.8\text{mm}$, $t_l = 3.3\text{mm}$, $t_2 = 4.2\text{mm}$, $t_2 = 1.8\text{mm}$ and the rest of the parameters as in Table 4.4	122
4.26 The simulated return loss of the UWB slot antenna with the narrow slot inscribed in the tuning stub	123
4.27 The measured return loss of UWB slot antenna	123
4.28 The measured radiation patterns at (a) 3.35GHz, (b) 6.5GHz and (c) 10GHz of the UWB slot antenna	124
4.29 The measured gain and radiation efficiency of band-notched UWB slot antenna	125
5.1 The simulated transfer function magnitudes in the azimuth and elevation planes of the (a) elliptical monopole, (b) band notched elliptical monopole, (c) inverted cone monopole, (d) band notched inverted cone monopole, (e) wide band slot, (f) band notched wide band slot antennas	130

5.2	The simulated antenna gains in the azimuth and elevation planes of the (a) elliptical monopole, (b) band notched elliptical monopole, (c) inverted cone monopole, (d) band notched inverted cone monopole, (e) wide band slot, (f) band notched wide band slot antennas	131
5.3	The simulated group delays in the azimuth and elevation planes of the (a) elliptical monopole, (b) band notched elliptical monopole, (c) inverted cone monopole, (d) band notched inverted cone monopole, (e) wide band slot, (f) band notched wide band slot antennas	132
5.4	The measured transfer function magnitudes in the azimuth and elevation planes of the (a) elliptical monopole, (b) band notched elliptical monopole, (c) inverted cone monopole, (d) band notched inverted cone monopole, (e) wide band slot, (f) band notched wide band slot antennas	134
5.5	The measured group delays in the azimuth and elevation planes of the (a) elliptical monopole, (b) band notched elliptical monopole, (c) inverted cone monopole, (d) band notched inverted cone monopole, (e) wide band slot, (f) band notched wide band slot antennas	135
5.6	The simulated impulse responses in the azimuth and elevation planes of the (a) elliptical monopole, (b) band notched elliptical monopole, (c) inverted cone monopole, (d) band notched inverted cone monopole, (e) wide band slot, (f) band notched wide band slot antennas	137
5.7	The measured impulse responses in the azimuth and elevation planes of the (a) elliptical monopole, (b) band notched elliptical monopole, (c) inverted cone monopole, (d) band notched inverted cone monopole (e) wide band slot and (f) band notched wide band slot antennas . .	139
5.8	The measured received pulses in the azimuth and elevation planes of the (a) elliptical monopole (b) band notched elliptical monopole, (c) inverted cone monopole, (d) band notched inverted cone monopole (e) wide band slot and (f) band notched wide band slot antennas . .	141

5.9	Simulated and measured transmitted pulses by two identical antennas in their face to face and side by side orientations. (a) elliptical monopole, (b) band notched elliptical monopole, (c) inverted cone monopole, (d) band notched inverted cone monopole, (e) wide band slot, (f) band notched wide band slot Antennas	146
A.1	Geometry of the square microstrip antenna designs with triangular slots (a) Design 1, (b) Design 2, (c) Design 3, (d) Design 4	171
A.2	Return loss S_{ii} for $i=1$ and 2 corresponding to ports 1 and 2, isolation between the ports (S_{2i}) and the power received by a standard horn (S_{3i}) for (a) Design 1, (b) Design 2, (c) Design 3 (switch OFF), (d) Design 3 (switch ON), and (e) Design 4	173
A.3	The simulated current distribution on the patch; Design 1 (a) at 1.65GHz when port 1 is excited with port 2 terminated in a matched impedance, (b) at 1.65GHz when port 2 is excited with port 1 terminated in a matched impedance; Design 2 (c) at 1.8GHz, (d) at 2.4GHz; Design 4 (e) at 900MHz, and (f) at 2.4GHz	174
A.4	The measured radiation patterns of the antenna; Design 1 (a) at 1.65GHz when excited at port 1 with port 2 terminated in a matched impedance, (b) at 1.65GHz when excited at port 2 with port 1 terminated in a matched impedance; Design 2 (c) at 1.8GHz, (d) at 2.4GHz; Design 4 (e) at 900MHz, and (f) at 2.4GHz	175
B.1	Geometry of the circular microstrip antenna designs with sector slot (a) Design 1, (b) Design 2, (c) Design 3, (d) Design 4	180
B.2	(a) Design 1: return loss S_{11} ; (b) Design 2: return loss S_{ii} for $i=1$ and 2 corresponding to ports 1 and 2, isolation between the ports (S_{21}) and the power received by a standard horn (S_{3i}); (c) Design 3: return loss S_{11} and the power received by a standard horn (S_{31}) for different switching states; and (d) Design 4: return loss S_{11} and the power received by a standard horn (S_{31})	183
B.3	The simulated current distribution on the patch for design 1 at (a) 1.79GHz ($\beta=147^\circ$) and (b) 2.47GHz ($\beta=70^\circ$)	184

- B.4 The measured radiation patterns of the antenna; Design 2 (a) at 1.83GHz, (b) at 2.43GHz; Design 4 (c) at 1.75GHz, (d) at 2.39GHz . 184

List of Tables

1.1	Features and advantages of UWB communications	8
1.2	Types of broadband antennas [Allen 2007]	16
1.3	Portable wide band antenna design parameters for MB-UWB and I-UWB applications [Oppermann 2004b]	25
3.1	Dimensions of the elliptical monopole antenna	63
3.2	Elliptical monopole antennas on different substrates	69
3.3	Dimensions of the simulated PIC antenna	76
3.4	Dimensions of the band-notched inverted cone antenna	88
4.1	Dimensions of the Koch slot antennas for different frequencies ($\epsilon_r=3.38$, $h=0.8\text{mm}$)	105
4.2	Dimensions of the Koch slot antenna ($g_l=g_w=0.5\text{mm}$, $g_f=5\text{mm}$) with a comparison between the computed (Cp.) and optimized (Op.) pa- rameters	111
4.3	Dimensions of the CPW-fed Koch slot antenna	116
4.4	Dimensions of the CPW-fed UWB slot antenna	118
5.1	FWHM, ringing (Ring.) and fidelity (Fid.) in the azimuth and ele- vation planes	143
5.2	Fidelity of the transmitted pulses	146

Glossary

1G	1 Generation
CDMA	Code Division Multiple Access
CPW	Coplanar Waveguide
DECT	Digital Enhanced Cordless Telecommunications
DSL	Differential Subscriber Line
FCC	Federal Communications Commission
FWHM	Full Width at Half Maximum
GPRS	General Packet Radio Service
GPS	Global Positioning System
GSM	Global System Mobile
HiperLAN	High Performance Radio LAN
I-UWB	Impulse UWB
IEEE	Institute of Electrical and Electronics Engineers
IP	Internet Protocol
LTI	Linear Time Invariant
MB-UWB	Multi-Band UWB
MC-UWB	Multi Carrier UWB
OFDM	Orthogonal Frequency Division Multiple Access
PCB	Printed Circuit Board
PCS	Personal Communications System

PDA	Personal Digital Assistant
PIFA	Planar Inverted-F Antenna
PILA	Planar Inverted-L Antenna
PSD	Power Spectral Density
Q-factor	Quality-factor
SNR	Signal to Noise Ratio
STIE	Space Time Integral Equation
U-NII	Unlicensed National Information Infrastructure
UMTS	Universal Mobile Telecommunications System
UWB	Ultra Wide-Band
VSWR	Voltage Standing Wave Ratio
WCDMA	Wideband Code Division Multiple Access
WiMAX	Worldwide Interoperability for Microwave Access
WLAN	Wireless Local Area Network
WPAN	Wireless Personal Area Network

Contents

Declaration	iii
Certificate	v
Acknowledgments	vii
1 Introduction	1
1.1 Modern Wireless Communication Systems	1
1.1.1 Ultra Wide-Band Communication (UWB) Systems . .	5
1.1.2 Antennas for Modern Wireless Communications	9
1.2 Broad-band Antennas: An Overview	11
1.2.1 UWB Antennas	16
1.3 Motivation for the Present Work	25
1.4 Thesis Organization	27
2 Methodology	31
2.1 Simulation and Optimization	32
2.2 The Antenna Transfer Characteristics	33
2.2.1 Choice of Source Pulse	38
2.2.2 Implementation in CST [®]	40
2.3 UWB Antenna Quality Measures	41
2.3.1 Frequency Domain Parameters	42
2.3.2 Time Domain Parameters	42
2.4 Fabrication	43
2.5 Antenna Measurements	44
2.5.1 Frequency Domain Parameters	45
2.5.2 Time Domain Parameters	50
2.6 Pulse Distortion Analysis: Fidelity Factor	52
2.7 Chapter Summary	54

3	Planar Broadband Monopole Antennas	55
3.1	Planar Monopole Antennas: Review	57
3.2	Elliptical Monopole Antenna	61
3.2.1	Geometry	62
3.2.2	Simulations	62
3.2.3	Design	70
3.2.4	Measurements	71
3.3	Printed Inverted Cone Monopole Antenna	72
3.3.1	Geometry	75
3.3.2	Design and Simulations	75
3.3.3	Measurements	78
3.4	Band-notched Antennas	80
3.4.1	Band-notched Elliptical Monopole Antenna	82
3.4.2	Band-notched Printed Inverted Cone Antenna	86
3.4.3	Dual Band-notched Elliptical Monopole Antenna	90
3.5	Chapter Summary	94
4	Planar Broadband Slot Antennas	97
4.1	Planar Broadband Slot Antennas: Review	98
4.2	Koch Fractal Slot Antenna	103
4.2.1	Geometry	104
4.2.2	Simulation and Design	104
4.2.3	Measurements	112
4.2.4	Dual-band Modified Koch Fractal Slot Antenna	114
4.3	UWB Slot Antenna	117
4.3.1	Geometry	118
4.3.2	Simulation and Design	118
4.3.3	Measurements	123
4.4	Chapter Summary	125

5	Transient Analysis	127
5.1	Spatio-Temporal Transfer Characteristics	127
5.2	Antenna Transfer Function	128
5.2.1	Simulation Study	128
5.2.2	Measurements with the Prototype Antennas	133
5.3	Impulse Response and UWB Quality Measures	136
5.4	Pulse Distortion Analysis	138
5.5	Chapter Summary	142
6	Conclusion	149
6.1	Thesis Summary and Conclusions	149
6.2	Suggestions for Future Work	153
	References	155
	Appendices	
A	Square patch antenna with triangular slots	169
B	Circular patch antenna with sector slot	179
	Resume of the Author	189

Introduction

Contents

1.1 Modern Wireless Communication Systems	1
1.1.1 Ultra Wide-Band Communication (UWB) Systems	5
1.1.2 Antennas for Modern Wireless Communications	9
1.2 Broad-band Antennas: An Overview	11
1.2.1 UWB Antennas	16
1.3 Motivation for the Present Work	25
1.4 Thesis Organization	27

This chapter surveys the current and emerging wireless communication standards used and highlights the significance of Ultra Wide-Band (UWB) communications. It further discusses the demand for compact & broad-band planar antennas for mobile applications. A review of the various broadband antenna types are done and their suitability for UWB applications is assessed. A description of the stimulus behind the present investigations is presented and we have concluded this chapter with the details of the organization of the present thesis.

1.1 Modern Wireless Communication Systems

There are few technologies that have had a more profound effect on human life than mobile communications. Its global growth is traced and compared with that of the fixed subscribers over the past fifteen years in Fig.1.1. As

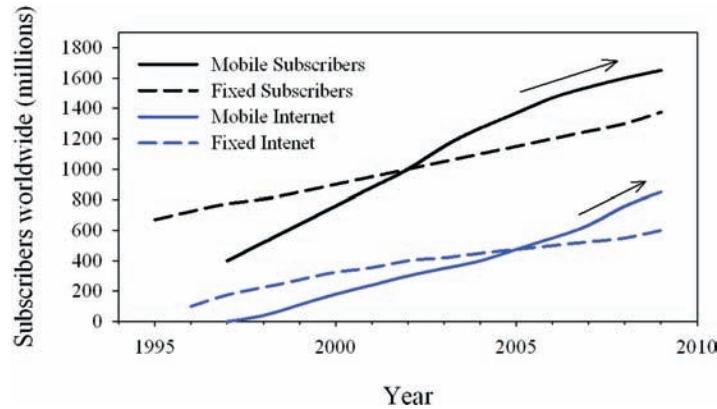


Fig. 1.1: Global growth in mobile and fixed subscribers [Kim 2003]

recently as about two decades ago no one had a mobile phone, while today 1.8 billion men, women and children depend on them and it now easily exceeds the number of land line users.

Apart from mobile telephone communications, Wireless Local Area Networks (WLANs), which came on the scene little more than a decade ago (1997), have also experienced phenomenal growth. The proliferation of WLAN hotspots in public places, such as at airport terminals, has been astounding. They have made their ways into our homes, riding on the back of xDSL and cable access modems, and are now integrated with WLAN Radio Access Points. As a result, the number of wireless internet subscribers is expected to overtake the number of wired internet users quite soon.

The backbone of modern wireless communication are the various commercial wireless standards used for its management and the allocated frequency bands that radio equipments use to transmit and receive data. They have continued to evolve from the first - 1G, to the present - 2G and 3G, to the future network system standards - 4G and 5G, that would support higher capacity digital systems with integrated and converged services with IP-based seamless networks. Its evolution over the last few decades along with their operating frequencies and fractional bandwidths (in %) are summarized and shown in Fig.1.2. Fractional bandwidth is the ratio of the signal bandwidth to the notional center frequency.

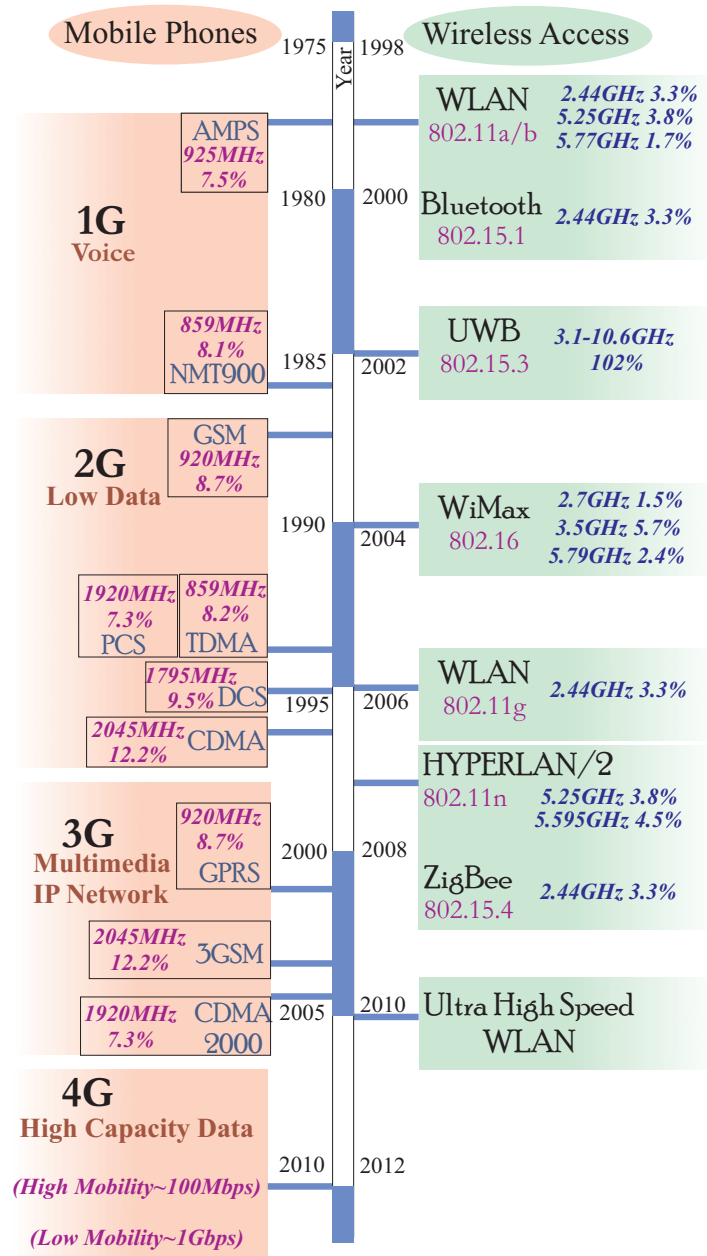


Fig. 1.2: Evolution of wireless communication technologies

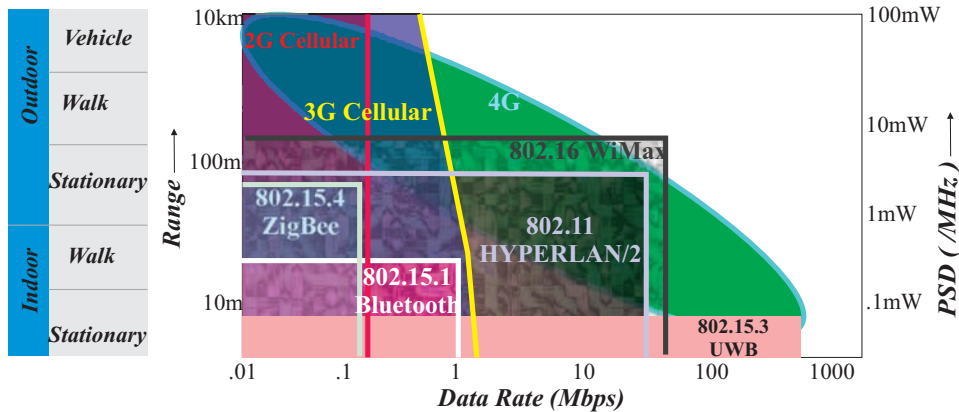


Fig. 1.3: Coverage, capacity and power spectral density comparisons

Worldwide today, Global System Mobile (GSM) is the most widely used cellular mobile standard and it also offers data communication services to users, although its rates are limited to just a few tens of Kbps [Yo 2007]. 3G, through suitable enhancements of the digital protocols have emerged with increased bandwidth and data rates (up to 2Mbps) and include standards like 3GSM, CDMA2000 and GPRS.

In contrast, originally designed to provide fixed data network extension, WLANs would support few hundreds of Mbps data transmission rates. WLAN systems typically operate in a range from 10 to 100m while wireless personal area network (WPAN) systems operate up to about 10m. WLAN (IEEE 802.11 family) and WPAN (IEEE 802.15 family) protocols are responsible for wireless data connections of various speeds and bandwidths to the internet for laptops, PDAs, and other wireless devices that operate in close proximity to one another and has evolved several times responding to the sustained user demands for higher bit-rates.

However, WLAN/WPANs do not offer the kind of mobility, which mobile systems do. In general there is a trade off between coverage and capacity. Fig.1.3 shows the relationship between some of the various standards, in terms of mobility (coverage) and capacity. Therefore as mobile communication systems seek to increase capacity, wireless data systems seeks to increase

coverage; subsequently they will both move towards convergence. The 802.16 WiMAX protocol appears to lend weight to this notion of convergence. It is one of the high-speed wireless broadband solutions that would provide greater than 70Mbps data rates to high-density medium-size areas (1000 to 5000m) such as city buildings, small and rural communities, and suburban malls.

For moving towards seamless roaming/handoff and the best connected services, 4G shall deploy single global cell core network to replace the cell network of 3G. Full IP will be applied in the network which can support different access method by integrating wireless wide and local area networks (IEEE 802.11a/b/g/n, IEEE 802.15 and IEEE 802.16) [Hui 2003]. The future, 5G mobile network is seen as user-centric concept instead of operator-centric as in 3G or service-centric concept as seen for 4G and the development is seen towards the user terminals. The terminals will have access to different wireless technologies at the same time and should be able to combine different flows from different technologies [Janevski 2009].

This increasing trend towards seamless integration of cellular networks such as GSM & 3G and WLAN & WPAN is a strong indicator for the inclusion of high-speed short range wireless in a comprehensive picture of future wireless networks [Oppermann 2004a]. UWB radio will deliver the essential new wireless bandwidth inexpensively, without using precious and scarce radio frequencies and hence has a significant role to play as an extension or complement to cellular technology in future mobile systems.

1.1.1 Ultra Wide-Band Communication (UWB) Systems

A UWB signal, in general, can be defined as the one whose fractional bandwidth, B_f , is greater than 0.25 or occupied a bandwidth of at least 500MHz at all times during the signal. B_f is defined as

$$B_f = \frac{2(f_h - f_l)}{f_h + f_l} \quad (1.1)$$

where f_h and f_l are the upper and lower edge frequencies, respectively. In 2002, the Federal Communications Commission (FCC) regulated the emission limits to -41.3dBm/MHz , for an allocated spectrum ranging from 3.1GHz to 10.6GHz [Commission 2002].

This led to the emergence of UWB technology based applications for commercial high-data-rate, short-range communications, radar systems and measurement. They include high-speed file transfers and printing, high-definition audio/video streaming and a myriad of other applications in the consumer electronics, personal computing and mobile communication arenas. The UWB systems should provide $\approx 50\text{Mbps}$ through buildings within a range of at least 20m , as well as higher rates (up to 1Gbps) at shorter distances. UWB circuits need very little power to achieve these data rates (around tens of mW), which is between one tenth and one hundredth of the power required by devices such as mobile telephones and existing WLANs for the equivalent data rates, respectively, and are thus ideal for battery-powered devices [Smyth 2004].

If we have a fixed amount of energy, we can either transmit a great deal of energy density over a small bandwidth or a very small amount of energy density over a large bandwidth. This is measured in terms of the power spectral density (PSD) which is defined as

$$PSD = \frac{P}{B} \quad (1.2)$$

where P is the power transmitted in watts (W), B is the bandwidth of the signal in hertz (Hz), and the unit of PSD is watts/hertz (W/Hz) or dBm/Hz on a logarithmic scale. For UWB systems, the energy is spread out over a very large bandwidth (hence the name ultra wide band) and in general, is of a very low power spectral density. This can be confirmed when UWB technology is compared with other wireless technologies as shown in Fig.1.3.

The maximum permitted power levels of the FCC approved UWB technology is low enough at 0.5mW over the entire 7.5GHz bandwidth (i.e. $PSD = -41.3\text{dBm/MHz}$, the same level as unintentional radiation from common

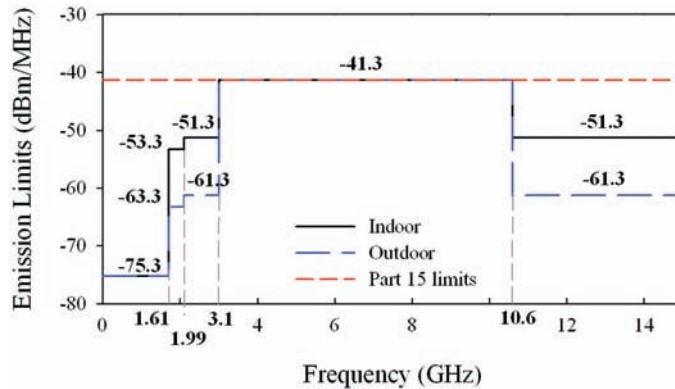


Fig. 1.4: FCC allocated spectral mask for UWB communications

electronics devices such as laptop computers). For wireless communications in particular, this allows UWB technology to overlay already available services such as the WiMAX and the IEEE 802.11 WLANs that coexist in the 3.1 to 10.6GHz.

In order to keep the interference to the minimum, the FCC and other regulatory groups specify spectral masks for different applications which shows the allowed power output for specific frequencies. The spectral mask allocated for UWB communications is shown in Fig.1.4. The major reasons for the extremely low allowed power output in the frequency bands 0.96GHz to 1.61GHz is due to pressure from groups representing existing services, such as mobile telephony, global positioning system (GPS) and military usage. However the most obvious technology that will require coexistence next to UWB is WLAN in the 5 to 6GHz spectrum. It is therefore essential, when designing a system, that the interference issue is considered.

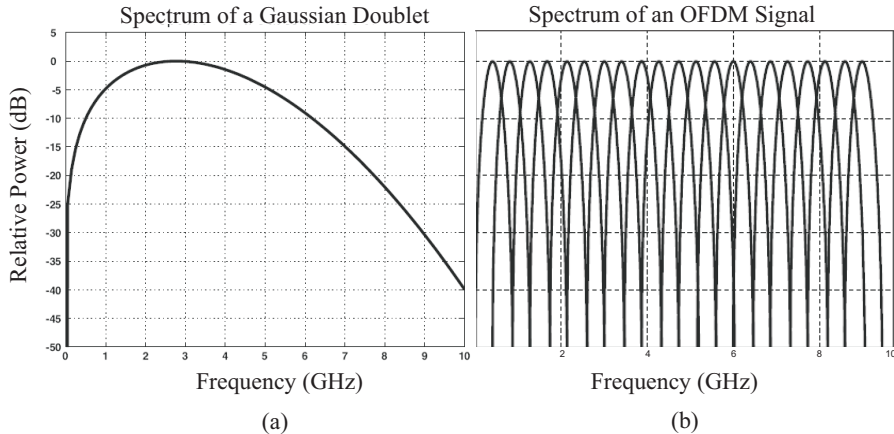
In short, the key attributes of UWB systems that make them suitable for high-speed WPANs are summarized in Table 1.1.

Unlike traditional narrow band systems, UWB generates short pulses and uses these pulses for data modulation. Therefore, UWB is alternatively referred to as impulse, carrierless or baseband transmission. However, UWB does not always have to be impulse or carrierless.

Essentially, UWB communications comes in one of two types,

Table 1.1: Features and advantages of UWB communications

<i>Features</i>	<i>Advantages</i>
Coexistence with current narrow band and wide band radio services	Avoids expensive licensing fees
Large channel capacity	Makes UWB systems perfect candidates for WPANs
Ability to work with low SNRs	Offers high performance in noisy environments
Low transmit power	Provides high degree of security with low probability of detection and intercept
Resistance to jamming	Reliable in hostile environments
High performance in multipath channels	Delivers higher signal strengths in adverse conditions
Superior penetration properties	Viable for through-the-wall communications and ground-penetrating radars
Carrierless transmission	Simple transceiver architecture at a reduced cost

**Fig. 1.5:** Comparison of (a) Impulse and (b) Multi carrier UWB spectrums.

- **Single Band:** Impulse radio falls in the category of single band UWB system and is based on sending very short duration pulses to convey information. In impulse radio, the signal that represents a symbol consists of serial pulses with a very low duty cycle. The pulse width is very narrow, typically in nanoseconds. As a result it has a better resolution of multi path in UWB channels. The small pulse width gives rise to a large bandwidth as shown in Fig.1.5(a). The high instantaneous power during the brief interval of the pulse

helps to overcome interference to UWB systems, but increases the possibility of interference from UWB to narrow band systems. Simple I-UWB systems can be very inexpensive to construct as it eliminates the need for up and down conversion and allows low-complexity transceivers.

- **Multi Band:** Since UWB can be any technique that generates signals occupying at least 500MHz of bandwidth within the spectrum mask placed by FCC [Commission 2002], the UWB systems can also be classified as multi-band based. Here, the 7500MHz of unlicensed spectrum can be considered to provide a number of UWB “bands” as shown in Fig.1.5(b) and can be exploited in many ways like by using multi-carrier (MC) or OFDM modulation with Hadamard or other spreading codes. MC-UWB is particularly well-suited for avoiding interference because its carrier frequencies can be precisely chosen to avoid narrow band interference to or from narrow band systems.

1.1.2 Antennas for Modern Wireless Communications

Several demands are placed on modern antennas designed for multi-frequency and multi-mode devices such as cellular phones, WLANs and WPANs. Fig.1.6 traces the progress in the antenna designs for mobile systems since its days of conception. Primarily, antennas need to have high gain, small physical size, broad bandwidth, versatility, embedded installation etc. depending on the type of application. For fixed applications such as cellular base stations and wireless access points, high gain and stable radiation coverage over the operating range are desired. For portable devices such as hand phones, personal digital assistants (PDAs) and laptop computers; compact, radiation efficient, omnidirectional antennas are preferred.

A few of its design challenges are discussed as follows:

- **Size:** Antennas for mobile terminals are desired to be small in physical size so that they can be embedded in devices or conform to device platforms. However the operation of electrically small antennas ($< \lambda/8$) is dictated by

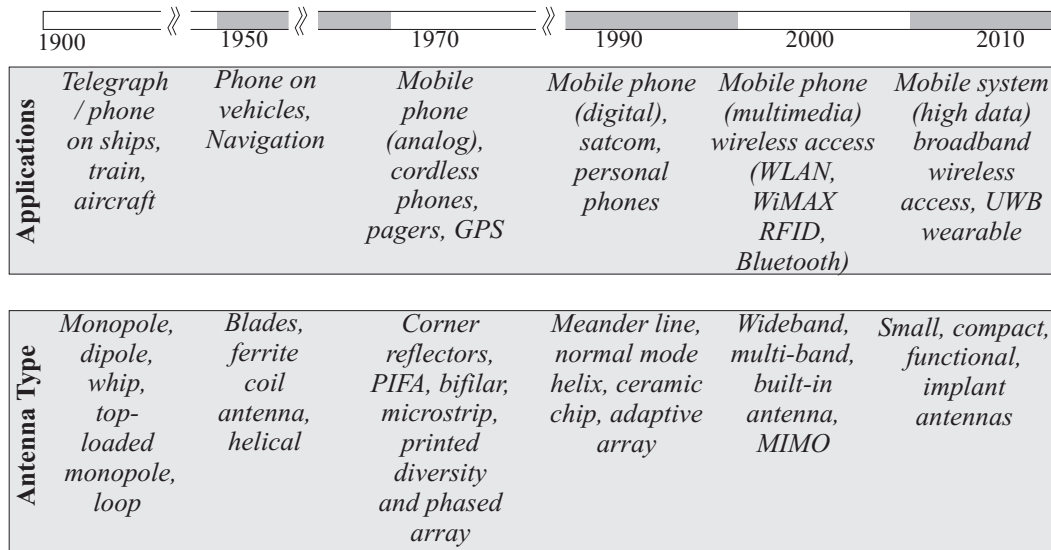


Fig. 1.6: Progress in antenna designs for mobile systems

fundamental relationships which relate their minimum Q-factor to the volume of the smallest sphere in which they can be enclosed, often referred to as the Chu-Harrington limit [Huang 2008]. The fundamental limitations of electrically small antennas are in terms of impedance bandwidth, gain and radiation efficiency.

In addition, one has to also respect limits that come from practical considerations of a compact antenna. For instance, smaller the mobile unit, greater will be the influence of the components located near the antenna on its performance. Efficient antennas are always preferred, so as to avoid frequent battery re-charging. Then there are the finite ground plane affects due to the radiating surface currents induced by the antenna element on the ground plane.

- **Bandwidth:** As can be observed from Fig.1.2, the fractional bandwidths for commercial mobile communication systems vary from 7% to 13% and reach up to 109% for UWB communications. The antennas used must have the required performance over the relevant operating frequency range.

Most importantly, the antennas should be well impedance-matched over the

operating frequency range. Antennas with broad bandwidths have additional advantages, such as to mitigate design and fabrication tolerances, to reduce impairment due to the installation environment, and most importantly, to cover several operating bands for multi-frequency or multi-mode operations.

In future, universal antenna solutions completely embedded into portable devices are desirable, which may cover frequencies from 800MHz to 11GHz or above in order to include all the existing wireless communication systems such as GSM900, GSM1800, PCS1900, WCDMA/UMTS (3G), 2.45/5.2/5.8GHz-ISM, U-NII, DECT, WLANs, European HiperLAN I, II, and the UWB systems as well.

- **Conformability:** For aesthetic reasons, antennas for portable devices has to be embedded. Owing to unique merits such as small volume, low manufacturing cost and easy integration into planar circuits, planar antennas are ideal candidates. In general, all antennas comprising planar or curved surface radiators or their variations and at least one feed are termed “planar antennas”. Printed microstrip patch antennas, slot antennas, suspended plate antennas, planar inverted-L and inverted-F antennas (PILAs and PIFAs), sheet monopoles and dipoles, roll monopoles, etc. are typical planar antennas used extensively in wireless communication systems.

In general, portable communication systems need low-cost compact planar antenna solutions with broad bandwidth and omni-directional radiation patterns.

1.2 Broad-band Antennas: An Overview

Broadband antennas are those which operate over a wide bandwidth. A working definition for the same would be as whose parameters - the impedance bandwidth, gain, polarization and radiation patterns, do not change significantly over about an octave or more. In this section, we will review the concept behind the operation of broadband radiators and, as it turns out in most cases,

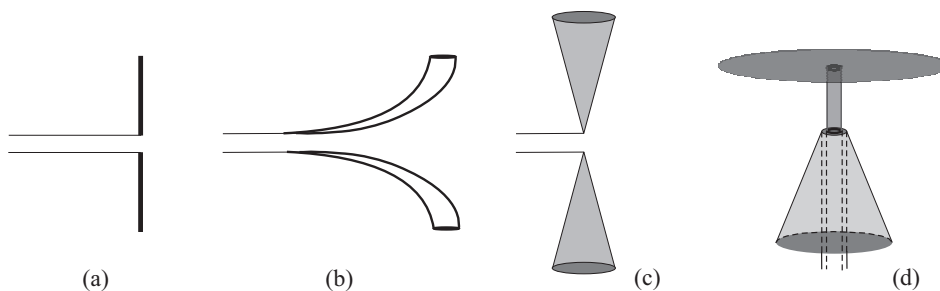


Fig. 1.7: (a) Wire dipole, (b) Twin Alpine horn, (c) Bicone, and (d) Discone antennas

it is rooted in having ‘a smooth physical structure’ [Stutzman 1981]. Such antennas usually require structures that do not emphasize abrupt changes in the physical dimensions involved but instead has smooth boundaries. Such physical structures tend to produce patterns and input impedances that changes smoothly with frequencies.

The difference between a transmission line and an antenna lies only in the amount of radiation generated and not in the geometry itself. For instance, an open ended two wire transmission line becomes an antenna if the spacing between the lines is large with respect to wavelength such that diffractions from the wires and wire ends do not cancel each other or incident fields in the exterior region [Chen 2007a]. A fundamental example would be a dipole antenna as in Fig.1.7(a). They fall under the category of resonant antennas whose bandwidths are generally low. For a resonant antenna, the waves traveling outwards from the feed point to the end of the antenna is reflected, setting up a standing wave type current distribution [Stutzman 1981].

If the strong localized diffractions on the antenna structure, which usually arise from abrupt discontinuities, is carefully controlled via critically designing the antenna geometry, a wide operating band is achieved. Common examples of such wide band antennas include rolled-edge horns, ridged horns [Bird 2007] and their planar versions like the tapered-slot antennas often called the Vivaldi antennas [Langley 1993], where the aim is to taper the antenna geometry to make a smooth transition from the input to the aperture.

Interestingly enough, even from an impedance bandwidth point of view,

we arrive at a similar tapered structure for a wide band operation as in the case of a twin Alpine-type horn shown in Fig.1.7(b) [Kraus 2005]. A two wire transmission line is opened out until the conductor separation is a wavelength or more. However, if the conductor spacing-diameter ratio is kept constant, a constant characteristic impedance over a wide frequency band is achieved. The result is a tapered graduation from the feed to the open end with a relatively constant unidirectional radiation pattern. These properties makes twin horn a classic broadband antenna. Unlike resonant antennas, reflected waves are minimized here and the input impedances are predominantly real as in the case of pure traveling waves on low loss uniform transmission lines. They can be easily classified under traveling wave antennas.

On the same line of thought, an infinite biconical antenna is analogous to an infinite uniform transmission line. The bicone would act as a guide for a spherical wave in the same way that a uniform transmission line acts as a guide for a plane wave. The input impedances of the infinitely long bicone is uniform and real; and it reduces with increase in the cone angle [Kraus 2005]. However, practical biconical antennas, shown in Fig.1.7(c), are finite and are analogous to a finite or terminated transmission line [Stutzman 1981]. Its input resistance becomes very large and the input reactance very small for an overall antenna length of approximately one wavelength similar to an ordinary dipole.

The overall pattern of a bicone is essentially the same as that of a dipole of length $< \lambda$ i.e. a solid revolution formed by a rotation of a figure of eight. It is significant to note that the terminal impedance of the thicker biconical antenna is more constant as a function of cone length than that of thinner antennas. Just as it is proven in case of cylindrical antennas, the thicker biconical antennas are more suitable for wide band applications. This is because a “fatter” structure will lead to a broader bandwidth since the current area and hence the radiation resistance is increased. The biconical antennas are thus one of the the earliest antennas used in broadband applications [Kraus 2005].

There are innumerable variations to the basic geometrical configurations

of bicones and monocones. Discone is one such example comprising of a disk and a cone as shown in Fig.1.7(d) [Balanis 1997]. The antenna performance as a function of frequency is similar to a high-pass filter. Below an effective cutoff frequency it becomes inefficient and produces severe standing waves in the feed line. At cutoff, the slant height of the cone is approximately $\lambda/4$. They have relatively constant input impedance and satisfactory pattern and gain over wide bandwidths with beam widths tending to become smaller. The antenna gains are larger with increasing frequency and that may be highly desirable and useful.

However, the antennas mentioned above are seldom used in portable/mobile devices due to their bulky size and high manufacturing costs. Therefore, planar versions of the bicones and monocones have been alternatively used in wireless communications because they have shown excellent performance in impedance and radiation along with their advantage of small size. The earliest planar dipole may be the bow-tie antenna invented by Brown-Woodward [Chen 2007b].

Planar monopole antennas are also widely reported. They can be excited by a coaxial cable vertically hosted above a large metal ground. The triangular monopole antenna is the planar versions of monocone antennas [Lin 2005]. The radiators of the planar monopole antennas can be of any shape for broad operating bandwidth. Square [Amman 1999], [Amman 2004], trapezoidal [Chen 2000b], diamond [Wu 2004b], pentagonal [Evans 1999], circular [Liang 2005b], semi-circular [Lee 2005], elliptical [Agrawal 1998], annular [Chen 2003b], square with semi-circular bottom [Anob 2001], printed inverted cone (PICA) [Suh 2004] etc. are few of the geometrical shapes of the radiators employed. Among the different configurations studied, the circular and especially the elliptical disk monopole appears to yields maximum bandwidth for similar overall dimensions [Agrawal 1998].

In mobile wireless applications, antennas are expected to be embeddable or easy to be integrated into wireless devices. Therefore, the antennas directly printed onto a printed circuit board (PCB) are the most promising

designs. Such antennas are usually constructed by etching the radiators onto a dielectric substrate and a ground plane around the radiators.

The planar broadband antennas proposed in the open literature mainly focus on the slot and monopole types. They have received considerable attention owing to their attractive merits, such as ultra wide frequency of operation, good radiation properties, simple structure and the ease of fabrication. The typical shapes of these monopole radiators are circle [Jianxin 2005], ellipse [Krishna 2007] and square [Gopikrishna 2007]. Printed wide slot antennas have also been widely reported especially those having a modified tuning stub, such as the fork-like stub [Sze 2001], [Qing 2003], [Chair 2004], [Hsu 2006], the rectangular stub [Chen 2003a], [Liu 2004a] and the circular stub [Jang 2003] inside a wide slot in the ground plane. A detailed literature review of the same is done in Chapter 3 and 4 of this thesis.

The other family of wide band antennas are called the frequency independent antennas. The desired feature for such antennas are frequency independent behavior of the input impedance and pattern. It is the emphasis on angles and complete removal of finite lengths which is the most distinctive feature of such antennas [Rumsey 1966]. The typical realization is an angular constant structure described only by the angles exhibiting scaling invariability.

Since in practical cases the physical size of the object is finite, a “truncation principle” can be applied. It says that ‘provided that if the overall current on the antenna decreases as we move away from the feed due to radiation, it is possible to define an active region within which if the actual finite structure is contained, truncation of the geometry does not modify the behavior of the antenna’ [Balanis 1997]. A typical example would be a finite biconical antennas and its planar counterpart - the bow-tie antennas.

There are other types of wideband antennas like the spiral and log-periodic antennas which shows frequency-independent characteristics but are based on different principles. Self complimentary antennas, characterized by self complimentary metallizations, are one such family of frequency independent antennas [Mushiake 1992]. By applying the Babinet’s principle, it is shown

that self complimentary structures have a constant input impedance [Balanis 1997]. Two-arm logarithmic spiral and archimedean spiral antennas are examples of antennas which realize the principle of frequency independence [Filipovic 2007].

Generating multiple resonances over the desired operating band is yet another principle of frequency independent operation for antennas like log periodic [Filipovic 2007] and fractal antennas [Kraus 2005]. Planar versions of the same are also reported like for example the planar log-periodic design which has its dipole elements with their one half etched on top layer and the other on the bottom layer of a substrate [Pantoja 1987] .

Since the requirements of antennas vary with applications and system designs, we can conclude this review on broad band antennas by categorizing the antennas discussed so far in terms of geometry and radiation characteristics as in Table. 1.2. Their suitability for high speed low power UWB communications systems is discussed in the following section.

Table 1.2: Types of broadband antennas [Allen 2007]

	Directional	Omni-directional
2 - D	Vivaldi Antenna Tapered Slot Antenna Log-periodic Antenna Planar Log-Spiral Antenna Conical Spiral Antenna	Planar Dipole Slot Antenna Printed Antenna on PCB
3 - D	TEM Horn Antenna Ridge Horn Antenna Reflector Antenna	Loaded Cylindrical Dipole Bi-conical Antenna Disc-cone Antenna Roll Antenna

1.2.1 UWB Antennas

The antenna requirements varies for the Multi-band (MB-UWB) and Impulse UWB (I-UWB) communications. Fig.1.8 plots the desired amplitude and phase response of the radiation fields of broadband antennas for the two types. In the case of MB-UWB, while a stable antenna gain (amplitude response)

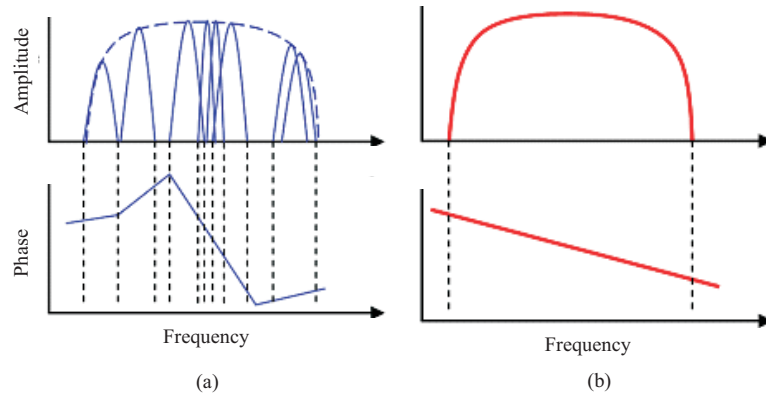


Fig. 1.8: The desired antenna response for (a) Multi-band/Multi-carrier and (b) Impulse UWB applications.

is a requirement, there are no constraints on the phase response as shown in Fig.1.8(a). The signal at any given time can be viewed as a narrow band signal and broad band antennas are used in such applications as multiple narrow bands.

I-UWB requires antennas that can cover multi-octave bandwidth in order to transmit pulses of the order of nano-seconds in duration with minimal pulse distortion. Since such systems do not necessarily employ modulation of a sinusoidal carrier, the signal at the antenna's input can be considered as the "message" signal and I-UWB antennas can be termed as "baseband pulse" antennas [Lamensdorf 1994]. Because the data may be contained in the shape or precise timing of the pulse, a clean impulse response can be considered as the primary requirement for a I-UWB antenna.

One of the challenges in implementation of UWB communication systems is the development of a suitable UWB antenna that would enhance the advantages promised by a pulsed communication system. To prevent distorting the pulse, an ideal I-UWB antenna should produce radiation fields with constant magnitude and a phase shift that varies linearly with frequency as shown in Fig.1.8(b).

1.2.1.1 Radiation of Large Fractional Bandwidth Pulses

The conventional nomenclature used to describe a broad band antenna performance (such as directivity, gain, VSWR, etc.) are not sufficient for evaluating antennas with baseband-pulse excitations as they are deduced by the time-harmonic (sine wave) solutions to Maxwell's equations. They are only suitable for antennas that are used for multiple narrow band services or channels. The Maxwell's equations can be applied in the case of radiation of UWB signals as well. On using a time domain approach, they manifest some interesting differences compared to the radiation of narrow band signals.

Radiation in free space occurs when the charges are accelerated and when the electric current encounters certain discontinuities in the antenna. There is also sometimes a partial time-delay derivative operation on the current density, from the various parts on the antenna, involved in the radiating process. Therefore, radiation manifests itself as a partial derivative in time and delay of the current.

The difference between wide band and narrow band signals is that the transmitted signals in narrow band systems are sine waves, so their time derivatives are also sine waves. The signal shape for narrow band signals remains sinusoidal throughout the radiation process. The wider the signal bandwidth, the more a signal shape differs from its time derivative in amplitude versus time [Siwiak 2004]. Hence the shape of the transmitting antenna current signal plotted versus time with respect to the input pulse will, in general, be different for different antenna orientations, size and shape.

An arbitrarily shaped antenna that supports surface currents $\mathbf{J}(\mathbf{r}', \tau)$ at points described by a vector r' pointing from the coordinate origin to the current density point and by a retarded time variable $\tau = t - R/c$ is shown in Fig.1.9. The retardation time, R/c , is explicitly the propagation time required for a disturbance to travel the distance R with velocity c . Using the space time integral equation (STIE) technique [Bennett 1978], which is a time-domain approach to electromagnetics, the general expression for the

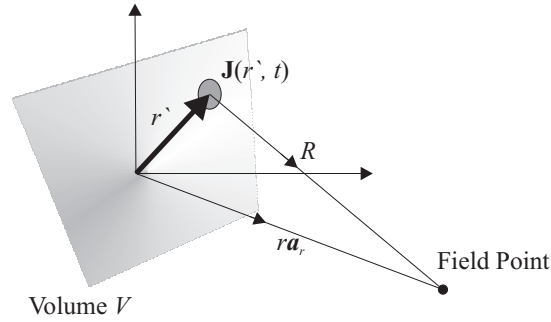


Fig. 1.9: Arbitrarily shaped antenna with surface currents $\mathbf{J}(r', t)$

magnetic far-zone field is

$$\mathbf{H}(r, t) = \frac{1}{4\pi r c} \int_V \frac{\partial}{\partial \tau} \mathbf{J}(r', \tau) \times \hat{a}_r dV' \quad (1.3)$$

where \hat{a}_r is a unit vector pointing in the direction of radiation. The electric far zone field is

$$\mathbf{E}(r, t) = -\eta_0 \hat{a}_r \times \mathbf{H}(r, t) \quad (1.4)$$

where η_0 is the intrinsic impedance of free space.

A key factor to note in the above equations is the appearance of the partial derivative in τ , which includes both time and delay. The magnetic field \mathbf{H} and the electric field \mathbf{E} are related to a time and delay derivative of the antenna current density which tends to lengthen the signal in time.

Furthermore, the retardation time R/c means that the radiated signal shape, as a function of time, will vary depending on where the observation point is relative to the antenna. Because of this, the radiated field signal shapes will be different from the signal shape supplied to the feed point of the antenna. On a similar line, the radiated fields of an ideal infinitesimal antenna would exactly be a time derivative of the transmitting signal everywhere in space because it is too small to impose any signal-distance delays on the antenna.

The receiving process is deduced from the principle of reciprocity in electromagnetic theory applied to the receiver antenna problem [Siviak 2004].

The principle allows us to write an expression for the voltage signal V_R at the receiving terminal of the antenna in terms of the current density $\mathbf{J}(r',\tau)$ that would be present if the receive antenna were used to transmit a feed-point current I_T ; and the the electric field E_{inc} due to the transmit antenna that would be incident on the receive-antenna location without the receive antenna being present.

$$\mathbf{V}_R(t) = -\frac{1}{I_T} \int_V \mathbf{E}_{inc}(r, t) \cdot \mathbf{J}(r', t) dV' \quad (1.5)$$

The effect, that is of interest to us here, is that the incident electric field undergoes a time delay before the fields impressed on the various parts of the antenna travel to the feed point to be summed up in the antenna load. There is no time derivative involved in receiving as there was in the transmitting process; however, the received voltage is not simply proportional to the incident electric field, but is rather a weighted summation of time-delayed points from the entire antenna surface. If the antenna were an infinitesimally small receiving antenna, then the time delays are zero and the received voltage is exactly proportional to the field strength.

Thus those antennas that appear to perform equally over wide frequency ranges when using narrow band signals, however performs very differently with impulse excitations. Broadband antennas for multi band operation are not necessarily effective for UWB signals. Antennas must be understood in their time-domain behavior as well, to observe the antenna effects on short pulses.

1.2.1.2 UWB Antenna Characterization by Spatio-Temporal Transfer Functions and Impulse Responses

There is a demand for both frequency domain and a time domain representation of UWB antennas. A common approach is to consider an impulse fed broadband antenna, that acts as a pulse shaping filter, as a linear time invariant (LTI) system [Sorgel 2005].

A system is a mathematical model that relates the output signal to the input signal of a physical process as shown in Fig.1.10. A linear system is the one which follows the superposition theorem, and it is said to be time-invariant if the input $x(t - t_0)$ produces a response $y(t - t_0)$ where t_0 is any real constant. In time domain analysis, the important objective is to find the impulse response of the system.

The impulse response $h(t)$ of an LTI system is defined as the response of the system when the input signal $x(t)$ is a delta function $\delta(t)$. The output $y(t)$ of an LTI system can be expressed as the convolution of the input signal $x(t)$ and the impulse response $h(t)$ of the system as shown below;

$$y(t) = h(t) \otimes x(t); \quad (1.6)$$

In the frequency domain, the Fourier transform of the above equation is

$$Y(\omega) = H(\omega)X(\omega); \quad (1.7)$$

where $H(\omega)$ is the Fourier transform of $h(t)$. The function $H(\omega)$ is called the transfer function or the frequency domain response of the LTI system. As the antenna characteristics also depend on the signal propagation direction (i.e. spatially dependent), the transfer functions and impulse responses modeling the UWB antennas are spatial vectors, $H(\omega, \theta, \phi)$ and $h(t, \theta, \phi)$ [Sorgel 2005].

The frequency-domain transfer function $H(\omega, \theta, \phi)$ and the time-domain impulse response $h(t, \theta, \phi)$ contains the complete information on the antenna behavior. It enables the assessment of two important antenna effects, namely, the ability of the antenna to effectively transmit and receive power and secondly, its distorting influence on the waveform to be transmitted or received.

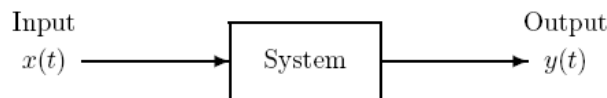


Fig. 1.10: Representation of a system with input $x(t)$ and output $y(t)$

This is quantified in the frequency domain in terms of parameters like antenna gain and group delay which can be deduced from the transfer function $H(\omega, \theta, \phi)$. A non-distorted structure is characterized by a constant group delay i.e. linear phase response. The nonlinearities in group delay indicate the resonant character of the device, which implicates the ability of the structure to store the energy. It results in ringing and oscillations of the antenna impulse response $h(t, \theta, \phi)$.

The dispersion can be analyzed from the envelope of the impulse response $h(t, \theta, \phi)$ by determining the time-domain parameters like its peak value, full width at half maximum (*FWHM*) and ringing. The time/frequency system model for UWB antennas and the deduction of the antenna parameters are discussed in detail in Chapter 2 of this thesis.

1.2.1.3 UWB Antenna Aspects

In the case of MB-UWB based communications, the antennas can be characterized like a classical narrow band antenna and all the earlier discussed types of broadband antennas including the log periodic antenna types are suitable [Sorgel 2003]. However the antennas for I-UWB applications need a closer look.

If in pulsed communications, the full FCC bandwidth from 3.1 to 10.6GHz is covered with the derivative of Gaussian pulse, then the transient behavior of the impulse response $h(t, \theta, \phi)$ of the antenna has to be taken in account. In this case, the impulse distortion in the time domain and in the spatial domain have to be examined for compatibility. An adverse behavior of the impulse response $h(t, \theta, \phi)$ can be characterized by [Weisbeck 2009]:

- low peak value;
- large width at half maximum;
- long ringing.

These have adverse effects on the system performance, like for example,

- reduces the received signal strength;
- distorts the pulse transmitted;
- limits the data rate in communications.

The various broadband antennas discussed previously needs to be analyzed for their time domain performance [Licul 2003]. Tapered waveguide antennas like the ridged horn antennas and Vivaldi antennas are based on the principle of traveling wave structures.

These structures have relatively high peak, short duration of the transient response envelope and hence low dispersion. The ringing which is due to the multiple reflections at the substrate edges and parasitic currents at the outer substrate edges, is relatively low. The ridged horn antennas find applications as standard antennas for UWB antenna characterization and the Vivaldi antennas are well suited for direct planar integration and also for UWB antenna arrays for radar and communications [Sorgel 2003]. Because of its non-resonant structure and that it offers proper radiation conditions for all frequencies within the given bandwidth, these antennas are ideal I-UWB antennas.

Biconical antennas are based on the principle of angle dependent structures. It has a near omni-directional pattern accompanied by a small ringing of the antenna. A planar example of the same is a bow-tie antenna which has reasonably compact dimensions when designed for the FCC UWB frequency band. Therefore this type of antenna can find applications in communications in mobile devices.

Spiral antennas based on the principles of self complimentary-frequency independent operation are however ill-suited for time-domain applications. This is because of the frequency dependent position of the radiating areas and therefore frequency dependent time delays. This results in broadening and reduction in peak values of the impulse response.

All antennas with closely placed multiple resonances or spurious surface currents are bad candidates and are disregarded for time-domain operations.

Among them is definitely the log periodic antennas [Sorgel 2003] and fractal antennas. Any UWB antenna with resonant elements broadens the radiated impulse i.e. increases the width and reduces the peak value of the impulse response.

For antennas that are electrically small, the impedance match is poor due to the high quality factor but the radiation pattern is almost constant. With a proper impedance transformation, the antennas can be made UWB. Typical candidates are the small monopole antennas and their planar approximations are the planar monopole antennas. They have omnidirectional radiation patterns with radiations in large elevation angles. Its impulse responses are short indicating small ringing. A good time domain behavior along with compact size makes them suitable as UWB antennas for portable communications. However, for smaller ground planes the matching is difficult for a 50Ω reference impedance. The finite ground planes also effects the stability of the radiation pattern versus frequency and the impulse radiating properties.

Hence, the choice of UWB antennas for portable, short-range applications is restricted to small and traveling wave antennas. Candidates for portable UWB applications are

- Planar monopole antennas;
- Bow-tie antennas;
- Small tapered slot antennas like Vivaldi antennas.

Some of the antenna specifications for portable UWB antennas for multi-band and I-UWB applications are given in Table 1.3.

Despite the approval of the FCC for UWB to operate over 3.1 to 10.6GHz, it may be necessary to notch-out portions of the band in order to avoid electromagnetic interference with the existing wireless networking technologies such as IEEE 802.11a in the U.S. (5.15 to 5.35GHz, 5.725 to 5.825GHz) and HIPERLAN/2 in Europe (5.15 to 5.35GHz, 5.47 to 5.725GHz). Therefore,

Table 1.3: Portable wide band antenna design parameters for MB-UWB and I-UWB applications [Oppermann 2004b]

MB-UWB	<i>Frequency Domain (3.1-10.6GHz)</i>	I-UWB
	Impedance : VSWR < 2	
	Pattern : Omnidirectional	
	Gain : 0dBi	
	Polarization : Constant	
	Radiation Efficiency : > 50%	
	<i>Time Domain</i>	
	Dispersion : Minimum	
	Fidelity : > 0.7	

UWB antennas with notched characteristics in the WLAN frequency band are most often desired.

1.3 Motivation for the Present Work

Since communication systems are trending towards high speed-seamless integration, it is important to evolve suitable broadband antennas. Applications, like UWB, requires additional parameters to be satisfied when it comes to pulsed communications. Here we have summarized the following technical and practical design goals for a UWB antenna:

- The antenna must be able to radiate or receive fast electromagnetic transients with frequencies between 3.1 and 10.6GHz.
- A criterion, to guarantee high mobility and hand held application, is compact dimensions and light weight.
- The antennas must be cheap for mass production

The issues concerning interference between wide band devices with other existing narrow band communication networks can be sorted by implementing filters to notch out the required frequency bands. However, since additional

filters would increase the size of the devices, embedded filters on the antenna is preferred.

Consumer electronics like wireless USB & next G bluetooth applications requires narrow planar antennas with a width of ≈ 11 to 24mm. However, with the reduction of antenna size, impedance bandwidth degrades. Since compact antennas show significant ground plane length/shape effects on its performance, it is important to design antennas resistant to it. The conflicting requirements of good performance and compact size make the design of such antennas challenging.

The aim of the thesis is to investigate the requirements for a wide band behavior of compact planar antenna designs. This work looks in detail the wide band performance of the monopole and slot antennas and identifies the design parameters of the same. Several novel designs on commercially available microwave substrates are proposed that could be successfully implemented in consumer electronics applications. It is important to characterize the designed UWB antennas in terms of their transient performance. To throw light on their suitability for pulse communications, their time-domain behavior is studied in the final part of the thesis.

The shortcoming of the planar antenna designs, usually reported, is that they are based on the lengthy trial and error method that involves computationally intensive full wave electromagnetic simulations. When one decides to design an antenna using a different dielectric substrate, the time consuming design process has to be fully repeated. In such circumstances, the designers are interested in having simple design formulas that provide a very good approximation to the final design when sophisticated EM analysis and design software packages are applied. This thesis addresses this issue and provides simple design formulas, which are suitable for the antennas designed. It is shown that the antenna design parameters obtained using the equations developed in this thesis do not differ much from the optimized values obtained using the commercial software

1.4 Thesis Organization

The thesis is divided in three sections as described below,

The first section is constituted by the first two chapters: the Introduction to the work and the Methodology adopted in the execution of the same. In this part we have discussed the evolution & future trends of modern mobile communication & wireless access and the significance of UWB communication. The conventional broad banding techniques for planar antennas are reviewed. Considering the design requirements of radiators for modern wireless communications, two general categories of planar wide band antennas namely Monopole and Slot-type are identified for further investigation.

The methodology for developing the antennas discussed involves simulation studies in CST Microwave Studio[®], fabrication of the same and measurements done with the test set up. The antenna measurements in the frequency domain for the return loss, radiation pattern and gain are described. The relevant theory behind the time domain characterization of the antenna, in terms of Full Width Half Maximum (*FWHM*), ringing and fidelity, which are deduced from the measurements, are explained.

The second section consisting of Chapters 3 & 4 concentrates on Broadband Monopole and Broadband Slot antennas respectively. In this section, a common approach is followed for the antenna development. We begin with a detailed literature review of the available designs belonging to this broad category, followed by a description on the evolution of the antennas presented. The proposed antenna designs are simulated and their resonant modes are identified. The antennas are CPW-fed for easy fabrication and better integration with monolithic microwave circuits except in some cases where it is microstrip-fed. The surface current and field distributions on the antenna at the resonant modes and their corresponding radiation patterns are analyzed in detail.

The results of the analysis along with the parametric studies have enabled us to deduce their design equations and design methodologies on any substrate

for the desired operating frequencies. The measured results of the fabricated antennas are then plotted with their corresponding simulated results which are found to conform well in all cases. Further, to notch out selected narrow band frequencies in the wide operating band, thin slot resonators are embedded in the antenna. Such adaptations are incorporated, optimized and measured on all the proposed designs.

There are two novel compact designs of planar monopole antennas presented: an elliptical antenna and an inverted cone antenna. These antennas perform well in terms of its impedance match and gain, over a wide band and easily comply with the FCC UWB frequency band of 3.1 to 10.6GHz. The radiation patterns are omni-directional but in case of the elliptical antenna they are distorted at the higher end of the spectrum. This is overcome by the inverted cone monopole antenna which has the advantage of a compact size as well. The slot resonators are engraved on either/both the radiator and ground plane to disable the antenna from functioning at the narrow band frequencies to be notched out. The photographs of the monopole antenna prototypes are shown in Fig.1.11(i) - (iv).

We have investigated the performance of planar slot antennas by designing a Koch fractal based slot antenna. The slot and feed geometry effects on the antenna performance are studied in detail. The antenna structure is compact and performs well over a frequency band wide enough to cover all the WLAN/WiMAX bands. An improved slot antenna design is presented next with a reduced size and enhanced bandwidth covering the FCC specified UWB band. This design has the additional advantage that its performance is independent of ground plane size making it suitable for wireless dongle applications. The photographs of the slot antenna prototypes are shown in Fig.1.11(v) - (vii).

In the third section presented in Chapter 5 of the thesis, we have investigated the influence of the antenna on radiation of a UWB pulse to confirm their suitability for I-UWB applications. The transfer function measurements are performed for both the azimuthal and elevation planes and their impulse

responses are deduced. This is successfully verified against the simulated results obtained using the time domain capabilities of CST Microwave Studio[®]. From the impulse responses, we have computed and compared parameters such as *FWHM* and ringing. The influence of the antenna on pulse transmissions is evaluated by convoluting the impulse response with a UWB pulse. The time domain distortions for the different designs are then characterized in terms of mathematically tractable parameters like Fidelity.

Finally we have concluded the thesis in Chapter 6 by compiling the overall work and their results along with a brief description on the scope for future study.

The appendices to the thesis explain the design and development of two types of microstrip slot antennas for dual band operation, suitably designed for mobile/wireless access standards like GSM 1.8GHz, WLAN 2.4GHz etc.

- **Appendix (A)**: Square patch antenna with triangular slots
- **Appendix (B)**: Circular patch antenna with a sector-slot

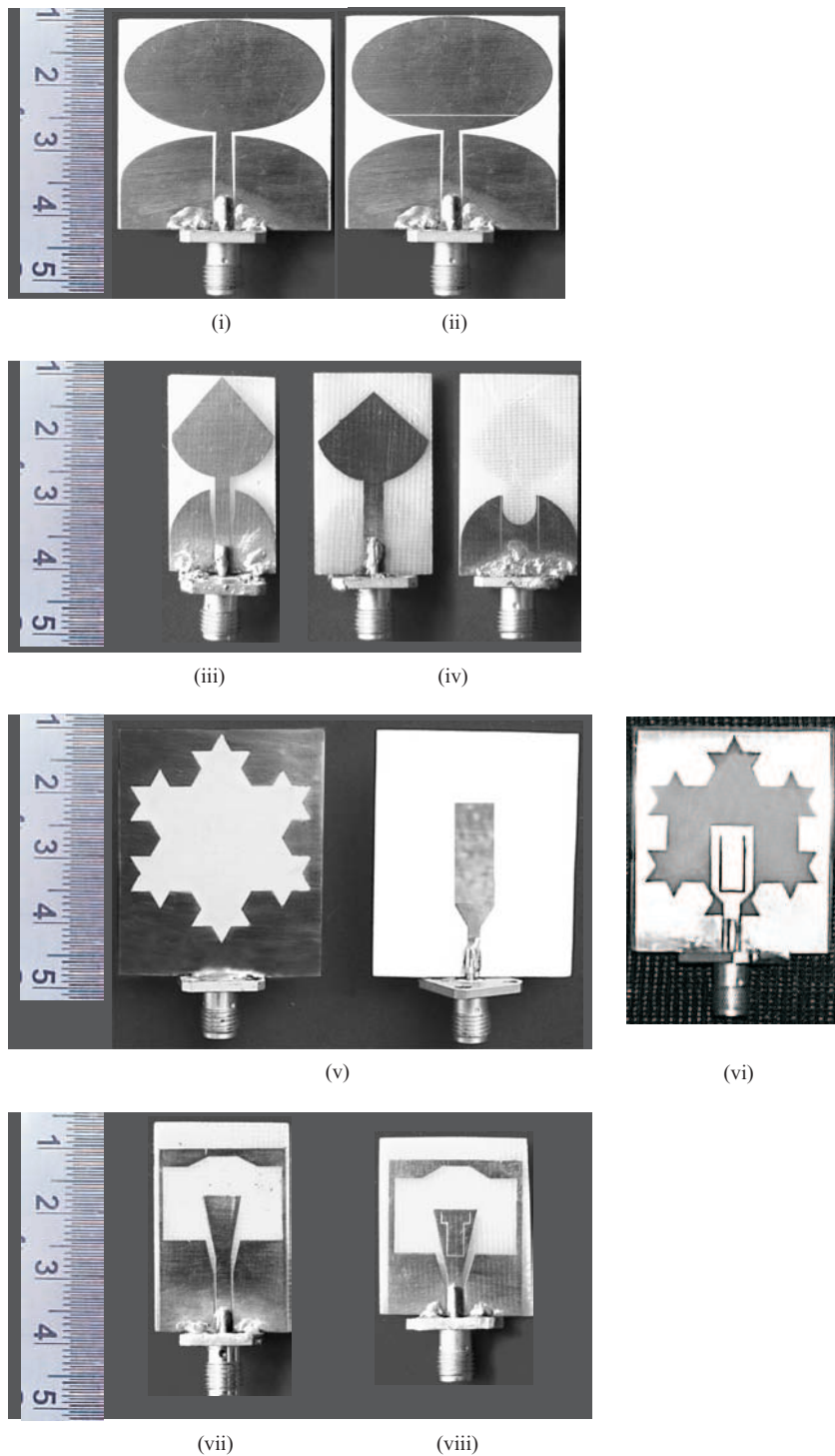


Fig. 1.11: Antenna prototypes (i) elliptical monopole, (ii) band notched elliptical monopole, (iii) inverted cone monopole, (iv) band notched inverted cone monopole, (v) Koch fractal slot, (vi) dual band Koch fractal slot, (vii) wide band slot, (viii) band notched wide band slot antennas

Methodology

Contents

2.1	Simulation and Optimization	32
2.2	The Antenna Transfer Characteristics	33
2.2.1	Choice of Source Pulse	38
2.2.2	Implementation in CST [®]	40
2.3	UWB Antenna Quality Measures	41
2.3.1	Frequency Domain Parameters	42
2.3.2	Time Domain Parameters	42
2.4	Fabrication	43
2.5	Antenna Measurements	44
2.5.1	Frequency Domain Parameters	45
2.5.2	Time Domain Parameters	50
2.6	Pulse Distortion Analysis: Fidelity Factor	52
2.7	Chapter Summary	54

This chapter presents a detailed account of the simulation, fabrication and measurement done for characterizing the antennas discussed in the following chapters. The antenna simulation studies are carried out using CST Microwave Studio[®]. The designs are parametrically analyzed and this, along with radiation pattern and current distribution studies, enables better understanding of their behavior and the formulation of design guidelines. The antennas are fabricated on microwave laminates by photolithography and measure-

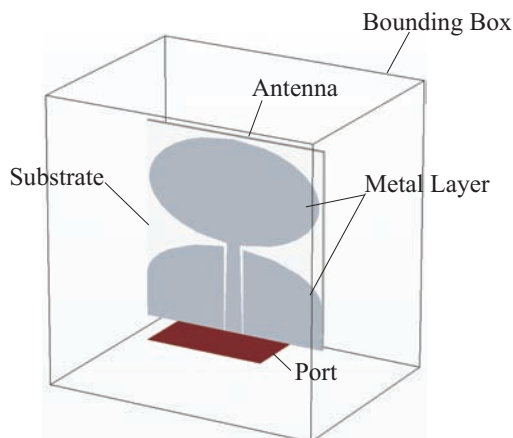


Fig. 2.1: CAD of the antenna in CST Microwave Studio[®]

ments are carried out at our test facility consisting of vector network analyzer and anechoic chamber. A detailed account of the measurement techniques, for frequency and time domain studies, are presented in this chapter.

2.1 Simulation and Optimization

The simulation models of the investigated antennas are developed in CST Microwave Studio[®]. It includes four different solvers and for our investigations, a time-domain solver is exploited. CST[®] is based on the description of electromagnetic problems by differential Maxwell equations that are solved by the finite difference method [CST 2009].

The antenna geometry is modeled in CST[®] by specifying the coordinates for each point of the structure along with appropriate material specifications as shown in Fig.2.1. The metallizations are specified as copper with a thickness of 0.01mm and substrates are assigned from either the in-built material data base or user-defined. The waveguide ports are assigned to excite the antennas. CST[®] gives the user an option to choose from its pre-defined templates like, in this case, the planar antenna template which automatically assigns the mesh type, mesh size etc. or it can as well be user-defined. The boundary conditions are set as open along the three coordinates. The frequency sweep is set over

the desired range of frequencies before the simulations are commenced.

From the simulated results, the antenna parameters like return losses, VSWR and the input impedances are plotted as a function of frequency. The antenna geometry can then be appropriately optimized for the desired impedance response. The radiation patterns, gain, current and field distributions are also determined at the specified frequencies.

2.2 The Antenna Transfer Characteristics

In the present thesis, the antenna is modeled as a Linear Time Invariant (LTI) system characterized by its spatio-temporal transfer function $H(\omega, \theta, \phi)$ [Mohammadian 2003] [Zwierzchowski 2003], whose magnitude and phase would completely define the antenna behavior. The antenna impulse response $h(t, \theta, \phi)$ can be calculated by inverse fourier transformation of its transfer function.

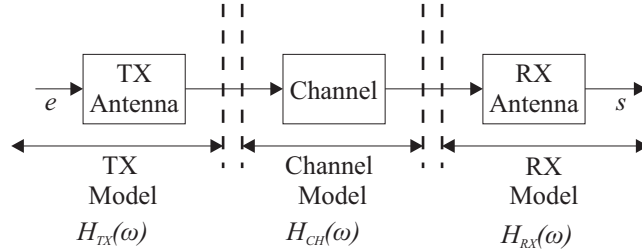


Fig. 2.2: Transmission model

Fig.2.2 presents a system model of a radio link made up of two antennas in free space under the approximation of far-field and line-of-sight propagation [Duroc 2007a]. It consists of three blocks: the TX antenna, the free space channel and the RX antenna. Each block is characterized by a transfer function $H_{TX}(\omega, \theta, \phi)$, $H_{CH}(\omega)$ and $H_{RX}(\omega, \theta, \phi)$, and associated impulse responses $h_{TX}(t, \theta, \phi)$, $h_{CH}(t)$ and $h_{RX}(t, \theta, \phi)$ respectively. The transient transmission is written in the frequency domain and the time domain, as

$$s(\omega) = H(\omega, \theta, \phi)e(\omega) = H_{TX}(\omega, \theta, \phi)H_{CH}(\omega, \theta, \phi)H_{RX}(\omega, \theta, \phi)e(\omega) \quad (2.1)$$

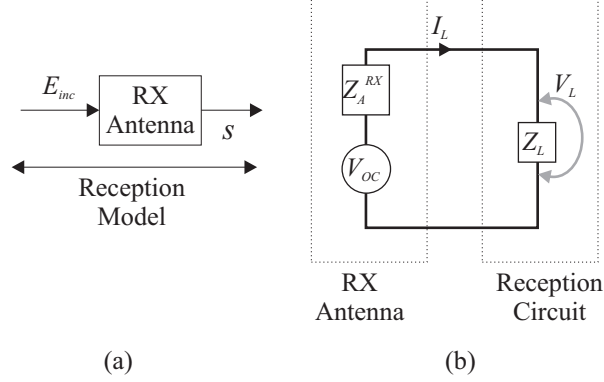


Fig. 2.3: (a) Antenna reception model and (b) its equivalent circuit

$$s(t) = h(t, \theta, \phi) \otimes e(t) = h_{TX}(t, \theta, \phi) \otimes h_{CH}(t, \theta, \phi) \otimes h_{RX}(t, \theta, \phi) \otimes e(t) \quad (2.2)$$

where $H(\omega, \theta, \phi)$ and $h(t, \theta, \phi)$ are the over all system transfer function and impulse response, respectively.

In order to deduce the transfer functions in terms of measurable parameters, the following analysis is carried out. Fig.2.3(a) and (b) represents the reception model for an antenna and its equivalent circuit, respectively. E_{inc} is the incident electric field and s is the output variable (e.g. V_{OC} , V_L or I_L). If $h_{eRX}(\omega, \theta, \phi)$ is defined as the receive (RX) antenna effective length, then the open circuit voltage at the terminals of the antenna with impedance Z_A^{RX} is [Balanis 1997]

$$V_{OC}(\omega) = h_{eRX}(\omega, \theta, \phi) E_{inc}(\omega, \theta, \phi) \quad (2.3)$$

or in terms of the V_L , the voltage across the load impedance Z_L , is

$$V_L(\omega) = \frac{Z_L}{Z_L + Z_A^{RX}} h_{eRX}(\omega, \theta, \phi) E_{inc}(\omega, \theta, \phi) \quad (2.4)$$

In time domain, V_L is

$$V_L(t) = \frac{Z_L}{Z_L + Z_A^{RX}} h_{eRX}(t, \theta, \phi) \otimes E_{inc}(t, \theta, \phi) \quad (2.5)$$

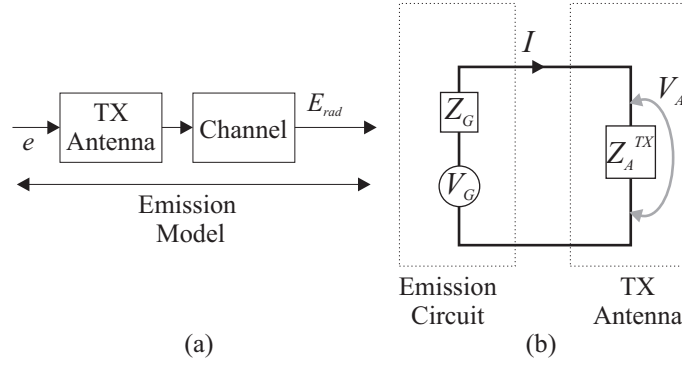


Fig. 2.4: (a) Antenna transmission model and (b) its equivalent circuit

The transmission model for an antenna and its equivalent circuit is shown in Fig.2.4(a) and (b), respectively. $E_{rad}(\omega, \theta, \phi)$ is the radiated electric far field at a space point defined by (θ, ϕ) , polar and azimuth angles, respectively. $e(\omega)$ is the considered input (e.g., voltage, current, or amplitude wave). Using eqn.(1.3) and (1.4) in the frequency domain, $E_{rad}(\omega, \theta, \phi)$ is

$$E_{rad}(\omega, \theta, \phi) = \frac{\eta_0}{4\pi dc} j\omega I(\omega) h_{eTX}(\omega, \theta, \phi) e^{-j\omega \frac{d}{c}} \quad (2.6)$$

where $h_{eTX}(\omega, \theta, \phi)$ is the effective length of the transmit (TX) antenna, $I(\omega)$ is the input current, c is the speed of light, η_0 is the free space intrinsic impedance (120Ω), d is the observation distance from the antenna. In terms of $V_G(\omega)$, the generator voltage at the antenna input, eqn.(2.6) is rewritten as

$$E_{rad}(\omega, \theta, \phi) = \frac{\eta_0}{4\pi dc} j\omega \frac{V_G(\omega)}{Z_G + Z_A^{TX}} h_{eTX}(\omega, \theta, \phi) e^{-j\omega \frac{d}{c}} \quad (2.7)$$

where Z_A^{TX} is the TX antenna input impedance and Z_G is the generator impedance. In time domain,

$$E_{rad}(t, \theta, \phi) = \frac{\eta_0}{4\pi dc} \frac{1}{Z_G + Z_A^{TX}} \frac{dV_G(t)}{dt} \otimes h_{eTX}(t, \theta, \phi) \otimes \delta(t - \frac{d}{c}) \quad (2.8)$$

It is important to emphasize that the transient response of the antenna $h_e(t, \theta, \phi)$ can introduce a spatio-temporal filter characteristic, that may be far apart from an ideal Dirac pulse which would otherwise characterize the

transmitting antenna as a mere differentiator in time.

The model of the transient transmission is then deduced by combining eqn.(2.4) and eqn.(2.7), where $E_{rad}(\omega, \theta, \phi)$ is incident on the antenna in reception. Considering the reflection coefficients (Γ_{TX} and Γ_{RX}) defined at the antenna ports as,

$$\Gamma_{TX}(\omega) = \frac{Z_A - Z_G^*}{Z_A + Z_G^*} \quad (2.9)$$

$$\Gamma_{RX}(\omega) = \frac{Z_A - Z_L^*}{Z_A + Z_L^*} \quad (2.10)$$

the expression for V_L in terms of V_G is

$$V_L(\omega) = \frac{j\omega\eta_0}{4\pi dc} \frac{Z_L(1 - \Gamma_{RX})(1 - \Gamma_{TX})}{4R_LR_G} h_{eRX}(\omega, \theta, \phi) h_{eTX}(\omega, \theta, \phi) V_G(\omega) e^{-j\omega \frac{d}{c}} \quad (2.11)$$

The system transfer function $H(\omega, \theta, \phi)$ is then,

$$H(\omega, \theta, \phi) = \frac{V_L(\omega)}{V_G(\omega)} \quad (2.12)$$

and comparing eqn.(2.11) and (2.12) with eqn.(2.1), we define the expressions for the transfer functions of the transmit and receive antennas, $H_{TX}(\omega, \theta, \phi)$ and $H_{RX}(\omega, \theta, \phi)$, respectively, as

$$H_{TX}(\omega, \theta, \phi) = j \frac{\omega}{c} \sqrt{\frac{\omega}{2\pi c}} \frac{(1 - \Gamma_{TX})}{2} \sqrt{\frac{\eta_0}{R_0}} h_{eTX}(\omega, \theta, \phi) \quad (2.13)$$

$$H_{RX}(\omega, \theta, \phi) = \sqrt{\frac{\omega}{2\pi c}} \frac{(1 - \Gamma_{RX})}{2} \sqrt{\frac{\eta_0}{R_0}} h_{eRX}(\omega, \theta, \phi) \quad (2.14)$$

where the free space channel transfer function $H_{CH}(\omega)$ is given by

$$H_{CH}(\omega) = \frac{\lambda}{4\pi d} e^{-j\omega \frac{d}{c}} = \frac{c}{2d\omega} e^{-j\omega \frac{d}{c}} \quad (2.15)$$

and the Z_G and Z_L are assumed equal to the reference impedance R_0 .

The impulse responses of the antenna in transmission and reception are calculated by taking the inverse fourier transform of eqn.(2.13) and (2.14),

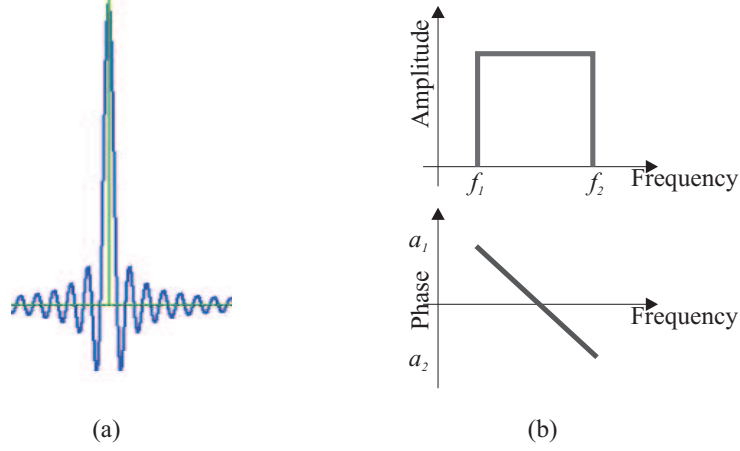


Fig. 2.5: Ideal UWB receiving antenna response (a) impulse response and (b) transfer function

respectively. The dimensional analysis of the eqn.(2.12) to (2.15) indicate that the units of the system transfer function and free space channel transfer function are dimensionless; and that of the TX and RX are $[m^{-1/2}]$ and $[m^{1/2}]$ respectively. The units of the impulse responses are $[m^{-1/2}s^{-1}]$ for TX and $[m^{1/2}s^{-1}]$ for RX antennas.

From eqn.(2.13) and (2.14), the TX and RX transfer functions holds a relation as

$$H_{TX}(\omega, \theta, \phi) = \frac{j\omega}{c} H_{RX}(\omega, \theta, \phi) \quad (2.16)$$

and their impulse responses

$$h_{TX}(t, \theta, \phi) = \frac{1}{c} \frac{dh_{RX}(t, \theta, \phi)}{dt} \quad (2.17)$$

which allows the verification of the Lorentz reciprocity, i.e.

$$h_{TX}(t) \propto \frac{\delta h_{RX}(t)}{\delta t}. \quad (2.18)$$

The consequence is that an ideal antenna (with $h_{RX}(t, \theta, \phi) = \delta(t)$) will radiate an electric field pulse that is proportional to the first-order time derivative of the input voltage pulse. An ideal receiving antenna will have a Dirac-

delta impulse response (independent of arrival angle) as shown in Fig.2.5(a), with the effect that the received voltage pulse will always have the same shape as the incident field pulse on the antenna.

In the frequency domain this will relate to an antenna transfer function with a constant amplitude response and a linear phase response (or constant group delay). In the real world (because of the FCC regulations for UWB communications) the received field pulse will always be band limited, and for practical purposes the required receiving antenna transfer function is one with a constant amplitude response and linear phase response within the 3.1 to 10.6GHz band [Papio-Toda 2007], as shown in Fig.2.5(b).

2.2.1 Choice of Source Pulse

In impulse radio, the signal that represents a symbol consists of serial pulses with a very low duty cycle. The pulse width is very narrow, typically in nanoseconds, and it can be any function which satisfies the spectral mask regulatory requirements. Several non-damped waveforms have been proposed in the literature for UWB systems, such as Gaussian, Rayleigh, Laplacian, cubic and modified Hermitian monocycles.

In all these waveforms, the goal is a nearly flat frequency domain spectrum over the bandwidth of the pulse with no DC component [Ghavami 2004]. In principle, all the impulses with the spectra wider than 500MHz, stipulated by the FCC, can be used as signals. However, the choice of the pulse shape is a key design decision in UWB systems. Given the stringent transmission power limitations, maximizing the received SNR requires efficient utilization of the bandwidth and power allowed by the FCC masks [Chen 2004a].

A Gaussian pulse has been the original proposal for UWB radar and communication systems [Taylor 1995]. However, its PSD has a direct current offset and hence will not radiate effectively. In addition, it does not fit in to the emission mask for any value of the pulse width.

One approach to the design of digital pulse shapers that comply with the

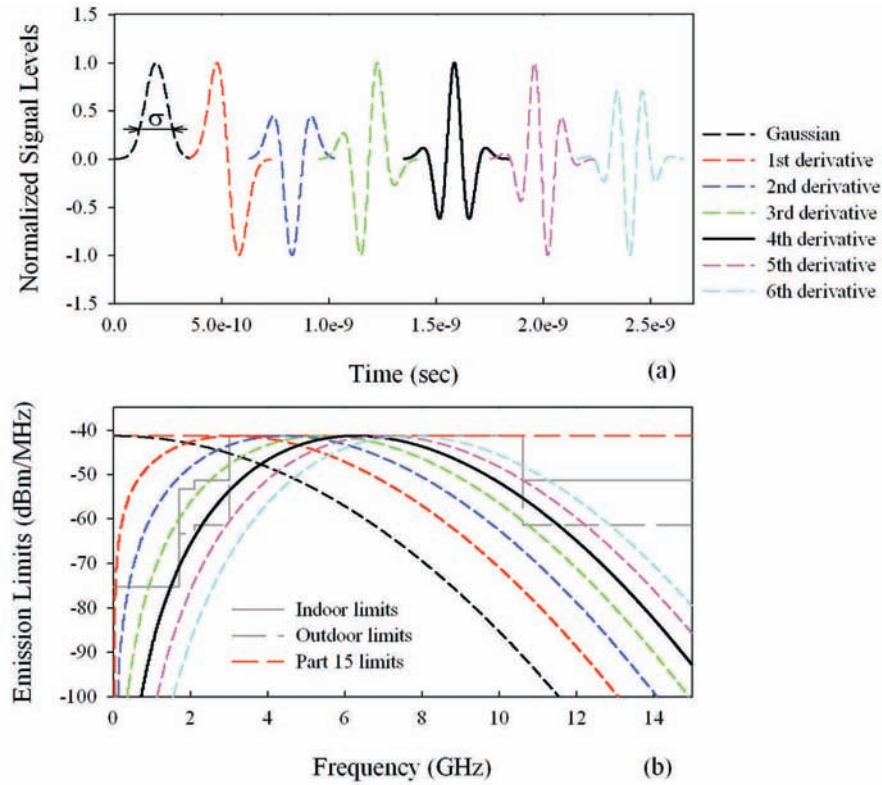


Fig. 2.6: Gaussian pulse and its derivatives (a) waveforms in the time domain and (b) their power spectral densities

FCC spectral masks is to employ prolate spheroidal wave functions to generate pulses from the dominant eigen vectors of a channel matrix that is constructed by sampling the spectral mask [Dilmaghani 2003], [Parr 2003], [Zhang 2004a]. The pulses generated from different eigenvectors are mutually orthogonal, but require a high sampling rate that could lead to implementation difficulties.

Another possible solution for this is to shift the center frequency and adjust the bandwidth so as to satisfy the requirements. This could be done by modulating the monocycle with a sinusoid to shift the center frequency and by varying the pulse width. Impulse radio being a carrier less system, modulation will increase the cost and complexity.

Other pulse shaping methods include exploiting the properties of Hermite orthogonal polynomials [Ghavami 2001], and fine-tuning higher-order derivatives of the Gaussian pulse [Sheng 2003].

Owing to unique temporal and spectral properties, a family of differentiated Gaussian pulses which resemble sinusoids modulated by a Gaussian envelope, $v_n(t)$, is widely used as the source pulses in the UWB systems.

$$v_n(t) = \frac{d^n}{d^n t} [e^{-2\pi(\frac{t}{\sigma})^2}]; \quad (2.19)$$

where the pulse parameter σ stands for the time in radians when $v_0(\sigma)=e^{-1}$, as shown in Fig.2.6(a) and n is the order of differentiation. Some of the higher-order derivative of gaussian pulses can match the UWB band directly, such as the fourth-order Rayleigh pulses as shown in Fig.2.6(b), with the σ chosen such that the pulse spectrum peaks at 5.5GHz. This is the waveform template chosen for pulse distortion analysis in this thesis. Note that the waveforms are shifted in X-axis for clearer distinction in Fig.2.6(a).

2.2.2 Implementation in CST[®]

To study the antenna effects when used in pulsed communications, the input voltage pulse $V_G(t)$ is specified in CST Microwave Studio[®] as

$$V_G(t) = A[3 - 6(\frac{4\pi}{T^2})(t - \tau)^2 + (\frac{4\pi}{T^2})^2(t - \tau)^4]e^{-2\pi(\frac{t-\tau}{T})^2}; \quad (2.20)$$

This pulse is a 4th derivative Gaussian pulse which conforms to the FCC spectral mask when $A=0.333$ and $T=0.175\text{nS}$. The radiated field pulses, $E_{rad}(t, \theta, \phi)$, are calculated on a sphere of radius 1m. The Fourier transforms of these two quantities are then calculated using an FFT.

The radiated electric fields are directly probed by inserting virtual probes over a wide range of angles in the two coordinate planes as shown in Fig.2.7. This simulation set up can be modeled as in Fig.2.4 and the transfer functions can be deduced using eqn.(2.7), (2.13) and (2.16). The impulse responses are deduced by taking the inverse fourier of the transfer functions. The antenna characteristics in the principal radiation planes are visually presented as color scaled plots in time or frequency in 2D for different antenna orientations,

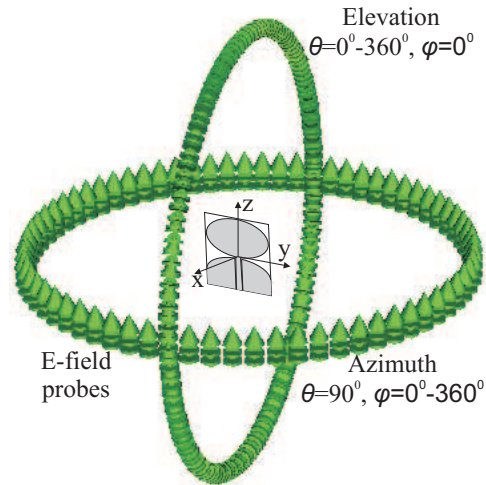


Fig. 2.7: Time domain simulation in CST Microwave Studio[®]

making it easy to comprehend the spatio-temporal behavior of the antennas.

2.3 UWB Antenna Quality Measures

The antenna model in Fig.2.2 covers all dispersive effects that result from a particular antenna structure (e.g. the varying group delay due to nonlinear phase response). The influences of frequency dependent matching and losses are also covered since the feeding network is included in the model. Thus quality measures of a particular UWB antenna, in terms of its ability to transmit and receive power and the distorting influence on the waveform to be transmitted or received, can be derived directly from its transient response [Sorgel 2005]. In this thesis, the antennas are characterized in terms of the receive transfer functions and impulse responses, since antenna transmit characteristics are assumed to be simply their derivatives. For the sake of simplification, the formulations are all given for the co-polarization.

2.3.1 Frequency Domain Parameters

The effective continuous wave gain pattern, $G_{eff}(\Omega)$, can be computed from the transfer function as follows [Duroc 2007b]:

$$G_{eff}(\omega, \theta, \phi) = \frac{2\omega}{c} |H(\omega, \theta, \phi)|^2 \quad (2.21)$$

where $H(\omega, \theta, \phi) = H_{RX}(\omega, \theta, \phi)$. The IEEE standard antenna gain [Balanis 1997], which excludes the losses due to mismatching, is easily calculated from $G_{eff}(\omega)$ by accounting for the antenna's input reflection coefficient $S_{11}(\omega)$:

$$G(\omega, \theta, \phi) = \frac{G_{eff}(\omega, \theta, \phi)}{1 - |S_{11}(\omega)|^2}. \quad (2.22)$$

In order to obtain the measures for distortion in the frequency domain, the group delay, $\tau_g(\omega)$, is defined as

$$\tau_g(\omega) = -\frac{d\phi(\omega)}{d\omega} = -\frac{d\phi(f)}{2\pi df} \quad (2.23)$$

where $H(\omega) = |H(\omega)|e^{j\phi(\omega)}$ with magnitude, $|H(\omega)|$ in $m^{1/2}$ and phase, $\phi(\omega)$ in radians. The group delay is the delay that a portion of the spectral energy at a given angular frequency ω encounters when transmitted through a filter. For minimum distortion, the group delay should be constant within the frequency band of interest, in which case the phase increases linearly with frequency.

2.3.2 Time Domain Parameters

The antenna effects on the signal transmission can be analyzed by considering the envelope of the transient response, which localizes the distribution of energy versus time and is a direct measure for the dispersion of the antenna. The Fourier transform of the transfer function gives a complex response, so a real valued antenna impulse response, $h_r(t, \theta, \phi)$, is used, as in

$$h_r(t, \theta, \phi) = \Re(h_{RX}(t, \theta, \phi)). \quad (2.24)$$

According to eqn.(2.5), the peak output voltage from an incident waveform depends on the peak value $p(\theta, \phi)$ of the antenna's transient response:

$$p(\theta, \phi) = \max|h_r(t, \theta, \phi)|. \quad (2.25)$$

A measure for the linear distortion of the antenna is the envelope width, which is defined as the full width at half maximum (*FWHM*) of the magnitude of the transient responses envelope:

$$FWHM_{0.5}(\theta, \phi) = t_2|_{p/2} - t_1|_{p/2}. \quad (2.26)$$

The duration in ringing is defined as the time until the envelope has fallen from the peak value to below a fraction α of the main peak:

$$Ringing_\alpha = t_2|_{\alpha p} - t_1|_{\alpha p}. \quad (2.27)$$

The lower bound for α is chosen according to the noise floor of the measurement. In order to compare the ringing of antennas with different gains under the constraint of constant noise floor, the fraction α is chosen to be $\alpha = 0.22$ (-13dB).

2.4 Fabrication

The antennas are generally fabricated on commercially available microwave substrates by photolithography. In our work, the antenna prototypes are mostly fabricated on FR4 Glass Epoxy which is a very cost effective alternative. First, the mask is created by printing the negative of the desired geometry on a transparent sheet. The single/double sided copper clad substrate is cleaned with acetone and dried. It is then uniformly coated with a negative photo resist and exposed to UV-radiation for a duration of 2 mins with the mask over it. The exposed photo resist hardens and those in the unexposed areas are washed off using a developer. The undesired metal portions are now

removed using Ferric Chloride (FeCl_3) solution. FeCl_3 dissolves the copper coating on the laminate except which is underneath the hardened photo resist layer. Finally, the laminate is washed in acetone solution to remove the hardened negative photo resist.

2.5 Antenna Measurements

The antennas, in general, are characterized by parameters like input impedance, efficiency, gain, effective area, radiation pattern, and polarization properties [Balanis 1997]. For narrow band applications, these are analyzed at the center frequency of the system. For wider bandwidths, the parameters become strongly dependent on frequency and they themselves are not enough to characterize the transient radiation behavior of the antennas. Their spatial dependent impulse response is required to understand the antenna performance when handling large fractional bandwidth pulses.

The transient response of the antenna can be measured either in the frequency domain followed by the the fourier transform or directly in the time domain. The measurements in time domain, using very short pulses or step functions as driving voltage, can be faster than measurements in the frequency domain. However, frequency domain measurements take advantage of the high dynamic range and the standardized calibration of the vector network analyzer [Sorgel 2005] and can make use of the existing test facility available for narrow band antenna measurements. The measurements in the present thesis are based on this method.

The frequency domain measurements of the antennas are carried out at our antenna measurement facility which includes network analyzers (HP8510C, R&S ZVB20 and Agilent PNA E8362B), spectrum analyzer, automated antenna positioner, broadband double-ridged horn antennas (2 to 20GHz) and anechoic chamber.

2.5.1 Frequency Domain Parameters

The methodology followed to determine the antenna parameters like impedance matching, VSWR, gain, efficiency, and radiation pattern is described here. Before the measurements are carried out, the losses associated with the cables and connectors needs to be nullified for measuring the scattering parameters (S) of the antenna under test (AUT) accurately. This is done by calibrating the network analyzer with known standards of open, short and matched loads for the frequency range of interest.

- **Input reflection coefficient and VSWR:** The reflection coefficient (Γ) at the antenna input is the ratio of the reflected voltage (current) to the incident voltage (current) and is same as the S_{11} when the antenna is connected at the port 1 of the network analyzer. It is a measure of the impedance mismatch between the antenna and the source line. The degree of mismatch is usually described in terms of input VSWR or the return loss. The return loss (RL) is the ratio of the reflected power to the incident power, expressed in dB as

$$RL = -20\log(|\Gamma|) = -20\log(|S_{11}|) = -|S_{11}|_{(dB)} \quad (2.28)$$

The voltage standing wave ratio ($VSWR$) is the ratio of the voltage maximum to minimum of the standing wave existing on the antenna input terminals. A well-matched condition will have return loss of 15dB or more. A VSWR equal to 2 gives a return loss of ≈ 10 dB and it is set as the reasonable limits for a matched antenna [Collin 2001].

The antenna input impedance is a complex quantity with a real and imaginary part, namely the antenna resistance and antenna reactance respectively. It is again a measure of the efficiency with which the antennas act as a transducer between the source and the propagating medium.

The AUT is connected at the calibrated ports of the analyzer and reflection mode is selected from the parameter menu. The input reflection coefficient,

$VSWR$ and input impedance are characterized using a single port calibration. The display is then set to give the $|S_{11}|_{dB}$ or the $-RL$ as a function of frequency. The return loss curve indicates good impedance matching at some frequencies (dips on the return loss curve) and they are regarded as the resonances of the antenna. The bandwidths are measured between the 2:1 $VSWR$ or -10dB $|S_{11}|_{dB}$ points of the plot. Similarly, $VSWR$, antenna impedance can as well be plotted against frequency by changing the output format.

- **Antenna Gain:** Antenna gain is the ratio of the intensity of an antenna's radiation in the direction of strongest to that of a reference antenna when both the antennas are fed by the same input power. If the reference antenna is an isotropic antenna, the gain is often expressed in units of dBi. The gain of the antenna is a passive phenomenon - power is not added by the antenna, but redistributed to provide more radiated power in certain directions than would be transmitted by an isotropic antenna.

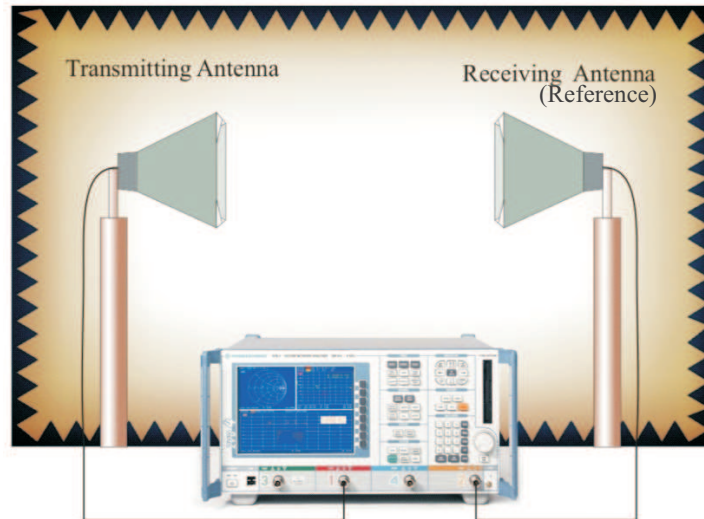
In this thesis, gain transfer method is used to calculate the absolute gain of the AUT [Balanis 1997]. The measurement setup is as shown in Fig.2.8. This method uses two standard wide band ridged horn antennas and the AUT. One of the antennas whose gain chart is available is chosen as the reference antenna ($G_{ref}(dB_i)$).

First, the two-antenna system made of the standard antennas are THRU calibrated for storing the reference gain in the analyzer as in Fig.2.8(a). Next, the reference antenna is replaced by the AUT as in Fig.2.8(b) and the transmission coefficient $|S_{21}|_{AUT(dB)}$, which is the relative gain, is recorded. The absolute gain can then be calculated as

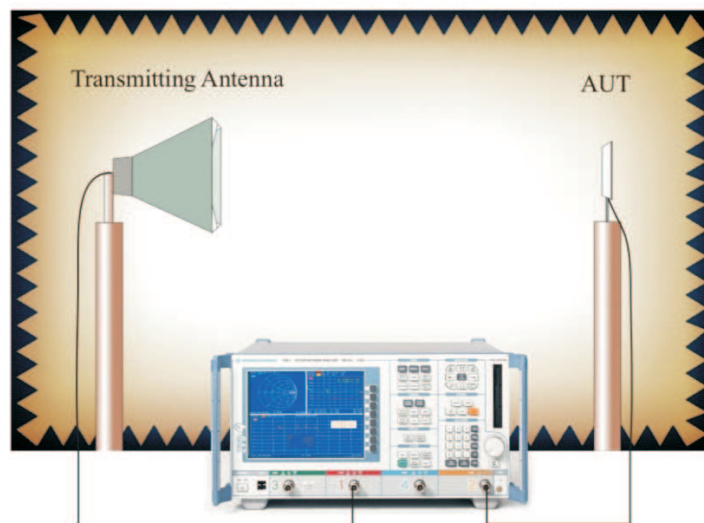
$$G(dB_i) = G_{ref}(dB_i) + |S_{21}|_{AUT(dB)} \quad (2.29)$$

This procedure is repeated for different antenna positions and the peak gain in dB_i is plotted all through the thesis.

- **Radiation Efficiency:** The IEEE definition of the antenna efficiency is



(a)



(b)

Fig. 2.8: Antenna measurement setup

the ratio of total radiated power to the net accepted power by the antenna at its terminals during the radiation process [IEE 1979]. A more reasonable definition would include the reflected power due to mismatch as an explicit loss and radiation efficiency is defined as the ratio of the total power radiated by the antenna to the net power applied at its terminals.

A method for assessing the efficiency over the UWB, that explicitly include mismatch reflected power as a loss term, is presented in [Schantz 2002]. This method is a modification of the Wheeler Cap method conventionally used to measure radiation efficiency of narrow band antennas. Rather than inhibiting radiation efficiency from the antenna to a radiation sphere with radius $r \approx \lambda/2\pi$ as in the narrow band approach, UWB Wheeler Cap method allows the antenna to radiate freely and then receive its own transmitted-reflected signal.

The power budget for a transmit antenna may be expressed in terms of power fractions. A fraction of the incident energy is dissipated in losses ($l \equiv \frac{P_{loss}}{P_{in}}$), a fraction is reflected away due to mismatch ($m \equiv \frac{P_{refl}}{P_{in}}$), and a fraction is radiated ($\eta \equiv \frac{P_{rad}}{P_{in}}$). Averaging over a suitable time interval and applying conservation of energy yields:

$$l + m + \eta = 1 \quad (2.30)$$

The spherical shell surrounding the AUT enforces a near ideal time reversal of the transmitted signal. Thus the antenna receives the reflected signal with negligible structural scattering, and the antenna mode scattering term is simply the mismatch fraction ($m=|S_{11-FS}|^2$). The receive and transmit efficiencies (η) are identical by reciprocity. The scattering coefficient inside the

UWB Wheeler Cap becomes:

$$\begin{aligned}
 |S_{11-WC}|^2 &= m + \eta^2 + \eta^2 m^1 + \eta^2 m^2 + \eta^2 m^3 \dots \\
 &= |S_{11-FS}|^2 + \eta^2 \sum_{n=0}^{\infty} |S_{11-FS}|^{2n} \\
 &= |S_{11-FS}|^2 + \eta^2 \frac{1}{1 - |S_{11-FS}|^2}
 \end{aligned} \tag{2.31}$$

which solves to yield the following result for radiation efficiency:

$$\eta = \sqrt{(1 - |S_{11-FS}|^2)(|S_{11-WC}|^2 - |S_{11-FS}|^2)} \tag{2.32}$$

For measurements, an oblate metallic chamber with diameter 70cm is used. First, the AUT is placed in free space and the return loss S_{11-FS} is measured. It is then placed at the center of the closed metallic chamber and the S_{11-WC} is measured. Finally, eqn.(2.32) is employed to calculate the radiation efficiency. The measurement is repeated several times and the average value at discrete frequency intervals is computed.

- **Radiation pattern:** The radiation pattern of an antenna is graphical representation of its radiation properties as a function of the space coordinates. This assumes a three dimensional (3-D) pattern. Because of the limits set by the practical measurement setup for measuring the 3-D pattern, usually patterns are measured in the three principal coordinate planes(XY, YZ, XZ) for antennas with omni-directional patterns. The far field patterns are measured at a distance $d > 2D^2/\lambda$, where D is the largest dimension of the antenna and λ is the smallest operating wavelength.

As shown in Fig.2.8(b), the AUT is connected to Port 1 and the standard ridged horn is connected to Port 2. The height and polarization of both antennas are aligned for maximum transmission ($|S_{21}|$) between them. The desired frequency points are selected for measurements. A THRU calibration is performed in this position which calibrates the S_{21} data to 0dB for every

frequency point selected.

In order to avoid any spurious reflections from the nearby objects, the time domain gating facility of the analyzer is implemented. The gate span is selected according to the largest dimension of the radiator. The antenna positioner is now set to home which sets the current position as 0^0 . The radiation pattern measurement software, ‘*Cremasoft*’ developed inhouse, controls the automated radiation pattern measurement process. The software is next evoked and the normalized S_{21} is measured. The number of frequency points are set according to convenience. The start angle, stop angle and step angle of the motor is also configured in ‘*Cremasoft*’ which then stores the measurements as a text file.

2.5.2 Time Domain Parameters

It is very important to assess the performance of the UWB antenna prototypes in the time domain apart from its conventional measurements in the frequency domain. The antennas intended for UWB systems need to possess superior pulse handling capabilities. This can be assessed directly in time domain as in [Shlivinski 1997], [Jongh 1997]. In this thesis, the measurements are carried out in the frequency domain and the time domain parameters are deduced by taking fourier transform and this is equally accurate as the direct time domain measurements [Sorgel 2005] [Yiqiong 2005].

2.5.2.1 Transfer Function Determination

The transfer function of the TX and RX antennas are determined from the measured values of S_{21} in the frequency domain. Using two identical standard wide band horn antennas oriented for bore-sight transmission, the following relations are derived from eqn.(2.1) and (2.16).

$$H_{TX}(\omega, \theta, \phi) = \sqrt{\frac{j\omega S_{21}(\omega, \theta, \phi)}{c} \frac{1}{H_{CH}(\omega)}} \quad (2.33)$$

$$H_{RX}(\omega, \theta, \phi) = \sqrt{\frac{cS_{21}(\omega, \theta, \phi)}{j\omega} \frac{1}{H_{CH}(\omega)}} \quad (2.34)$$

where the H_{CH} is as given in eqn.(2.15). This enables the characterization of the reference antenna.

With the reference antenna as the TX antenna and the AUT as the receive antenna, the receive transfer function of the AUT is deduced for multiple orientations by

$$H_{RXAUT}(\omega, \theta, \phi) = \frac{S_{21}(\omega, \theta, \phi)}{H_{CH}(\omega)H_{TX}(\omega, \theta, \phi)}. \quad (2.35)$$

Eqn.(2.16) allows the determination of the corresponding TX transfer function. In order to obtain physical results, the phase of the transmission coefficient S_{21} should be unwrapped correctly.

2.5.2.2 Implementation in MATLAB[®]

The impulse responses are deduced from the measured transfer functions by taking their inverse fast fourier transforms (IFFT) but with certain precautions. The measured data used in this thesis is over a frequency range 2 to 12GHz. The data is complemented by zero padding for 0 to 2GHz and 12GHz to f_{max} where $f_{max}=64$ GHz. It is assumed that the antenna's response is so poor out of band that the data obtained is clearly dominated by noise and it might be advantageous to blank or zero data in those frequency ranges [McLean 2008]. To correspond to the spectrum of a real signal, the conjugate of the zero-padded data is taken and reflected to the negative frequencies resulting in a spectrum which is symmetric around DC. The IFFT of the resulting measured data in frequency domain gives a real impulse waveform.

Fig.2.9 plots the measured transfer function amplitudes and impulse responses of the standard wide band horn antenna characterized as explained above. The response is near-ideal with relatively constant amplitude of the transfer functions and a receive impulse response which is similar to a Dirac-

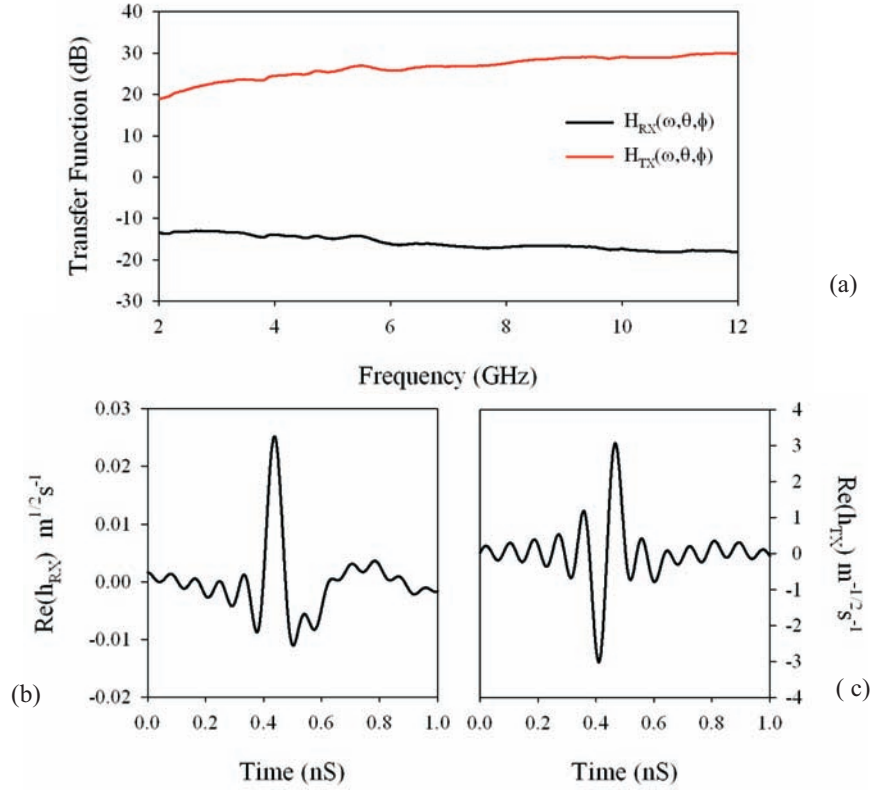


Fig. 2.9: Measured characteristics of the standard wide band horn antenna (a) transfer function amplitudes, (b) receive impulse response and (c) transmit impulse response

delta function.

2.6 Pulse Distortion Analysis: Fidelity Factor

Ideally, an impulse antenna should faithfully replicate the transmitted pulse on reception. But the changes in the phase center position and radiation characteristics alter the integrity of the transmitted pulses. The non-linearity in the antenna phase response leads to pulse dispersion. In addition, its radiation characteristics also have a significant impact on its performance. Any distortion of the signal in the frequency domain causes distortion of the transmitted pulse shape, therefore increases the complexity of the detection mechanism at the receiver.

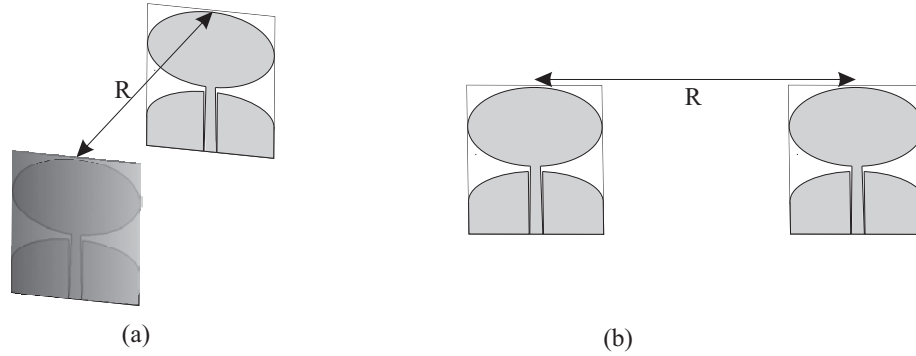


Fig. 2.10: Transmit-receive antenna orientations (a) face to face and (b) side by side

The antenna gain should be smooth across the frequency band in order to avoid frequency selective distortion of the transmitted pulse. Since the antenna gain typically appears different from different angles, the shape of received pulse show spatial dependence [Fortino 2008].

From the spatio-temporal antenna impulse responses, we are able to calculate the pulse distortions introduced by the antenna along different orientations. These distortions are often quantized as the fidelity factor which is a measure of the faithfulness with which a device reproduces the time shape of the input signal. For UWB systems, the commonly used receivers are based on the pulse energy detection or correlation with the template waveform. Therefore we need to examine the pulse distortions by calculating the fidelity factor [Lamensdorf 1994].

The fidelity between waveforms $x(t)$ and $y(t)$ is generally defined as

$$F = \max \frac{\int x(t) \cdot \int y(t - \tau) dt}{\sqrt{\int |x(t)|^2 \cdot dt \int |y(t)|^2 \cdot dt}} \quad (2.36)$$

where τ is the delay which is varied to maximize the numerator. The fidelity parameter F , is the maximum of the cross-correlation function and compares only shape of the waveforms not the amplitudes. It is deduced from the measured and simulated data for different RX antenna orientations, with $y(t)$ as the incident and $x(t)$ as the received waveform [Klemm 2005].

To assess antenna performance as a system, we have considered a pair of the designed planar antennas. One antenna is assumed to be transmitting and the other receiving. The distance between the transmitting and the receiving antennas is 120cms of free space, which is more than 12 wavelengths at the lowest frequency of the considered band of operation i.e. the antennas are in the far field of each other. The antennas are oriented in two extreme cases: face to face and side by side as in Fig.2.10 and their corresponding fidelity factors are determined with respect to the input pulse waveform [Telzhensky 2006].

2.7 Chapter Summary

This chapter has discussed the methodology to simulate, optimize and fabricate the various planar antennas mentioned in the following chapters of the thesis. It has deduced the complete theory behind the transfer function characterization and the transient analysis of the antennas, along with their simulation and measurement techniques. The performance of the UWB antennas are assessed not only in terms of the conventional antenna parameters like $VSWR$, return loss, gain and radiation pattern but also in terms of the UWB quality measures derived from its transient analysis like the peak, $FWHM$, ringing and group delay. The antenna's ability to effectively transmit-receive a UWB pulse waveform are also discussed and estimated in terms of the Fidelity factor.

Planar Broadband Monopole Antennas

Contents

3.1	Planar Monopole Antennas: Review	57
3.2	Elliptical Monopole Antenna	61
3.2.1	Geometry	62
3.2.2	Simulations	62
3.2.3	Design	70
3.2.4	Measurements	71
3.3	Printed Inverted Cone Monopole Antenna	72
3.3.1	Geometry	75
3.3.2	Design and Simulations	75
3.3.3	Measurements	78
3.4	Band-notched Antennas	80
3.4.1	Band-notched Elliptical Monopole Antenna	82
3.4.2	Band-notched Printed Inverted Cone Antenna	86
3.4.3	Dual Band-notched Elliptical Monopole Antenna	90
3.5	Chapter Summary	94

In this chapter we have concentrated on the development of broadband monopole antennas. We begin with a detailed literature review of the available designs belonging to this broad category, followed by a description on the evolution of the antenna designs presented. The designs are then simulated and their resonant modes are identified. The antennas are mostly CPW-fed for easy fabrication and better integration. The surface current & field distributions on the antenna and their radiation patterns at the resonant modes are analyzed in detail.

The results of the analysis along with the parametric studies have enabled us to deduce their design equations and design methodologies on any substrate for the desired operating frequencies. The performance of the fabricated antennas are then experimentally verified and are found to conform reasonably well with the simulated responses in all cases. Further, to notch out select narrow band frequencies in the wide operating band, thin resonator slots are embedded in the antenna. Such adaptations are incorporated, optimized and experimentally verified for all the proposed designs.

There are two novel designs of compact planar monopole antennas presented in this chapter: an elliptical monopole and an inverted cone antenna. These antennas perform well in terms of its impedance match and gain, over a wide band and easily comply with the FCC approved UWB frequencies of 3.1 to 10.6GHz. The radiation patterns which are desired to be omni-directional however are distorted at the higher end of the spectrum in the case of the elliptical antenna. This is overcome by the inverted cone monopole antenna design which has the advantage of a compact design as well. The slot resonators are engraved on either/both the radiator and ground plane to disable the antenna from functioning at the select narrow band frequencies.

The antennas prove to be suitable for broadband mobile applications in terms of their physical requirements and wide band characteristics. Their suitability for pulsed UWB applications are confirmed by investigating their effects on large fractional bandwidth pulses and this is carried out in Chapter 5.

3.1 Planar Monopole Antennas: Review

One of the most popular antennas employed in mobile and wireless communications systems are the monopole antennas. These antennas are generally convenient to match to 50Ω and are unbalanced, thus eliminating the need for a balun, which may have a limited bandwidth. The simplest member of the family is the quarter-wave monopole above a perfect ground plane.

The impedance bandwidth achievable for the quarter-wave monopole antenna is dependent on the radius of the cylindrical stub and increases with radius. This is true up to a point where the stepped radius from the feed probe to the cylindrical element becomes abrupt. Tapering this transition is often employed in wide band elements, such as bi-conical dipoles and conical monopoles [Amman 2003b].

A simpler and cost effective technique is to replace the cylindrical stub of a conventional monopole with a planar element, yielding a planar monopole. The different polygonal monopole shapes have already been mentioned in Section 1.2 of Chapter 1. There are different techniques employed to improve the impedance band. They include the use of shorting pins [Lee 1999] [Amman 2003a], beveling techniques [Amman 2001], offset feed [Amman 2004], double feed [Antonino-Daviu 2003], trident feed [Wong 2005b], etc. The monopoles have been further modified by arranging trapezoidal monopoles orthogonally with a circular patch shorted to the ground placed on top [Lau 2005], square monopoles orthogonally [Anob 2001] etc. But such ultra wide band metal-plate monopole antennas always need a perpendicular metal ground plane.

In comparison, the printed monopole antennas are of a smaller volume and are suitable for integrating with MMICs. It consists of a monopole patch and a ground plane, both printed on the same or opposite sides of a substrate, while a microstrip line or CPW is located in the middle of the ground plane to feed the monopole patch. One of its earliest type is a Tab monopole [Johnson 1997]. Many regular geometrical shapes have been em-

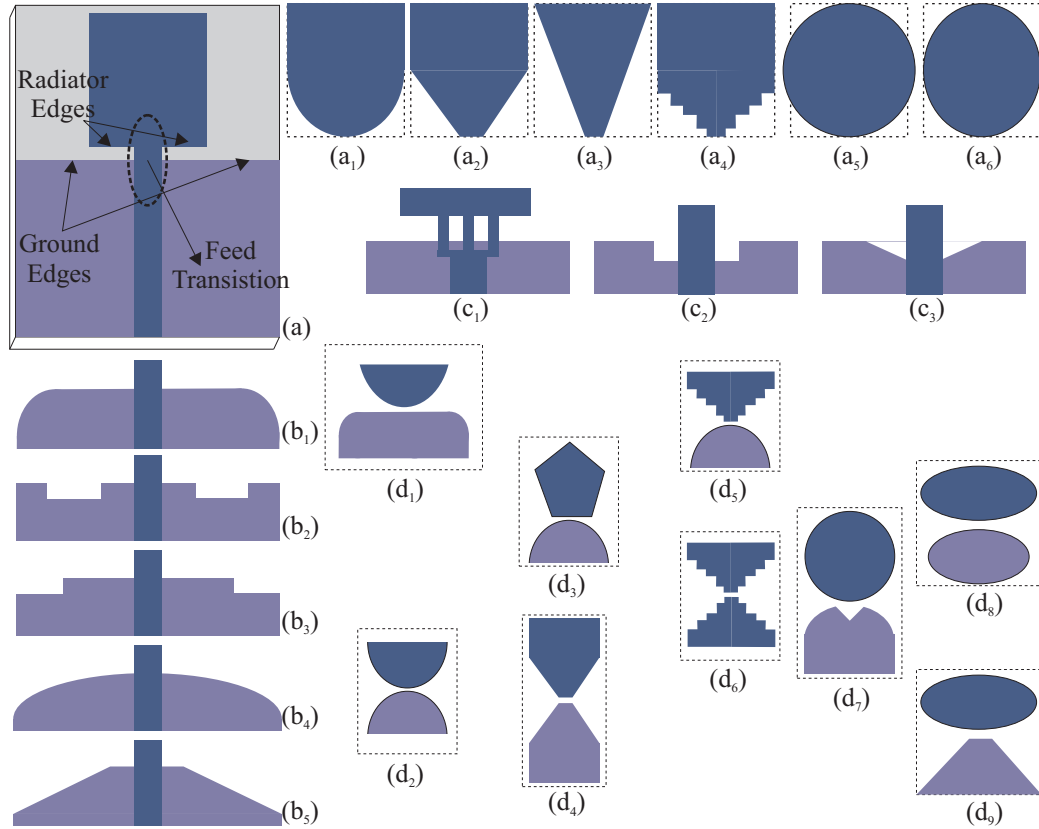


Fig. 3.1: Different modifications on planar monopole antenna for wide band characteristics

ployed as the monopole radiators with or without ground plane modifications for the desired effects [Chen 2007b].

The simplest of all would be a square or rectangular monopole antenna [John 2005] but their wide band impedance matching is limited unless modifications are made on the patch/feed geometry. On examining the reported antenna geometries on planar wide band monopoles, we can categorize the modifications made on the basic geometry, shown in Fig.3.1, in to three: radiator edges, ground edges and feed transition modifications.

The different radiator types that have been reported are square monopole with semi-circular base [Ray 2007], trapezoidal [Peyrot-Solis 2007], triangular [Ray 2006] [Lin 2005], stepped rectangular patch [Choi 2004], circular [Liang 2005b], elliptical [Thomas 2007] and they are shown in Fig.3.1(a1-

a₆). The radiator edge near the ground is an important parameter which affects the antenna performances and they have even been characterized by binomial functions for ultra wide band performance [Ling 2007].

Even though such curved radiators along with straight ground edge gives wide band performance, the antenna size can be reduced by making ground plane and feed modifications. The ground edges have been slotted [Gopikrishna 2007], rounded [Dong 2009], notched [Wu 2007b], curved and hexagonal [Wu 2007a], as shown in Fig.3.1(b₁-b₅). The feed transitions have been trident shaped [Wu 2008] or with slits on the ground plane for improved bandwidth performance [Bao 2007] [Peyrot-Solis 2007] as in Fig.3.1(c₁-c₃).

In this context, the use of the terms of planar monopoles requires an extra explanation. The initial structure of planar monopole formed by a square patch vertically positioned above a horizontal ground plane and fed from a coaxial line was introduced in [Amman 1999]. The extension of this concept was made in [Liang 2005b], where the patch and the finite size ground were proposed to be formed on one plane. The justification for the use of the name “planar monopole” in [Amman 1999] stemmed from the fact that a coaxially fed wire monopole was stretched and became planar.

However, the structure introduced in [Liang 2005b] and the ones that followed includes a finite ground plane. In cases where the antenna size is made compact by patch and ground modifications, both “planar monopole” and “finite ground” can be considered as radiating elements and the entire structure resembles a planar dipole antenna.

Several of the compact planar monopoles reported, falls in this category and some are shown in Fig.3.1(d₁-d₉). Typical examples with their sizes are the semi-elliptical dipole antennas (33x31mm²) [Zhang 2008], semi-circular patches as radiator and ground (25x25mm²) [Su 2006], pentagonal radiator with curved ground (50x58mm²) [Shrivastava 2007], hexagonal radiating elements (22x31.3²) [Kwon 2004], stepped radiator elements (19x21mm²) [Vasylychenko 2008], stepped radiator with curved ground (25x26mm²) [Cho 2006], circular patch with curved ground and a V-shaped slot on the ground at

the feed transitions (38x28mm²) [Yoon 2004], elliptical radiating elements (20x23mm²) [Xia 2008] and elliptical radiator and a trapezoidal ground plane for very wide band operations (140x108mm²) [Zhong 2007].

This gives us an additional view on the operation of the planar monopoles. These antenna elements feature a slot between the “monopole” and “ground”, which as our studies reveal, plays an important role in obtaining wide band behavior. This is because it forms a traveling wave type antenna.

This can be confirmed when we look at the fact that several such antennas have been reported where the planar monopoles exhibit a wide band behavior even when they have large slots inscribed in the radiator patch. For example, elliptical monopole with a circular slot inscribed [Yan 2008], crescent shaped monopole [Azenui 2007], annular ring shaped radiator [Liang 2005a], half annular ring monopole [Kan 2007]. [Fortino 2008] reports compact UWB planar monopole antenna which has large slots inscribed in both the radiator and ground.

The review of the planar monopole antennas confirms the requirement for a tapered transformation from the feed to the antenna edges so as to have a gradual impedance variation among the different resonant modes excited. The ground and radiator edges basically operates as a pair of opposing tapered slot lines which makes them inherently wide band. However, their radiation patterns may deviate from the desired omnidirectional behavior as the tapered slot line antennas are relatively directional.

Another implication of the tapered slot approximation is that it tends to have the position of its phase center, the region of maximum radiation, varying while operating over a large band frequencies. This would have an impact on its time domain response as discussed in Section 1.2.1.1 of Chapter 1.

In this chapter, we begin by investigating an elliptical monopole antenna to study the impact of antenna geometry on its wide band matching and radiation patterns. Further, we modify the antenna design to optimize their performance for portable UWB applications.

The elliptical monopole antenna has an ellipse as the radiator and another

ellipse with a rectangular base as the ground. Based on the literatures reviewed, the elliptical geometry appears to be an ideal choice. The novelty of the antenna designed lies in its simplicity. It is based on a Euclidean geometry and would make its design equations simpler. Its inherently tapered radiator-ground interface, makes them impedance matched over a wide band.

The antenna is CPW-fed with compact dimensions of 31x32mm². A detailed parametric analysis is carried out to throw light on its operation. A much compact printed inverted cone monopole antenna design with dimensions 14x30mm² is presented in the following section which better suits the new-generation portable UWB applications.

3.2 Elliptical Monopole Antenna

The planar elliptical antenna is fundamentally derived from a volcano smoke antenna [Kraus 2005]. It is one of the earliest wide band antenna designs with a “fat” monopole and gradual tapering of the inner and outer conductors of a coaxial transmission line; an appearance reminiscent of a volcanic crater and a puff of smoke.

Theoretically, the radiators of the planar monopole antennas can be of any shape for broad operating bandwidth. Small and gradual discontinuities are desired for a reflection less transducer action over wide frequencies. The planar monopole antennas with ellipse-shaped radiating elements are known to operate effectively over a wide frequency band, making them natural candidates for broadband applications [Agrawal 1998].

One may think that since the transformation is performed by just lower portion of the ellipse it is possible to use a half ellipse. However, simulations show that the diffraction caused by the sharp edge of the half ellipse degrades the performance. Hence, the upper part of the element was also rounded into an ellipse.

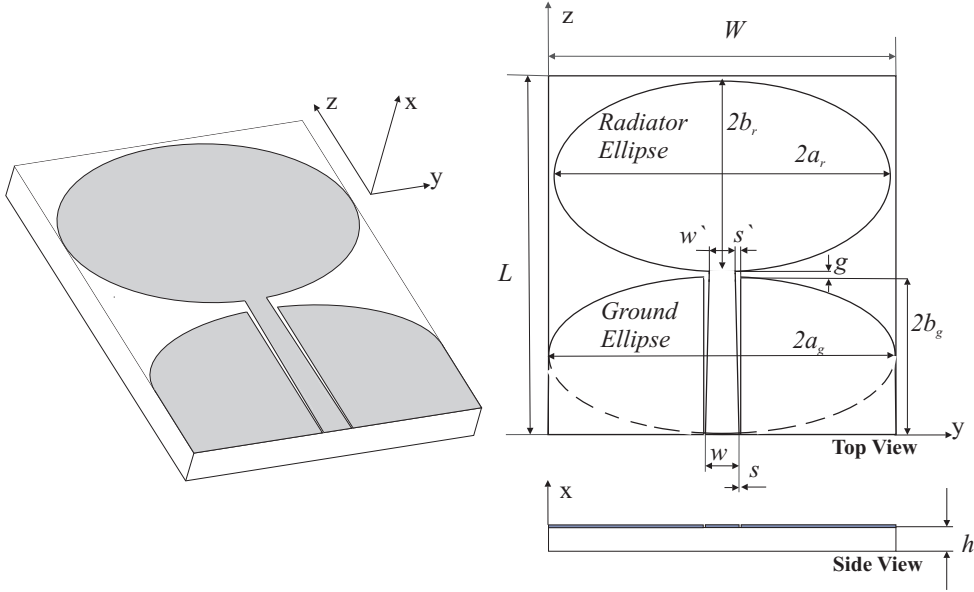


Fig. 3.2: Geometry of the elliptical monopole antenna

3.2.1 Geometry

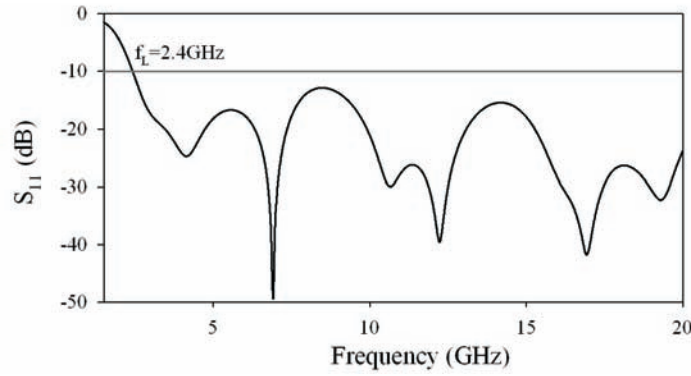
The geometry of the elliptical monopole is shown in Fig.3.2. It consists of elliptical radiator patch and an elliptical ground plane with a rectangular base. The radiator and ground ellipse dimensions are chosen as $(a_r \text{ \& } b_r)$ and $(a_g \text{ \& } b_g)$ as the semi-major and minor axes, respectively. The radiator is fed by a CPW line, with its center strip tapered from a 50Ω feed impedance at the connector end to the impedance at the edge of the radiator ellipse. The center strip width and the gap at the feed end is (s, w) and at the radiator edge (s', w') , respectively. The antenna is printed on one side of a substrate with height h and permittivity ϵ_r . The overall dimensions of the antenna is denoted by width W and length L .

3.2.2 Simulations

In this section, the performance of the antenna is investigated through simulations. Fig.3.3 illustrates the simulated return loss ($S_{11(dB)} = -RL_{dB}$) of an optimal design of the antenna with parameters as in Table 3.1, where all the

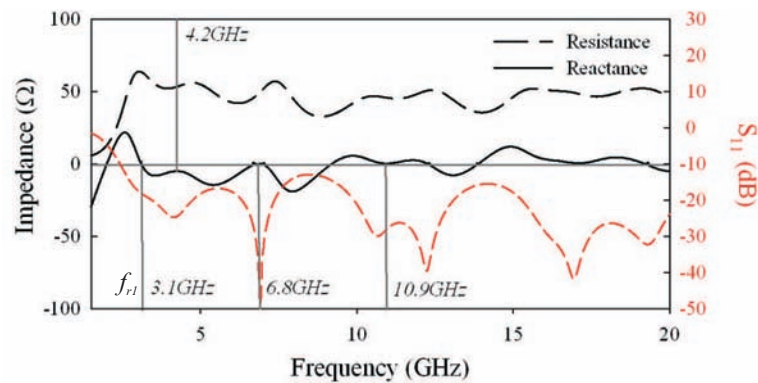
Table 3.1: Dimensions of the elliptical monopole antenna

ϵ_r	h	w	s	a_r	b_r	a_g	b_g	g	s'	w'	L	W
3.3	0.8	3	0.2	15	8.5	15.5	7	0.55	0.55	2.3	32	31

**Fig. 3.3:** Simulated return loss curve of an elliptical monopole antenna

antenna dimensions are in mms. The simulated -10dB bandwidth appears to span an extremely wide frequency range from 2.4GHz to more than 20GHz.

In order to identify the resonance modes of the antenna, its input impedance is plotted against frequency in Fig.3.4. Traditionally, the zero crossings on the reactance curve are identified as resonances which in this case compares well with the dips in the return loss curve. Four resonances are identified from the plots, the first (f_{r1}) at 3.1GHz, then 4.2GHz, 6.8GHz, and 10.9GHz. From an impedance point of view, the antenna designed appears as an ideal candidate

**Fig. 3.4:** Simulated input impedance curve of an elliptical monopole antenna

for UWB communications in the 3.1 to 10.6GHz.

3.2.2.1 Surface Current & Field Distributions and 3D Radiation Patterns

The return loss or the input impedance can only describe the behavior of an antenna as a lumped load at the end of a feeding line. The detailed EM behavior of the antenna is revealed by examining the surface current distributions and the radiation patterns.

The surface current distribution of the antenna and E-field distribution on the substrate close to the resonance frequencies and their corresponding simulated 3D radiation patterns are plotted in Fig. 3.5. The current is mainly distributed on the conductor edges of the radiator and ground ellipses, which gives an indication about the dependence of antenna geometry on the resonant frequencies.

At the first (3.1GHz) and second (4.2GHz) resonance frequencies, the distributions are similar and the antenna has a dipole like behavior where the current is oscillating and has a pure standing wave pattern along most part of the ellipse edge. This is ascertained by their doughnut shaped radiation pattern. However, the distribution is more confined in the gap between radiator and ground edges near the feed at the second resonance. The parametric analysis discussed in the following section would confirm this dependence of the second resonance on the gap g .

The distribution at 6.2GHz and 10.2GHz indicates that they are the second and third harmonics of the fundamental resonance modes. Animations of the same indicates that the current is traveling along the lower edge, but oscillating at the top edge. Consequently the antenna phase center position no longer remain constant. The radiation patterns also appears to loose its omnidirectionality in the XY plane. At the second harmonic frequency (6.2GHz), the gain increases along $\theta=30^\circ$ in the YZ plane. At the third (10.2GHz), it is more directional towards the sides ($\pm Y$ axis). It can be concluded from these

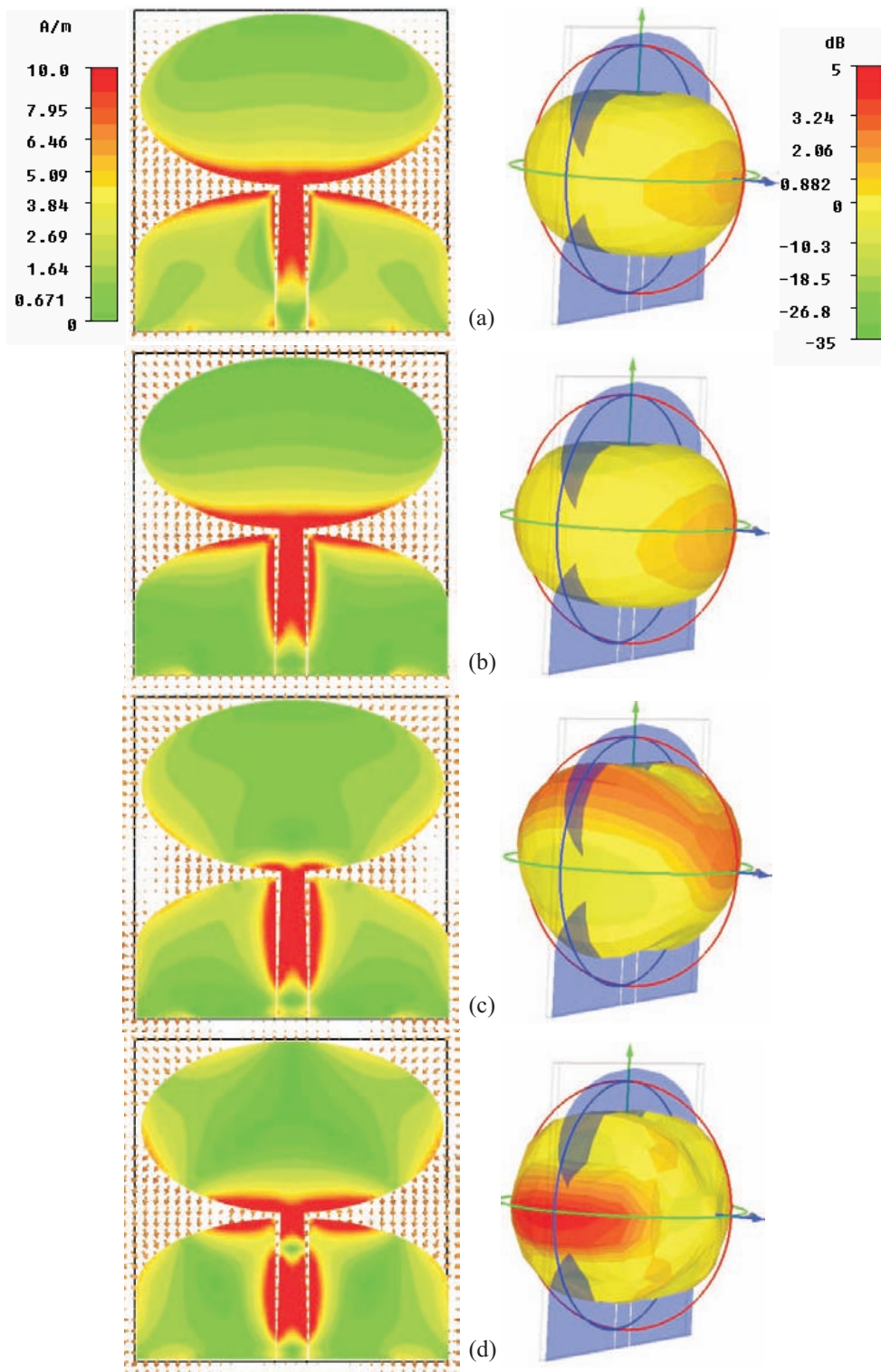


Fig. 3.5: Simulated surface currents and E-field distribution on an elliptical monopole antenna along with its simulated radiation patterns at (a) 3.1GHz, (b) 4.2GHz, (c) 6.2GHz, and (d) 10.2GHz.

observations that the radiation pattern is omnidirectional at the lower side of the operating band but deteriorates at higher frequencies.

3.2.2.2 Parametric Analysis

Further insight on the antenna performance is obtained by carrying out a detailed parametric analysis. Fig.3.6 shows the simulated return loss curves for different antenna dimensions. A significant observation from the plots is that a wide band impedance matching ($S_{11} < -10\text{dB}$) is inherently achieved for the elliptical monopole antenna considered, in spite of variations in its parameters. However, it shows a shift in the lowest resonance frequency f_{r1} , with the radiator height (b_r), ground height (b_g) and their gap (g).

Fig.3.6(a) plots the antenna return losses as b_r is varied from 8.5mm to 4.5mm. A shift in the antenna frequencies towards a higher range can be noted with a distinct increase in f_L from 2.4GHz to 3.4GHz. This confirms the monopole type operation of the antenna, where decrease in the radiator length increases the resonant frequency.

But the second resonant frequency is observed to slightly reduce as b_r is decreased. This is due to the fact that the tapered gap between the radiator and ground patch is decreased as b_r is reduced while keeping a_r same. This corresponds well with the observations from the surface current/field distributions at the second resonance.

Fig.3.6(b) notes little change in f_{r1} with variations in a_r as the radiator length b_r is unchanged here. However, as a_r reduces from 17mm to 9mm, the second resonance increases from 4.2GHz to 4.7GHz, again confirming its dependence on the radiator ground tapered gap. Similar observations can be obtained in Fig.3.6(d) with variations in the ground width a_g with an exception at the first harmonic frequency which is lowered as a_g is increased.

As the ground height b_g decreases from 11mm to 5mm, Fig.3.6(c) shows that the antenna resonances are disturbed and show an increase with a distinct shift in f_L from 2.1GHz to 2.6GHz. This would mean that the ground plane

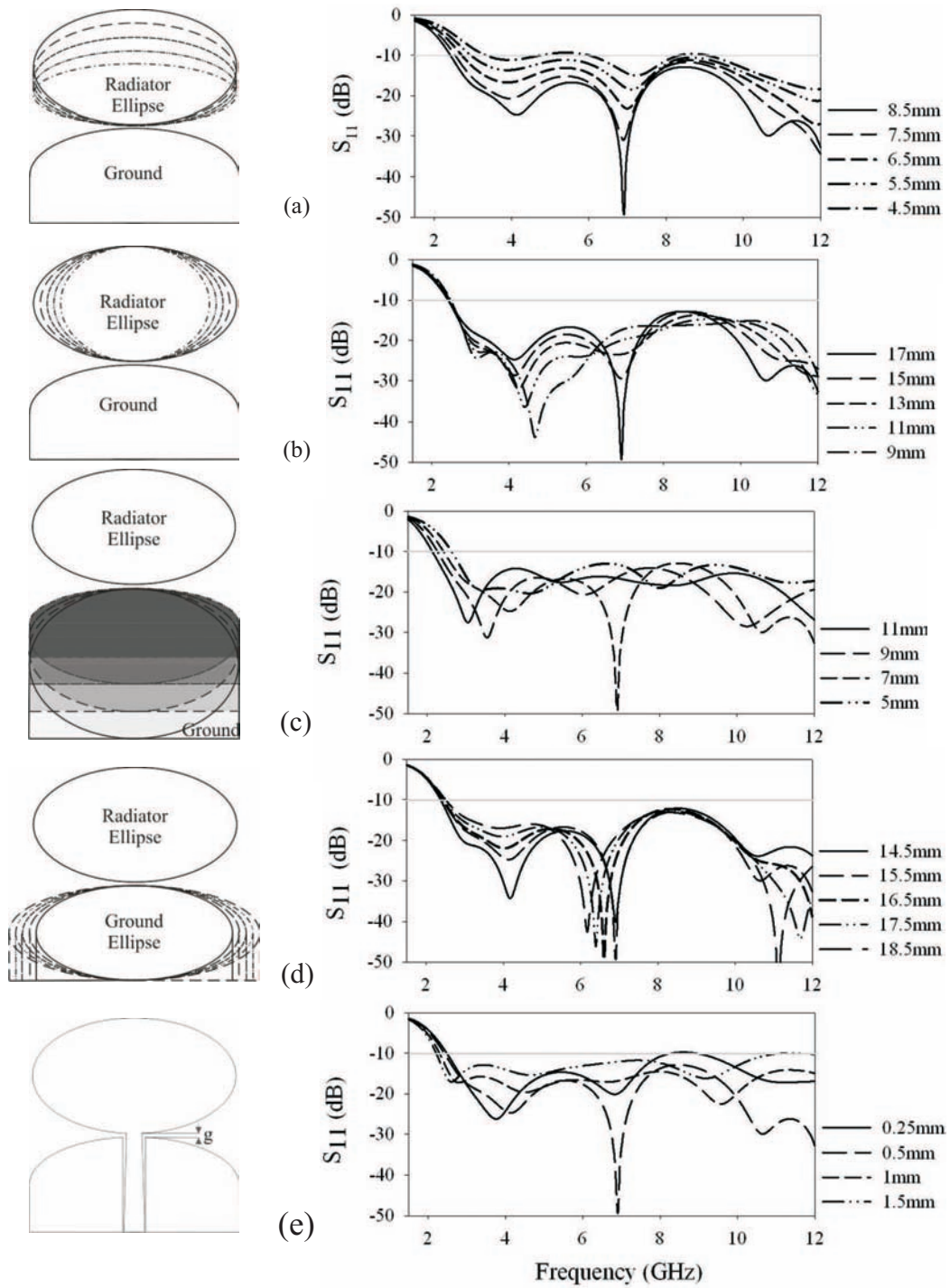


Fig. 3.6: Simulated return loss curves for different values of (a) b_r , (b) a_r , (c) b_g , (d) a_g , and (e) g with the rest of the parameters as in Table 3.1

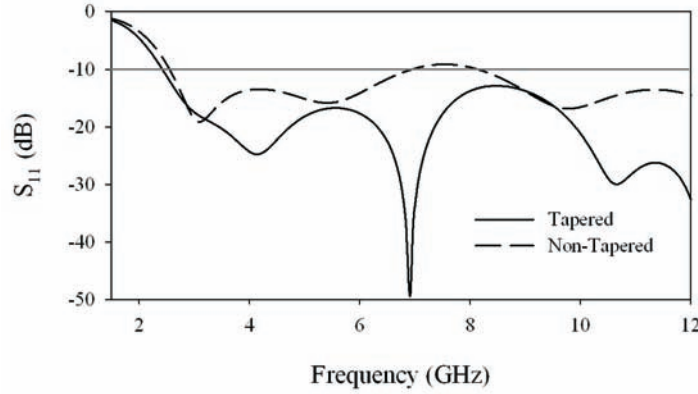


Fig. 3.7: Simulated return loss curves for antenna with and without feed tapering

is also a part of the antenna. The current distribution on the ground plane affects the characteristics of the antenna. The monopole as well as the ground plane forms an equivalent quasi-dipole antenna.

Finally, as the gap g is varied from 1.5mm to 0.25mm, Fig.3.6(e) shows that f_{r1} is slightly increased from 2.7GHz to 3.2GHz and the second resonance decreases from 4.8GHz to 3.7GHz. The antenna continues to be impedance matched over the whole band for the different values of g .

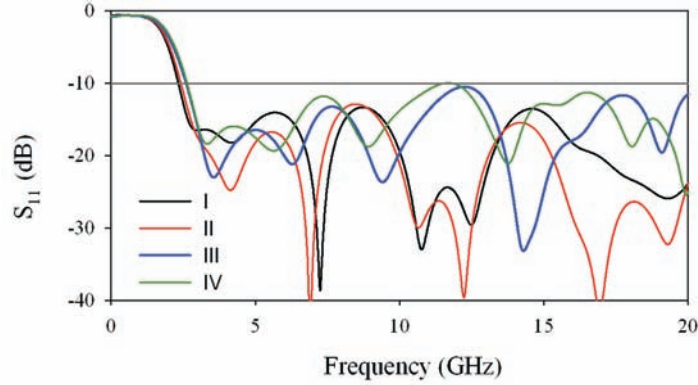
As noted before, the center conductor of the CPW feed in the designed antenna is tapered from the 50Ω line at the feed end to higher impedance at the radiator edge. To better understand the influence of tapering, the antenna return loss is plotted with and without the tapering in Fig.3.7.

As can be observed, the impedance matching is improved by feed tapering. Even though f_L and f_{r1} remain relatively unchanged, the second resonance stands affected. It is noted that the second resonance and the rest of the harmonic frequencies are decreased due to tapering. Basically, the tapered CPW line acts as an impedance transformer matching the 50Ω impedance of the SMA connector to the elliptical monopole with the ground plane acting as a component to form the distributed matching network with the monopole.

Finally the antenna is designed on substrates with different permittivity and heights. Corresponding to the substrate chosen, 50Ω CPW feed lines are designed and tabulated in Table 3.2. The rest of the antenna dimensions

Table 3.2: Elliptical monopole antennas on different substrates

Antenna	Laminate	ϵ_r	$h(\text{mm})$	$w(\text{mm})$	$s(\text{mm})$	$f_{r1}(\text{GHz})$
I	RT/duroid [®] 5880	2.2	1.57	3.08	0.16	3.07
II	Nelco NH9320	3.3	0.8	3	0.2	3.1
III	FR4 Epoxy	4.4	1.6	2.7	0.35	3.25
IV	RT/duroid [®] 6006 Epoxy	6.15	1.27	2.4	0.5	3.34

**Fig. 3.8:** Simulated return loss curves for the elliptical monopole antennas designed on different substrates

remain same as in Table 3.1. The return loss curves of the antenna designed on different substrates are plotted in Fig.3.8.

The same geometry gives wide band impedance matching with very little variation in f_L for the different substrates used. This is due to the monopole like radiation at the lower frequencies where the finite substrate dimensions confines most of the field lines in air. While the f_{r1} remains relatively undisturbed by the substrate, the higher harmonics do vary significantly.

Hence the following conclusions can be drawn from the analysis; the antenna behaves like a quasi-dipole at the lower frequencies with its characteristic doughnut shaped radiation pattern. As a result, antenna dimensions b_r , b_g and g are principally relevant for the lower frequency operations.

At higher frequencies, the traveling waves along the tapered edges of the antenna dominates and hence behaves like a tapered slot antenna. The waves traveling through the slots cause directional radiation patterns in the XY plane. As a result, we obtain a wide beam in the direction along the slot

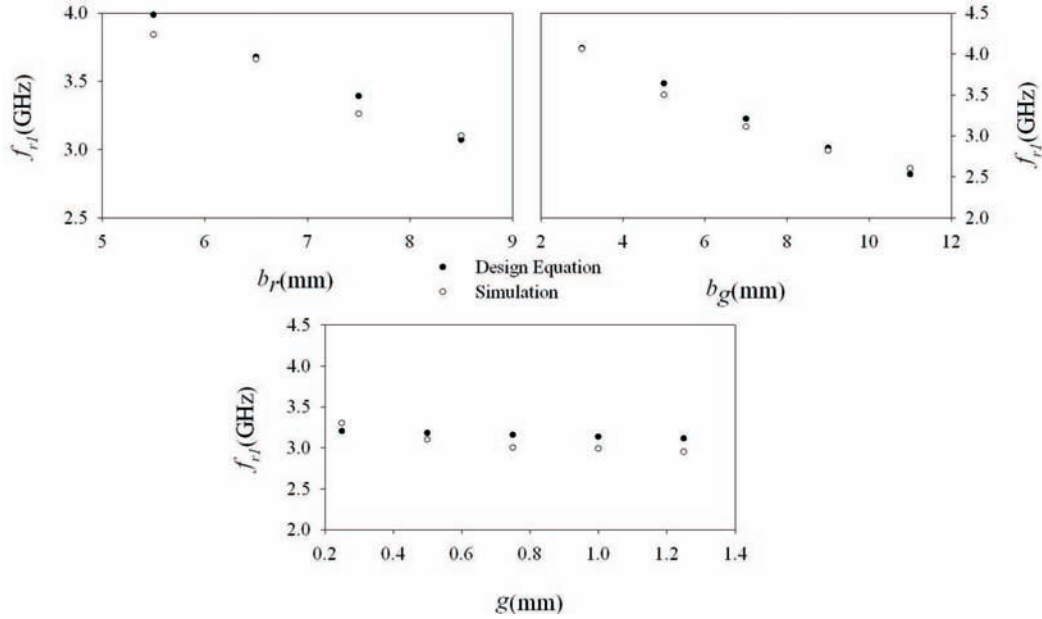


Fig. 3.9: Simulated and calculated f_{r1} plotted for different b_r , b_g and g values

while shallow nulls are observed in the directions orthogonal to the slot.

3.2.3 Design

The planar elliptical monopole antenna is a very wide band design where the lowest resonance is found to be critically determined by the antenna dimensions. Hence, an approximate equation for f_{r1} is deduced as

$$f_{r1}(GHz) = \frac{0.33c}{2b_r + 2b_g + g/(1 - \varepsilon_{eff})^2} \quad (3.1)$$

where ε_{eff} is the effective permittivity of a CPW waveguide [Simons 2001] with center strip width w' and slot width s' and c is the speed of light.

The validity of the equations are verified by designing elliptical monopole antennas with different values of b_r , b_g and g with rest of the dimensions as in Table 3.1. Wide band impedance matching is consistently observed in all cases. The f_{r1} , which is varied over a range of 2GHz to 4GHz for different antenna dimensions, are found to compare well with the computed ones deduced from eqn.(3.1) and are plotted in Fig.3.9.

The following assumptions on the antenna dimensions are also observed to be valid:

$$\begin{aligned}
 e &\approx 0.5, \\
 b_r &\approx b_g, \\
 s' &\approx g \approx 0.55mm, \\
 W &\approx 2a_g, \\
 L &\approx 4b_r + g
 \end{aligned} \tag{3.2}$$

where e is the eccentricity of the radiator/ground ellipse.

The antenna is characteristically wide band in nature, but the lower edge of the operating band can be suitably varied according to demand. Based on the observations aforementioned, a simple design procedure for the elliptical monopole antenna on the different commercially available laminates, as in Table 3.2, is explained below.

- Design a 50Ω CPW line on a substrate with permittivity ε_r and thickness h .
- Calculate ε_{eff} of a CPW waveguide with center strip width w and slot width s and
- Calculate b_g and the rest of the parameters using eqn.(3.1) and (3.2) for the desired f_{r1}

Once the geometrical parameters are deduced as per the steps described, the antenna design can be optimized using any commercial EM software.

3.2.4 Measurements

A prototype of the antenna was fabricated on a substrate of $\varepsilon_r = 3.3$ and $h = 0.8mm$ with the parameters as in Table 3.1 and 3.2. Return loss measurements indicate a wide band width from 2.5 to $>12GHz$, which is validated by simulations as shown in Fig.3.10. The slight deviation at lower frequencies could be due to the the soldering effect of the SMA connector and its mechanical tolerance on the finite ground plane current distribution which is

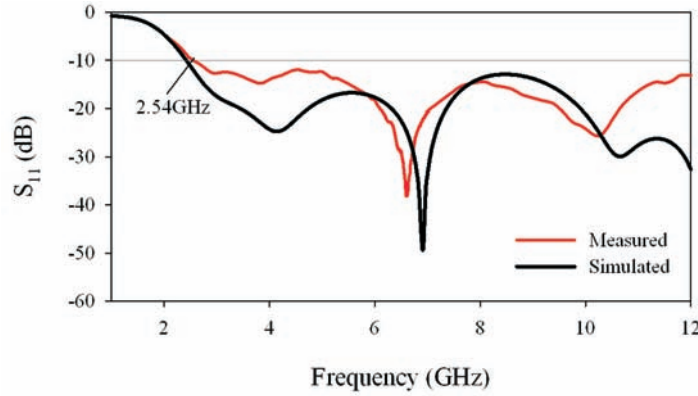


Fig. 3.10: Measured return loss of the elliptical monopole antenna

not accounted in the simulation. The normalized radiation patterns of the antenna for co-polarization and cross-polarization in the X-Y, Y-Z and X-Z planes for three different frequencies are shown in Fig.3.11. The patterns are stable throughout the band and resembles that of a monopole; omnidirectional in the azimuth (X-Y) and bidirectional in the elevation (Y-Z and X-Z) at the lower resonance as shown in Fig.3.11(a).

However at 6.5GHz, instead of a figure of eight in the elevation plane, the pattern appears raised to around $\theta=30^\circ$ as shown in Fig.3.11(b). At 9.5GHz, as shown in Fig.3.11(c), the pattern is slightly directional towards the $\pm Y$ axis. The measured patterns compare well with the simulated pattern shown in Fig. 3.5 and the polarization of the antenna is along the Z direction.

Measured peak gain of the antenna is shown along with its radiation efficiencies in Fig.3.12. The gain appears to range between 0.5 to 5dBi and the radiation efficiencies remain above 85% throughout the band.

3.3 Printed Inverted Cone Monopole Antenna

As discussed in Section 1.2.1.1 of Chapter 1, the radiated antenna far-field is the weighted sum of time delay derivatives of its surface currents. So all frequencies contained in the pulse should be radiated from the same point on the antenna for minimum pulse distortion. This makes electrically small

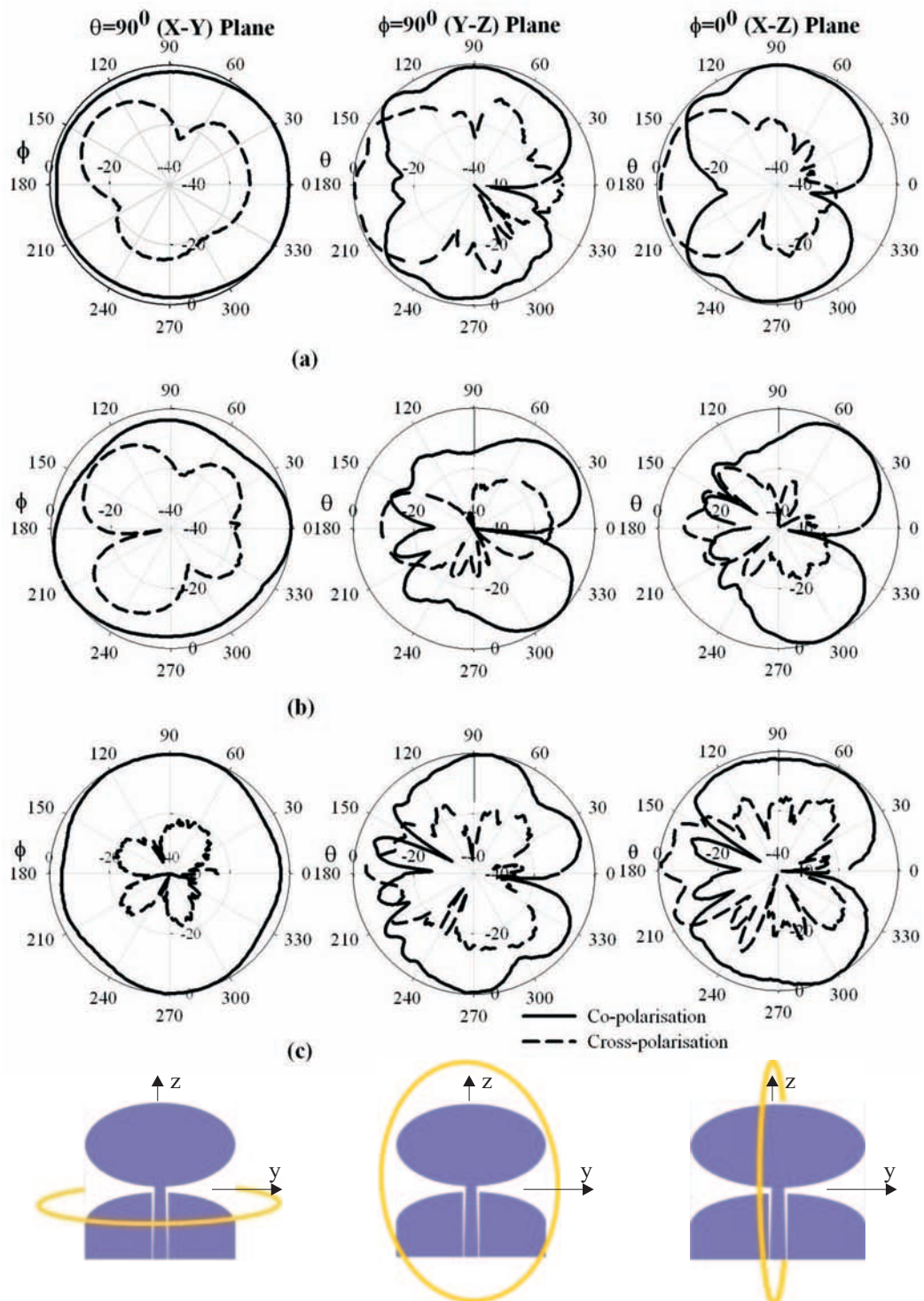


Fig. 3.11: Measured radiation patterns of the elliptical monopole antenna at (a) 3.5GHz, (b) 6.5GHz and (c) 9.5GHz

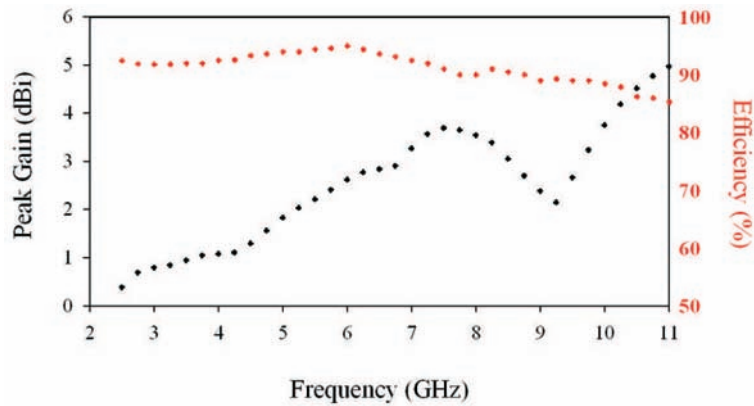


Fig. 3.12: Measured peak gain and radiation efficiency of the elliptical monopole antenna

compact antennas a good candidate for low power small range UWB radios. The compact size would also appreciate its suitability for the new-generation portable equipments.

The planar inverted cone (PIC) monopole antenna shows excellent wide band characteristics since it belongs to the bi-conical family of antennas. [Suh 2004] reports a very wide band behavior exhibited by a PIC antenna, however, the design is mounted on a large ground plane and is not suitable for portable communication systems. A planar version of the same but inscribed within a cone shaped slot and microstrip fed is reported in [Cheng 2008]. However, it is large in size ($60 \times 60 \text{mm}^2$) and fails to retain its wide band matching when the size is reduced.

Most of the surface currents in the elliptical monopole is distributed along the tapered slot between the two radiation patches. There are small currents in areas far away from the center of the antenna and makes little contributions to the radiation performance. Hence, smaller antennas can be constructed by carefully cutting the unimportant parts of the radiating patches without creating any abrupt discontinuity. As a result, elliptical monopole is reduced to an inverted cone shape and can achieve the same radiation performance if their sizes are readjusted properly along with similar changes to the ground patch. The design of the PIC antenna discussed in this section incorporates

a U-shaped slot on the ground patch near the feed transition as well. The overall size of the antenna is reduced to $14 \times 30 \text{mm}^2$.

3.3.1 Geometry

Fig.3.13 shows the geometry of the proposed printed inverted cone antenna. The ground plane of the antenna is shaped as a semi-ellipse near the radiating patch with dimensions b_g and a_g . An elliptical slot with b_{g1} and a_{g1} as major and minor axes is engraved on the ground edge and it is further shaped in to a U-shaped slot. The radiator patch is of length b_r and is an inverted cone (α) with a circular base of radius a_r .

The antenna is printed on FR4 substrate and fed by a 50Ω CPW line. The tapering of the ground and the radiator edges ensures matching at the higher frequencies of the UWB spectrum and the U-shaped slot at the ground edge, near the radiator, ensures mid-band matching.

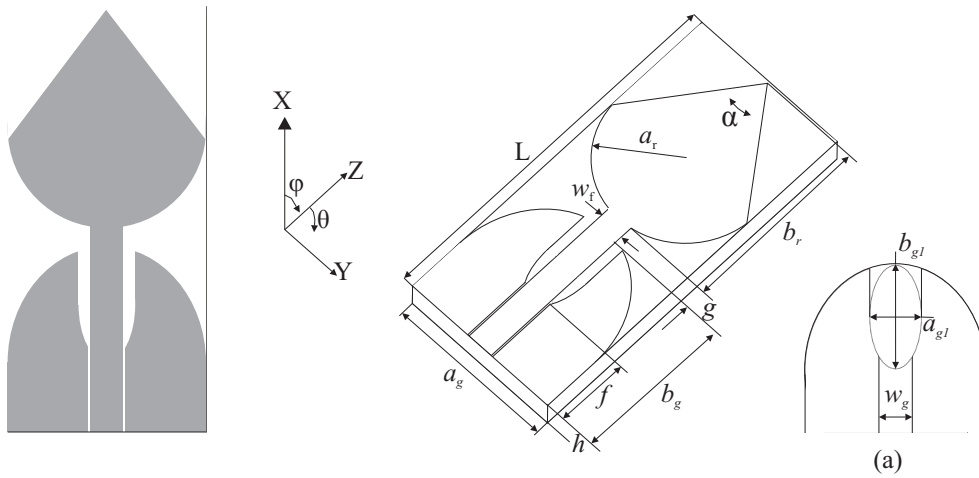


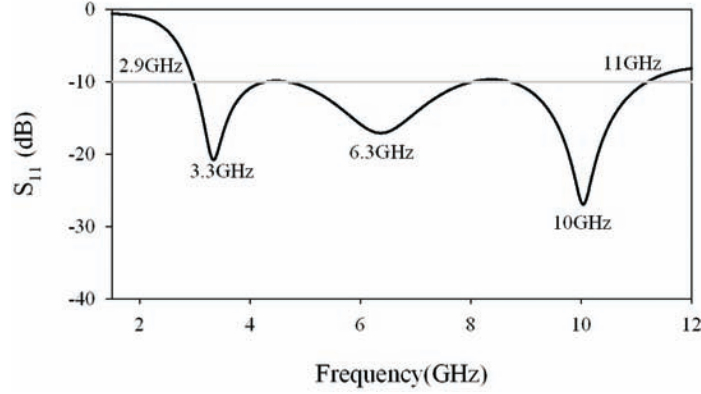
Fig. 3.13: Geometry of the inverted cone monopole antenna (a) ground plane with dimensions

3.3.2 Design and Simulations

The design equation deduced for the first resonance f_{r1} for an elliptical monopole antenna (eqn.(3.1)) continues to stand valid in this case as well. It is slightly

Table 3.3: Dimensions of the simulated PIC antenna

ε_r	a_g	L	h	a_r	b_r	α	g	w_f	f	b_g	b_{g1}	a_{g1}	w_g
4.4	14	30	1.6	7	15.3	74.5	1.75	2.3	6.2	12.8	4	8	2.58

**Fig. 3.14:** Simulated return loss curves of the inverted cone monopole antenna

modified in this case to take into account the dimensions of the PIC and is

$$f_{r1}(GHz) = \frac{0.33c}{b_r + b_g + g/(1 - \varepsilon_{eff})^2} \quad (3.3)$$

where ε_{eff} is the effective permittivity of a CPW waveguide near the feed transition (center strip w_g and gap $(\frac{a_g - w_f}{2})$) and c is the speed of light. The following assumptions are also made:

$$\begin{aligned} b_g &\approx b_r, \\ a_r &\approx b_r/2, \\ a_g &\approx b_g \end{aligned} \quad (3.4)$$

The dimensions of the designed antenna is deduced for $f_{r1} = 3.3GHz$ and are optimized using the simulation software for UWB operation. It is tabulated in Table 3.3.

The simulated return loss of the antenna is shown in Fig.3.14 which shows that the antenna covers the UWB spectrum from 2.9GHz to around 11GHz with resonances at 3.3GHz, 6.3GHz and 10GHz. Fig.3.15 shows the surface currents & field distributions on the antenna along with their corresponding

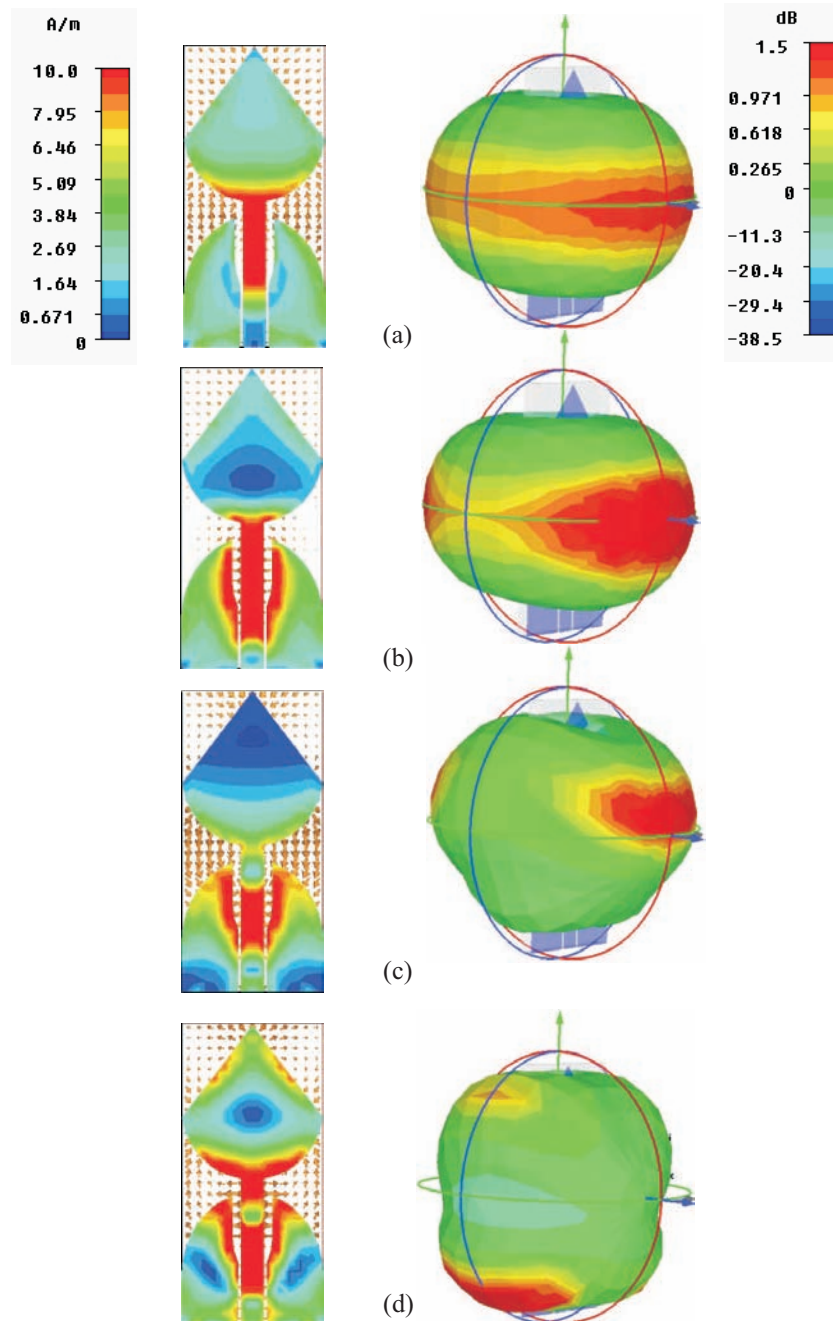


Fig. 3.15: Simulated surface current and E-field distributions on the inverted cone monopole antenna along with its simulated radiation patterns at (a) 3.3GHz, (b) 6.3GHz, (c) 9GHz, and (d) 10.6GHz.

3D radiation patterns at 3.3GHz, 6.3GHz, 9GHz, and 10.6GHz.

Antenna surface currents, shown in Fig.3.15, indicate that they are mainly restricted to areas near the U-shaped slot over most of the UWB frequencies. The slot appears to have a significant influence on the antenna behavior by maintaining its phase center position almost constant. It is also noted that the antenna performs in an oscillating or standing wave mode almost throughout the UWB band. It diverts from this behavior at the end of the spectrum (at 10.6GHz) with the current traveling and oscillating at the extreme ends of the geometry, and creating a pattern maximum along $\theta = \pm 30^\circ$.

When compared to the elliptical monopole, the gain seems to have been reduced which could be attributed to the reduced size. However, the antenna exhibits near perfect omni-directional pattern almost throughout the UWB spectrum.

3.3.3 Measurements

Fig.3.16 plots the measured return loss curves along with its simulated ones and they appear to compare well. It indicates a broad impedance bandwidth from 2.8GHz to 11GHz for $S_{11} < -10$ dB.

The radiation pattern is measured at three different frequencies and is plotted in Fig.3.17, for co and cross-polarizations. The patterns are observed to be stable and omnidirectional and behave similar to the simulated pattern

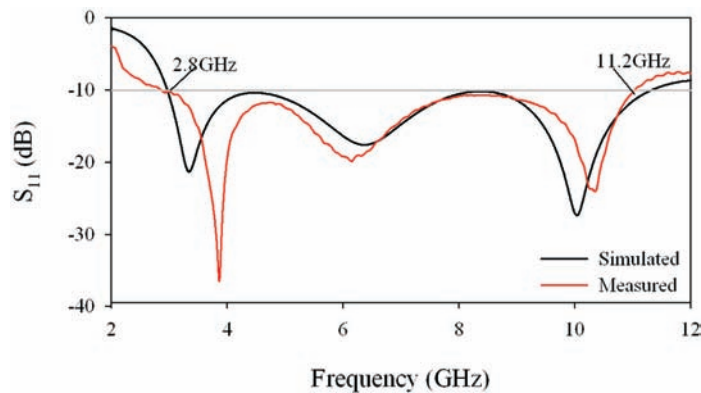


Fig. 3.16: Measured return loss of the inverted cone monopole antenna

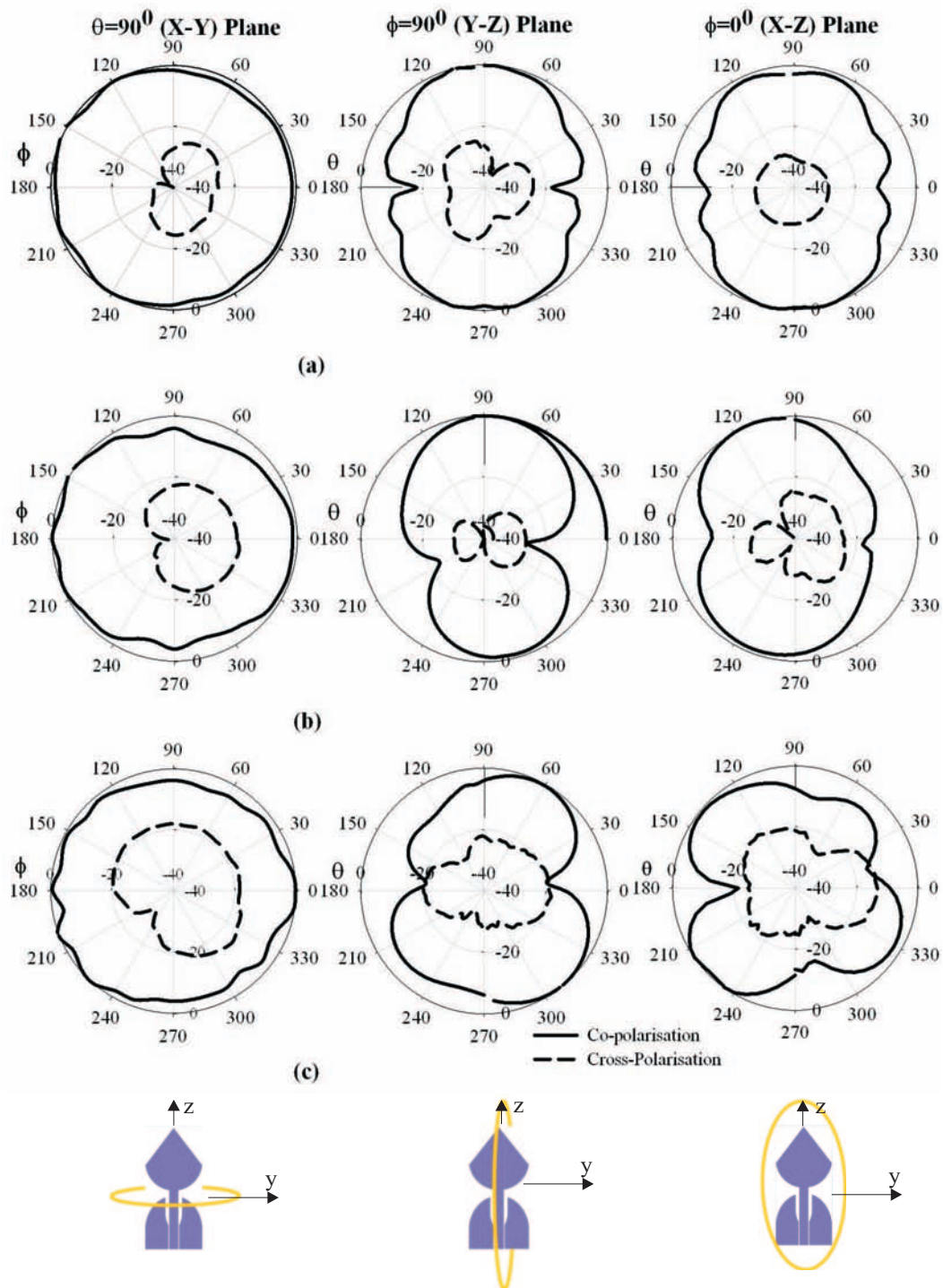


Fig. 3.17: Measured radiation patterns of the inverted cone monopole antenna at (a) 3.3GHz, (b) 6.3GHz and (c) 9.5GHz

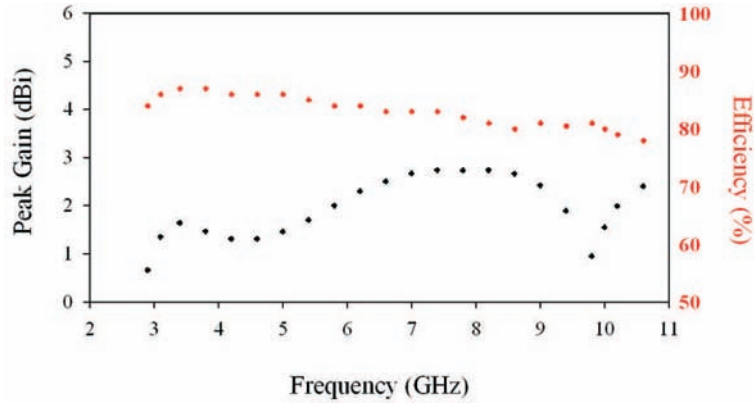


Fig. 3.18: Measured peak gain and radiation efficiency of the inverted cone monopole antenna

in Fig.3.15. The antenna polarization is along the Z axis and has very low cross-polarization as a result of the compact cross-section size of the antenna. The measured gain and radiation efficiency plotted in Fig.3.18 indicate an average gain of 2dBi and an efficiency $>80\%$ through out the UWB frequency range.

The measurement of such compact antennas is however very sensitive to the presence of the RF cable located in the near field of the AUT. The slight differences between simulations and measurements are caused by neglecting the parasitic effects of the cable and connector in the simulations and measurements.

3.4 Band-notched Antennas

Because of the existence of other wireless standards, such as IEEE 802.11a or HIPERLAN/2 operating in the 4.9 to 5.9GHz, an additional requirement for UWB antennas is to reject some bands within the ultra wide pass band. In these cases, UWB antennas with notched characteristics at certain bands are desired. The function of rejecting certain frequencies can be accomplished within the wireless transceiver by employing a band rejection filter. This calls for allocating a suitable area within the transceiver for such a device. This

requirement can be significantly relaxed by introducing the band rejection function within the UWB antenna structure.

The literature review shows a number of methods that are used to achieve the band-notch function. They can be basically categorized in to two groups; the first group include the technique of adding a perturbation in the antenna's radiating element. Such a perturbation usually consists of a slot carved in the antenna's radiating element like cutting away rectangular portion from the upper elliptical patch [Zhang 2008], inverted U-shaped slot in the radiator patch [Vasylchenko 2008], two T-shaped stubs inside an ellipse slot cut in the radiation patch [Hong 2007], a tuning stub in the ring monopole [Gao 2006], an arc shaped slot on the circular disk [Wong 2005a], two slits within the elliptic radiating element [Bahadori 2007].

In the second group, a perturbation on the antenna feeding line and ground plane, rather than on the antenna's radiating element itself, is added. They include U-slot defected ground structure (DGS) in the ground of the feed line [Yin 2008], a compact coplanar waveguide (CPW) resonant cell [Qu 2006a], a pair of square half-wavelength ring resonators on the ground plane [Dong 2009], L-shaped slots in the ground plane [Pancera 2007]. The perturbation would act as a band stop filter whose stop band is exactly the unwanted 5 to 6GHz frequency interval.

There are of course other band-notch techniques like introducing split ring resonators [Kim 2006], employing a Koch-curve-shaped slot [Lui 2006], a parasitic open-circuit element within the printed slot antenna [Lui 2005], attaching parasitic elements near the radiating patch [Kim 2005] [Abbosh 2009].

In this section, we have incorporated thin slot resonators within the elliptical monopole radiator patch and the ground plane of the inverted cone antenna to notch out the 5 to 6GHz WLAN bands. The investigations include a parametric analysis by varying the slot dimensions. This is further extended to the design of dual band-notched elliptical monopole antenna where a combination of dual slots in the ground or a slot in the ground as well as patch is implemented for a multiple band performance.

3.4.1 Band-notched Elliptical Monopole Antenna

The band reject mechanism is achieved for the elliptical monopole antenna by introducing a narrow $\lambda/2$ thin horizontal slot inside the patch as shown in Fig.3.19.

3.4.1.1 Simulation and Design

The simulated return loss of the antenna for different slot parameters namely the slot length s_l , width t , and position w_l & d from the edge of the radiator ellipse are plotted in Fig.3.20. The dimensions of elliptical antenna remains same as in Table 3.1.

It is observed from Fig.3.20(a) that the center frequency of the notched band is determined by the slot length s_l and is approximately

$$s_l = \frac{\lambda_g}{2} \quad (3.5)$$

where $\lambda_g = \lambda_0 / \sqrt{\epsilon_{eff}}$, $\epsilon_{eff} \approx (\epsilon_r + 1) / 2$ and λ_0 is the free space wavelength at the rejection frequency. This is confirmed in Fig.3.20(b) which shows that on keeping s_l constant and changing the slot position, the notch frequency remains same but the matching varies.

Fig.3.20(c) shows the dependence of the notched bandwidth with slot

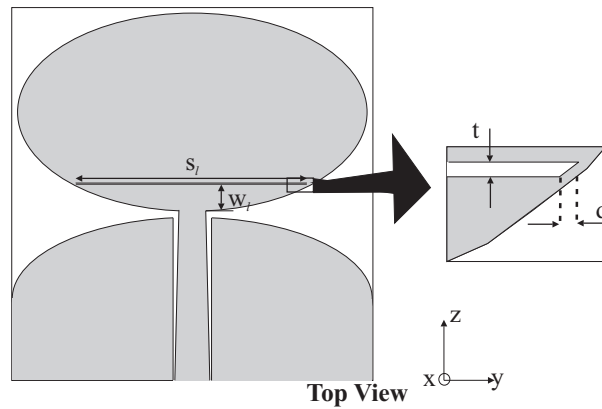


Fig. 3.19: Geometry of a notched elliptical monopole antenna

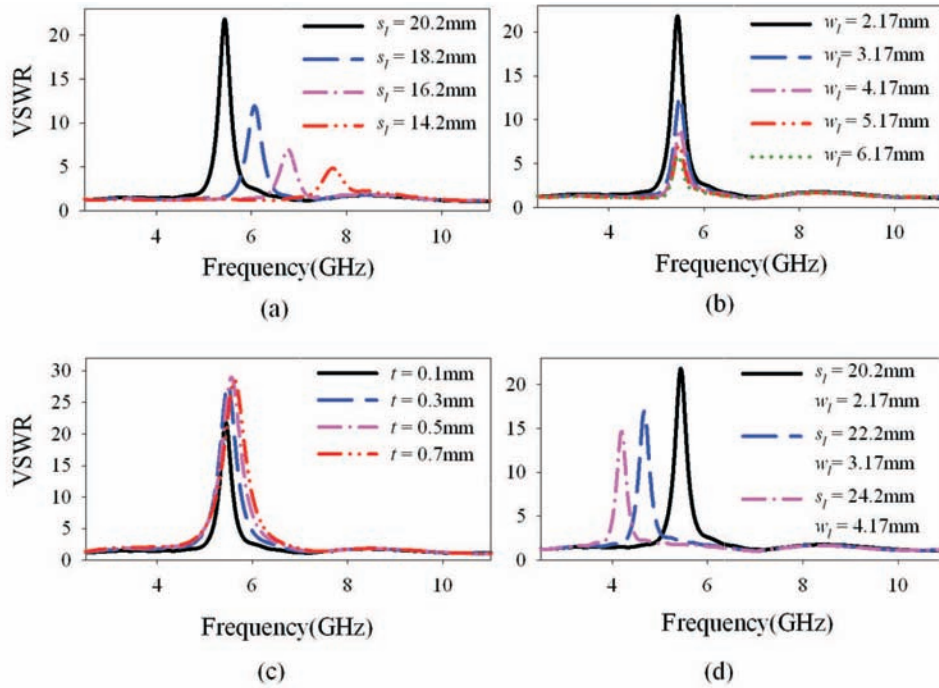


Fig. 3.20: VSWR variations of a notched elliptical monopole antenna for different (a) slot lengths s_l with $w_l = 2.17\text{mm}$ and $t = 0.1\text{mm}$, (b) slot positions w_l with $s_l = 20.2\text{mm}$ and $t = 0.1\text{mm}$, (c) slit widths t with $s_l = 20.2\text{mm}$ and $w_l = 2.17$, (d) slit lengths s_l and slit position w_l with $d = 0.2\text{mm}$ and $t = 0.1\text{mm}$.

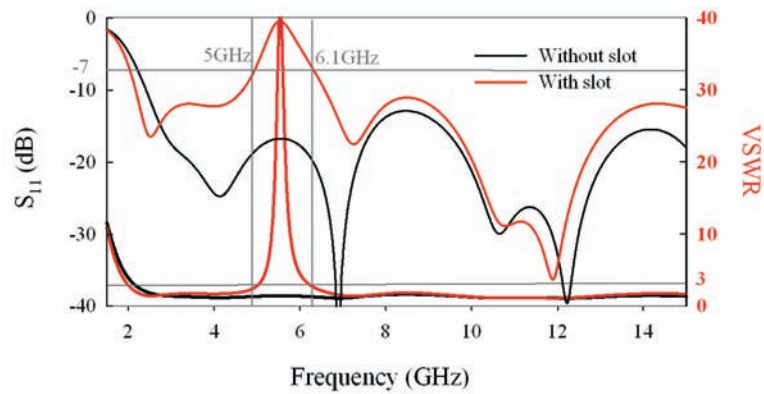


Fig. 3.21: Simulated return loss and VSWR curves of a notched elliptical monopole antenna with and without the slot

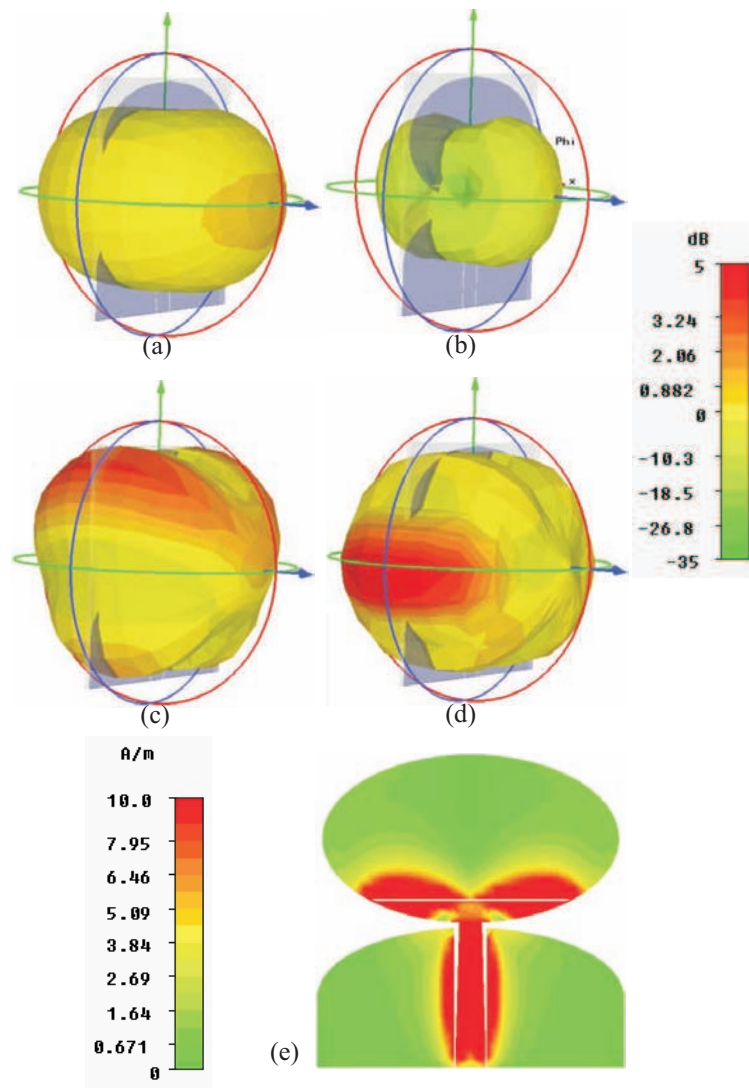


Fig. 3.22: Simulated radiation patterns of a notched elliptical monopole antenna at (a) 3.1GHz, (b) 5.45GHz, (c) 7.0GHz, and (d) 10.2GHz and (e) the current distribution at 5.45GHz.

thickness t . So while the slot length s_l is fixed for the select notch frequency, its bandwidth can be adjusted by changing its thickness t . From the parametric studies, it is observed that the best result, that is maximum signal rejection at the desired notched frequency band, is obtained when a $\lambda/2$ long slot is placed at minimum distance d from the patch edge. This is confirmed in Fig.3.20(d) with $d = 0.2\text{mm}$, for different notched frequencies.

The dimensions of the slot inscribed in the radiator ellipse is deduced using

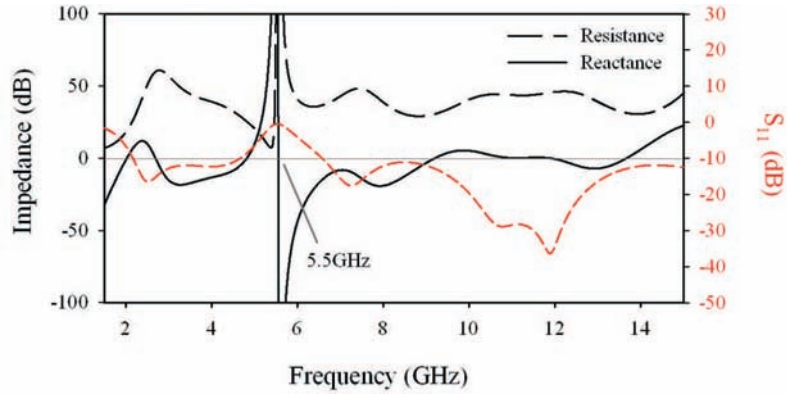


Fig. 3.23: Simulated impedance and return loss of a notched elliptical monopole antenna

eqn.(3.5) at a notch frequency of 5.45GHz and are as follows; $s_l = 20.2\text{mm}$, $t = 0.1\text{mm}$, $d = 0.2\text{mm}$ and $w_l = 2.17\text{mm}$. Fig.3.21 plots the simulated return loss and VSWR with and without the slot. We can see that the antenna resonances remain unaffected due to the presence of the slot except in the frequency band 5 to 6.1GHz where a large VSWR is noted.

The band-notched property is also observed in Fig.3.22, where the simulated 3D patterns plotted at 3.1GHz, 7.0GHz, and 10.2GHz remains similar to the corresponding plots of the elliptical monopole antenna, without the slot, shown in Fig.3.5 except at the notched frequency of 5.45GHz. At 5.45GHz, a distinct reduction in radiation of more than 10dB is noted along all directions. Fig.3.22(e) shows that the surface current distribution appears stronger around the slot at the notched frequency of 5.45GHz. It is more concentrated at the farthest sides of the slot and is oppositely directed along its lower and upper edges. This leads to destructive interference of the excited surface currents in the patch.

The $\lambda_g/2$ long horizontal slot behaves like a parallel combination of two shorted $\lambda_g/4$ long slots resulting in a high input impedance at 5.45GHz and causing the antenna to be non-radiating at that frequency. The antenna input impedance plot in Fig.3.23 records a large resistance and a zero crossing on the reactance curve at 5.45GHz validating our arguments.

3.4.1.2 Measured Results

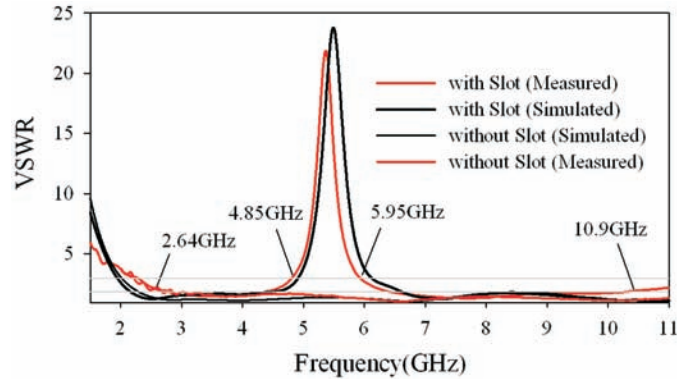


Fig. 3.24: Measured VSWR curves of a notched elliptical monopole antenna

The simulated and measured VSWR of this antenna with and without the slot is plotted in Fig.3.24. Good agreement between the simulated and measured results is observed. It reveals a 2:1 VSWR bandwidth from 2.64GHz to 10.9GHz. The VSWR remains high (>3) in the 4.85 to 5.95GHz band with a very large value (>20) occurring around 5.45GHz. In the pass band, the VSWR of the original UWB antenna is only slightly affected by the presence of the slot.

The measured radiation patterns in the X-Y, Y-Z and X-Z planes of the antenna at the notched frequency is plotted in Fig.3.25. The pattern at 5.45GHz has been normalized w.r.t that at 3.5GHz. We can observe a reduction in gain by ≈ 10 dB along all directions uniformly.

Fig.3.26 plots the measured gain which shows relatively constant values in the pass band with a large decrease in gain in the rejected band which goes as low as -13dB compared to the rest of the band. Corresponding dip in the radiation efficiency can also be noted here.

3.4.2 Band-notched Printed Inverted Cone Antenna

For compact antennas like the inverted cone UWB antenna discussed in Section 3.3 of this chapter, accommodating a half wavelength slot resonator in

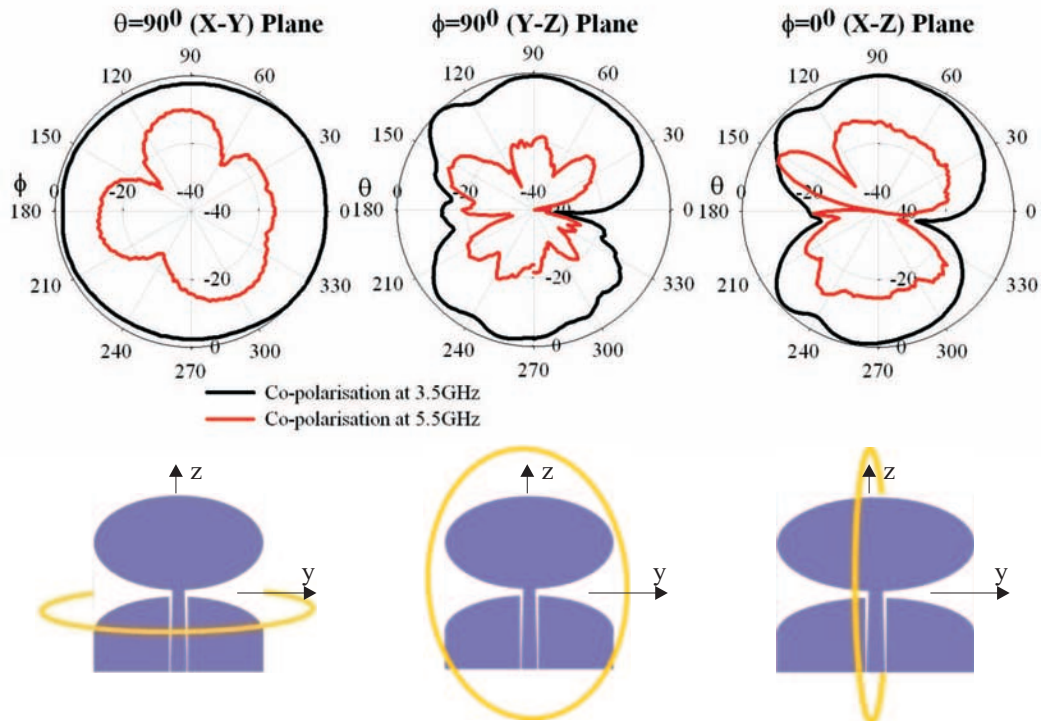


Fig. 3.25: Measured radiation patterns of a notched elliptical monopole antenna

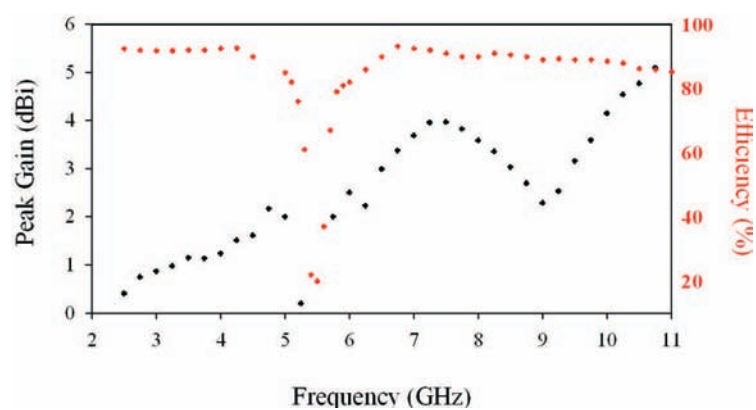


Fig. 3.26: Measured peak gain and radiation efficiency of a notched elliptical monopole antenna

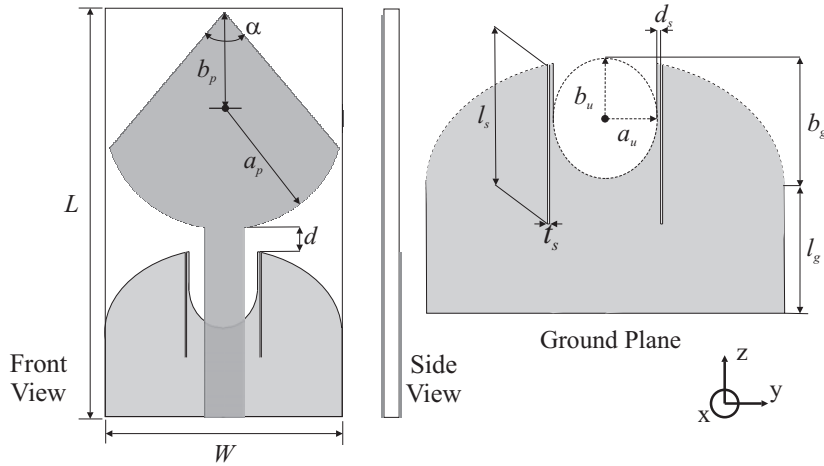


Fig. 3.27: Geometry of a notched PIC monopole antenna

Table 3.4: Dimensions of the band-notched inverted cone antenna

ϵ_r	W	L	h	a_p	α	w_f	b_r	g	b_g	b	a_u	b_u	d	l_s	t_s
4.4	18	30	1.6	9	86	2.8	15.3	1.8	12.7	7.5	2.6	3	0.3	8.2	0.1

the radiating patch, to filter out the 5 to 6GHz WLAN bands, would be a challenge due to the space constraints imposed. Instead, we have incorporated a pair of symmetrically placed quarter wavelength slot resonators etched in the ground plane for the band-notch action. Fig.3.27 shows the geometry of the band-notched inverted cone monopole antenna. In this case the inverted cone is fed by a 50Ω microstrip line.

3.4.2.1 Simulated and Measured Results

Fig.3.28 plots the simulated VSWR of a UWB antenna optimized to notch out the 5.2/5.8GHz WLAN frequencies. The dimensions (in mm) of the antenna are tabulated in Table 3.4. The antenna with the slots record a VSWR >3 for frequencies from 5.2 to 5.9GHz which goes as high as VSWR ≈ 7 at 5.5GHz. For other frequencies in the pass band, the response remains similar to that of the antenna designed without the slots.

The quarter wavelength slot resonators are open at one end and their

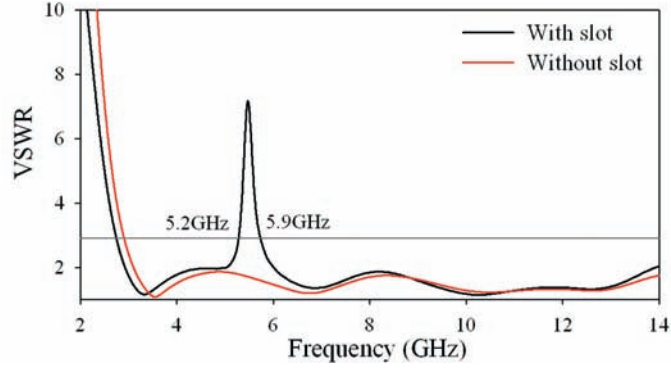


Fig. 3.28: Simulated VSWR curves of a notched PIC monopole antenna

length (l_s) is deduced as

$$l_s = \frac{\lambda_g}{4} \quad (3.6)$$

where $\lambda_g = \lambda_0 / \sqrt{\epsilon_{eff}}$, $\epsilon_{eff} \approx (\epsilon_r + 1) / 2$ and λ_0 is the free space wavelength at the rejection frequency. However, a sharper notched band is observed as the slots are located closer to the microstrip feed-monopole transition.

The surface current distribution at 5.5GHz in Fig.3.29 shows that most of the currents are surrounding the slots at the notched frequency with a maxima at its shorted end and a minima at its open ends. It is the destructive interference of the surface currents that causes the antenna to be non-radiative at the notched frequency.

The measured VSWR and return loss of this antenna with and without the slot resonators are plotted in Fig.3.30. For the antenna without the slot resonators, the VSWR characteristics reveal UWB behavior with a 2:1 VSWR bandwidth from 3.07GHz to >12 GHz. When the quarter wave slot resonators are introduced, the VSWR is high (≈ 6) at 5.5GHz. The value of VSWR > 3 is noted in the 5.1 to 5.9GHz band and is only slightly affected in the pass band.

The measured radiation pattern of the antenna at 5.5GHz that has been normalized w.r.t that at 3.5GHz is plotted in Fig.3.31. We can observe a reduction in gain by ≈ 10 dB along all directions uniformly.

The gain and radiation efficiency of the antenna is measured and plotted

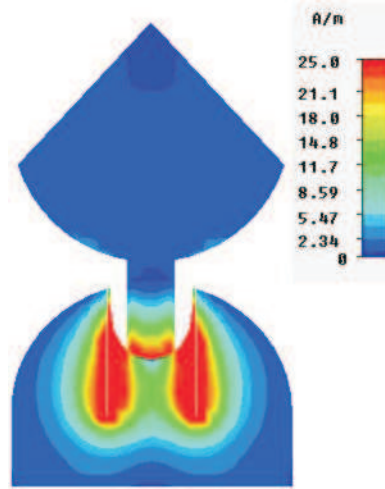


Fig. 3.29: Surface current distribution at 5.5GHz of a notched PIC monopole antenna

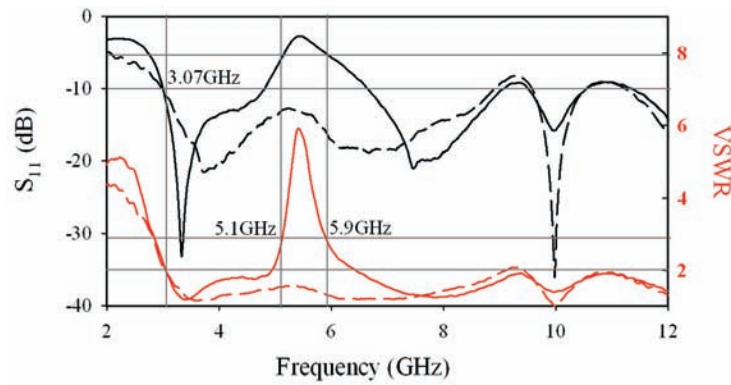


Fig. 3.30: Measured return loss and VSWR curves of a notched pic monopole antenna

in Fig.3.32. An average gain of 2dBi is noted throughout the operating band except at the notched frequency where dip >10 dB is obtained. The antenna designed has a radiation efficiency of more than 80% in the pass band and reduction in the rejected band.

3.4.3 Dual Band-notched Elliptical Monopole Antenna

The multiple slots etched on the elliptical monopole antenna, that filter out the undesired frequencies without disturbing the antenna characteristics in

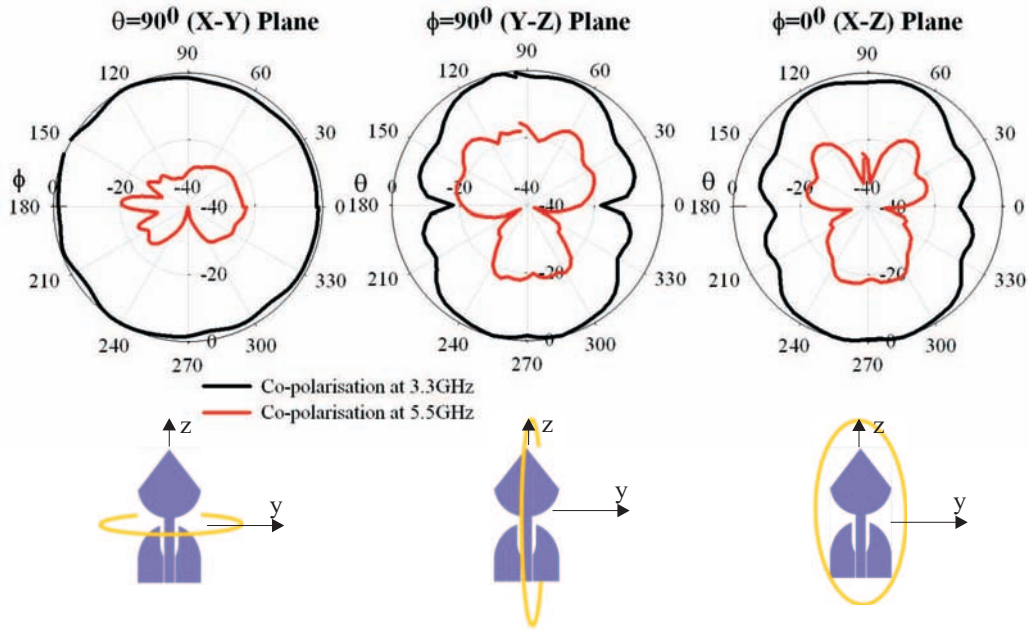


Fig. 3.31: Measured radiation patterns of a notched PIC monopole antenna

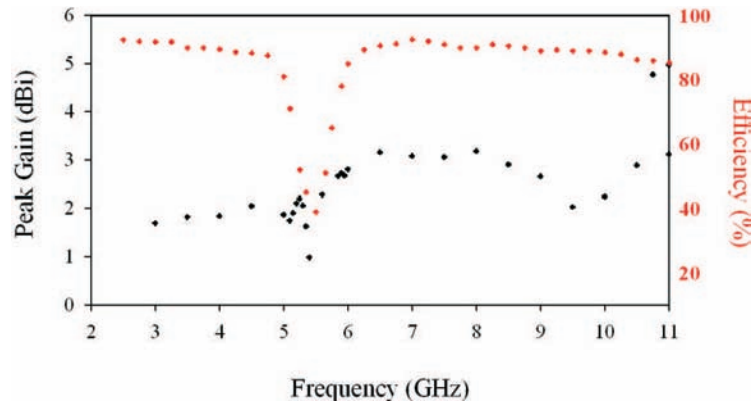


Fig. 3.32: Measured peak gain of a notched pic monopole antenna

the rest of the band, is presented in this section. Two types of combination slots are used to reject dual bands of choice as shown in Fig.3.33. Antenna design 1 employs two U-shaped thin slots in the radiator ellipse where each measure half a wavelength at their corresponding reject frequencies. Similarly, antenna design 2 employs a U-shaped half-wavelength slot resonator in the radiator ellipse and dual symmetrically placed quarter-wavelength L-shaped slot resonators in the ground patch, all measured at their corresponding reject

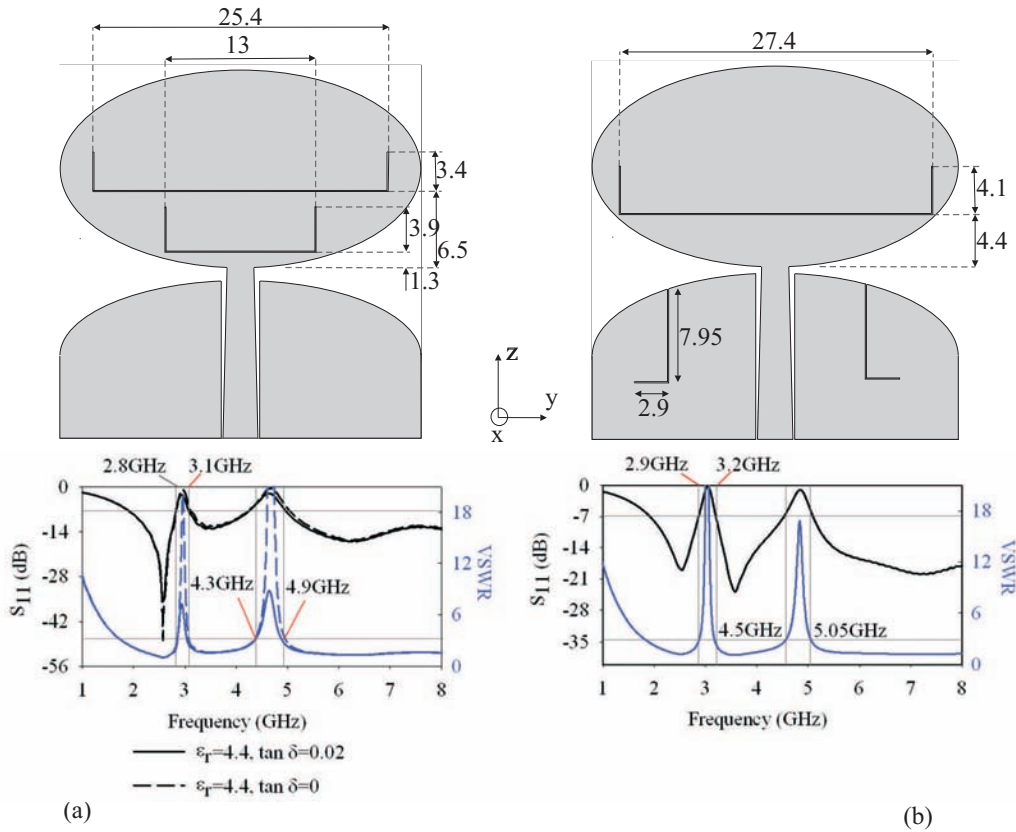


Fig. 3.33: Geometry and simulated return loss of a dual-notched elliptical monopole antenna (a) Design 1 (b) Design 2

frequencies.

The dimensions of the elliptical monopole remains the same as given Table 3.1 and 3.2 where the antenna 1 is designed on FR4 ($\epsilon_r=4.4$ and $\tan\delta=0.02$) and antenna 2 on NH9320 substrate ($\epsilon_r=3.3$ and $\tan\delta=0.0012$).

The simulated return loss of the designed antennas are plotted in Fig.3.33 where a VSWR >3 is recorded for frequencies 2.8 to 3.1GHz and 4.3 to 4.9GHz for design 1 and for frequencies 2.9 to 3.2GHz and 4.5 to 5.05GHz for design 2. While design 2 records large VSWRs (>10) in the notched bands, design 1 records relatively lower rejection (VSWR >5) in the notched bands. It is also interesting to note that when antenna design 1 was simulated on an FR4 substrate with no loss ($\tan\delta=0$) a sharp increase in the VSWRs (>10) are noted in the rejected bands (Fig.3.33(a)). Therefore the substrate loss factor

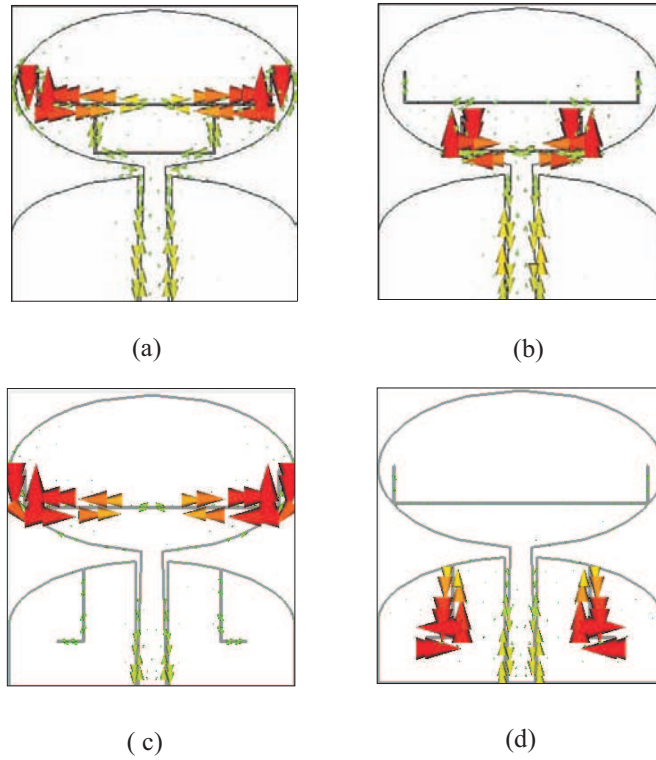


Fig. 3.34: Surface current distribution on a dual-notched elliptical monopole antenna; Design 1 at (a) 3GHz, (b) 4.6GHz and Design 2 at (c) 3GHz and (d) 4.8GHz

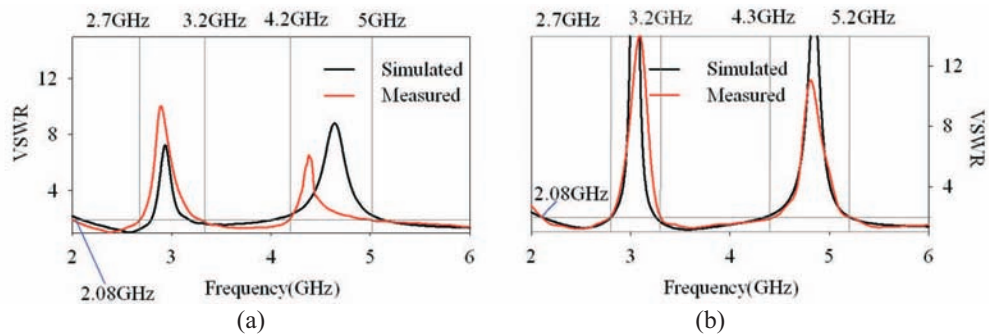


Fig. 3.35: Measured VSWR of a dual-notched elliptical monopole antenna (a) Design 1 (b) Design 2

appears to have an impact on the rejection capability in the notched band.

The destructive interference of the antenna radiation at the reject frequencies is confirmed from the surface currents on the antenna which is particularly concentrated around the slots as shown in Fig.3.34.

Fig.3.35 plots the measured return loss of the antenna which shows reasonable comparison with simulated plots. The slots rejects 2.7 to 3.2GHz and 4.2 to 5.1GHz and gives a triple band performance from 2.08 to 2.7GHz, 3.2 to 4.2GHz and 5.1 to >10GHz. Thus it covers the 2.5 to 2.69GHz, 3.4 to 3.69GHz, and 5.25 to 5.85GHz WiMAX bands and the IEEE 802.11 WLAN standards of the 2.4GHz (2.4 to 2.484GHz), 5.2GHz (5.15 to 5.35GHz) and 5.8GHz (5.725 to 5.825GHz) bands. The antennas designed are suitable for operation as WLAN/WiMAX antennas for portable equipments.

3.5 Chapter Summary

In this chapter, we have presented two designs of broadband planar monopole antennas, namely the elliptical monopole and inverted cone monopole. The planar elliptical monopole antenna has a wide band operation (2.54GHz to >12GHz), simple structure and nearly omnidirectional radiation patterns at the lower end of the spectrum. The antenna has the convenience of compact size (31x32mm²) and a CPW feed. It is composed of a monopole element and a finite ground plane and both the radiator (monopole element) and ground plane contribute to the field radiation. The monopole and the ground plane forms a quasi-dipole antenna at its lowest resonance. The extremely wide impedance band is ensured by the exponential impedance transformer arrangement between the ground and the patch.

The antenna appears to be an ideal candidate for the 3.1 to 10.6GHz UWB operation from the frequency domain studies. Since the antenna operates over a multi-octave bandwidth, it would be excellent to transmit pulses of the order of a nanosecond in duration with minimal distortion. However neither its radiation pattern remain omnidirectional nor its phase center location remain constant over the whole bandwidth as would have been desired. This would in turn mean that the pulse transmission would differ according to their space coordinates and that it may be distorted. The space dependency & distortion of the pulse transmitted/received is predicted here but its extent and whether

it is within the tolerable limits can only be determined by the transfer function characterization of the antenna which involve both the amplitude and phase of the radiated fields. This is studied in detail in Chapter 5.

The inverted cone monopole antenna presented in the following section has a reduced size ($14 \times 32 \text{mm}^2$) and wide band operation (2.8 to 11.2GHz). It appears to be perfectly ideal for UWB hand held applications with a compact size, stable & omnidirectional antenna pattern and an almost constant regions of radiation, otherwise called the phase center. From this we can predict that the antenna should exhibit pulse transmission with minimum distortion and independent of the space coordinates. However, the analysis of the antenna performance, in terms of any ringing if at all present, would be complete only by looking at its transient response which is studied in detail in Chapter 5.

In final section of this chapter, the designed wide band antennas are adapted to coexist with existing WLAN bands (5.2/5.8GHz) with minimum interference. A thin half wavelength long slot resonator is inscribed on the radiator patch of the elliptical monopole antenna to filter out the 5 to 6GHz frequencies. Similar performance is achieved by dual symmetrically placed quarter wavelength slot resonators inscribed on the ground patch of the inverted cone monopole antenna. The time domain performance of these antennas for assessing their suitability for UWB applications is carried out in Chapter 5. Finally, a combination of such multiple slots are implemented to adapt the designed elliptical monopole antenna for triple band operation particularly for the 2.5/3.5/5.5GHz WiMAX as well as the 2.4/5GHz WLAN standards.

Planar Broadband Slot Antennas

Contents

4.1	Planar Broadband Slot Antennas: Review	98
4.2	Koch Fractal Slot Antenna	103
4.2.1	Geometry	104
4.2.2	Simulation and Design	104
4.2.3	Measurements	112
4.2.4	Dual-band Modified Koch Fractal Slot Antenna	114
4.3	UWB Slot Antenna	117
4.3.1	Geometry	118
4.3.2	Simulation and Design	118
4.3.3	Measurements	123
4.4	Chapter Summary	125

In this chapter, we have investigated the performance of planar slot antennas. We begin by designing a Koch fractal based slot antenna along with a detailed study of their slot & feed geometry effects on the antenna performance. The antenna structure is compact and performs well over a frequency band wide enough to cover all the WLAN/WiMAX bands. A UWB slot antenna design is presented next with a reduced size and an enhanced bandwidth covering the FCC specified UWB frequencies. This design has the unique advantage of its performance being independent of ground plane size making it suitable for wireless dongle applications.

4.1 Planar Broadband Slot Antennas: Review

In the search for low profile, light weight and wide band antennas, there has been particular emphasis given to printed slot antennas, especially wide-slot antennas, as they are completely planar and have a wide operating bandwidth [Yoshimura 1972] [Kahrizi 1993].

The technique is to excite a narrow rectangular slot with a simple microstrip feed line as in [Yoshimura 1972] and [Pozar 1986]. In [Yoshimura 1972], the feed point is shifted from the center of the slot and is short-circuited through the dielectric substrate. A similar technique of feed point shifting close to the slot end is used in [Pozar 1986]. In both cases, the offset of the feed point leads to impedance matching in a narrow frequency band with $\approx 20\%$ bandwidth .

The geometrical and physical parameters of the slot as well as the feed network are also observed to affect the bandwidth of slot antennas. By considering a slot antenna as an aperture with a known electric field distribution, it is possible to obtain its fields [Balanis 1997]. Using the antenna field, the radiated and stored energies can be found and a quality factor (Q) is defined for the antenna which is a function of the antenna dimensions. It is shown that for a rectangular slot antenna, as the slot width is increased, the Q decreases or equivalently bandwidth increases.

This increase is much faster for the smaller antenna widths and decreases as the width increases beyond a certain range [Behdad 2004]. This is because as the width of the slot increases, the radiation resistance of the slot increases which leads to impedance mismatch between the slot and microstrip line. This in turn would reduce the impedance bandwidth of the antenna [Kahrizi 1993]. However, terminating the open end of the feed line within the width of the slot have been reported as a means for increasing the bandwidth of the wide rectangular slot antenna in [Shum 1995] even though substantial bandwidth improvement could not be achieved.

When a T-shaped microstrip tuning stub is used to excite a wide rectan-

gular aperture, a relatively broad bandwidth is noted ($\approx 58\%$) from 1.5 to 3.2GHz [Kim 2000]. Similarly, modifications in the shape of the slot can also result in broadband operation as in [Chen 2000a] where a semi-circular slot and a protruding square shape is used to realize a bandwidth of 46%.

Experimental results show that by choosing suitable combinations of feed and slot shapes and tuning their dimensions, good impedance bandwidth and stable radiation patterns can be obtained. Wide-slot antennas with different slot shapes such as triangular [Chen 2005] [Liu 2004b], square [Sze 2001] [Chen 2003a], rectangular [Wu 2004a], rhombus [Jan 2007], pentagonal [Rajgopal 2009], hexagonal [Jan 2005], L-shaped [Dissanayake 2008], circular, elliptical [Li 2006] [Angelopoulos 2006] have been investigated.

Different feed shapes are also reported like the simple extension of the microstrip [Jan 2005] and CPW [Jan 2006] [Chiou 2003], fork like [Sze 2001] [Qing 2003] [Chair 2004], rectangular [Chen 2003a], triangular [Liu 2004b], circular [Qu 2006b], elliptical [Angelopoulos 2006], U-shaped [Li 2006] etc. In wide-slot antennas, a high level of the electromagnetic coupling to the feed line results due to the large size of the slot. Therefore, varying the feed shape or slot shape will change the coupling which means that this technique can be used to control the impedance matching.

In addition to these regular shapes of the slot and feed types, there has been several other modifications reported for a wide band operation. In [Chiou 2003], conducting strips are incorporated on each corners diagonally to achieve bandwidths greater than 60%. A similar approach is followed in [Sze 2003] where a broadband circular polarization is achieved by protruding a T-shaped metallic strip from the ground towards the slot center and feeding the square slot antenna using a 50Ω CPW with a protruded signal strip at 90° to T-shaped strip.

Different types of feed for the simple rectangular aperture have been reported to operate over varying range of frequencies with different bandwidths. [Sze 2001] reports a wide aperture, of size 54mm x 54mm, fed by a fork like tuning stub realizing a bandwidth of 1GHz centered around 2GHz. [Chen 2003a]

reports over 60% bandwidth around 2GHz when a rectangular aperture, of size 44mm x 44mm, is fed by a rectangular stub. In [Jang 2001], an inverted T-shaped microstrip tuning stub excites a wide aperture to operate from 1.877 to 5.638GHz ($\approx 114\%$).

[Chair 2004] reports a CPW fed fork shaped tuning stub exciting a rectangular aperture of size 32.2mm x 21mm and optimized for operation in the FCC approved UWB band of 3.1 to 10.6GHz. [Qing 2003] also records a similar geometry for UWB operation. [Lin 2006] reports a very compact UWB slot antenna design which has a rectangular aperture fed by a rectangular stub where the aperture size is restricted to 13mm x 23mm .

Further review of the literature reveals that the feed-slot gap significantly affects the antenna bandwidth. The effects of feed-slot combination and feed-gap widths are studied in [Liu 2004b] for UWB operation of the antenna. For the study, an antenna with an arc-shaped slot and a square patch feed and another antenna that has a triangular shape slot and an equilateral triangular-patch feed are used to achieve around 100% bandwidth.

Detailed investigations in the above design indicates that rounded corners in the slot can improve the bandwidth and [Qu 2006c] reports an improvement as high as 158%. A simpler version of the above antennas are proposed in [Denidni 2006] wherein the authors have used a circular slot and a circular tuning stub to realize an antenna with as much as 110% bandwidth. In [Habib 2006], the use of stubs other than the circular one to excite the circular slot is explored. It reveals that slots and stubs of similar geometry can result in the widest possible bandwidth of all the possible combinations. [Cheng 2008] is based on similar principle but with an inverted cone geometry with a circular base. As an extension, ellipses of different ellipticity for the ground as well as the tuning stub is studied [Angelopoulos 2006]. Their studies propose the use of an elliptical design for compact applications and a circular design for wider bandwidth.

Tapering the feed gap is another technique which is observed to improve the impedance bandwidth. This can be either achieved by tapering the feeding

line as in [Li 2006] [Yoon 2006] or introducing a narrow slot on the ground edges beneath the feed as in [Chen 2006] [W.-F. Chen 2008].

The electric field distribution (or the magnetic current) in the slot is identical to the electric current distribution on a complimentary wire. The electric field everywhere is normal to the surface of the slot antenna except in the region of the slot. Hence the currents in the sheet can be directly deduced from the distribution of the electric field in the slot. Consequently, the radiated field of the magnetic current element within the slot boundaries should include the contribution of the electric current flowing on the metal surface. As a result the wide slot antennas features a dependence of the frequencies of operation on the slot geometries. [Li 2006] derives an empirical relation for the lower edge frequency in terms of the elliptical slot dimensions by regarding it as an equivalent magnetic surface. [Chen 2005] and [Chen 2006] relates the slot perimeter to the lowest operating frequency.

However, the performance of the antenna printed on a PCB can be significantly affected by the shape and size of the ground plane of the antenna which is usually located electrically close to the radiator, particularly for devices with limited space such as a W-USB dongle [Zhang 2004b] [Chen 2004b] [Kwon 2003]. In addition, the printed UWB antenna consisting of a planar radiator and system ground plane is essentially an unbalanced design, where the electric currents are distributed on both the radiator and the ground plane so that the radiation from the ground plane is inevitable. Such a ground-plane effect causes severe practical engineering problems such as design complexities and deployment difficulties.

An investigation was performed to study the effects of a housing device on the antenna performance in [Bahadori 2007]. The hosting device was represented by a metal box. It was shown that if the antenna is placed vertically, the main features of its performance does not change significantly. In [Su 2007], a U-shaped, metal-plate monopole, fabricated from bending a simple metal plate onto a foam base of width 20mm is reported. Small ground-plane length effects on the antenna impedance bandwidth have also been observed which

makes them well suitable for internal, UWB-antenna applications in wireless USB dongles with various possible system ground-plane or PCB lengths. A small slotted PCB-printed UWB antenna is presented in [Chen 2007c] which has a rectangular notch cut vertically from the printed radiator and a strip asymmetrically attached to the radiator. The effects of the ground plane and RF cable on the antenna performance are reported to have been suppressed greatly.

In contrast to planar dipole/monopole antennas which have relatively large electric near-fields that are prone to undesired coupling with near-by objects, slot antennas have relatively large magnetic near-fields that tend not to couple strongly with near-by objects [Schantz 2003]. Thus, slot antennas are ideal candidates for applications wherein near-field coupling is required to be minimized like in the case of USB Dongle type applications as discussed before.

In this section, there are two types of antenna designed. In the first type, the concept of space filling characteristics of fractal curves which has been used in the design of compact and multi band patch antennas [Werner 2003] is applied for the design of wide slot antennas with reduced size. There exists a contradiction between enlarging the impedance bandwidth and enhancing the radiation pattern bandwidth by widening the slot [Kim 2000]. So, in the design presented, a Koch snowflake fractal shaped slot, whose the perimeter increases by 33% with every iteration without increasing the overall size is implemented.

The Koch snowflake fractal shaped slot is employed for a compact and wide band antenna operation. The antenna designed has a bandwidth sufficient enough to cover the 2.4/5.2/5.8GHz WLAN and 2.5/3.5/5.5GHz WiMAX bands. The over all size of the antenna is 29mm x 38mm. A CPW-fed modified Koch snowflake slot antenna operating over a dual wide frequency bands covering the WLAN and WiMAX bands are also designed.

The second type of antenna designed is a UWB slot antenna which employs a near-rectangular slot with a tapered tuning stub. The antenna operates from 2.9 to 11GHz and is only 20mm in width. The antenna performance is found

to be tolerant to any changes in the length of the ground conductor and finds applications in wireless USB dongles. The antenna is further improved so as to coexist with the WLAN communication bands, by notching out the 5 to 6GHz frequencies.

4.2 Koch Fractal Slot Antenna

In this section, a Koch snowflake fractal shaped slot is employed for a compact and wide band operation covering 2.2 to 6.3GHz. The designed antenna is observed to have a relatively stable and omnidirectional radiation pattern throughout the operational band.

Design equations are empirically deduced relating the size of the slot with the lowest resonance of the operating band. The optimized dimensions of the tuning stub and the ground, for a wide band operation, are also presented. The validity of the derived equations are verified by designing the antenna on different substrates and when scaled for operation in different frequency bands.

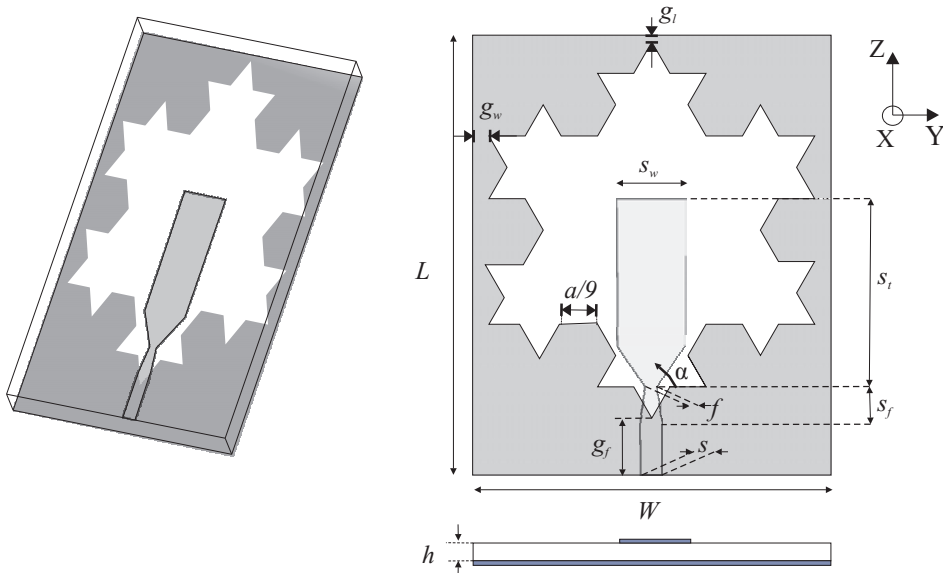


Fig. 4.1: Geometry of the Koch fractal slot antenna

4.2.1 Geometry

The geometry of the microstrip-fed Koch fractal based slot antenna is illustrated in Fig.4.1. The antenna is implemented on a low loss substrate of thickness h and permittivity ϵ_r . A Koch fractal slot is printed on one side of the substrate and is fed by a 50Ω microstrip line along with a tuning stub printed on the other side.

4.2.2 Simulation and Design

We begin this section with a detailed parametric study of the antenna performance for different iterations and sizes of the Koch fractal slot and for different ground plane sizes. It also looks at the effects of flaring the tuning stub. Based on this as well as the surface current and aperture field distribution on the antenna, design equations are derived.

4.2.2.1 Effect of the Fractal Geometry

The basic geometry of the slot is an equilateral triangle of side a , on which repeated iterations lead to the Koch snowflake geometry as shown in Fig.4.2. The simulated return loss of antenna I, with parameters as in Table 4.1 and dimensions in mm, for various iteration stages of the fractal geometry is plotted in Fig.4.3.

As can be observed, the resonant frequencies of the slot antenna decrease with the increase in the number of iterations. It is also noted that the Koch

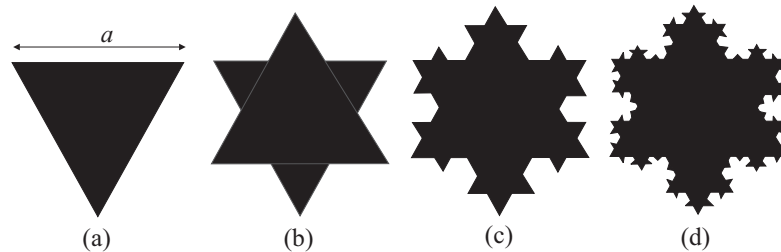
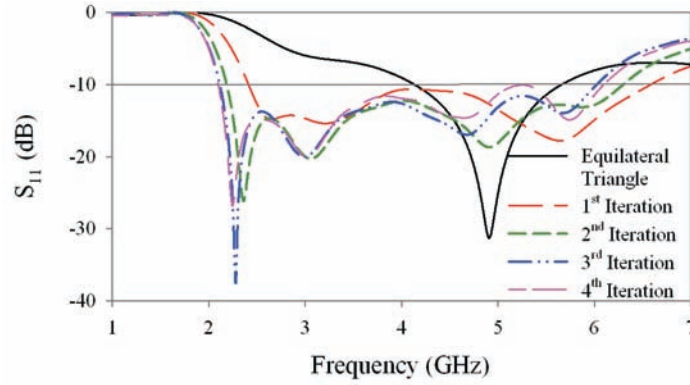


Fig. 4.2: Koch snowflake geometry in its different iteration stages (a) basic geometry, (b) 1st iteration, (c) 2nd iteration, and (d) 3rd iteration.

Table 4.1: Dimensions of the Koch slot antennas for different frequencies ($\epsilon_r=3.38$, $h=0.8\text{mm}$)

Ant.	W	L	a	s	g_l	g_w	g_f	s_w	s_f	s_t	f	α
I	29	38	28	1.8	0.6	0.5	5	7	3.7	17.3	1	60^0
II	20.5	27	19.5	1.8	0.6	0.5	5	5	3.0	12.6	0.6	57^0
II	47	57.5	45	1.8	0.6	0.5	5	12	5.3	26.4	1.2	60^0

fractal geometry improves the coupling between the feed stub and the slot, in turn enhancing the impedance bandwidth of the slot antenna. The operating band of the antenna shifts from 4.1 to 5.6GHz to 2.2 to 6.3GHz as the number of iterations increase to 2. Further increase in the iteration order is observed to cause only minor changes in the operating frequencies.

**Fig. 4.3:** Simulated return loss of the Koch fractal slot antenna for different iterations of the slot

4.2.2.2 Effect of Slot Size

To get further insight on the effect of slot geometry on the antenna performance, the proposed second iteration Koch slot antennas are designed with three different slot sizes, namely antennas I, II and III, as tabulated in Table 4.1. The return loss plotted in Fig.4.4 shows that over 90% bandwidth is observed for all the antennas and their first resonant frequency, f_{r1} is lowered from 3.9 to 1.5GHz as the size of the slot is increased from 19.5 to 45mms .

To understand the dependence of slot geometry on the antenna behavior, the surface current distributions on the antennas are plotted at f_{r1} , in

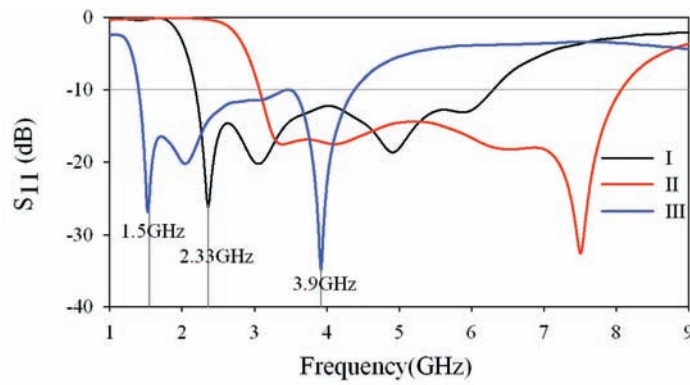


Fig. 4.4: Simulated return loss of the Koch fractal slot antenna for different sizes of the Koch slot

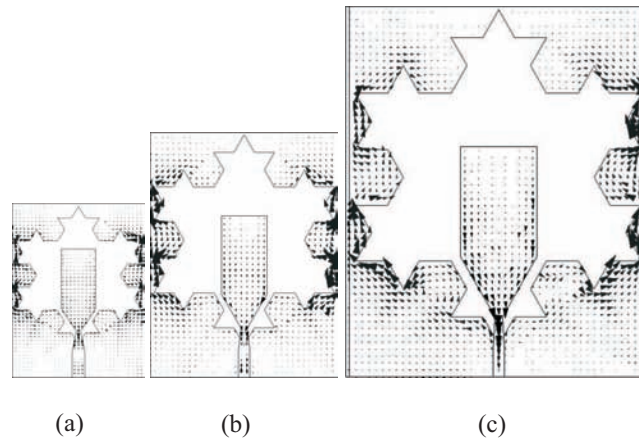


Fig. 4.5: Current distribution on (a) antenna II at 3.9GHz, (b) antenna I at 2.33GHz, and (c) antenna III at 1.5GHz

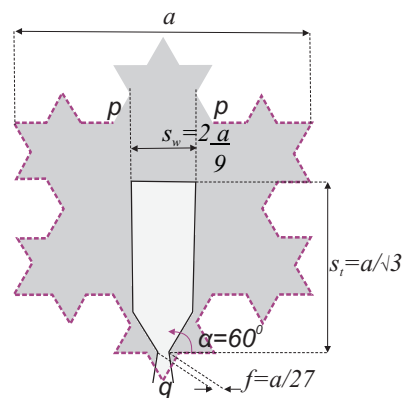


Fig. 4.6: Dimensions of the Koch slot antenna in terms of slot size 'a'

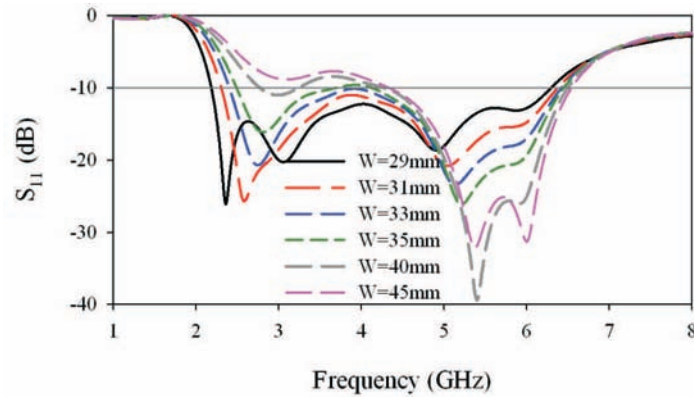


Fig. 4.7: The simulated return loss of the second iteration Koch slot (antenna I) for various ground widths W with rest of the parameters remaining same as in Table 4.1

Fig.4.5(a), (b) and (c). In all the cases, the surface current is observed to be following the fractal slot edges and a half wavelength variation in current is observed along the slot boundary ‘ pq ’ as shown in Fig.4.6.

4.2.2.3 Effect of Ground Size

Simulations indicate that the ground length L has minor influence on the antenna performance while the width W has a prominent effect on the wide band matching of the slot antenna. While g_l has almost negligible effect, length l_f is found to affect the antenna response when reduced to less than 4.0mm. Therefore, for the design of a compact antenna, the values of g_l and l_f are fixed at 0.5mm and 5mm respectively.

Fig.4.7 plots the variation in the return loss of antenna I as W is varied over a range from 29mm to 45mm with rest of the parameters remaining same as in Table 4.1. It is observed that as the width reduces, the impedance matching at the lower frequencies improve. The value of g_w of the antenna is fixed at 0.5mm for an optimum performance in terms compact size and broad bandwidth.

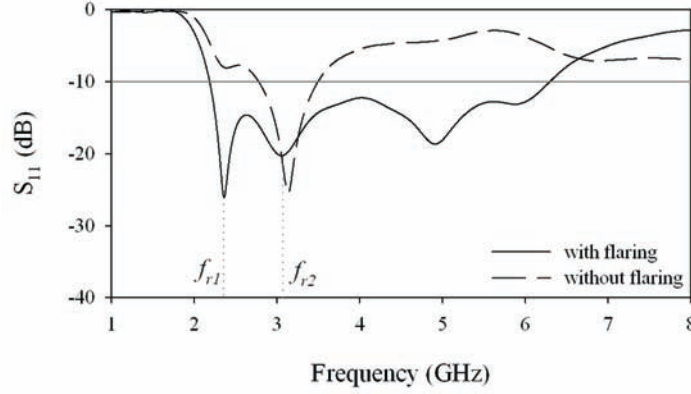


Fig. 4.8: The simulated return loss of second iteration Koch slot (antenna I) with ($\alpha=90^\circ$) and without ($\alpha=0^\circ$) the flaring in the tuning stub

4.2.2.4 Effect of Tuning Stub

Fig.4.8 plots the effect of flaring of tuning stub on the return loss of the antenna. It is observed that a broad impedance bandwidth is observed when the flare angle α is 60° . In the proposed design, a second resonance observed at f_{r2} , is similar to that of a quarter wave monopole where the stub length s_t corresponds to approximately $\lambda/4$ and is computed as

$$f_{r2} = \frac{c}{4s_t\sqrt{\epsilon_{eff}}} \quad (4.1)$$

where $\epsilon_{eff} \approx (\epsilon_r + 1)/2$ and c is the speed of light.

The flaring of the tuning stub guarantees a smooth change in impedance from one resonant mode to the other. With this a smooth transition between the resonances at f_{r1} and f_{r2} and its higher order modes, a wide band operation of the antenna is achieved.

4.2.2.5 Aperture Electric Fields

The aperture field plotted at f_{r1} , f_{r2} and at higher resonances corresponds to different modes of field distribution. The field distributions shown in Fig. 4.9(a) and (b), at $f_{r1}=2.4\text{GHz}$ and $f_{r2}=3\text{GHz}$, are the fundamental modes excited in the antenna. This conforms with the simulation studies carried out

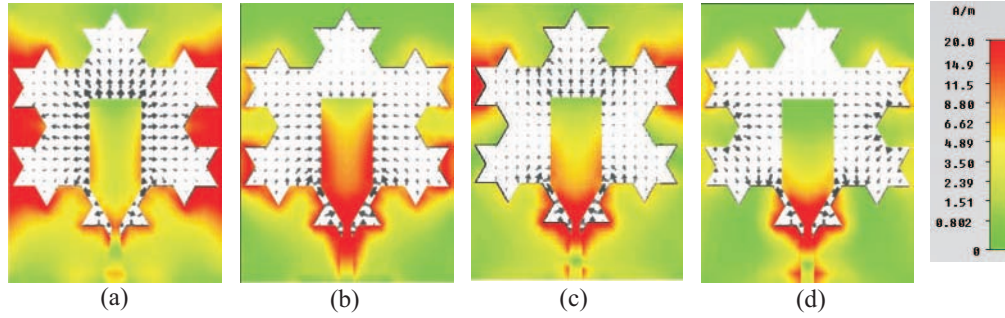


Fig. 4.9: Electric field in the antenna aperture and their surface current distributions at (a) 2.4GHz, (b) 3GHz, (c) 4.95GHz and (d) 6GHz

in the previous sections, where resonance at f_{r2} is by virtue of the tuning stub acting like a quarter wave monopole and f_{r1} is due to slot boundary surrounding the stub.

Their higher derivatives are excited at 4.95GHz and 6GHz and are shown in Fig.4.9(c) and (d). Strong Y-field components on either sides of the stub cancel in the far field for all cases resulting in linear polarization along the Z-axis.

4.2.2.6 Design

Based on the above observations, equations for designing the wide band Koch slot antenna are summarized as follows

- Feed line: Choose the width of the microstrip feed line s for 50Ω impedance on a substrate with permittivity ϵ_r and thickness h .
- Slot Geometry: For the desired frequency band of operation, calculate the slot dimension a . With reference to Fig.4.6, the boundary of the slot (pq) and the wavelength (λ_{r1}) at the first resonant frequency f_{r1} of the antenna is related as

$$\lambda_{r1} = 2pq. \quad (4.2)$$

The fractal nature of the slot enables deduction of the boundary pq in terms

of the side a of the basic equilateral triangle geometry as

$$pq = \frac{20a}{9}. \quad (4.3)$$

Corresponding to the first resonance frequency f_{r1} , a can be computed from the following equation after substituting eqn.(4.3) in eqn.(4.2),

$$a = \frac{67.5}{f_{r1}}. \quad (4.4)$$

where a is in mm and f_{r1} is in GHz.

- Ground: Based on the simulation studies, the dimensions are fixed for optimum performance as below,

$$\begin{aligned} g_l = g_w &= 0.5mm \\ g_f &= 5mm. \end{aligned} \quad (4.5)$$

- Tuning Stub: The dimensions of the tuning stub is also deduced in terms of the slot dimension a and shown in Fig.4.6 as

$$\begin{aligned} s_t &= \frac{a}{\sqrt{3}} \\ s_f &= \frac{\sqrt{3}a}{18} \\ s_w &= \frac{2a}{9} \\ f &= \frac{a}{27} \\ \alpha &= 60^\circ. \end{aligned} \quad (4.6)$$

Using the parameters so computed, antennas designed on different substrates and for different frequencies are tabulated in Table 4.2 where all dimensions are in mm. The computed dimensions are optimized slightly for wide band matching by simulations and their return losses are plotted in Fig.4.10. As noted in Table 4.2 and Fig. 4.10, the resonances of these antennas, especially

Table 4.2: Dimensions of the Koch slot antenna ($g_l=g_w=0.5\text{mm}$, $g_f=5\text{mm}$) with a comparison between the computed (Cp.) and optimized (Op.) parameters

Ant.	ϵ_r	WXL	a	h	s	s_t		s_w		s_f		f		α		$f_{r1}(\text{GHz})$		$f_{r2}(\text{GHz})$		band (GHz)
						Cp.	Op.	Cp.	Op.	Cp.	Op.	Cp.	Op.	Cp.	Op.	Cp.	Op.	Cp.	Op.	
I	3.38	29X38	28	0.8	1.8	16.2	17.3	6.2	7	2.7	3.7	1	1	60	60	2.4	2.36	2.92	3.05	2.15-6.3
II	3.38	20.5X27	19.5	0.8	1.8	11.2	12.6	4.3	5	1.9	3	0.7	0.6	60	57	3.4	3.38	4.1	4.11	3-8.1
III	3.38	47X57.5	45	0.8	1.8	26	26.4	10	12	4.3	5.3	1.7	1.2	60	60	1.5	1.53	1.9	2.04	1.4-4.3
IV	2.3	29X38	28	0.8	2.4	16.2	17.9	10	7	2.7	5.3	1	1	60	60	2.4	2.43	3.3	3.1	2-2-7
V	2.65	29X38	28	1	2.8	16.2	17.9	6.2	7	2.7	3.7	1	1	60	60	2.4	2.4	3.1	2.82	2.18-6.5
VI	3.38	29X38	28	1.6	3.6	16.2	16.3	6.2	7	2.7	3.7	1	1	60	60	2.4	2.4	3.1	3	2.15-5.9
VII	4.4	29X38	28	0.8	1.5	16.2	16.8	6.2	6.6	2.7	3.7	1	1.2	60	62	2.4	2.31	2.71	3.15	2.15-6.1

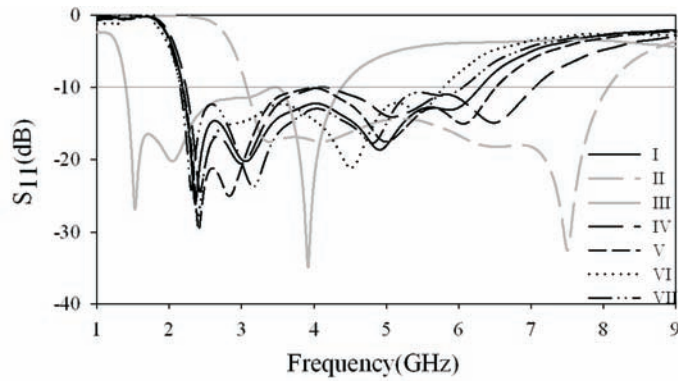


Fig. 4.10: Simulated return loss of the antennas in Table 4.2

f_{r1} , show only slight deviation from the computed values and there is wide impedance matching throughout the band.

4.2.3 Measurements

A prototype of the antenna I is fabricated on a substrate of $\epsilon_r=3.38$, $h=0.8\text{mm}$ with the parameters given in the Table 4.2 and its impedance and radiation characteristics were measured. The antenna return loss is plotted in Fig.4.11 with simulated results and it shows good agreement. The 10dB bandwidth of the antenna is from 2.33GHz to 6.19GHz with resonances at 2.45GHz, 3.2GHz and 5.4GHz. Thus the antenna covers the 2.4 to 2.484GHz, 5.15 to 5.35GHz, and 5.725 to 5.825GHz WLAN bands, and the 2.5 to 2.69GHz, 3.4 to 3.69GHz,

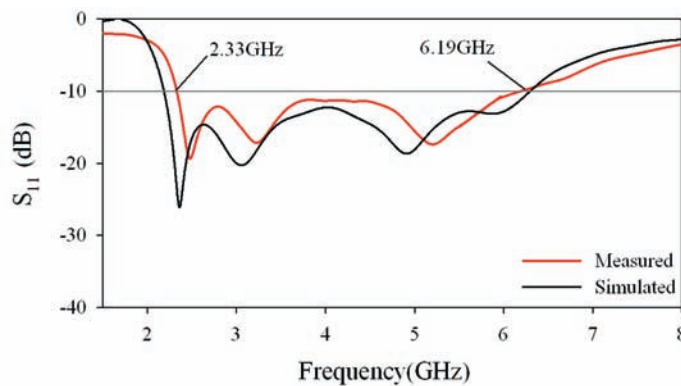


Fig. 4.11: Measured return loss of the Koch slot antenna

and 5.25 to 5.85GHz WiMAX bands.

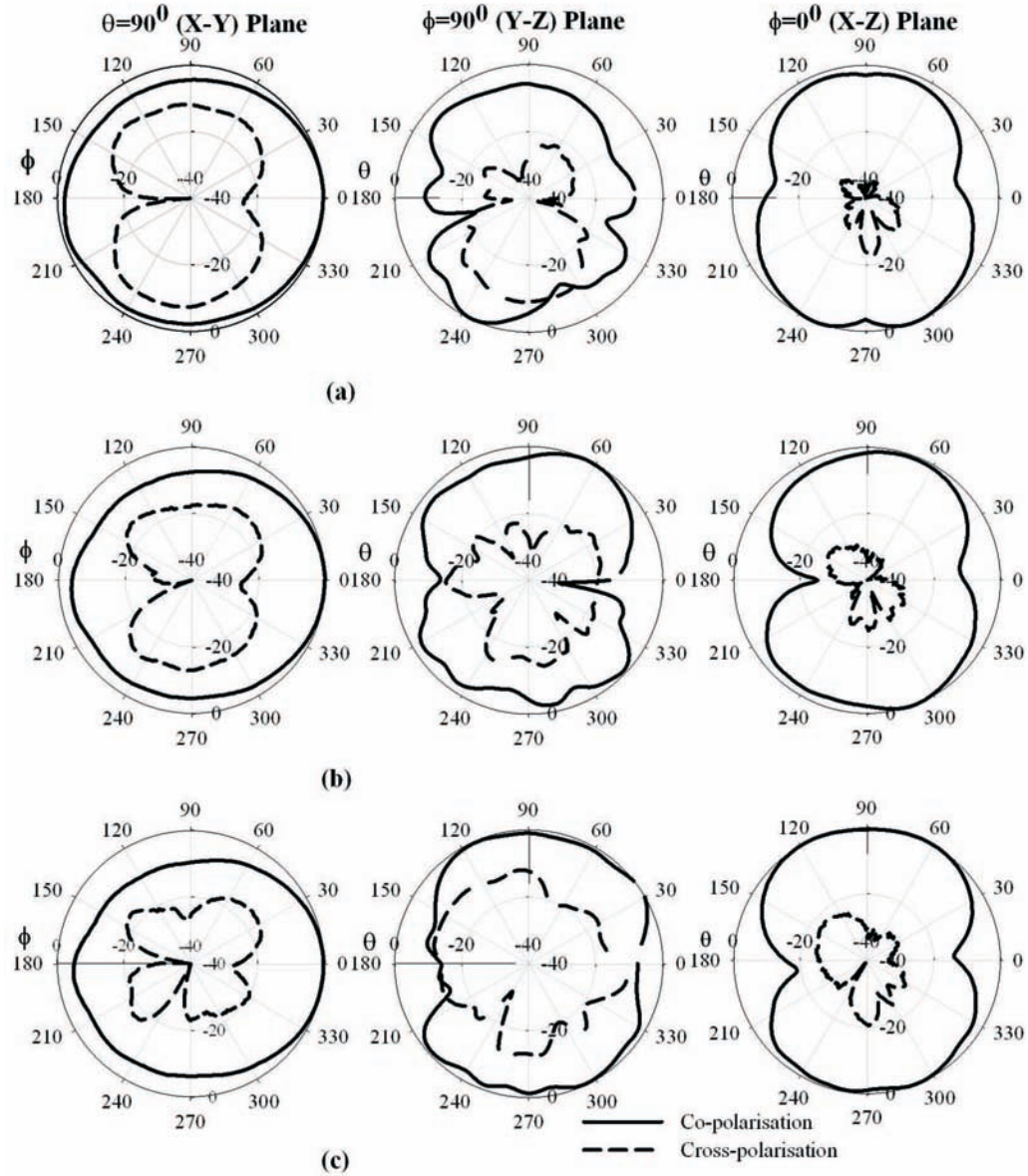


Fig. 4.12: Measured radiation pattern of the Koch slot antenna at (a) 2.45GHz (b) 3.2GHz and (c) 5.4GHz

The measured radiation patterns of the antenna in the X-Y, Y-Z and X-Z planes of the antenna for three different frequencies are shown in Fig.4.12. The patterns are stable throughout the band and are omnidirectional in the azimuthal plane (X-Y) and bidirectional in the elevation planes (Y-Z and X-

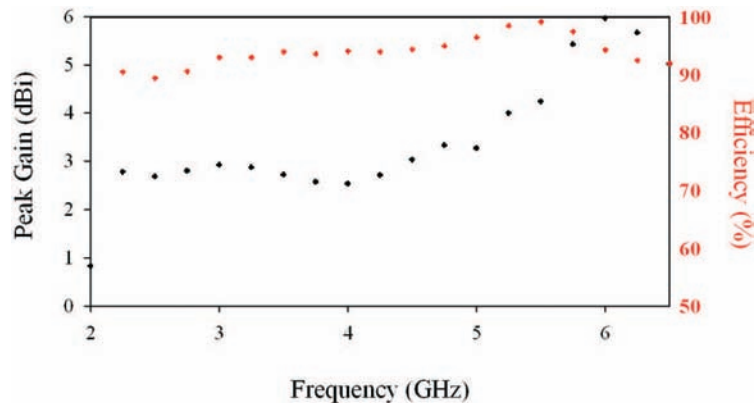


Fig. 4.13: Measured peak gain and radiation efficiency of Koch slot antenna

Z) throughout the band. Polarization of the antenna is along the Z direction. Cross-polarization is observed in the X-Y plane due to the strong horizontal component of aperture electric field.

Measured peak gain of the antenna is plotted in Fig.4.13 along with its radiation efficiency. The plots show that the gain remains above 2.0dBi and also indicates that the antenna radiation efficiency is greater than 90% throughout the operating band.

4.2.4 Dual-band Modified Koch Fractal Slot Antenna

In this section, we present a CPW-fed modified Koch snowflake slot antenna operating over dual frequency bands. The CPW feed makes them more suitable for compact wireless communication devices owing to its features like uni-planar structure, easy fabrication and circuit integration.

Even though a wide-band antenna operating from 2.3 to 6GHz is sufficient, a dual band antenna design would significantly relax the requirements imposed upon the filtering electronics within the wireless device for multi-band applications and would be cost-effective. A half wavelength tuning slot is integrated with the wide-band Koch slot antenna for the filter action. This way the antenna achieves dual wide-band operation satisfying the WLAN and WiMAX bands simultaneously along with a compact profile by virtue of the

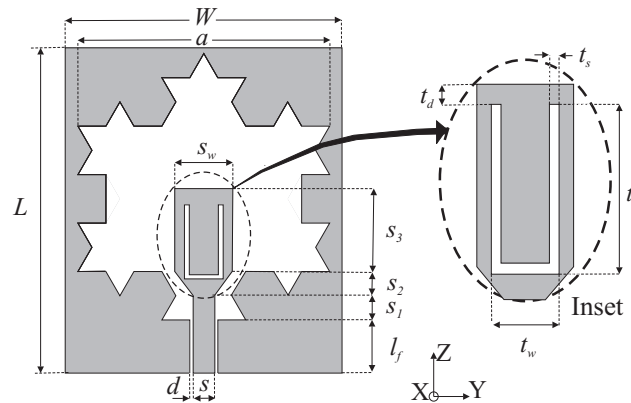


Fig. 4.14: Geometry of the CPW-fed modified Koch fractal slot antenna

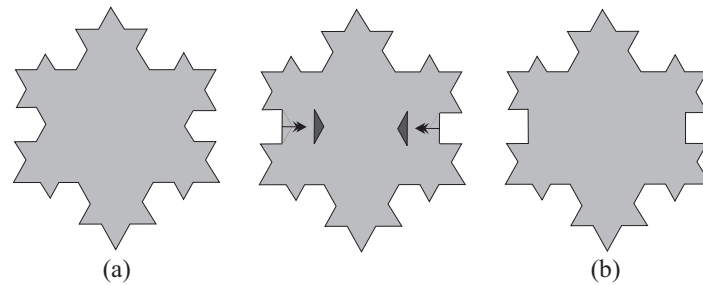


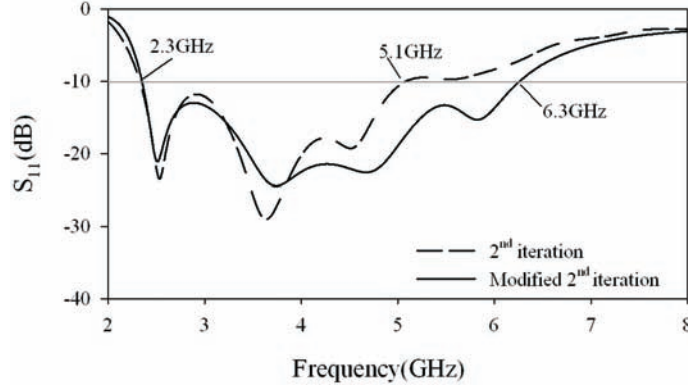
Fig. 4.15: Evolution from (a) the 2^{nd} iteration Koch slot to (b) the modified 2^{nd} iteration Koch slot

Koch fractal based slot geometry.

The configuration of the proposed modified Koch slot antenna for dual band operation is illustrated in Fig.4.14. The modified Koch snowflake slot is fed by a 50Ω CPW feed along with a tuning stub embedded with a U-shaped slot. The antenna is implemented on a low loss substrate of relative permittivity ϵ_r and thickness h . Fig.4.15 shows the evolution of the modified Koch slot from the 2^{nd} iteration Koch slot. It is observed that with the modified slot, the operating bandwidth of the antenna is improved from 2.3 to 5.1 to 2.36 to 6.26GHz as shown in Fig.4.16. The antenna parameters are tabulated in Table 4.3 where all dimensions are in mm.

Table 4.3: Dimensions of the CPW-fed Koch slot antenna

ϵ_r	W	L	h	a	l_f	d	s	s_1	s_2	s_3	s_w
4.4	28.5	33.5	1.6	26	5.5	0.35	2.2	2.5	2.5	9.1	6.2

**Fig. 4.16:** Simulated return loss of the CPW-fed Koch slot antenna and the CPW-fed modified Koch slot antenna

4.2.4.1 Modified Koch Slot Antenna with a Narrow Slot Resonator

A half wavelength U-slot etched out on the tuning stub of the wide-band antenna notches out the corresponding frequency (f_{notch}) leading to a dual wide-band operation. Fig.4.17 plots the simulated return loss of the antenna for different slot lengths. As the length of the slot increases from 19.6mm ($t_l = 7.8$ mm) to 21.6mm ($t_l = 9.3$ mm), the notched frequency shifts from 5.0 to 4.3GHz, following the eqn.(4.7).

$$s_l \approx \frac{c}{2f_{notch}\sqrt{\epsilon_{eff}}} \quad (4.7)$$

where $\epsilon_{eff} \approx (\epsilon_r + 1)/2$ and c is the speed of light.

4.2.4.2 Measurements

The simulated and measured return loss of the antenna plotted in Fig.4.18, show good agreement. The -10dB bandwidth of the wide-band antenna (without the slot) is 3.77GHz (2.33 to 6.1GHz). With the tuning slot, the antenna gives dual wide-band performance with a -10dB bandwidth of 1.57GHz in

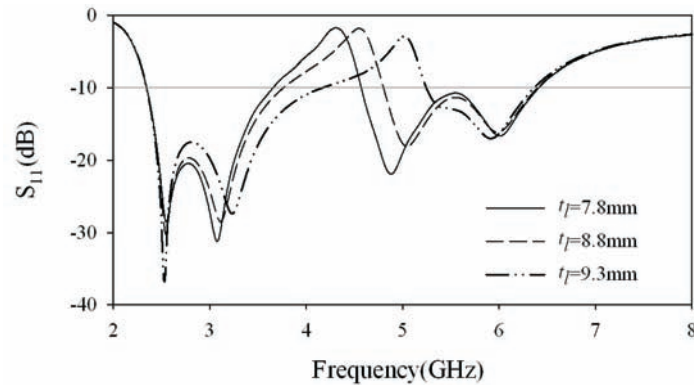


Fig. 4.17: Simulated return loss of the antenna for different slot resonator lengths (t_l) with $t_w=4\text{mm}$ and $t_s=0.5\text{mm}$ and rest of the parameters as in Table. 4.3

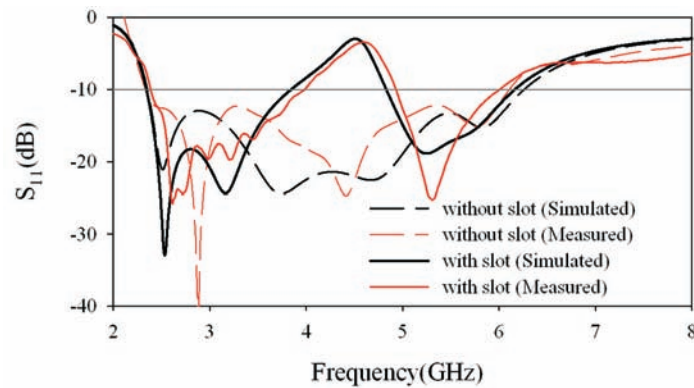


Fig. 4.18: Measured return loss of the antenna with and without the slot with $t_l=8.8\text{mm}$, $t_w=4\text{mm}$, $t_s=0.5\text{mm}$ and rest of the parameters as in Table. 4.3

the lower band (2.38 to 3.95GHz) and 1.1GHz in the upper band (4.95 to 6.05GHz). Thus, it covers the 2.4 to 2.484GHz, 5.15 to 5.35GHz, and 5.725 to 5.825GHz WLAN bands, and the 2.5 to 2.69GHz, 3.4 to 3.69GHz, and 5.25 to 5.85GHz WiMAX bands.

4.3 UWB Slot Antenna

In this section, a compact UWB printed slot antenna is described, suitable for integration with the printed circuit board (PCB) of a wireless, universal, serial-bus (WUSB) dongle. The design comprises of a near-rectangular slot fed by a CPW printed on a PCB of size $20 \times 30\text{mm}^2$. It has a large bandwidth covering

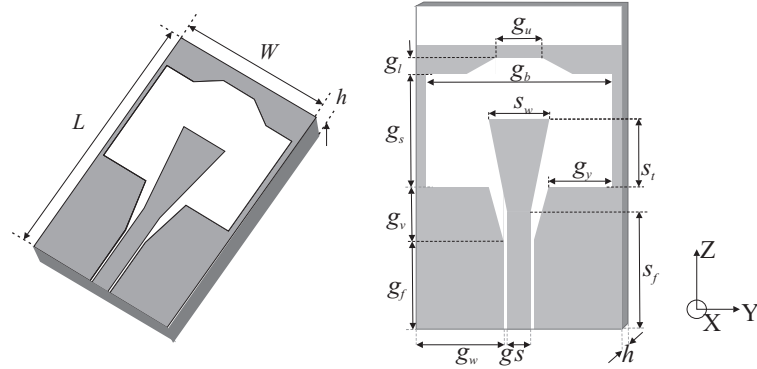


Fig. 4.19: Geometry of the CPW-fed UWB slot antenna

Table 4.4: Dimensions of the CPW-fed UWB slot antenna

ϵ_r	W	L	h	g_u	g_b	g_l	g_s	g_r	g_f	s	g	g_y	s_t	s_w	s_f
4.4	20	29	1.6	4.7	18	1.7	11.5	5.5	9	2.4	0.3	6.5	7	6.2	12

the 3.1 to 10.6GHz UWB band, with omnidirectional radiation patterns.

Further, a notched band centered at 5.45GHz WLAN bands is obtained within the wide bandwidth by inserting a narrow slot inside the tuning stub. Details of the antenna designed are described and measured results of the fabricated prototype are discussed.

4.3.1 Geometry

Fig.4.19 shows the geometry of the slot antenna. The antenna consists of a near-rectangular aperture etched out from the ground plane of a PCB and a CPW-fed tapered tuning stub. The CPW feed is designed for 50Ω on FR4 substrate with $\epsilon_r=4.4$ and thickness $h=1.6\text{mm}$. Since the feed and the ground are implemented on the same plane, only one layer of substrate with single-sided metallization is used, making the antenna easy and cost-effective to manufacture.

4.3.2 Simulation and Design

The simulated return loss of the designed slot antenna with parameters as in Table. 4.4 is plotted in Fig.4.20. It indicates that the antenna covers the 3.1 to

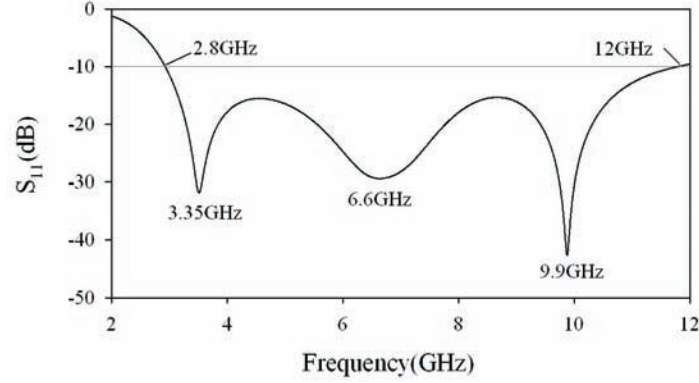


Fig. 4.20: Simulated return loss of the antenna with the parameters as in Table. 4.4

10.6GHz UWB frequencies with three distinct resonances, 3.35GHz, 6.5GHz and 10GHz. A smooth transition from one antenna mode to another enables a wide band impedance matching. In this case, it is achieved by tapering the tuning stub and by smoothening the slot boundary especially near the feed and at the top of the tuning stub.

The surface current distribution on the antenna along with its aperture electric field at its resonances are plotted in Fig.4.21. It indicates that the first resonance (at 3.35GHz) is due to the slot geometry since longest current path is following the slot boundary. A half wavelength variation is observed along the slot boundary ‘*ab*’ (shown in Fig.4.21(a)) and follows eqn.(4.8).

$$ab = \frac{\lambda_{o1}}{2\sqrt{\epsilon_{eff}}} \quad (4.8)$$

where λ_{o1} is the free space wavelength at the first resonance and $\epsilon_{eff} \approx (\epsilon_r + 1)/2$.

The second resonance (at 6.6GHz) is due to the monopole like behavior of the tuning stub as in eqn.(4.9).

$$s_t = \frac{\lambda_{o2}}{4\sqrt{\epsilon_{eff}}} \quad (4.9)$$

where λ_{o2} is the free space wavelength at the second resonance. The third resonance (at 9.9GHz) is observed to be a higher order mode which is confirmed

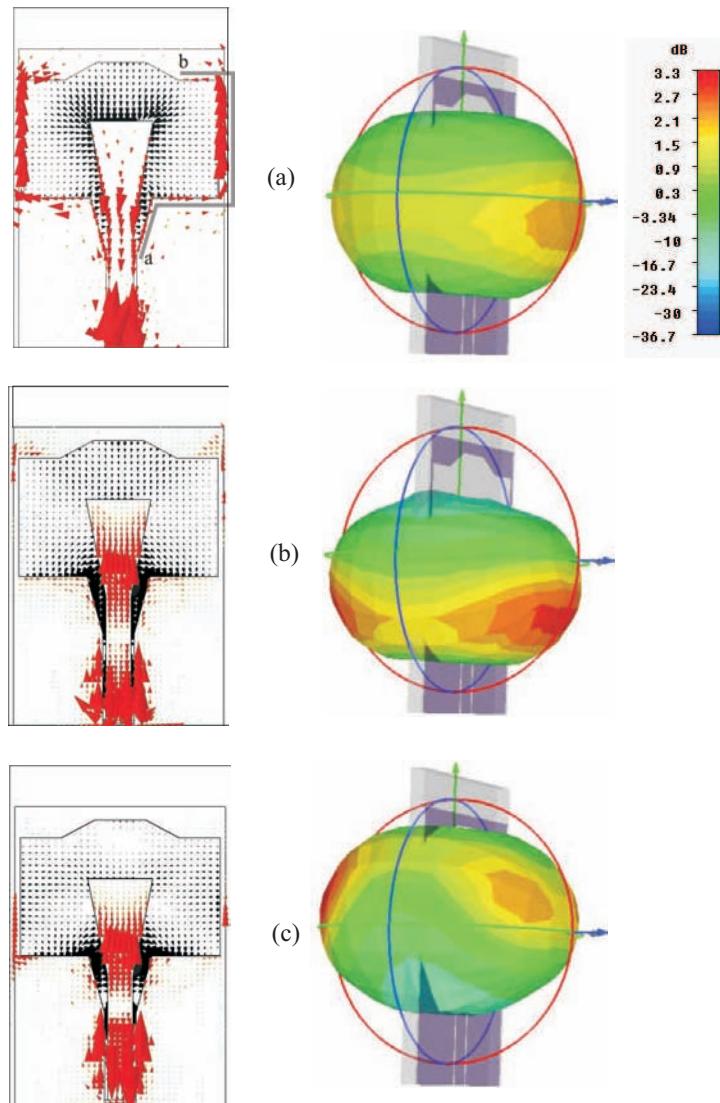


Fig. 4.21: Surface current distribution and aperture electric field of the slot antenna at (a) 3.35GHz, (b) 6.6GHz and (c) 9.9GHz

from the aperture field distribution as plotted in Fig.4.21(c).

The overall size of the proposed UWB antenna is compact ($20 \times 30 \text{mm}^2$) with its width comparable with practical, wireless USB dongles. However, while integrating the UWB antenna with the system ground plane of USB dongles, with lengths typically ranging at 70mm, generally the antenna performance gets de-tuned. Hence to prove the suitability of the proposed design for WUSB applications, the effect of the ground plane length on the antenna

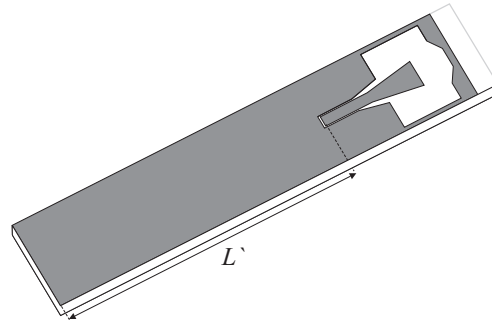


Fig. 4.22: The UWB slot antenna integrated with the system ground plane of USB dongles

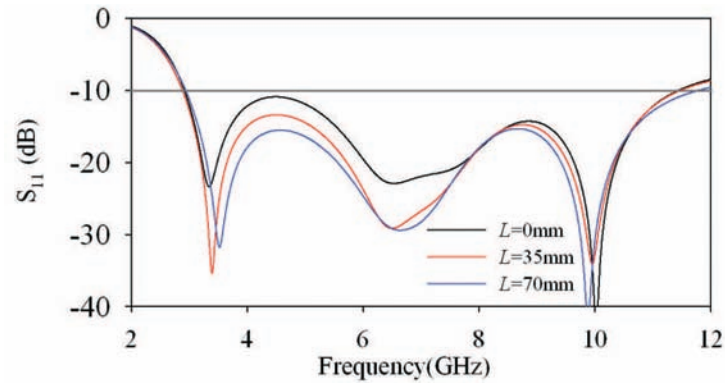


Fig. 4.23: The return loss of the UWB slot antenna for different ground lengths L'

needs to be studied.

Fig.4.23 plots the return loss of the antenna for different ground lengths (L') as shown in Fig.4.22. It shows that there is negligible variation in the matching and the impedance bandwidth of the antenna for different values of L' . Fig.4.24(a-c) plots the surface current distribution on the antenna integrated with the PCB of a USB dongle. It is observed that the majority of the electric currents are concentrated around the slot with very little current on the rest of the ground plane. As a result, the performance of the antenna is insensitive to the system ground plane of the USB.

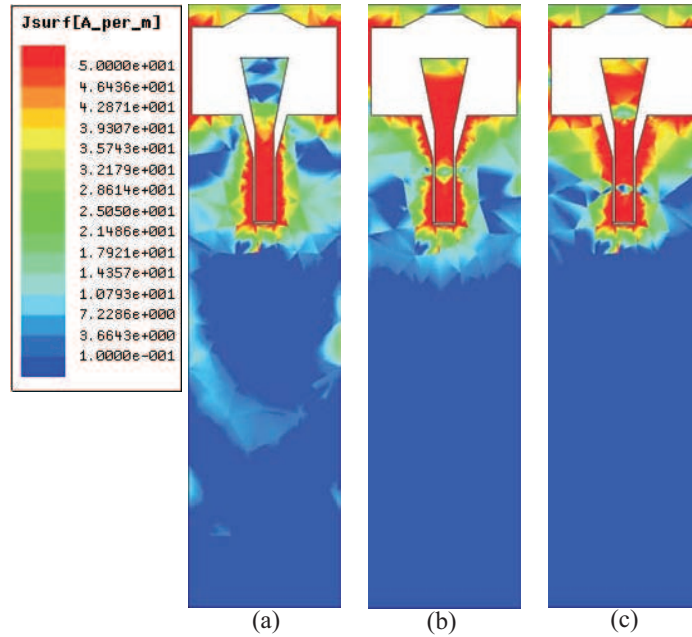


Fig. 4.24: The surface current intensity distribution on UWB slot antenna with $L'=75\text{mm}$ at (a) 3.3GHz, (b) 6.5GHz, (c) 10GHz

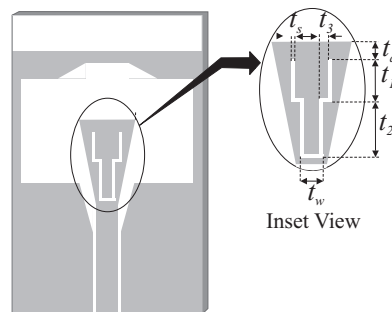


Fig. 4.25: The UWB slot antenna with a slot resonator inscribed with $t_s = 0.3\text{mm}$, $t_d = 1.4\text{mm}$, $t_w = 1.8\text{mm}$, $t_l = 3.3\text{mm}$, $t_2 = 4.2\text{mm}$, $t_2 = 1.8\text{mm}$ and the rest of the parameters as in Table 4.4

4.3.2.1 Band-notched UWB Slot Antenna

A narrow half wavelength slot embedded in the tuning stub is incorporated in the design to notch out the undesired WLAN frequencies in the 5.15 to 5.825GHz band as shown in Fig.4.25. Fig.4.26 which plots the simulated return loss of the UWB slot antenna with the narrow slot inscribed shows good rejection with a VSWR > 9 observed at 5.5GHz.

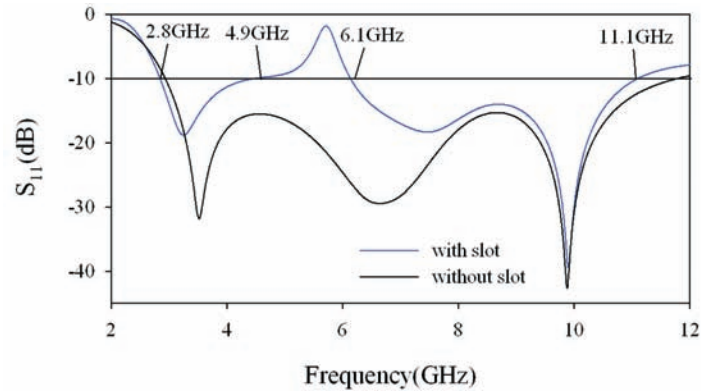


Fig. 4.26: The simulated return loss of the UWB slot antenna with the narrow slot inscribed in the tuning stub

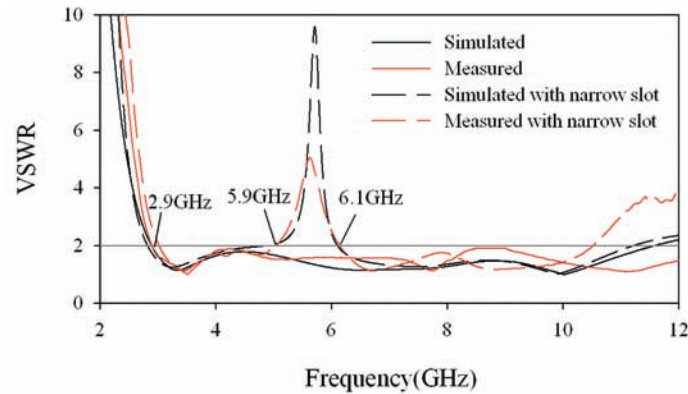


Fig. 4.27: The measured return loss of UWB slot antenna

4.3.3 Measurements

The measured VSWR of this antenna with and without the slot in the tuning stub is plotted in Fig.4.27 and is validated with the simulated results. The VSWR characteristics reveal UWB behavior with a 2:1 VSWR bandwidth from 2.9GHz to 11GHz. When the slot is introduced in the tuning stub a high VSWR (> 4) occurs at around 5.5GHz. In the pass band, the VSWR of the antenna is only slightly affected by the presence of the slot in the tuning stub.

The measured radiation patterns in the X-Y, Y-Z and X-Z planes of the antenna for three different frequencies are shown in Fig.4.28. The patterns are stable throughout the band and resembles that of a monopole; omnidirec-

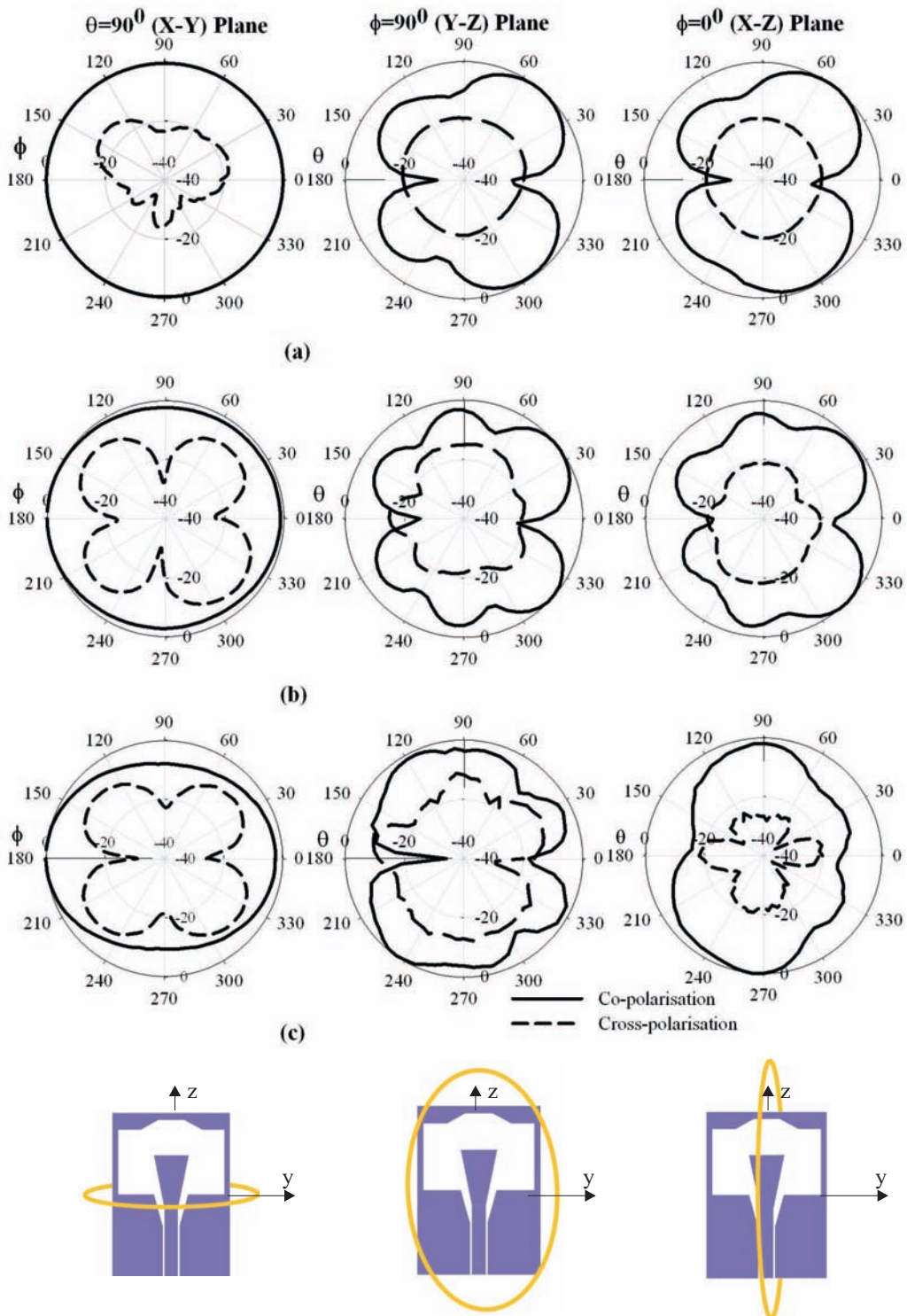


Fig. 4.28: The measured radiation patterns at (a) 3.35GHz, (b) 6.5GHz and (c) 10GHz of the UWB slot antenna

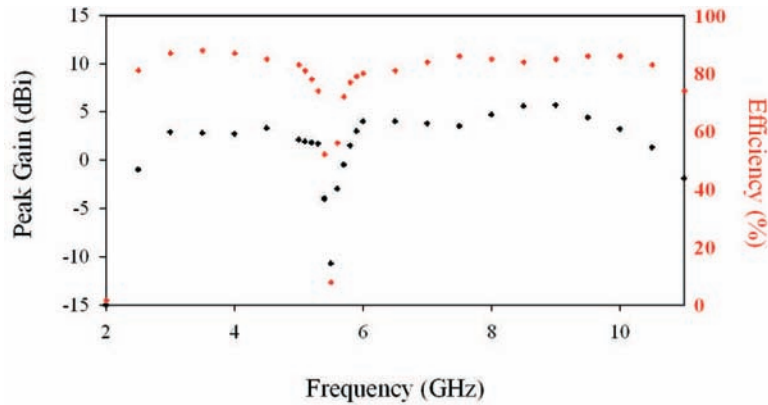


Fig. 4.29: The measured gain and radiation efficiency of band-notched UWB slot antenna

tional in the H-plane (X-Y) and bidirectional in the E-planes (Y-Z and X-Z) throughout the band. Polarization of the antenna is along the Z direction.

Measured peak gain of the antenna is plotted in Fig.4.29 along with the radiation efficiency. The plots show a peak gain above 2dBi throughout the band except at the notched frequency where it is as low as -13dB while the radiation efficiency is more than 85% in the pass band.

4.4 Chapter Summary

Two types of broadband slot antennas, (a) Koch fractal slot and (b) UWB slot antenna, are presented in this chapter. The compact Koch fractal slot antenna is designed to operate 2.3 to 6.2GHz. Simulated results showed that the introduction of a Koch fractal slot instead of the triangular slot geometry lowers the frequency of operation. Use of a compact ground plane improves the coupling between the slot and feed line along with a reduction in the overall size of the antenna. Wide band matching is ensured by an optimized tapered tuning stub.

Empirical equations are deduced and validated to design the Koch slot antenna on different substrates. Measured results indicate a large impedance bandwidth with relatively stable and omnidirectional radiation patterns which

makes the design suitable for broadband wireless communication applications. The bandwidth of the antenna is wide enough for WLAN 2.4/5.2/5.8GHz and WiMAX 2.5/3.5/5.5GHz operations.

A CPW-fed modified Koch fractal printed slot antenna is presented next. The antenna has the advantage of CPW feed and the 2nd iteration Koch slot is modified for a bandwidth covering 2.3 to 6.3GHz. A half wavelength tuning slot is integrated within the wide-band Koch slot antenna for the filter action which in this case is optimized to notch out 4 to 5GHz. This way the antenna achieves dual wide-band operation satisfying the WLAN (2.4 to 2.48GHz, 5.15 to 5.35GHz in the United States and 5.725 to 5.825GHz in Europe) and WiMAX bands (2.5 to 2.69GHz/ 3.4 to 3.69GHz/ 5.25 to 5.85GHz bands) simultaneously along with a compact profile by virtue of the Koch fractal based slot geometry.

In the final section, a compact UWB slot antenna fed by a CPW suitable for wireless USB dongle applications is presented. The impedance bandwidth of the designed antenna ranges from 2.9 to 11GHz. A half-wave length slot inscribed on the tuning stub is also incorporated in the design to notch out the 5.4GHz WLAN band. The antenna features all the desirable characteristics demanded by UWB communication systems such as adequate impedance bandwidth and stable radiation patterns throughout the ultra-wide band. In addition to compact size, the antenna is insensitive to ground plane length variations, making it suitable for WUSB dongle and mobile UWB applications.

However, to ascertain the performance of the antenna for transmission of short UWB pulses of nano-seconds duration, the UWB slot antenna needs to be analyzed in time domain. This aspect of the antenna is studied in detail in Chapter 5.

Transient Analysis

Contents

5.1 Spatio-Temporal Transfer Characteristics	127
5.2 Antenna Transfer Function	128
5.2.1 Simulation Study	128
5.2.2 Measurements with the Prototype Antennas	133
5.3 Impulse Response and UWB Quality Measures . . .	136
5.4 Pulse Distortion Analysis	138
5.5 Chapter Summary	142

In this chapter, the transfer characteristics and the transient responses of the UWB planar antennas described in Chapters 3 & 4 are investigated and compared. These antennas are well-matched in the 3.1 to 10.6GHz communication bands. Since they may behave differently while transmitting/receiving large fractional bandwidth pulses, their time-domain studies are of extreme importance for high speed pulsed communications. The theory behind the simulations and measurements are discussed in Chapter 2. Measurements are performed in the azimuth and elevation planes and are verified with the simulations carried out using CST-Microwave Studio[®].

5.1 Spatio-Temporal Transfer Characteristics

In this thesis, three UWB antenna designs and their 5 to 6GHz band-notched versions, namely, the elliptical monopole, the printed inverted cone (PIC)

monopole and the slot antennas are optimized to have an impedance bandwidth wide enough to cover the 3.1 to 10.6GHz UWB frequencies. Their design aspects are discussed in Chapter 3 & 4. In this chapter they are assessed for their suitability for pulsed UWB applications by examining their transient responses.

With the transfer function characterization process, the transient response of the antenna is analyzed and the effects of the antenna on the waveform of the transmitted pulse are predicted. Efforts can be made on the transceiver circuit side to compensate for any unwanted effects caused by antenna. For example, in the receiver circuit, the gain of the low noise amplifier can be increased at a certain frequency range, where the magnitude of the antenna transfer function is relatively low. It is even possible to pre-distort the waveform in the transmitter circuit in such a manner that, when the distorted pulse passes through the antenna, it is distorted for the second time in such a way that its original waveform is recovered.

5.2 Antenna Transfer Function

With the antenna modeled as an LTI filter, the transfer characteristics which holds the complete information of the antenna performance, is investigated in this section. As discussed in Section 2.2.3, the frequency domain parameters of the antenna, namely gain and group delay, are then deduced from its receive transfer function $H_{RX}(\omega)$.

5.2.1 Simulation Study

Fig.5.1 shows the plot of the transfer function magnitudes ($|H_{RX}(\omega)|$ in dB), derived from simulations as described in Section 2.2 of Chapter 2. The plot has different orientation angles; $\phi = 0^\circ$ to 360° at $\theta = 90^\circ$ for the azimuth and $\theta = 0^\circ$ to 360° at $\phi = 0^\circ$ for the elevation planes; that are depicted on the horizontal axis and frequencies are marked on the vertical axis. Since the

antenna radiation properties are directly proportional to its transfer characteristics, this plot provides a two-dimensional evaluation of the antenna radiation along its different orientations over the entire range of operating frequencies.

As can be observed from the plots in the azimuthal planes, the designed antennas are omnidirectional for frequencies below 7GHz. The doughnut shape is confirmed from the elevation plane plot which shows a wide angular coverage with nulls at $\theta = 0^\circ$ and $\theta = 180^\circ$. The transfer function magnitudes of band-notched designs in Fig.5.1(b),(d), and (f) show clear nulls, over all orientation angles, at the notched frequencies in the 5 to 6GHz WLAN bands.

However, some of the designed antennas have squinted radiation properties at the higher frequencies. Especially in case of the elliptical monopole antennas (Fig.5.1(a)&(b)) where sharp nulls are observed for frequencies $> 7\text{GHz}$ between $\phi=30^\circ$ to 150° and $\phi=210^\circ$ to 330° in the azimuth. The rest of the antennas show nulls around $\phi=90^\circ$ and 270° at the higher end of the spectrum. The inverted cone monopole antenna shows a constant magnitude of the transfer function almost through out the UWB spectrum except for frequencies $> 10\text{GHz}$.

To get an insight into the antenna performance, the antenna gain and group delay, deduced as in eqn.(2.22) and (2.23) of Chapter 2, are plotted in Fig.5.2 and Fig.5.3. More than 10dB reduction in the antenna gain is recorded in the 5 to 6GHz band of the band-notched designs as shown in Fig.5.2(b),(d), and (f). Corresponding discontinuity is observed in the group delay plots Fig.5.3(b),(d), and (f).

Peak gains of 4dBi, 2.0dBi and 3dBi are observed in the Fig.5.2, for the elliptical monopole, the inverted cone monopole and the slot antenna designs respectively and they compare well with their corresponding measured peak gains reported in Chapters 3 & 4. The designed antennas show a group delay response within the range of $\pm 0.3\text{nS}$ over the entire operating frequency range. It can be noted that the inverted cone monopole antenna exhibits a uniform group delay as shown in Fig.5.3(c).

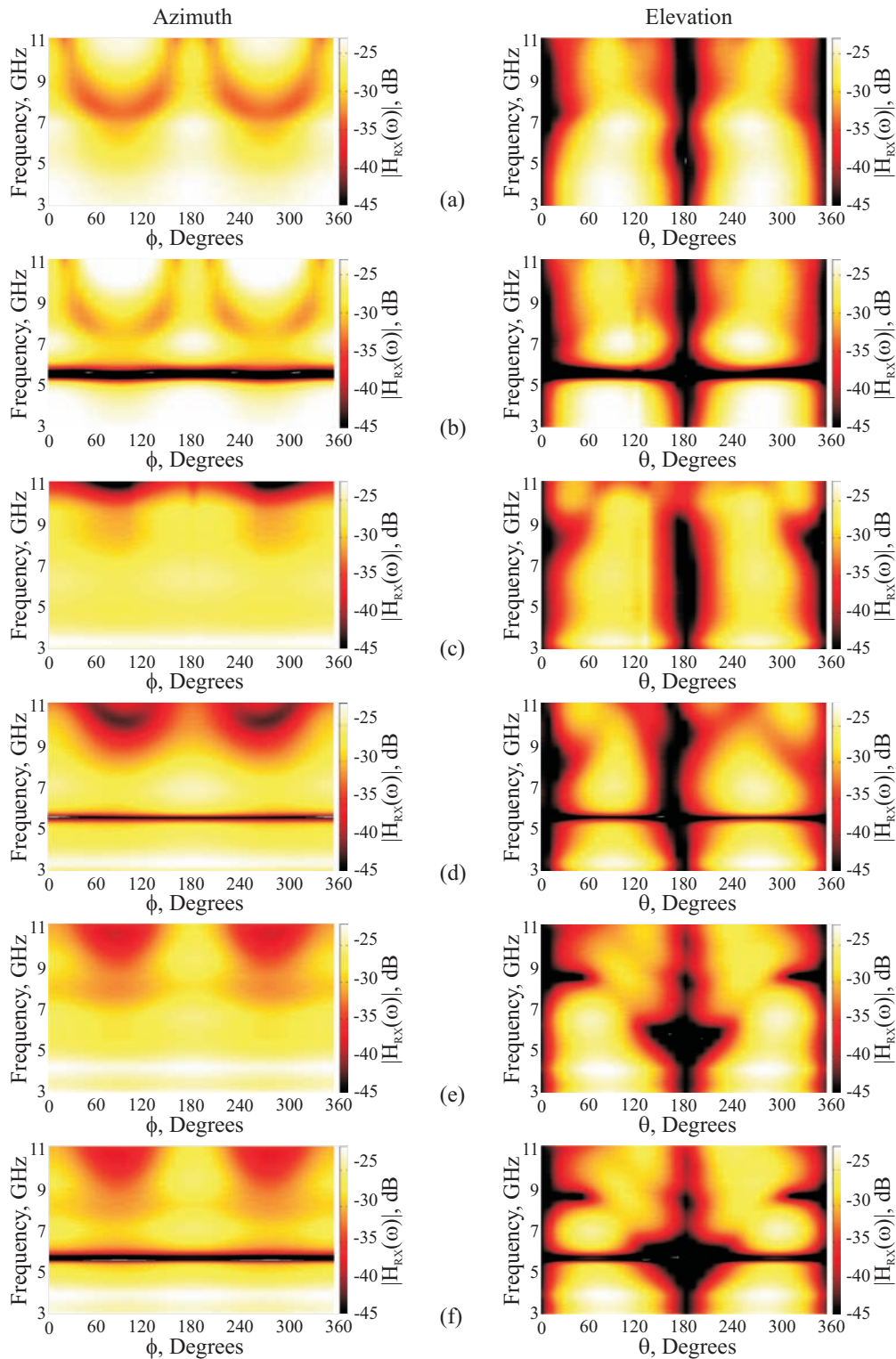


Fig. 5.1: The simulated transfer function magnitudes in the azimuth and elevation planes of the (a) elliptical monopole, (b) band notched elliptical monopole, (c) inverted cone monopole, (d) band notched inverted cone monopole, (e) wide band slot, (f) band notched wide band slot antennas

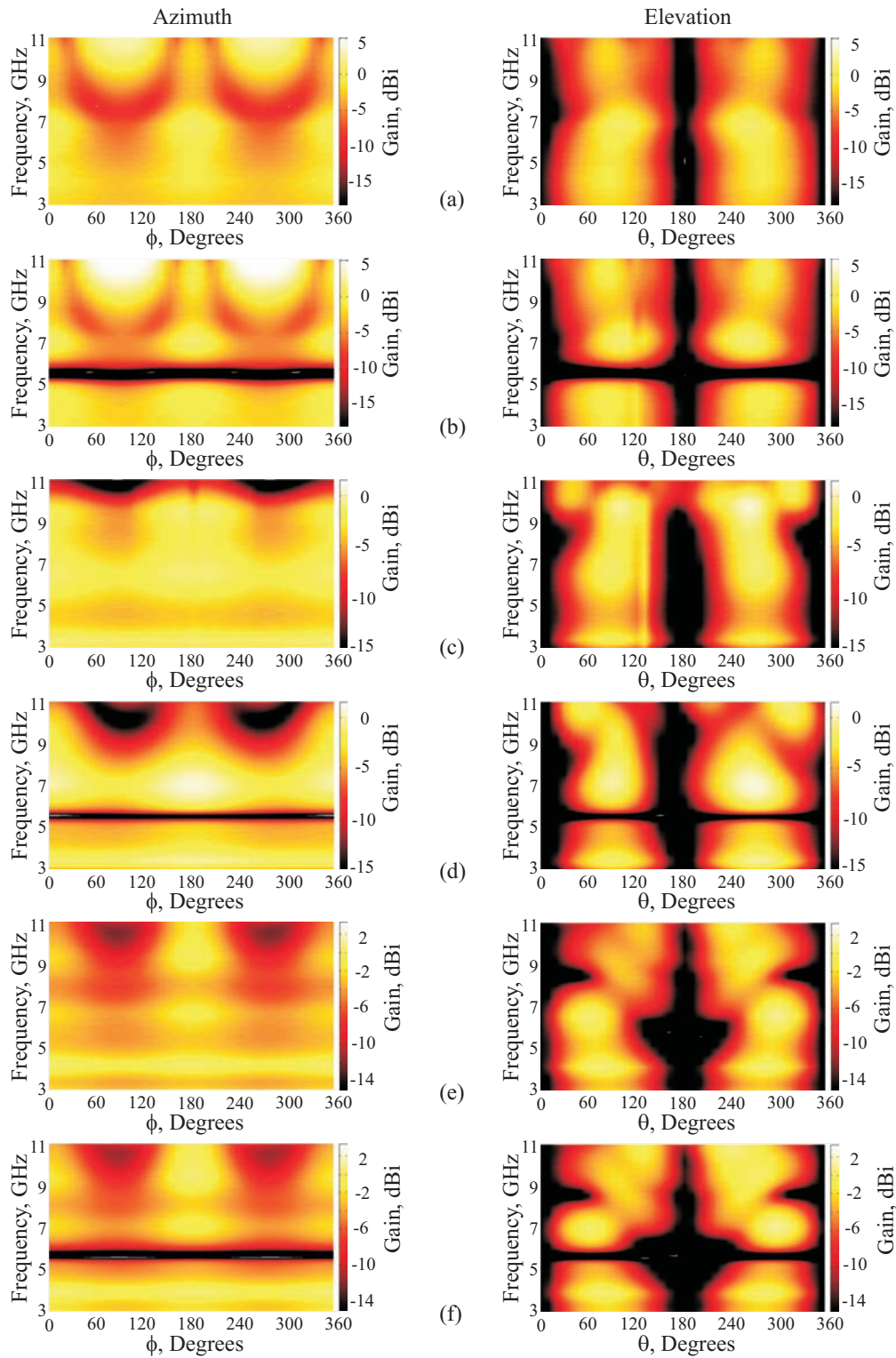


Fig. 5.2: The simulated antenna gains in the azimuth and elevation planes of the (a) elliptical monopole, (b) band notched elliptical monopole, (c) inverted cone monopole, (d) band notched inverted cone monopole, (e) wide band slot, (f) band notched wide band slot antennas

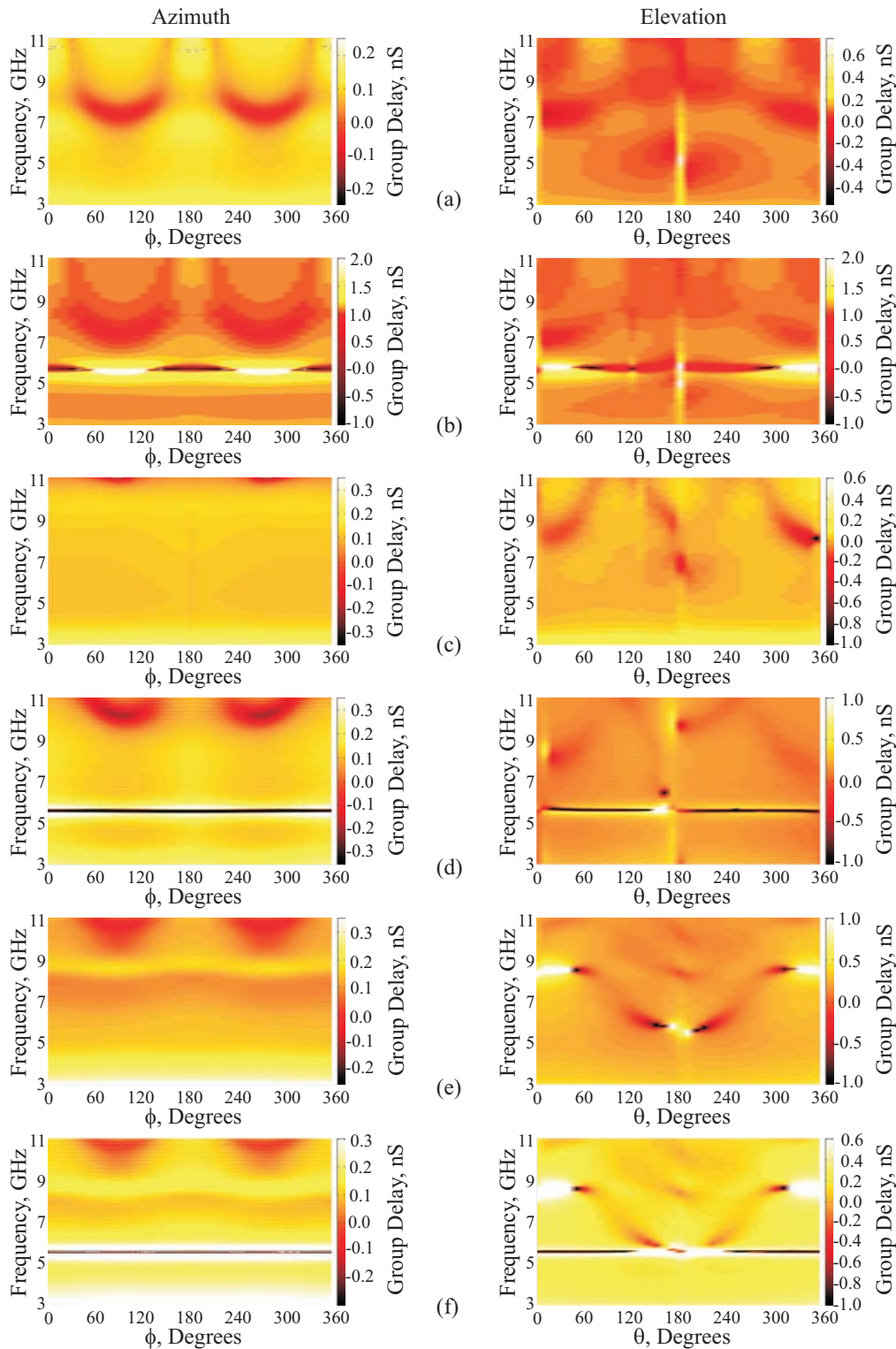


Fig. 5.3: The simulated group delays in the azimuth and elevation planes of the (a) elliptical monopole, (b) band notched elliptical monopole, (c) inverted cone monopole, (d) band notched inverted cone monopole, (e) wide band slot, (f) band notched wide band slot antennas

5.2.2 Measurements with the Prototype Antennas

The procedure for the transfer characteristics measurements are as explained in Sections 2.5.2 of Chapter 2. The transmitting and receiving antennas are positioned in their far-fields, at a distance of 25cms for measurements. the source power levels of the VNA is set at +10dBm to improve the signal to noise ratio (S/N) of the measured data. Measurements are performed in steps of 30° .

The measured antenna transfer function amplitudes are plotted in the azimuthal plane and in the elevation planes and shown in Fig.5.4. It can be observed that they compare well with the intensity variations in the simulated transfer characteristics plotted in Fig.5.1.

The group delay deduced from the phase of the measured transfer function as in eqn.(2.23) of Chapter 2, is plotted in Fig.5.5 for two extreme angles $\phi=0^{\circ}$ and 90° in the azimuth and $\theta=0^{\circ}$ and 90° in the elevation. Except at the notched frequencies of the band notched designs (Fig.5.5(b), (d) and (f)) and at $\theta=0^{\circ}$, 180° in the elevation plane, the measured group delay is within the tolerable range of $\pm 1\text{nS}$.

Among the UWB antennas designed in this thesis, all exhibit reasonably good performance with a constant group delay and a steady transfer function magnitude within the operating frequency range. Some deviations are observed at the higher end of the UWB spectrum where the transfer function magnitude varies for different antenna orientations. The inverted cone monopole shows minimum spatial variations among the antennas investigated. The superior performance of the inverted cone monopole is confirmed from the antenna transfer function and group delay measurements as well.

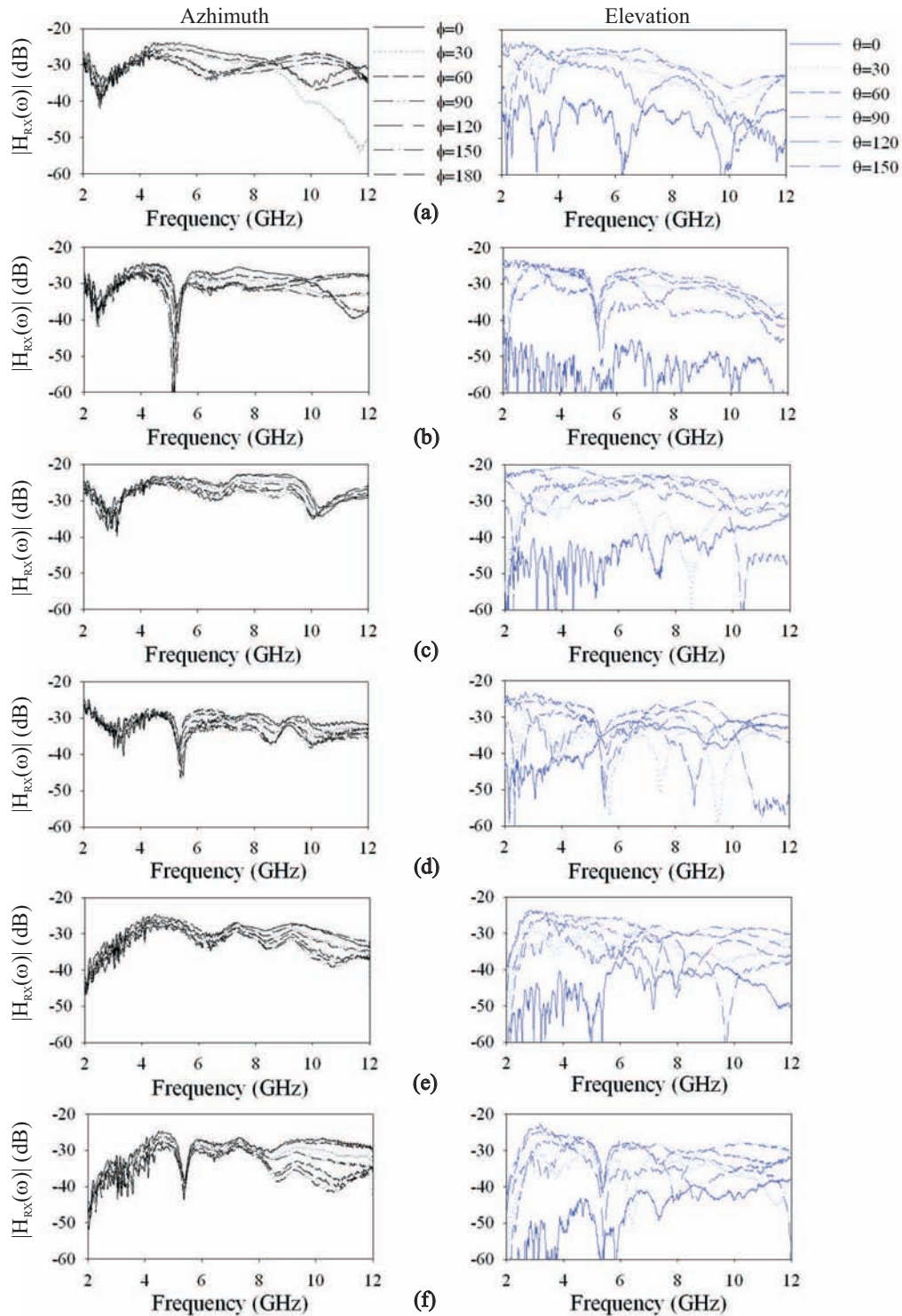


Fig. 5.4: The measured transfer function magnitudes in the azimuth and elevation planes of the (a) elliptical monopole, (b) band notched elliptical monopole, (c) inverted cone monopole, (d) band notched inverted cone monopole, (e) wide band slot, (f) band notched wide band slot antennas

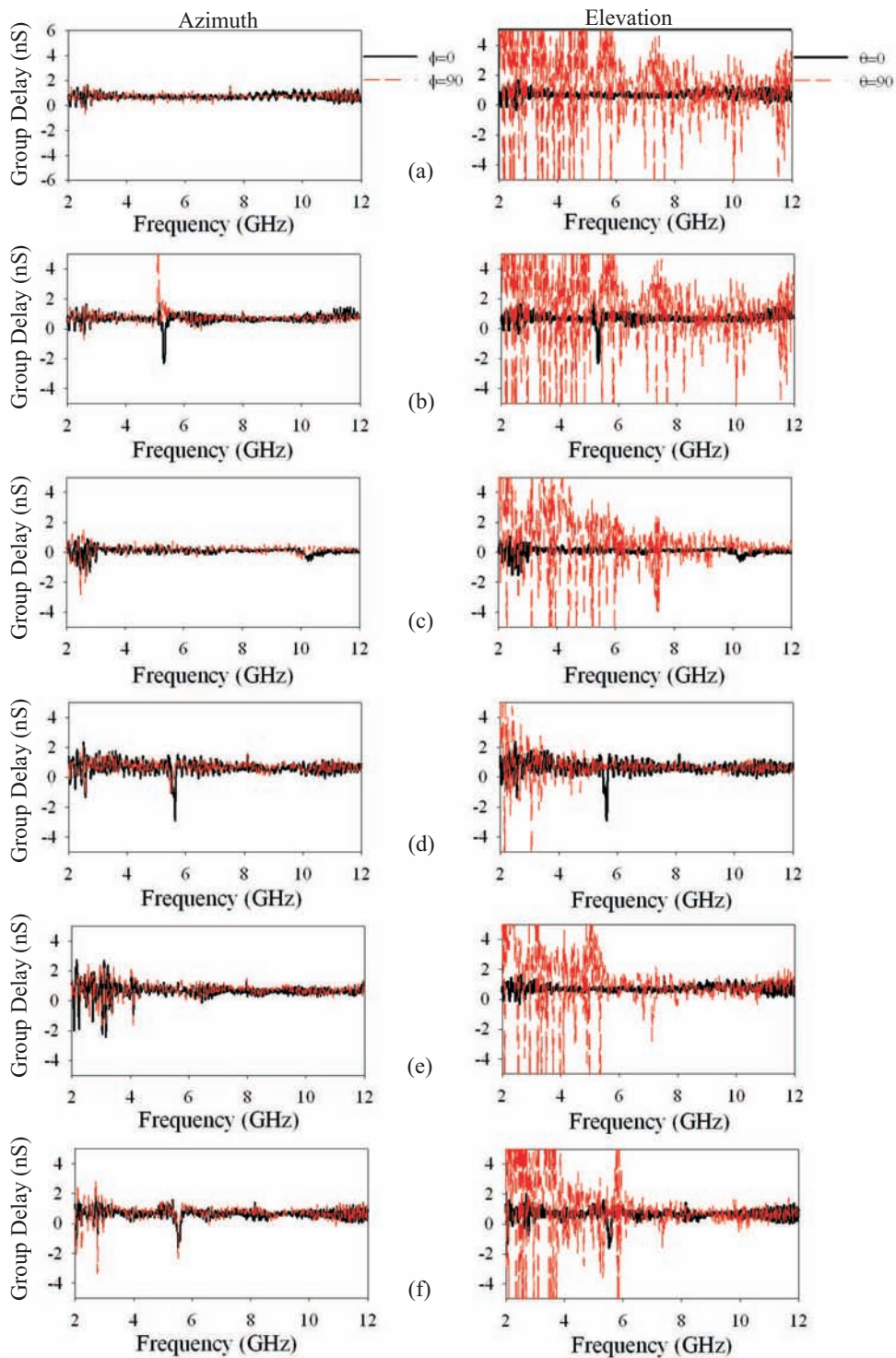


Fig. 5.5: The measured group delays in the azimuth and elevation planes of the (a) elliptical monopole, (b) band notched elliptical monopole, (c) inverted cone monopole, (d) band notched inverted cone monopole, (e) wide band slot, (f) band notched wide band slot antennas

5.3 Impulse Response and UWB Quality Measures

The transient behavior of the antennas are assessed from their impulse responses which are obtained by taking the inverse fourier transform of their transfer functions. The UWB antenna quality measures, namely the FWHM and ringing are directly deduced from the magnitude of the impulse response envelop as in Section 2.3.2 of Chapter 2. An ideal antenna for UWB portable applications should show a uniform impulse response performance for different antenna orientations with minimum FWHM and ringing.

The simulated antenna impulse responses are derived from their corresponding transfer functions plotted in Fig.5.1 and the envelopes of their real terms are shown in Fig.5.6. Even though all of them are within the acceptable range of performance in the azimuth as well as elevation, the extent of any amplitude degradation noted in their antenna transfer function leaves a signature in their impulse response behavior.

We can notice that the nulls in the transfer function plots in the elevation plane at $\theta = 0^0$ and 180^0 corresponds well with their impulse response plots. In case of the band notched designs, shown in Fig.5.6(b), (d), and (f), an increase in the number of ripples is clearly visible. The pattern degradation at higher frequencies observed especially in case of the elliptical monopole between $\phi=30^0$ to 150^0 and 210^0 to 330^0 in the azimuth, leads to an increased ringing along those orientation angles. This in turn makes the impulse responses slightly non-uniform in the azimuth. Predictably the inverted cone monopole comes out with a superior behavior in terms of its transient response with a uniform response in azimuth and wide angle performance in elevation with minimum ringing.

The impulse response deduced from the measured transfer functions are plotted for different orientation angles in the azimuth and elevation planes in Fig.5.7. Most of the responses resemble the delta function. The increase in

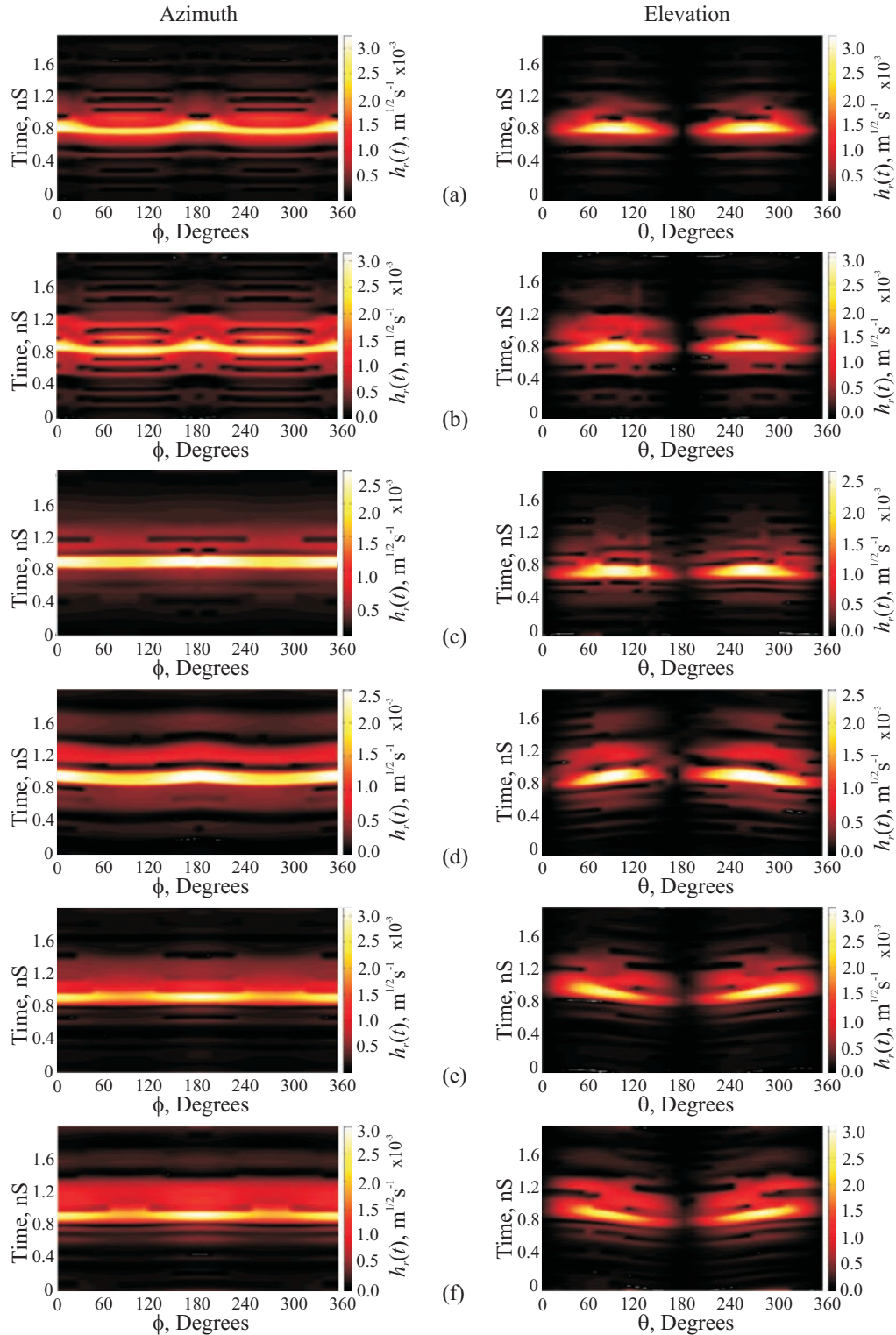


Fig. 5.6: The simulated impulse responses in the azimuth and elevation planes of the (a) elliptical monopole, (b) band notched elliptical monopole, (c) inverted cone monopole, (d) band notched inverted cone monopole, (e) wide band slot, (f) band notched wide band slot antennas

ringing is clearly observed in the case of the band notched antenna designs in Fig.5.7(b), (d), and (f).

To compare the antenna performance qualitatively, their simulated and measured FWHM and ringing, derived using eqn.(2.26) and (2.27), are tabulated in Table 5.1. They appear to compare well and a narrow FWHM ($< 200\text{pS}$) is seen in azimuth and within $\pm 60^\circ$ of elevation in most cases. The band-notched antenna designs record a clear increase in ringing ($> 400\text{pS}$).

The planar elliptical and the inverted cone monopole show superior transient response with the latter having a uniform response and minimum spatial variations in the azimuth. In the case of the slot antenna, even though it shows a reasonably good performance in the azimuth it has a slightly narrower performance in the elevation plane. This corresponds well with the magnitude distortion noted in their transfer function plots in the elevation plane, shown in Fig.5.1(e) and (f).

5.4 Pulse Distortion Analysis

Antenna effects on nano-second pulses are studied using the method outlined in Section 2.6 of Chapter 2. The template pulse chosen is 4th derivative Gaussian as shown in Fig.2.6 of Chapter 2. The measured and simulated normalized pulses in the azimuth and elevation planes are plotted in Fig.5.8.

It is observed that the measured and simulated received pulses agree well. The band-notched designs record an increase in pulse dispersion complying well with their impulse response characteristics studied in the previous section. Their fidelity factors, tabulated in Table 5.1, record values $> 90\%$ in the azimuth plane except in the case of band-notched where it is $> 80\%$. The inverted cone monopole gives a superior performance with a fidelity $> 95\%$ reported uniformly in the azimuth.

The antenna performance as a transmit-receive system is assessed based on the method outlined in Section 2.6 in Chapter 2. The simulated and measured output pulses for both face to face and side by side orientations of

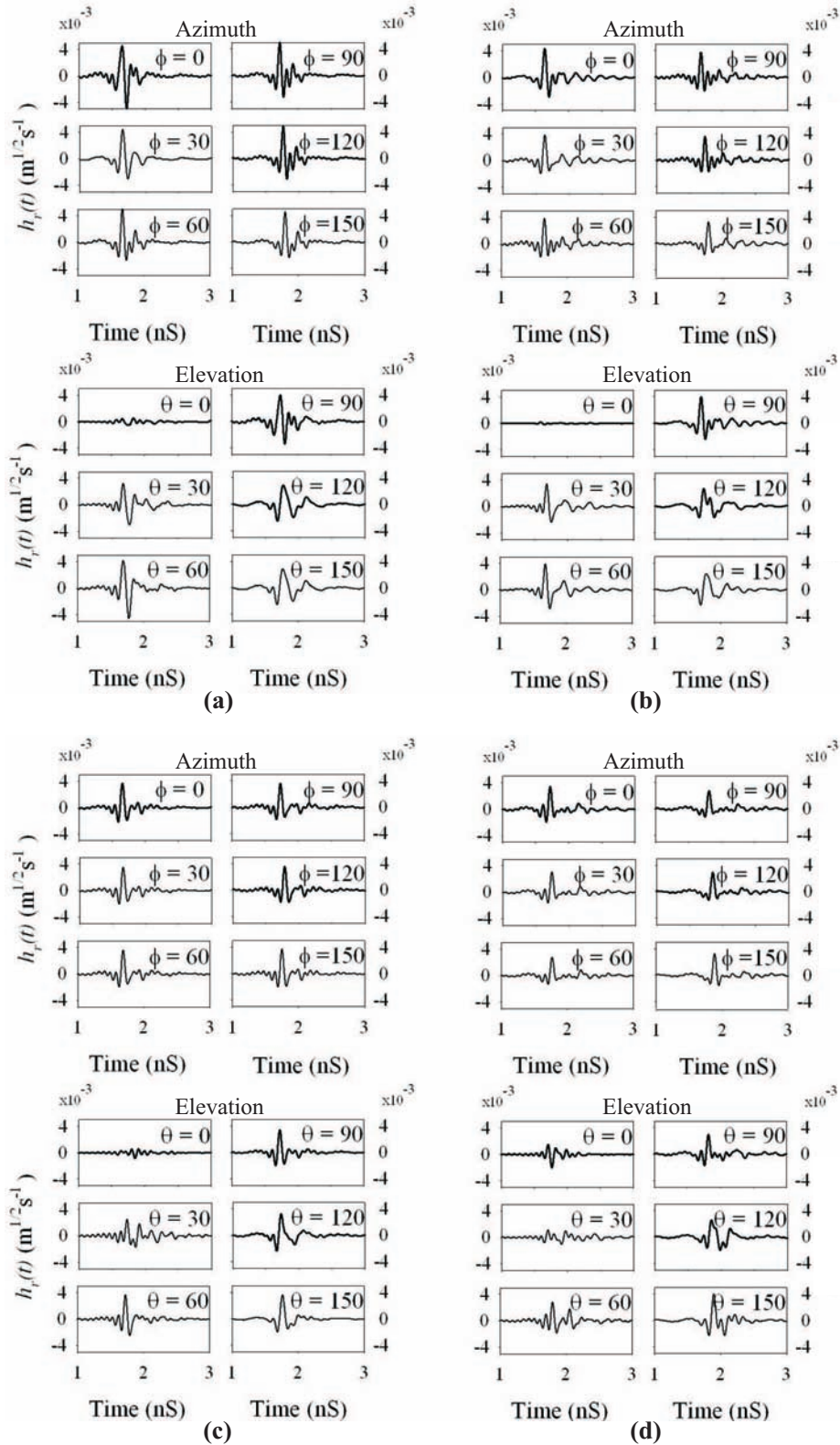


Fig. 5.7: The measured impulse responses in the azimuth and elevation planes of the (a) elliptical monopole, (b) band notched elliptical monopole, (c) inverted cone monopole, (d) band notched inverted cone monopole (e) wide band slot and (f) band notched wide band slot antennas

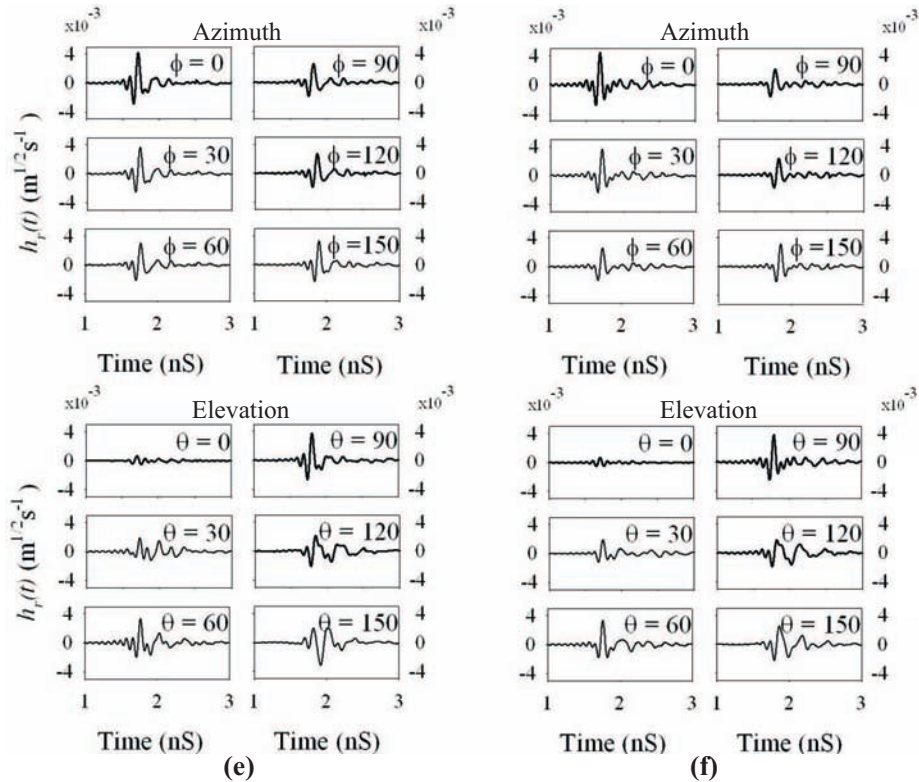


Fig. 5.7: Continued from the previous page

the antennas are plotted with respect to the normalized face to face response and is plotted in Fig.5.9. It can be observed that they compare well and that the band notched designs exhibit visible ringing effects.

In the case of the elliptical monopole antennas (Fig.5.9(a) and (b)) even though the output pulses are slightly distorted, they remain acceptable. But the maximum amplitude of the received waveform for the side by side case is about 20% lower than that of the face to face case. The inverted cone and slot antennas show very little difference in the face to face and side by side cases. The fidelity factor for the simulated and measured pulses are tabulated in Table 5.2 for the antennas in their face to face and side by side orientations.

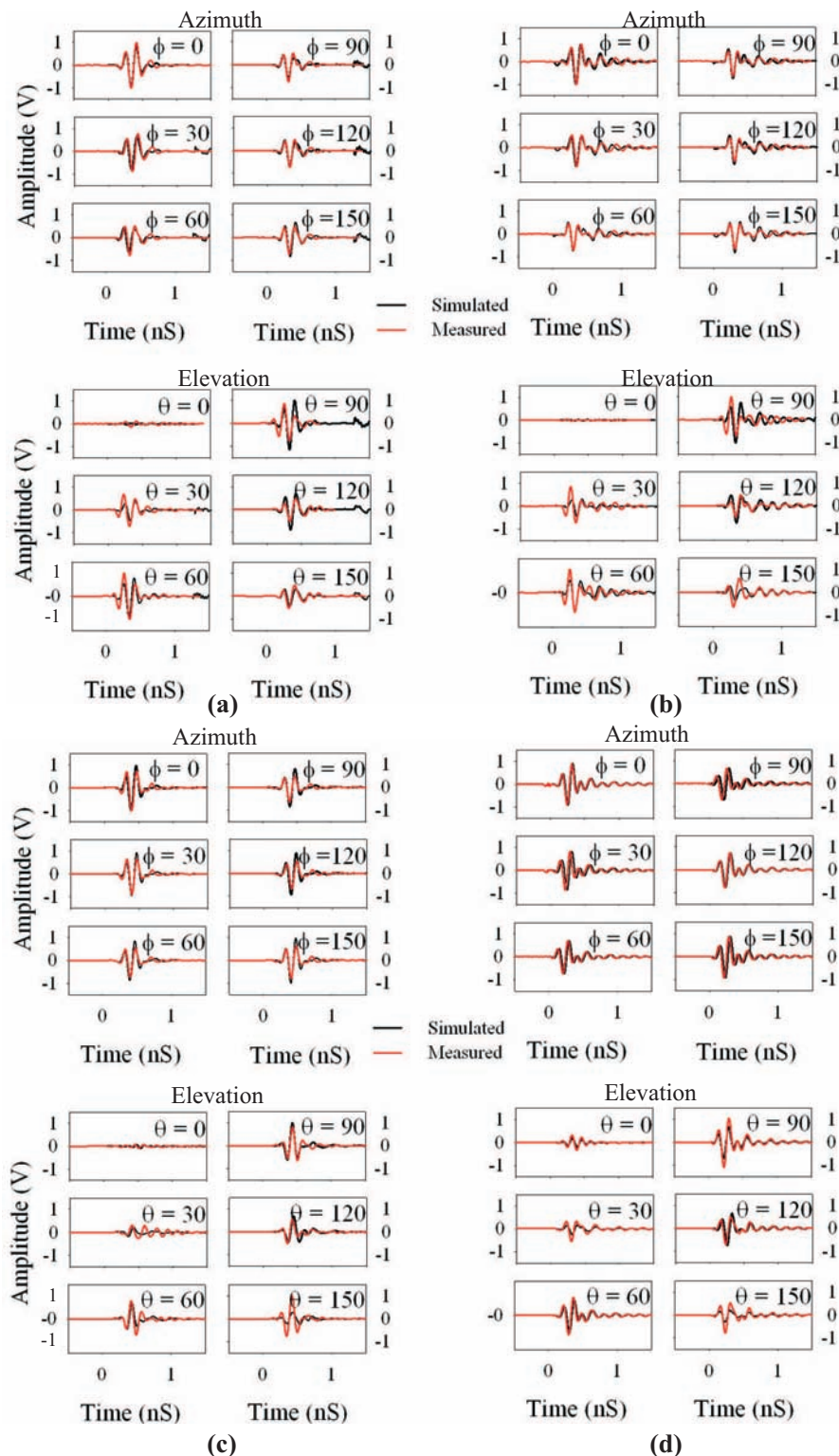


Fig. 5.8: The measured received pulses in the azimuth and elevation planes of the (a) elliptical monopole (b) band notched elliptical monopole, (c) inverted cone monopole, (d) band notched inverted cone monopole (e) wide band slot and (f) band notched wide band slot antennas

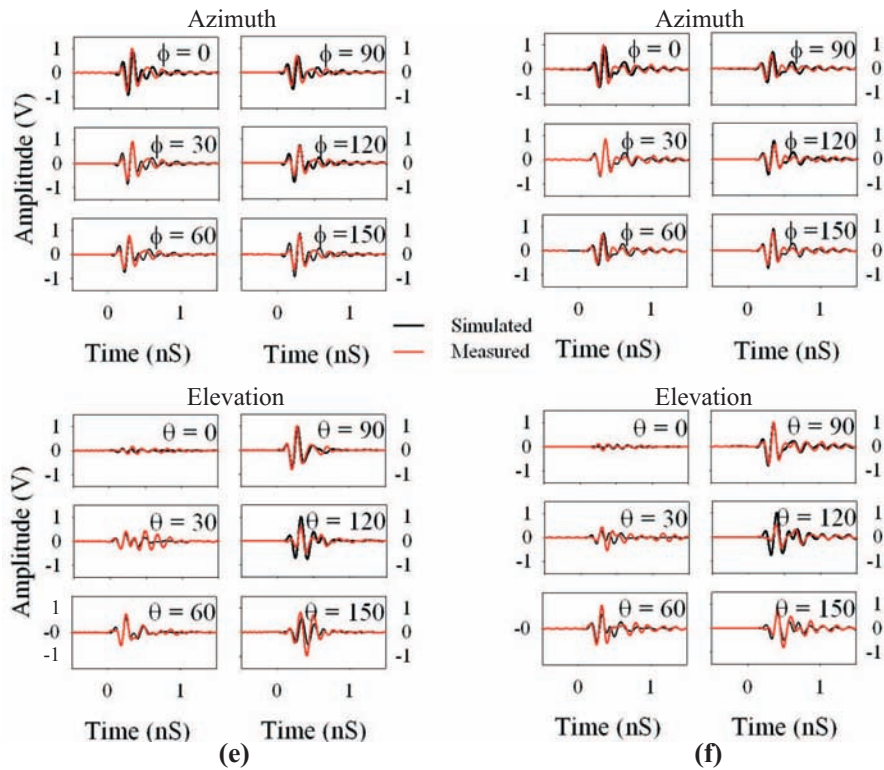


Fig. 5.8: Continued from the previous page

5.5 Chapter Summary

In this chapter, the spatio-temporal transfer characteristics of the antennas presented in this thesis for UWB operation are studied. This would confirm their suitability for pulsed UWB applications and is quantified further by their pulse distortion analysis. Any distortion in the frequency domain and any abrupt discontinuity in the antenna geometry is reflected in the time domain as dispersion. The FWHM and ringing measures this dispersion. Fidelity, which is the cross correlation of the transmitted and received pulses, measures the antenna effects on the transmitted pulse.

The study reveals a close correspondence between the geometry of the antenna with its performance in the time domain. The surface current distribution analysis has revealed a relative shift in the phase center for the different frequencies of operation in the case of the planar elliptical monopole antenna.

Table 5.1: FWHM, ringing (Ring.) and fidelity (Fid.) in the azimuth and elevation planes

				Angle						
				ϕ or θ in degrees						
				0	30	60	90	120	150	180
Elliptical Monopole	Azimuth	FWHM	Sim.	143	144	96	104	116	134	136
			pS	Meas.	192	176	123	117	125	133
		Ring.	Sim.	248	224	312	316	320	228	249
			pS	Meas.	256	320	336	327	345	318
		Fid.	Sim.	96.8	96	93	92	93	95.4	96.7
			%	Meas.	95.5	94.6	93.5	93.3	94.8	93.5
	Elevation	FWHM	Sim.	189	132	125	142	135	146	175
			pS	Meas.	268	176	152	198	178	244
		Ring.	Sim.	240	228	210	246	292	296	320
			pS	Meas.	396	157	276	250	340	377
		Fid.	Sim.	74	97.8	96.5	96.8	95.9	90.1	84
			%	Meas.	83	94.7	93.7	95	92.3	98.2
Band-notched Elliptical Monopole	Azimuth	FWHM	Sim.	134	108	103	109	118	113	135
			pS	Meas.	128	135	112	117	109	114
		Ring.	Sim.	380	376	336	344	375	390	384
			pS	Meas.	440	488	420	408	416	456
		Fid.	Sim.	88	86.6	82.6	82	81.9	86.8	89
			%	Meas.	81.7	81.7	80	80.15	80.3	81.8
	Elevation	FWHM	Sim.	157	192	98	134	112	96	173
			pS	Meas.	208	152	120	128	132	600
		Ring.	Sim.	585	380	386	376	372	370	569
			pS	Meas.	600	488	408	448	508	506
		Fid.	Sim.	67	90.1	86.7	88	84.4	74.3	80.5
			%	Meas.	60	70.7	80	81.8	81.5	72.3

The antenna is relatively large in size when compared to the rest (width $\approx 30\text{mm}$). So, for certain frequencies, the surface currents from different parts of the antenna combine out of phase while receiving a signal depending on the antenna orientations. By reciprocity, the antenna exhibits this feature in transmitting mode as well. The result is a distorted radiation pattern which in this case occurs at the upper end of the UWB spectrum. This deviation from the omni-directional pattern is confirmed in the transfer function of the

Table 5.1: FWHM, ringing (Ring.) and fidelity (Fid.) in the azimuth and elevation planes (Continued)

				Angle						
				ϕ or θ in degrees						
				0	30	60	90	120	150	180
Inverted Cone Monopole	Azimuth	FWHM	Sim.	142	146	152	154	150	146	142
			Meas.	144	141	128	112	119	127	144
		Ring.	Sim.	320	328	314	327	320	328	329
			Meas.	312	309	320	336	315	328	314
		Fid.	Sim.	95.6	95.5	95.2	95.2	95	95.3	95.6
			Meas.	95.5	95.4	95.5	95.7	95.5	95.6	95.2
	Elevation	FWHM	Sim.	175	124	136	142	147	138	166
			Meas.	190	144	148	144	152	150	188
		Ring.	Sim.	476	276	280	320	294	292	315
			Meas.	664	566	160	312	360	316	421
		Fid.	Sim.	79	80.8	95.3	95.6	95.4	87.4	64.3
			Meas.	68	61.4	95.5	95.3	95.04	90.3	77.9
Band-notched Inverted Cone Monopole	Azimuth	FWHM	Sim.	121	112	104	96	100	112	110
			Meas.	144	149	157	155	153	149	145
		Ring.	Sim.	424	428	425	432	427	431	430
			Meas.	552	464	470	472	456	460	462
		Fid.	Sim.	92.7	91.1	90.5	89.9	90.4	91.1	91.3
			Meas.	90	92	90.2	90.1	90.3	89.6	90.2
	Elevation	FWHM	Sim.	179	175	189	121	147	200	310
			Meas.	350	210	198	144	167	200	290
		Ring.	Sim.	550	408	414	424	420	428	523
			Meas.	667	534	590	551	496	584	615
		Fid.	Sim.	84.4	90.9	90.3	92.7	88	87.1	83
			Meas.	65	76.3	87.9	90	88.4	86	69

antenna and reflected in their transient responses.

In the case of the inverted cone monopole, the phase center is relatively constant over the entire UWB spectrum except for frequencies $>10\text{GHz}$ and has a compact size (width $\approx 14\text{mm}$). As a result the antenna shows excellent time domain performance which is uniform in azimuth and a wide angle of operation in elevation. But this is at the cost of a slightly reduced gain. The slot antenna performance falls in between. Its size is $\approx 20\text{mm}$ and has a

Table 5.1: FWHM, ringing (Ring.) and fidelity (Fid.) in the azimuth and elevation planes (Continued)

			Angle							
			ϕ or θ in degrees							
			0	30	60	90	120	150	180	
Slot Antenna	Azimuth	FWHM pS	Sim.	120	125	171	183	175	125	121
			Meas.	112	128	144	160	152	135	120
		Ring. pS	Sim.	296	350	409	413	401	296	245
			Meas.	248	256	432	440	437	224	184
		Fid. %	Sim.	92.3	91.4	89.4	88.6	90.6	93	94
			Meas.	92.25	91.1	90.5	87.9	88.14	92.5	93.9
	Elevation	FWHM pS	Sim.	430	224	208	120	112	104	136
			Meas.	350	288	244	112	127	152	128
		Ring. pS	Sim.	552	312	320	295	272	420	570
			Meas.	671	400	432	248	432	480	413
		Fid. %	Sim.	75	79	80.7	92.3	91.8	86	80
			Meas.	75	68	86	92	86.5	86	75.8
Band-notched Slot Antenna	Azimuth	FWHM pS	Sim.	114	118	134	189	126	113	118
			Meas.	128	126	136	152	144	136	121
		Ring. pS	Sim.	394	406	422	426	418	394	374
			Meas.	411	448	413	442	416	427	409
		Fid. %	Sim.	90.7	90	89.4	86.5	87.7	89.7	91
			Meas.	90	89.4	87	84.3	86	88.4	90.5
	Elevation	FWHM pS	Sim.	409	118	119	114	255	276	290
			Meas.	388	129	121	127	300	281	315
		Ring. pS	Sim.	612	392	311	395	418	452	473
			Meas.	650	299	399	408	416	440	519
		Fid. %	Sim.	68.5	61.5	87.7	90.7	88.3	83	76.1
			Meas.	68	61.8	87.2	90	84	81.3	69.7

response which does vary in azimuth but it is better than that of the planar elliptical antenna.

Thus we can conclude here, that even though a wider bandwidth is ensured by a smooth impedance transformation in the antenna geometry at the cost of its increased size, it is basically the antenna phase center location over the operating frequency range which determines its suitability for the pulsed UWB operation. As studies reveal in the case of the inverted cone and the

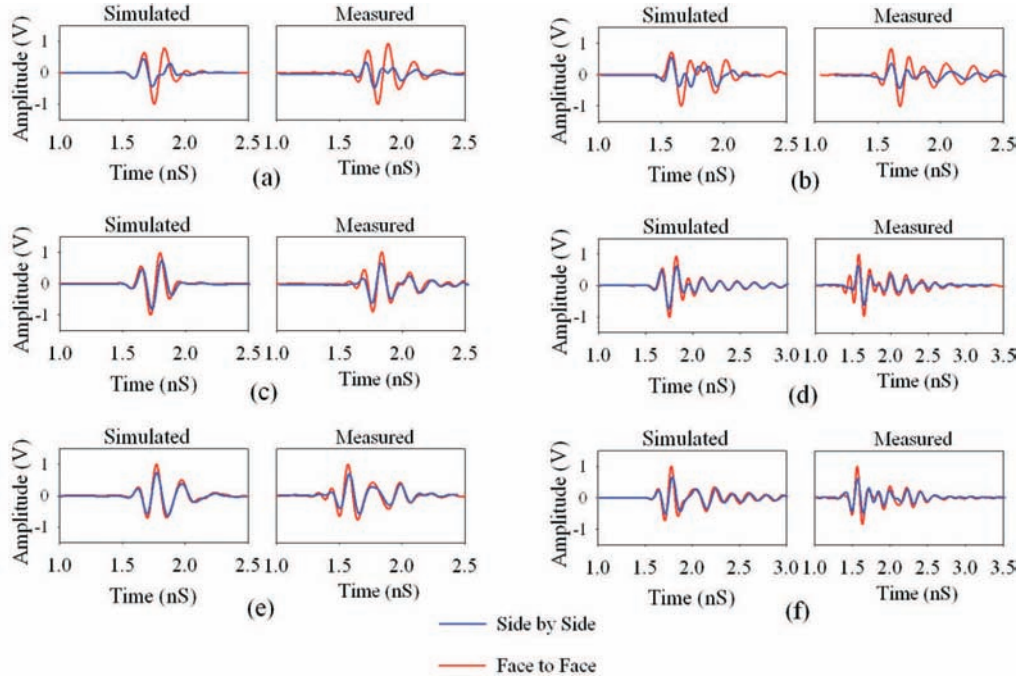


Fig. 5.9: Simulated and measured transmitted pulses by two identical antennas in their face to face and side by side orientations. (a) elliptical monopole, (b) band notched elliptical monopole, (c) inverted cone monopole, (d) band notched inverted cone monopole, (e) wide band slot, (f) band notched wide band slot Antennas

Table 5.2: Fidelity of the transmitted pulses

Antenna	Fidelity (%)			
	Face to Face		Side by Side	
	Simulated	Measured	Simulated	Measured
Elliptical Monopole	96	89	85	81
Band-notched Elliptical Monopole	89	83	78	73
Inverted Cone Monopole	95	92	95	91.6
Band-notched Inverted Cone Monopole	91	87	91	86.2
Slot Antenna	93	90	89	87.3
Band-notched Slot Antenna	90	89	87	85

slot antenna, a compact size with good impedance matching within the UWB 3.1 to 10.6GHz band and a uniform response in terms of the space coordinates would be better option for portable UWB applications than antennas with a large bandwidth and that consume PCB space. The retardation caused by any displacement in the antenna phase center location, if any, by such compact antennas (width $\approx 20\text{mm}$) is negligible for nano-sec pulses .

Conclusion

Contents

6.1 Thesis Summary and Conclusions	149
6.2 Suggestions for Future Work	153

This chapter sums up the results and highlights the achievements of the research work carried out. This is followed by few suggestions for future work. The results presented in the thesis have been published by the author in different international journals and conferences.

6.1 Thesis Summary and Conclusions

The aim of the thesis was to investigate the design requirements of compact planar antennas for wide band applications. Two types of antennas belonging to this class were identified: monopole and slot antennas; and four novel compact antennas were designed, namely elliptical monopole, inverted cone monopole, Koch fractal slot and wide band slot antenna

The evolution of the designed antennas were investigated in detail to have an insight into their wideband behavior. As the studies reveal, the key to a broadband antenna performance lies in having a smooth transition from the feed to the ground edges. On observing the geometry of all the antennas designed in this thesis, we can notice that abrupt discontinuities in their geometry, especially near the feed-radiator transitions, have been avoided. As a consequence, the impedance change from one resonance mode to the other is minimized, resulting in wideband performance of the antenna.

The design aspects, based on the geometrical parameters of the antenna, were first investigated. The simulation studies, in terms of their return loss and current/field distribution on the antenna at different resonances, reveal their dependence on the antenna dimensions. Dimensional parameters, critically determining the resonances and wideband impedance matching of the antenna, were identified and simple empirical relations were deduced. These equations, whose validity was also verified, can help the antenna designer to deduce the antenna geometry on any desired substrate for the desired frequency range of operation. The deduced geometry can act as a precursor to the final design optimized using any of the simulation softwares.

The designs also incorporates thin slot resonators inscribed within the radiator and/or ground patch to reject narrow frequency bands. Such embedded filters avoids the use of additional filters in the circuits which may not be desired for portable wireless systems with space constraints.

A brief summary of the different antennas designed are;

1. Elliptical monopole antenna

This antenna has a wide band operation (2.54GHz to >12GHz), simple structure and an omnidirectional radiation patterns especially at the lower end of the spectrum. The elliptical monopole as well as the ground plane forms a quasi-dipole antenna at its lowest resonance and the extremely wide impedance band is ensured by the gradual impedance transformation arrangement between the ground and the patch. The antenna is CPW fed with a size-31x32mm², gain ranging between 0.5 to 5dBi and radiation efficiency greater than 85% over the operating frequency range. They have been reported in *Publication no.1*.

The narrow slot resonators are incorporated in this design to reject single and dual frequencies. A thin half wavelength long slot resonator is inscribed on the radiator patch to filter out the 5 to 6GHz frequencies. A combination of such multiple slots are implemented, either on the radiator patch or on the radiator as well as the ground, to adapt the an-

tenna for triple band operation particularly suited for the 2.5/3.5/5.5GHz WiMAX as well as the 2.4/5GHz WLAN standards. The results are reported in *Publication no. 2*.

2. Inverted cone monopole antenna

This antenna has a reduced size (14mmx32mm) and a wide band of operation (2.8 to 11.2GHz). The radiator patch is a printed inverted cone with a circular base and ground is a semi-ellipse with a U-shaped slot at the feed radiator transition. The slot appears to have a significant influence on the antenna behavior by maintaining its region of radiation almost constant. It is also noted that the antenna performs in an oscillating or standing wave mode through out the UWB band. Hence it appears to be perfectly ideal for UWB hand held applications with a compact size, stable & omnidirectional antenna pattern. The antenna gain averages around 2dBi and radiation efficiency $> 80\%$ is noted in the operating band.

This design also incorporates dual symmetrically placed quarter wavelength slot resonators inscribed on the ground patch to notch out the 5 to 6GHz WLAN frequencies. These results have been reported in *Publications no. 3 & 4*.

3. Koch fractal slot antenna

The introduction of a Koch fractal slot instead of the triangular slot geometry is observed to lower the frequency of operation along with wide band matching. The slot antenna employs the fractal slot geometry, in combination with a compact ground plane and a tapered tuning stub, to perform over a wide band. The antenna is microstrip fed and has a size-29x38mm², operating over a band wide enough to cover the WLAN 2.4/5.2/5.8GHz and WiMAX 2.5/3.5/5.5GHz bands with a gain ranging between 2.5 to 5.5dBi and radiation efficiency $> 85\%$ over the entire operating frequency range.

A CPW-fed version of the same antenna, with a slightly modified Koch slot, is presented for similar operating frequencies. This design also includes a half wavelength narrow slot resonator inside the tuning stub optimized to filter out the 4 to 5GHz band. The publications related to this work are *Publications no. 5 & 6*.

4. Wide band slot antenna

This is a compact UWB slot antenna, of width-20mm and fed by a CPW line, operating over a range from 2.9 to 11GHz. The antenna features all the desirable characteristics demanded by UWB communication systems such as adequate impedance bandwidth and stable radiation patterns throughout the ultra-wide band with a gain and radiation efficiency $> 2\text{dBi}$ and 85%, respectively, over the operating frequency range.

In addition, the antenna is insensitive to ground plane length variations, making it suitable for WUSB dongle and mobile UWB applications. This design also include a half-wave length slot inscribed on the tuning stub to notch out the 5.4GHz WLAN band and they have been reported in *Publications no. 7 & 8*.

The antennas designed for UWB operation from 3.1 to 10.6GHz has been further analyzed for their time domain response in the final section of the thesis to confirm their suitability for pulsed UWB applications. The transfer function measurements are performed for both the azimuthal and elevation planes and their impulse responses are deduced. The impulse response of the antennas are then characterized in terms of FWHM and ringing. A narrow FWHM ($< 200\text{pS}$) is seen in azimuth plane and within $\pm 60^\circ$ of elevation plane. The band-notched antenna designs record a clear increase in ringing ($> 400\text{pS}$). The inverted cone antenna exhibits the minimum variation in FWHM and ringing values for the different angular positions.

The antenna effects on nano-second pulses are measured in terms of the fidelity factor and values $> 90\%$ in the azimuth plane is recorded for all antennas except in case of band-notched where it is $> 80\%$. The inverted cone

monopole gives a superior performance with a fidelity $>95\%$ reported uniformly in the azimuth.

All of the UWB designs proposed in this thesis can provide ultra wide bandwidth. However, in the case of elliptical monopole, even though a wider bandwidth is ensured by a smooth impedance transformation in the antenna geometry, a distortion in the pattern is observed at higher frequencies since the region of radiation does not remain constant. This distortion in the frequency domain gets reflected in the transient response of the antenna and the performance varies with azimuth angle.

The inverted cone and the slot antenna, by virtue of their near omnidirectional pattern over the whole bandwidth, exhibits relatively uniform transient response for different space coordinates. This can be easily attributed to their compact size, which inevitably lead to minimum phase difference between the surface currents from the different parts of the antenna. The performance of all the designed UWB antennas are, however, within tolerable limits which makes them all suitable for pulsed UWB applications.

6.2 Suggestions for Future Work

The following are some of the prospects for future work:

The transfer function measurements performed in this thesis have been restricted to the two orthogonal planes. For better understanding of the 3-dimensional antenna radiation properties, an automated measurement setup may be devised in future to measure at different spherical coordinates of the antenna.

A direct time domain measurements may also be performed in future for all the designed antennas involving a nano-sec pulse generator and a wideband digital storage oscilloscope.

The antennas designed in this thesis have been printed on lossy substrates. Instead, they may be designed on low temperature co-fired ceramic (LTCC) substrates in future which have the advantage of direct integration with mono-

lithic microwave circuits.

Even though the miniaturization of the antennas designed is a feasible future prospect, the techniques to achieve ground-independent UWB antenna performance may be stressed in order to enhance their prospect of adoption in practical applications. Diversity UWB antenna may also be investigated for the same reasons. When the antenna is built on a portable device, the impact from human body may also be considered.

UWB systems operate at extremely low power level which limits its transmission range. In order to enhance the quality of the communication link and improve channel capacity and range, directional systems with high gain are required for some applications. Therefore, research on UWB directional antenna and antenna array may be carried out especially because the design of wideband arrays gives great difficulties in element spacing.

Due to the low power level operation of UWB systems, a typical UWB receiver requires a low-noise amplifier. Antenna integration with low-noise amplifier may be investigated in future.

Future radio systems, such as software defined radio and cognitive radio concepts give rise to significant challenges for antenna design and in particular reconfigurable antenna design. Wideband antennas with bandwidths over a decade are desired in the search mode. An external switching/tuning may be used to narrow the bandwidth while improving the search sensitivity. This would require that a narrow band and a wideband antenna may be integrated into the same volume and they may be designed to operate in either of the modes electronically.

References

- [Abbosh 2009] A. M. Abbosh and M. E. Bialkowski. *Design of UWB planar band-notched antenna using parasitic elements*. IEEE Trans. Antennas Propag., vol. 57, no. 3, pages 796–799, 2009.
- [Agrawall 1998] P. A. Agrawall, G. Kumar and K. P. Ray. *Wideband planar monopole antenna*. IEEE Trans. on Antennas Propag., vol. 46, no. 2, pages 294–295, 1998.
- [Allen 2007] B. Allen, M. Dohler, E. E. Okon, W. Q. Malik, A. K. Brown and D. J. Edwards. *Ultra-wideband antennas and propagation for communications, radar and imaging*. John Wiley and Sons, Inc., 2007.
- [Amman 1999] M. J. Amman. *Square planar monopole antenna*. In Proceedings of IEE Nat.Conf. Antennas Propagation, numéro 461, pages 37–40, 1999.
- [Amman 2001] M. J. Amman. *Control of the impedance bandwidth of wide-band planar monopole antennas using a beveling technique*. Microw. Opt. Techno. Lett., vol. 30, no. 4, pages 229–232, 2001.
- [Amman 2003a] M. J. Amman. *A wide-band shorted planar monopole with bevel*. IEEE Trans. Antennas Propag., vol. 51, no. 4, pages 901–903, 2003.
- [Amman 2003b] M. J. Amman and Z. N. Chen. *Wideband monopole antennas for multi-band wireless systems*. IEEE Ant. Propag. Mag., vol. 45, no. 2, pages 146–150, 2003.
- [Amman 2004] M. J. Amman and Z. N. Chen. *An asymmetrical feed arrangement for improved impedance bandwidth of planar monopole antennas*. Microw. Opt. Techn. Lett., vol. 40, no. 2, pages 156–158, 2004.
- [Angelopoulos 2006] E. S. Angelopoulos, A. Z. Anastopoulos, D. I. Kaklamani, A. A. Alexandridis, F. Lazarakis and K. Dangakis. *Circular and elliptical CPW-fed slot and microstrip-fed antennas for ultrawideband applications*. IEEE Antennas Wireless Propag. Lett., vol. 5, pages 294–297, 2006.
- [Anob 2001] P. V. Anob, K. P. Ray and G. Kumar. *Wideband orthogonal square monopole antennas with semi-circular base*. IEEE Int. Symp. Antennas and Propagat., vol. 3, pages 294–297, 2001.

- [Antonino-Daviu 2003] E. Antonino-Daviu, M. Cabedo-Fabres, M. Ferrando-Bataller and A. Valero-Nogueira. *Wideband double-fed planar monopole antennas*. *Electron. Lett.*, vol. 39, pages 1635–1636, 2003.
- [Azenui 2007] N. C. Azenui and H. Y. D. Yang. *A printed crescent patch antenna for ultrawideband applications*. *IEEE Ant. Wireles. Propag. Lett.*, vol. 6, pages 113–116, 2007.
- [Bahadori 2007] K. Bahadori and Y. Rahmat-Samii. *A miniaturized elliptic-card UWB antenna with WLAN band rejection for wireless communications*. *IEEE Trans. Antennas Propag.*, vol. 55, no. 11, pages 3326–3332, 2007.
- [Balanis 1997] C. A. Balanis. *Antenna theory: analysis and design, IInd Ed.* John Wiley and Sons, Inc., 1997.
- [Bao 2007] X. L. Bao and M. J. Ammann. *Investigation on UWB printed monopole antenna with rectangular slitted groundplane*. *Microw. Opt. Technol. Lett.*, vol. 49, no. 7, pages 1585–1587, 2007.
- [Behdad 2004] N. Behdad and K. Sarabandi. *Dual resonant slot antennas for wireless applications*. *Proc. IEEE AP-S Int. Symp.*, pages 1931–1934, 2004.
- [Bennett 1978] C. L. Bennett and G. F. Ross. *Time-domain electromagnetics and its applications*. *Proceedings of the IEEE*, vol. 66, no. 3, pages 299–318, 1978.
- [Bird 2007] T. S. Bird and A. W. Love. volume *Antenna Engineering Handbook*, Chapter 14, Horn antennas. McGraw-Hill, 2007.
- [Chair 2004] R. Chair, A. A. Kishk and K. F. Lee. *Ultrawide-band coplanar waveguide fed rectangular slot antenna*. *IEEE Antennas Wireless Propag. Lett.*, vol. 3, no. 1, pages 227–229, 2004.
- [Chen 2000a] W.-S. Chen, C. C. Huang and K. L. Wong. *A novel microstrip-line fed printed semicircular slot antenna for broad band application*. *Microw. Opt. Technol. Lett.*, vol. 26, no. 4, pages 237–239, 2000.
- [Chen 2000b] Z. N. Chen and M. Y. W. Chia. *Impedance characteristics of trapezoidal planar monopole antenna*. *Microw. Opt. Technol. Lett.*, vol. 27, no. 2, pages 120–122, 2000.
- [Chen 2003a] H. D. Chen. *Broadband CPW-fed square slot antennas with a widened tuning stub*. *IEEE Trans. Antennas Propag.*, vol. 51, no. 8, pages 1982–1986, 2003.

- [Chen 2003b] Z. N. Chen, M. J. Ammann, M. Y. W. Chia and T. S. P. See. *Circular annular planar monopoles with EM coupling*. IEE Proc. Microw. Antennas, Propagat., vol. 150, no. 4, pages 269–273, 2003.
- [Chen 2004a] Z. N. Chen, X. H. Wu, H. F. Li, N. Yang and M. Y. W. Chia. *Considerations for source pulses and antennas in UWB radio systems*. IEEE Trans. Antennas Propag., vol. 52, no. 7, pages 1739–1748, 2004.
- [Chen 2004b] Z. N. Chen, N. Yang, Y. X. Guo and M. Y. W. Chia. *An investigation into measurement of handset antennas*. IEEE Trans. Instrum. Meas., vol. 54, no. 3, pages 1100–1110, 2004.
- [Chen 2005] W. S. Chen and F. M. Hsieh. *A broadband design for a printed isosceles triangular slot antenna for wireless communications*. Microw. J, vol. 48, no. 7, pages 98–112, 2005.
- [Chen 2006] W. S. Chen. *A novel broadband design of a printed rectangular slot antenna for wireless applications*. Microw. J, vol. 49, no. 1, pages 122–130, 2006.
- [Chen 2007a] C-C. Chen. volume Antenna Engineering Handbook, Chapter 19, Ultrawide bandwidth antenna design. McGraw-Hill, 2007.
- [Chen 2007b] Z. N. Chen. *Antenna Engineering Handbook, Chapter 37, Broadband planar antennas for high-speed wireless communications*. McGraw-Hill, 2007.
- [Chen 2007c] Z. N. Chen, T. S. P. See and X. Qing. *Small printed ultrawideband antenna with reduced ground plane effects*. IEEE Trans. Antennas Propag., vol. 55, no. 2, pages 383–388, 2007.
- [Cheng 2008] S. Cheng, P. Hallbjörner and A. Rydberg. *Printed slot planar inverted cone antenna for ultrawideband applications*. IEEE Antennas Wireless Propag. Lett., vol. 7, pages 18–21, 2008.
- [Chiou 2003] J. Y. Chiou, J. Y. Sze and K. L. Wong. *A broad-band CPW-fed strip-loaded square slot antenna*. IEEE Trans. Antennas Propag., vol. 51, no. 4, pages 719–721, 2003.
- [Cho 2006] Y. J. Cho, K. H. Kim, D. H. Choi, S. S. Lee and S.-O. Park. *A miniature UWB planar monopole antenna with 5-GHz band-rejection filter and the time-domain characteristics*. IEEE Trans. Antennas Propag., vol. 54, no. 5, pages 1453–1461, 2006.
- [Choi 2004] S. H. Choi, J. K. Park, S. K. Kim and J. Y. Park. *A new ultrawideband antenna for UWB applications*. Microw. Opt. Techno. Lett., vol. 40, no. 5, pages 399–401, 2004.

- [Collin 2001] R. E. Collin. *Foundations for microwave engineering, IIInd Ed.* John Wiley and Sons, Inc., 2001.
- [Commission 2002] Federal Communications Commission. *First report and order, revision of Part 15 of commission's rule regarding ultra-wide band transmission systems.* FCC 02-48, 2002.
- [CST 2009] *User's Manual.* CST-Microwave Studio, 2009.
- [Denidni 2006] T. A. Denidni and M. A. Habib. *Broadband printed CPW-fed circular slot antenna.* Electron. Lett., vol. 42, no. 3, pages 135–136, 2006.
- [Dilmaghani 2003] R. S. Dilmaghani, M. Ghavami, B. Allen and H. Aghvami. *Novel UWB pulse shaping using prolate spheroidal wave functions.* Proc. IEEE Int. Symp. on Personal, Indoor and Mobile Radio Communications, Beijing, vol. 1, pages 602–606, 2003.
- [Dissanayake 2008] T. Dissanayake and K. P. Esselle. *UWB performance of compact L-shaped wide slot antennas.* IEEE Trans. Antennas Propag., vol. 56, no. 4, pages 1183–1187, 2008.
- [Dong 2009] Y. D. Dong, W. Hong, Z. Q. Kuai and J. X. Chen. *Analysis of planar ultrawideband antennas with on-ground slot band-notched structures.* IEEE Trans. Antennas Propag., vol. 57, no. 7, pages 1886–1893, 2009.
- [Duroc 2007a] Y. Duroc, A. Ghiotto, T.-P. Vuong and S. Tedjini. *UWB antennas: systems With transfer functions and impulse response.* IEEE Trans. on Antennas and Propagat., vol. 55, no. 5, pages 1449–1451, 2007.
- [Duroc 2007b] Y. Duroc, T.-P. Vuong and S. Tedjini. *A time/frequency model for ultrawideband antennas.* IEEE Trans. on Antennas and Propagat., vol. 55, no. 8, pages 2342–2350, 2007.
- [Evans 1999] J. A. Evans and M. J. Ammann. *Planar trapezoidal and pentagonal monopoles with impedance bandwidths in excess of 10:1.* IEEE Antennas and Propagation Society International Symposium, vol. 3, pages 1558–1561, 1999.
- [Filipovic 2007] D. S. Filipovic and T. Cencich. *Antenna Engineering Handbook, Chapter 13, Frequency Independent Antennas.* McGraw-Hill, 2007.

- [Fortino 2008] N. Fortino, J.-Y. Dauvignac, G. Kossiavas and R. Staraj. *Design optimization of UWB printed antennas for omnidirectional pulse radiation*. IEEE Trans. on Antennas and Propagat., vol. 56, no. 7, pages 1875–1881, 2008.
- [Gao 2006] Y. Gao, B. L. Ooi and A. P. Popov. *Band-notched ultra-wideband ring-monopole antenna*. Microw. Opt. Technol. Lett., vol. 48, no. 1, pages 125–126, 2006.
- [Ghavami 2001] M. Ghavami, L. B. Michael and R. Kohno. *Hermite function based orthogonal pulses for UWB communication*. Proc. Int. Symp. on Wireless Personal Multimedia Communications, pages 437–440, 2001.
- [Ghavami 2004] M. Ghavami, L. B. Michael and R. Kohno. *Generation of ultra wideband waveforms*. In Ultra Wideband Signals and Systems in Communication Engineering. John Wiley and Sons, Inc., 2004.
- [Gopikrishna 2007] M. Gopikrishna, D. D. Krishna, C. K. Aanandan, P. Mohanan and K. Vasudevan. *Square monopole antenna for ultra wide band communication applications*. Journal of Electro-Magnetic Waves and Application (JEMWA), vol. 21, pages 1525–1537, 2007.
- [Habib 2006] M. A. Habib and T. A. Denidni. *Design of a new wideband microstrip-fed circular slot antenna*. Microw. Opt. Technol. Lett., vol. 48, no. 5, pages 919–923, 2006.
- [Hong 2007] C.-Y. Hong, C.-W. Ling, I.-Y. Tarn and S.-J. Chung. *Design of a planar ultrawideband antenna with a new band-notch structure*. IEEE Trans. on Antennas and Propagat., vol. 55, no. 12, pages 3391–3397, 2007.
- [Hsu 2006] S. H. Hsu and K. Chang. *Ultra-thin CPW-fed rectangular slot antenna for UWB applications*. Proc. IEEE AP-S Int. Symp., pages 2587–2590, 2006.
- [Huang 2008] Y. Huang and K. Boyle. *Antennas from theory to practice*. John Wiley and Sons, Inc., 2008.
- [Hui 2003] S. Y. Hui and K. H. Yeung. *Challenges in the migration to 4G mobile systems*. IEEE Communications Magazine, pages 54–59, December, 2003.
- [IEE 1979] *IEEE Standard Test Procedures for Antennas*. IEEE Std 149-1979, 1979.

- [Jan 2005] J.-Y. Jan, C.-Y. Hsiang, J.-W. Sul, Y.-T. Cheng and W.-S. Chen. *Printed microstrip-line-fed wideband slot antenna with a hexagonal slot*. Proc. IEEE AP-S Int. Symp., pages 569–572, 2005.
- [Jan 2006] J.-Y. Jan and C.-Y. Hsiang. *Wideband CPW-fed slot antenna for DCS, PCS, 3G and Bluetooth bands*. Electron. Lett., vol. 42, no. 24, pages 1377–1378, 2006.
- [Jan 2007] J. Y. Jan and J. C. Kao. *Novel printed wideband rhombus like slot antenna with an offset microstrip fed line*. IEEE Antennas Wireless Propag. Lett., vol. 6, pages 249–251, 2007.
- [Janevski 2009] T. Janevski. *5G mobile phone concept*. Proceedings of the 6th IEEE Conference on Consumer Communications and Networking Conference, pages 823–824, 2009.
- [Jang 2001] Y. W. Jang. *Large bandwidth double T-shaped microstrip fed single layer single slot antenna*. Microw. Opt. Technol. Lett., vol. 30, no. 3, pages 185–187, 2001.
- [Jang 2003] Y. W. Jang. *A circular microstrip-fed single-layer single-slot antenna for multi-band mobile communications*. Microw. Opt. Technol. Lett., vol. 37, pages 59–62, 2003.
- [Jianxin 2005] L. Jianxin, C. C. Chiau, X. Chen and C. G. Parini. *Study of a printed circular disc monopole antenna for UWB systems*. IEEE Trans. Antennas Propag., vol. 53, no. 11, pages 3500–3504, 2005.
- [John 2005] M. John and M. J. Ammann. *Optimization of impedance bandwidth for the printed rectangular monopole antenna*. Microw. Opt. Technol. Lett., vol. 47, no. 2, pages 153–154, 2005.
- [Johnson 1997] J. M. Johnson and Y. Rahmat-Samii. *The tab monopole*. IEEE Trans. Antennas Propag., vol. 45, no. 1, pages 187–188, 1997.
- [Jongh 1997] R. K. De Jongh, M. Hajian and L. P. Ligthart. *Antenna time-domain measurement techniques*. IEEE Ant. Propag. Mag., vol. 5, no. 39, pages 7–12, 1997.
- [Kahrizi 1993] M. Kahrizi, T. K. Sarkar and Z. A. Maricevic. *Analysis of a wide radiating slot in the ground plane of a microstrip line*. IEEE Trans. Antennas Propag., vol. 41, pages 29–37, 1993.
- [Kan 2007] H.K. Kan, W.S.T. Rowe and A.M. Abbosh. *Compact coplanar waveguide-fed ultrawideband antenna*. Electron. Lett., vol. 43, no. 12, pages 654–656, 2007.

- [Kim 2000] M. K. Kim, K. Kim, Y. H. Suh and I. Park. *A T-shaped microstrip-line-fed wide slot antenna*. Proc. IEEE AP-S Int. Symp., pages 1500–1503, 2000.
- [Kim 2003] Y. Kim, B. J. Jeong, J. Chung, C.-S. Hwang, J. S. Ryu, K.-H. Kim and Y. K. Kim. *Beyond 3G: vision, requirements, and enabling technologies*. IEEE Communications Magazine, pages 120–124, March, 2003.
- [Kim 2005] K. H. Kim, Y. J. Cho, S. H. Hwang and S. O. Park. *Band-notched UWB planar monopole antenna with two parasitic patches*. Electron. Lett., vol. 41, no. 14, pages 783–785, 2005.
- [Kim 2006] J. Kim, C. S. Cho and J. W. Lee. *5.2GHz notched ultra wide band antenna using slot-type SRR*. Electron. Lett., vol. 42, no. 6, pages 315–316, 2006.
- [Klemm 2005] M. Klemm, I. Z. Koves, G. F. Pederson and G. Troster. *Novel small-size directional antenna for UWB WBAN/WPAN applications*. IEEE Trans. on Antennas and Propagat., vol. 53, no. 12, pages 3884–3896, 2005.
- [Kraus 2005] J. D. Kraus and R. J. Mahefka. *Antennas for all applications, 3rd Edn*. Tata McGraw-Hill, 2005.
- [Krishna 2007] D. D. Krishna, M. Gopikrishna, C. K. Aanandan, P. Mohanan and K. Vasudevan. *Compact coplanar waveguide-fed ultrawideband antenna*. International Journal on Wireless and Optical Communications, vol. 4, no. 2, pages 183–194, 2007.
- [Kwon 2003] D. Kwon and Y. Kim. *Suppression of cable leakage current for edge-fed printed dipole UWB antennas using leakage-blocking slots*. IEEE Antennas Wireless Propag. Lett., vol. 5, pages 183–186, 2003.
- [Kwon 2004] D. H. Kwon and Y. Kim. *CPW-fed planar ultra wideband antenna with hexagonal radiating elements*. Proc. IEEE AP-S Int. Symp., vol. 3, pages 2947–2950, 2004.
- [Lamensdorf 1994] D. Lamensdorf and L. Susman. *Baseband-pulse-antenna techniques*. IEEE Antennas and Propagation Magazine, vol. 36, no. 1, pages 20–30, 1994.
- [Langley 1993] J.D.S. Langley, P.S. Hall and P. Newham. *Novel ultrawide-bandwidth Vivaldi antenna with low cross-polarization*. Electron. Lett., vol. 29, no. 23, pages 2004–2005, 1993.

- [Lau 2005] K.-L. Lau, P. Li and K.-M. Luk. *A monopolar patch antenna with a very wide impedance bandwidth*. IEEE Trans. Antennas Propag., vol. 53, no. 2, pages 655–661, 2005.
- [Lee 1999] E. Lee, P. S. Hall and P. Gardener. *Compact wideband planar monopole antenna*. Electron. Lett., vol. 35, no. 35, pages 2157–2158, 1999.
- [Lee 2005] J. W. Lee, C. S. Cho and J. Kim. *A new vertical half disc-loaded ultra-wideband monopole antenna (VHDMA) with a horizontally top-loaded small disc*. IEEE Antennas and Wireless Propagat. Letters, vol. 4, pages 198–201, 2005.
- [Li 2006] P. Li, J. Liang and X. Chen. *Study of printed elliptical/circular slot antennas for ultrawideband applications*. IEEE Trans. Antennas Propag., vol. 54, no. 6, pages 1670–1675, 2006.
- [Liang 2005a] J. Liang, C.C.Chiau, X. Chen and C.G.Parini. *CPW-fed circular ring monopole antenna*. Proc. IEEE AP-S Int. Symp., pages 500–503, 2005.
- [Liang 2005b] J. Liang, C. C. Chiau, X. Chen and C. G. Parini. *Study of a printed circular disc monopole antenna for UWB systems*. IEEE Trans. on Antennas Propag., vol. 53, no. 11, pages 3500–3504, 2005.
- [Licul 2003] S. Licul, J. A. N. Noronha, W. A. Davis, D. G. Sweeney, C. R. Anderson and T. M. Bielawa. *A parametric study of time-domain characteristics of possible UWB antenna architectures*. Proc. IEEE AP-S Int. Symp., pages 3110–3114, 2003.
- [Lin 2005] C.C. Lin, Y.C. Kan, L.C. Kuo and H.R. Chuang. *A planar triangular monopole antenna for UWB communication*. IEEE Microwave Wireless Compon. Lett., no. 15, pages 624–626, 2005.
- [Lin 2006] Y.-C. Lin and K.-J. Hung. *Compact ultrawideband rectangular aperture antenna and band-notched designs*. IEEE Trans. Antennas Propag., vol. 54, no. 11, pages 3075–3081, 2006.
- [Ling 2007] C.-W. Ling, W.-H. Lo, R.-H. Yan and S.-J. Chung. *Planar binomial curved monopole antennas for ultrawideband communication*. IEEE Trans. Antennas Propag., vol. 55, no. 9, pages 2622–2624, 2007.
- [Liu 2004a] Y. Liu, K. L. Lau and C. H. Chan. *Microstrip-fed wide slot antenna with wide operating bandwidth*. Proc. IEEE AP-S Int. Symp., vol. 3, pages 2285–2288, 2004.

- [Liu 2004b] Y. F. Liu, K. L. Lau, Q. Xue and C. H. Chan. *Experimental studies of printed wide-slot antenna for wide-band applications*. IEEE Antennas Wireless Propag. Lett., vol. 3, pages 273–275, 2004.
- [Lui 2005] W. J. Lui, C. H. Cheng and H. B. Zhu. *Frequency notched printed slot antenna with parasitic open-circuit stub*. Electron. Lett., vol. 41, no. 20, pages 1094–1095, 2005.
- [Lui 2006] W. J. Lui, C. H. Cheng and H. B. Zhu. *Compact frequency notched ultra-wideband fractal printed slot antenna*. IEEE Micro. Wireless Comp. Lett., vol. 16, no. 4, pages 224–226, 2006.
- [McLean 2008] J. S. McLean and R. Sutton. *Considerations for source pulses and antennas in UWB radio systems*. Proc. IEEE Int. Conf. on Ultra-wideband, vol. 2, pages 113–116, 2008.
- [Mohammadian 2003] A. H. Mohammadian, A. Rajkotia and S. S. Soliman. *Characterization of UWB transmit-receive antenna systems*. IEEE Conf. on Ultra-wideband Systems and Technology, pages 157–161, 2003.
- [Mushiake 1992] Y. Mushiake. *Self-complimentary antennas*. IEEE Antennas Propagat. Mag., vol. 34, pages 23–29, 1992.
- [Oppermann 2004a] I. Oppermann. *The role of UWB in 4G*. In Wireless Personal Communications, volume 29, pages 121–133. Kluwer Academic Publishers, 2004.
- [Oppermann 2004b] I. Oppermann, M. Hamalainen and J. Iinatti. *UWB theory and applications*. John Wiley and Sons, Inc., 2004.
- [Pancera 2007] E. Pancera, D. Modotto, A. Locatelli, F. M. Pigozzo and C. De Angelis. *Novel design of UWB antenna with band-notch capability*. European Microwave Week 2007, ECWT, Munich, 2007.
- [Pantoja 1987] R. Pantoja, A. Sapienza and F. M. Filho. *A microwave printed planar log-periodic dipole array antenna*. IEEE Trans. on Antennas and Propagat., no. 35, pages 1176–1178, 1987.
- [Papio-Toda 2007] A. Papio-Toda, W. Sorgel, J. Joubert and W. Wiesbeck. *UWB antenna transfer property characterization by FDTD simulations*. INICA 2007 International Conference on Antennas, Munich, pages 81–85, 2007.
- [Parr 2003] B. Parr, B. Cho, K. Wallace and Z. Ding. *A novel ultra-wideband pulse design algorithm*. IEEE Communications Letters, vol. 7, no. 5, pages 219–221, 2003.

- [Peyrot-Solis 2007] M. A. Peyrot-Solis, J. A. Tirado-Mendez and H. Jardón-Aguilar. *Design of multiband UWB planarized monopole using DMS technique*. IEEE Antennas Wireless Propag. Lett., vol. 6, pages 77–79, 2007.
- [Poazar 1986] D. M. Pozar. *Reciprocity method of analysis for printed slot antenna and slot-coupled microstrip antennas*. IEEE Trans. Antennas Propag., vol. 34, no. 12, pages 1439–1466, 1986.
- [Qing 2003] X. Qing, M. Y. W. Chia and X. Wu. *Wide-slot antenna for UWB applications*. Proc. IEEE AP-S Int. Symp., vol. 1, pages 834–837, 2003.
- [Qu 2006a] S.-W. Qu, J. L. Li and Q. Xue. *A band-notched ultrawideband printed monopole antenna*. IEEE Antennas Wireless Propag. Lett., vol. 5, pages 495–498, 2006.
- [Qu 2006b] S.-W. Qu, J.-L. Li and Q. Xue. *Broadband microstrip-line-fed wide slot antenna with improved patterns*. Electron. Lett., vol. 42, no. 16, 2006.
- [Qu 2006c] S. W. Qu, C. Ruan and B. Z. Wang. *Bandwidth enhancement of wide-slot antenna fed by CPW and microstrip line*. IEEE Antennas Wireless Propag. Lett., vol. 5, pages 15–17, 2006.
- [Rajgopal 2009] S. K. Rajgopal and S. K. Sharma. *Investigations on ultra-wideband pentagon shape microstrip slot antenna for wireless communications*. IEEE Trans. Antennas Propag., vol. 57, no. 5, pages 1353–1359, 2009.
- [Ray 2006] K.P. Ray and Y. Ranga. *Ultra-wideband printed modified triangular monopole antenna*. Electron. Lett., vol. 42, no. 19, pages 1081–1082, 2006.
- [Ray 2007] K.P. Ray, Y. Ranga and P. Gabhale. *Printed square monopole antenna with semicircular base for ultra-wide bandwidth*. Electron. Lett., vol. 43, no. 5, pages 13–14, 2007.
- [Rumsey 1966] V. H. Rumsey. *Frequency independent antennas*. New York: Academic, 1966.
- [Schantz 2002] H. G. Schantz. *Radiation Efficiency of UWB Antennas*. Proceedings of the 2002 IEEE UWBST Conference, 2002.
- [Schantz 2003] H. G. Schantz. *UWB magnetic antennas*. Proc. IEEE AP-S Int. Symp., vol. 3, pages 604–607, 2003.

- [Sheng 2003] H. Sheng, P. Orlik, A. M. Haimovich, L. J. Cimini and J. Zhang. *On the spectral and power requirements for ultra-wideband transmission*. Proc. IEEE Int. Conf. on Communications, pages 738–742, 2003.
- [Shlivinski 1997] A. Shlivinski, E. Heyman and R. Kastner. *Antenna characterisation in the time domain*. IEEE Trans. on Antennas and Propagat., vol. 45, pages 1140–1149, 1997.
- [Shrivastava 2007] V. Shrivastava and Y. Ranga. *Ultra wide band CPW-fed printed pentagonal antenna with modified ground plane for UWB applications*. Proc. IEEE AP-S Int. Symp., page not known, 2007.
- [Shum 1995] S. M. Shum, K. F. Tong, X. Zhang and K. M. Luk. *FDTD modelling of microstrip-line-fed wide slot antenna*. Microw. Opt. Techno. Lett., vol. 10, no. 10, pages 118–120, 1995.
- [Simons 2001] R. N. Simons. *Coplanar Waveguide Circuits, Components, and Systems*. page 11. John Wiley and Sons, Inc., 2001.
- [Siwiak 2004] K. Siwiak and D. McKeown. *Ultra-wideband radio technology*. John Wiley and Sons, Inc., 2004.
- [Smyth 2004] P. Smyth. *Ultra-wideband and its capabilities*. In Mobile and Wireles Communications, Key Technoloies and Future Applications, BT Communication Technology Series 9, pages 81–100. The Institution of Engineering and Technology, London, UK, 2004.
- [Sorgel 2003] W. Sorgel, C. Waldschmidt and W. Wiesbeck. *Transient responses of a vivaldi antenna and a logarithmic periodic dipole array for ultra wideband communication*. Proc. IEEE AP-S Int. Symp., pages 592–595, 2003.
- [Sorgel 2005] W. Sorgel and W. Wiesbeck. *Influence of antennas on ultra-wideband transmisson*. EURASIP J. App. Signal Processing, pages 296–305, 2005.
- [Stutzman 1981] W. L. Stutzman. In Antenna theory and design. John Wiley and Sons, Inc., 1981.
- [Su 2006] S.-W. Su and K.-L. Wong. *Printed band-notched ultra wideband quasi-dipole antenna*. Microw. Opt. Techno. Lett., vol. 48, no. 3, pages 418–420, 2006.
- [Su 2007] S.-W. Su, J.-H. Chou and K.-L. Wong. *Internal Ultrawideband Monopole Antenna for Wireless USB Dongle Applications*. IEEE Trans. Antennas Propag., vol. 55, no. 4, pages 1180–1183, 2007.

- [Suh 2004] S. Y. Suh, W. L. Stutzman and W. A. Davis. *A new ultrawideband printed monopole antenna: the planar inverted cone antenna (PICA)*. IEEE Trans. on Antennas and Propagat., vol. 52, no. 5, pages 1361–1364, 2004.
- [Sze 2001] J. Y. Sze and K. L. Wong. *Bandwidth enhancement of a microstripline fed printed wide-slot antenna*. IEEE Trans. on Antennas and Propagat., vol. 49, no. 7, pages 1020–1024, 2001.
- [Sze 2003] J. Y. Sze and K. L. Wong. *Bandwidth enhancement of a microstrip line fed printed wide slot antenna*. IEEE Trans. Antennas Propag., vol. 49, no. 7, pages 194–196, 2003.
- [Taylor 1995] J. D. Taylor. *Introduction to ultrawideband radar systems*. CRC Press, 1995.
- [Telzhensky 2006] N. Telzhensky and Y. Leviatan. *Planar differential elliptical UWB antenna optimization*. IEEE Trans. on Antennas and Propagat., vol. 54, no. 11, pages 3400–3405, 2006.
- [Thomas 2007] K. G. Thomas and N. Lenin. *Ultra wideband printed monopole antenna*. Microw. Opt. Technol. Lett., vol. 49, no. 5, pages 1082–1085, 2007.
- [Vasylchenko 2008] A. Vasylchenko, W. D. Raedt and G. A. E. Vandenbosch. *Design and parametric analysis of a very compact UWB antenna with band rejection feature*. Proc. of iWAT2008, vol. 3, pages 430–433, 2008.
- [W.-F. Chen 2008] C.-C. Tsai W.-F. Chen and C.-Y. Huang. *Compact wide-slot antenna for ultra-wideband communications*. Electron. Lett., vol. 44, no. 15, pages 892–893, 2008.
- [Weisbeck 2009] W. Weisbeck, G. Adamiuk and C. Sturm. *Basic properties and design principles of UWB antennas*. Proceedings of the IEEE, vol. 97, no. 2, pages 372–385, 2009.
- [Werner 2003] D. H. Werner and S. Ganguly. *An overview of fractal antenna engineering research*. IEEE Ant. and Prop. Mag., vol. 5, no. 1, pages 38–57, 2003.
- [Wong 2005a] K. L. Wong, Y. W. Chi, C. M. Su and F. S. Chang. *Band-notched ultra-wideband circular-disk monopole antenna with an arc-shaped slot*. Microw. Opt. Technol. Lett., vol. 45, no. 3, pages 188–191, 2005.

- [Wong 2005b] K.-L. Wong, C. H. Wu and S.-W. Su. *Ultra-wideband square planar metal-plate monopole antenna with a trident shaped feeding strip*. IEEE Trans. Antennas Propag., vol. 53, no. 4, pages 1262–1268, 2005.
- [Wu 2004a] J. W. Wu, H. M. Hsiao, J. H. Lu and S. H. Chang. *Dual broadband design of rectangular slot antenna for 2.4 and 5GHz wireless communication*. Electron. Lett., vol. 40, no. 23, 2004.
- [Wu 2004b] X. H. Wu, Z. N. Chen and N. Yang. *Optimization of planar diamond antenna for single/multiband UWB wireless communications*. Microw. Opt. Techno. Lett., vol. 42, no. 6, pages 451–455, 2004.
- [Wu 2007a] Q. Wu, R. Jin, J. Geng and M. Ding. *Pulse preserving capabilities of printed circular disk monopole antennas with different grounds for the specified input signal forms*. IEEE Trans. Antennas Propag., vol. 55, no. 10, pages 2866–2873, 2007.
- [Wu 2007b] Q. Wu, R. Jin, J. Geng and J. Lao. *Ultra-wideband rectangular disk monopole antenna with notched ground*. Electron. Lett., vol. 43, no. 11, pages 605–606, 2007.
- [Wu 2008] Q. Wu, R. Jin, J. Geng and M. Ding. *Printed omni-directional UWB monopole antenna with very compact size*. IEEE Trans. Antennas Propag., vol. 56, no. 3, pages 896–899, 2008.
- [Xia 2008] Y.Q. Xia and Z.G. Duan. *Compact CPW-fed dual ellipses antenna for ultra-wideband system*. Electron. Lett., vol. 44, no. 9, pages 567–567, 2008.
- [Yan 2008] X.-R. Yan, S.-S. Zhong and G.-Y. Wang. *Compact printed monopole antenna with 24:1 impedance bandwidth*. Electron. Lett., vol. 44, no. 2, 2008.
- [Yin 2008] K. Yin and J. P. Xu. *Compact ultra-wideband antenna with dual bandstop characteristic*. Electron. Lett., vol. 44, no. 7, pages 453–454, 2008.
- [Yiqiong 2005] J. S. Yiqiong, S. Aditya and C. L. Law. *Transfer function characterization of UWB antennas based on frequency domain measurement*. 8th European Conference on Wireless Technology, London, pages 277–280, 2005.
- [Yo 2007] D. M. K. Ah Yo and R. Emrik. *Antenna Engineering Handbook, Chapter 2, Frequency bands for military and commercial applications*. pages 9–14. McGraw-Hill, 2007.

- [Yoon 2004] H. Yoon, H. Kim, K. Chang, Y. J. Yoon and Y. H. Kim. *A study on the UWB antenna with band-rejection characteristic*. Proc. IEEE AP-S Int. Symp., no. 2, pages 1784–1787, 2004.
- [Yoon 2006] H. K. Yoon, Y. Lim, W. Lee and Y. J. Yoon. *UWB wide slot antenna with band-notch function*. Proc. IEEE AP-S Int. Symp., pages 3059–3062, 2006.
- [Yoshimura 1972] Y. Yoshimura. *A microstrip line slot antenna*. IEEE Trans. Microwave Theory Tech., vol. MTT-20, pages 760–762, 1972.
- [Zhang 2004a] H. Zhang and R. Kohno. *SSA realization in UWB multiple access systems based on prolate spheroidal wave functions*. Proc. IEEE Wireless Communications and Networking Conf., pages 1794–1799, 2004.
- [Zhang 2004b] Y. Zhang, Z. N. Chen and M. Y. W. Chia. *Effects of finite ground plane and dielectric substrate on planar dipoles for UWB applications*. Proc. IEEE AP-S Int. Symp., pages 2512–2515, 2004.
- [Zhang 2008] J.-P. Zhang, Y.-S. Xu and W.-D. Wang. *Microstrip-fed semi-elliptical dipole antennas for ultrawideband communications*. IEEE Trans. Antennas Propag., vol. 56, no. 1, pages 241–245, 2008.
- [Zhong 2007] S.-S. Zhong, X.-L. Liang and Wei Wang. *Compact elliptical monopole antenna with impedance bandwidth in excess of 21:1*. IEEE Trans. Antennas Propag., vol. 55, no. 11, pages 3082–3086, 2007.
- [Zwierzchowski 2003] S. Zwierzchowski and P. Jazayeri. *Derivation and determination of the antenna transfer function for use in ultra-wideband communications*. Proc. Wireless, Calgary, Alberta, Canada, pages 533–543, 2003.

Square patch antenna with triangular slots

Multi frequency microstrip antennas use a single structure for communication at different frequencies, thus giving the benefits of space, cost and mobility in different cellular networks [1]. These antennas generally have two types of applications in the telecommunication area: systems in which two types of standards are combined such as personal handsets combining GSM and DCS 1800 modes in Europe, and applications in which different frequencies are used for transmission and reception such as personal satellite communications and cellular network systems.

Numerous designs for dual frequency microstrip antennas are available in literature. In many cases, the resonances are at adjacent orthogonal modes so that the radiation is orthogonally polarized at the same/dual frequencies. Consequently, such an antenna finds applications in frequency reuse or simultaneous transmit-receive operation at the same frequency [2].

In land mobile communication systems, performance is deteriorated as a result of multi-path propagation. Multi-path effects can be reduced by polarization diversity or by using dual linearly polarized antennas [3-4]. The use of dual polarizations can also double the number of channels available in the limited bandwidth. However for simultaneous receive and transmit operation, a higher level of isolation between the orthogonal modes excited in the antenna is needed for avoiding crosstalk [5].

Design of compact square microstrip patch antennas with triangular slots inscribed for a dual polarized/dual frequency operation, suitably designed for mobile/wireless access standards like GSM 1.8GHz and WLAN 2.4GHz frequencies, is presented in this section.

The four different types of antennas designed in this section are, namely,

- Design 1: a dual linearly polarized square microstrip antenna with triangular slots,
- Design 2: a dual frequency dual polarized square microstrip antenna with a bow tie shaped-slot,
- Design 3: an electronically switchable dual frequency dual polarized square microstrip antenna with triangular slots,
- Design 4: a dual frequency square microstrip antenna with fractal based slots.

A size reduction is achieved in all the designs by means of reactive loading in the form of slots on the surface of the patch. Such loading increases the surface current path and the electrical length of the element, which leads to a reduction of the patch size for a given resonant frequency [6]. Hence such designs are highly desired in the new-generation wireless applications due to their compact size and dual frequency/dual polarized operation.

Geometry

The basic configuration of the proposed microstrip antennas, for exciting dual frequencies and dual polarizations, is shown in Fig.A.1 with dimensions in mm. A square patch with the triangular slots, symmetric with respect to the patch diagonals and printed on a substrate with $\varepsilon_{r1}=4.4$ & $h_1=1.6\text{mm}$, is electromagnetically coupled to 50Ω microstrip feed lines fabricated on a substrate with $\varepsilon_{r2}=3.1$ & $h_2=1.6\text{mm}$.

Fig.A.1(a) shows a square microstrip patch with two triangular slots for single frequency dual polarized operation at 1.65GHz. Fig.A.1(b) shows a bow-tie shaped slotted patch antenna, which is obtained when the two diagonally symmetric triangular slots inscribed in the square patch are overlapped. This should lower the resonant frequency of the square patch because of the increase in the surface current path by virtue of the slot.

Electronically switchable microstrip antenna with triangular slots is shown in Fig.A.1(c), which has a PIN diode connected across the slots. The diode can be switched ON or OFF by applying DC voltage which is isolated using

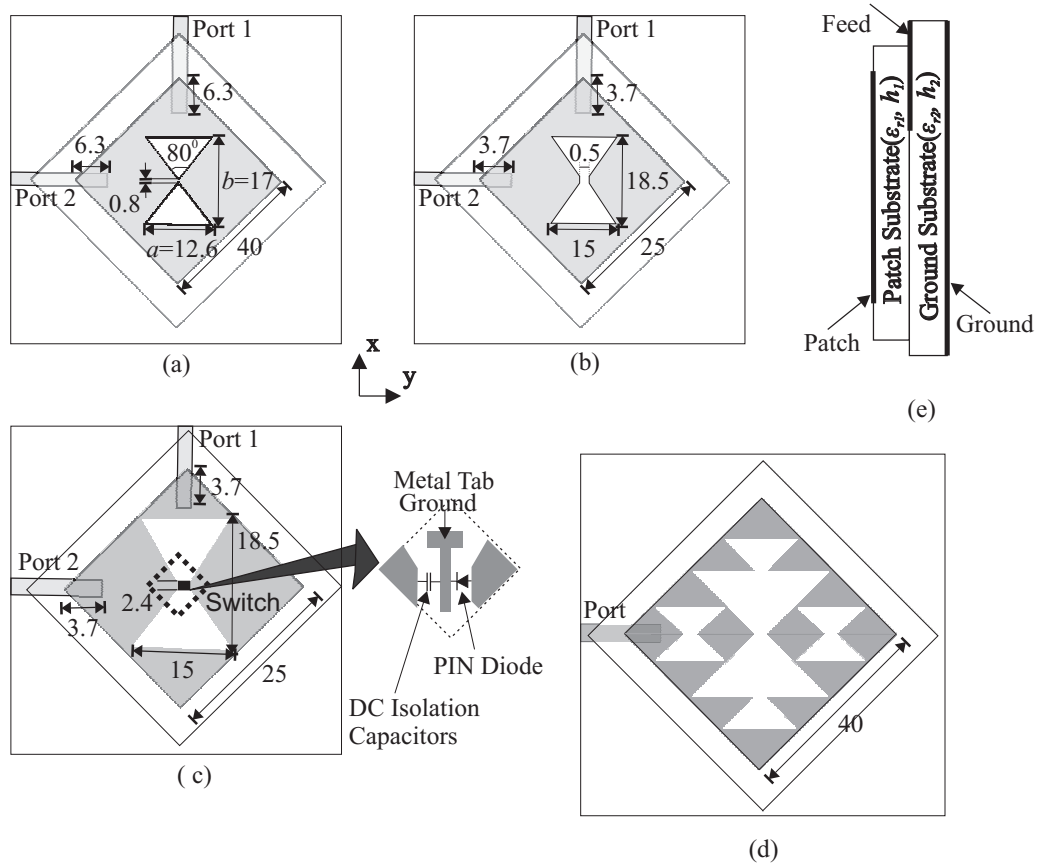


Fig. A.1: Geometry of the square microstrip antenna designs with triangular slots (a) Design 1, (b) Design 2, (c) Design 3, (d) Design 4

a capacitor. When the diode is in the ON state they essentially behave as a short circuit and the RF signal is guided through the PIN diode. They are represented by conductive metal tabs. On the other hand, when the PIN diode is in the OFF state, they behave as open circuit. It has been established that, these simplified implementations of switches should provide acceptable representations for the actual switches [7]. According to the switching state of the PIN diode, the antenna operates as a dual frequency dual polarization antenna at 1.8GHz and 2.4GHz or as a dual linearly polarized antenna at 2.4GHz.

The design 4, shown in Fig.A.1(d), consists of a square microstrip patch antenna embedded with modified Sierpinski gasket slots. It has been shown that fractal shapes by virtue of its self similarity property can be successfully applied to the design of multi-band antennas [8, 9]. This, combined with

the fact that slot loaded microstrip patches exhibits size reduction, has been applied here to design a compact patch antenna with fractal based slots to operate at multiple bands.

Simulations and Measurements

The simulated and measured return loss (S_{ii} with $i=1$ for port 1 and $i=2$ for port 2) of the designed antennas along with the isolation between the ports (S_{21}) is plotted in Fig.A.2. The effect of the slots, inscribed on the square patch, on the antenna radiating properties is studied by comparing the power received from the antennas and an un-slotted square patch of the same size and is plotted in Fig.A.2. A standard horn antenna (at port 3) is used to receive the co-polarized power from the antennas all placed at the same distance.

To have an insight on the polarization behavior of the antennas, their current distributions at the resonant frequencies are plotted in Fig.A.3, where the darker areas represents higher intensity. The co and cross-polarized antenna radiation patterns are measured and plotted in Fig.A.4, when either of the ports are excited while the other is match terminated.

Results and Conclusion

The following are the results of the different compact square microstrip patch antennas, designed for dual frequency orthogonally polarized operation, presented in this section. The results of this work has been reported by the author in various international journals and conferences.

- Design 1: reported in *Publication no. 9*;

It is observed from Fig.A.2(a) that the antenna exhibits a single frequency dual polarized operation at 1.65GHz and an isolation greater than 36dB. It is also observed that the gain of the proposed antenna, operating at a lower frequency, is comparable with that of the un-slotted square patch of the same size.

The current distribution on the patch at 1.65GHz, when either of the two ports is excited, depicted in Fig.A.3(a) & (b), shows that the polarization

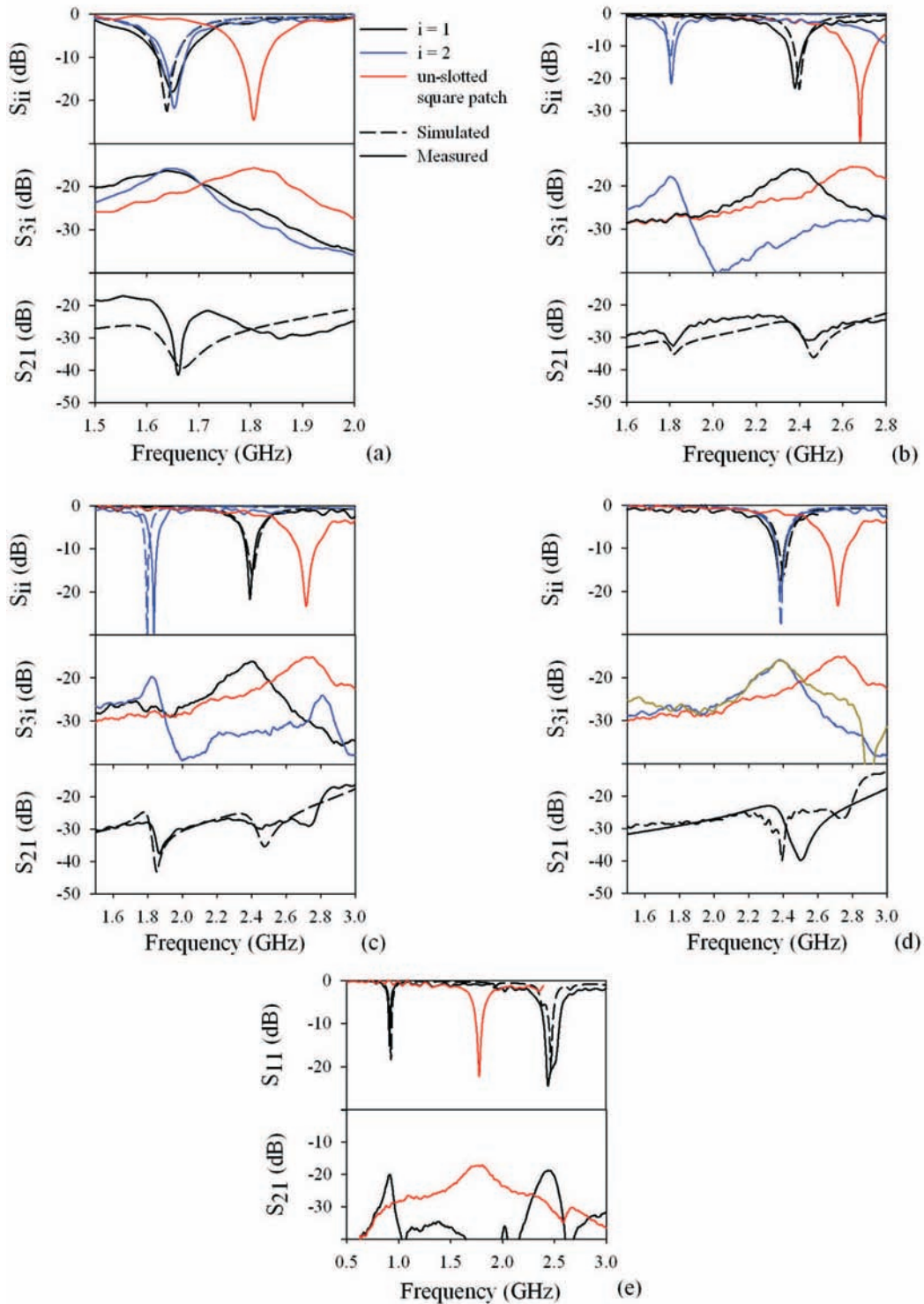


Fig. A.2: Return loss S_{ii} for $i=1$ and 2 corresponding to ports 1 and 2, isolation between the ports (S_{2i}) and the power received by a standard horn (S_{3i}) for (a) Design 1, (b) Design 2, (c) Design 3 (switch OFF), (d) Design 3 (switch ON), and (e) Design 4

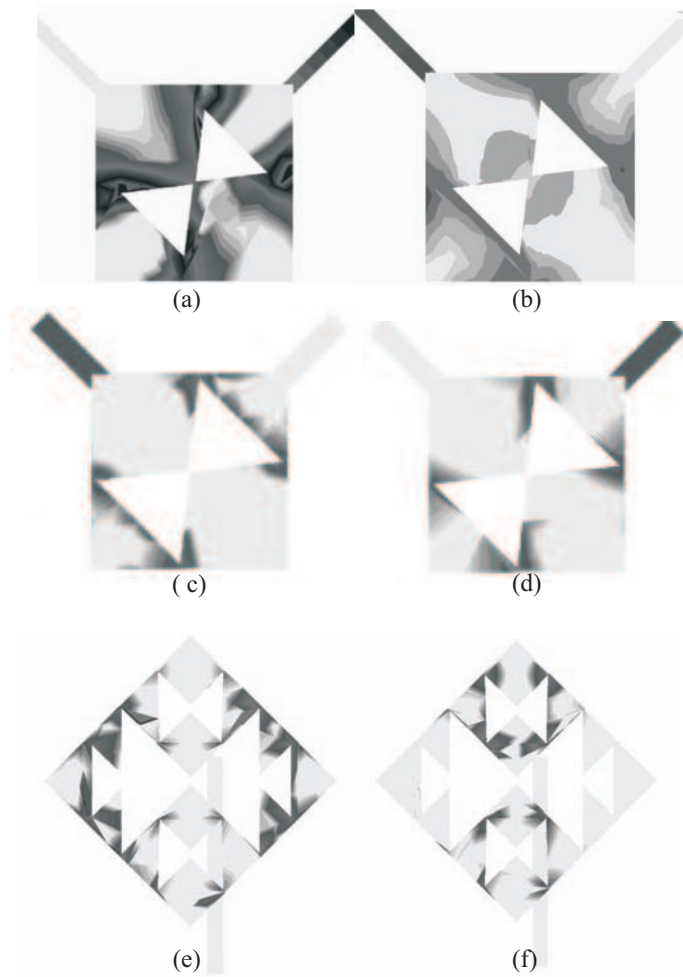


Fig. A.3: The simulated current distribution on the patch; Design 1 (a) at 1.65GHz when port 1 is excited with port 2 terminated in a matched impedance, (b) at 1.65GHz when port 2 is excited with port 1 terminated in a matched impedance; Design 2 (c) at 1.8GHz, (d) at 2.4GHz; Design 4 (e) at 900MHz, and (f) at 2.4GHz

is along the diagonals of the square patch. The isolation between them is improved by adjusting the feed position in the region where the electric field on the patch obtained by feeding the other port is minimum.

For a single frequency operation, it is critical that the surface currents around the slot in both the orthogonal directions have to traverse equal lengths. The resonant frequency of the proposed antenna can be varied by varying the dimensions of the slot uniformly. Simulation studies show that a minimum resonant frequency of 1.5GHz is observed for $a=17\text{mm}$

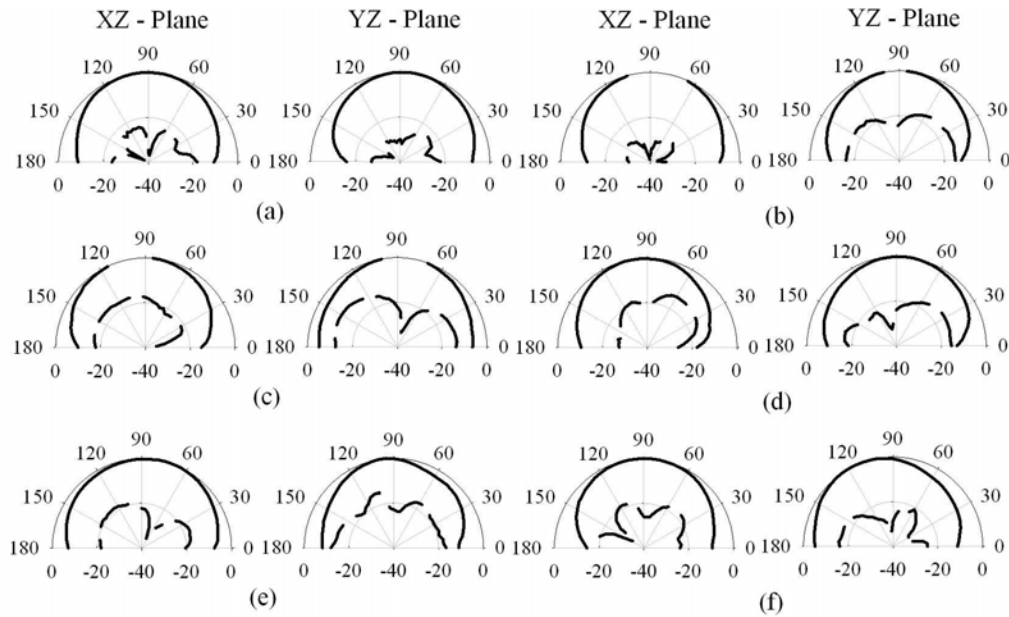


Fig. A.4: The measured radiation patterns of the antenna; Design 1 (a) at 1.65GHz when excited at port 1 with port 2 terminated in a matched impedance, (b) at 1.65GHz when excited at port 2 with port 1 terminated in a matched impedance; Design 2 (c) at 1.8GHz, (d) at 2.4GHz; Design 4 (e) at 900MHz, and (f) at 2.4GHz

and $b=21.2\text{mm}$ while the rest of the antenna parameters remain same. For the same resonant frequency, an un-slotted patch has a side dimension of 49.5mm where as the proposed antenna side is only 40mm. Hence, a size reduction of 35% is as well achieved.

- Design 2: reported in *Publication no. 10*;

Fig.A.2(b) shows that the antenna resonates at 1.81GHz and 2.39GHz when excited at ports 2 and 1 respectively and an isolation better than 30dB is observed. The radiated power from the antenna excited at one of the ports with the other is terminated in its matching impedance is compared with an un-slotted square patch of the same size. It is observed that the proposed antenna operates at a lower frequency when compared to the un-slotted square patch, with out significant reduction in gain.

The simulated current distributions on the patch at the two resonances are given in Fig.A.3(c) & (d), which shows that at the higher resonance frequency (2.39GHz), the antenna is linearly polarized along $\pm X$ axis

and for the lower resonance (1.81GHz), it is along $\pm Y$ axis.

For a resonance at 1.8GHz, an un-slotted square patch has a dimension of 41mm^2 where as the proposed antenna size is only 25mm^2 . Hence, a size reduction of 63% is achieved. This configuration would be useful in GSM (1.8GHz) and WLAN (2.4GHz) applications.

- Design 3: reported in *Publication no. 11*;

It is observed, from Fig.A.2(c) & (d), that the antenna exhibits dual band orthogonal polarization at 1.8GHz (port 2) and 2.4GHz (port 1), when the diode is in OFF state. When diode is in ON state, it exhibits dual linear polarizations at 2.4GHz. Isolation better than 30dB is observed between the ports.

The radiation characteristics of the antenna for different diode states is compared with a simple square patch antenna of the same size, which resonates at 2.75GHz. It shows that the frequencies of operation have been reduced, when compared to an un-slotted patch, with their relative gains comparable under different switching state of the diode but with a slight reduction at 1.8GHz (port 2).

- Design 4: reported in *Publication no. 12*;

It is observed, from Fig.A.2(e), that the antenna resonates at two distinct frequencies, 900MHz and 2.43GHz with bandwidths 15MHz (893 MHz to 908MHz) and 150MHz (2.40GHz to 2.55GHz) respectively. For resonance at 900MHz, the dimensions of an un-slotted patch would be $83 \times 83\text{mm}$ where as in the present design it is only $40 \times 40\text{mm}$. Hence there is 77% size reduction.

The simulated current distribution on the patch antenna, shown in Fig.A.3(e) & (f), indicate that the higher resonant frequency of patch is due to the smaller slots and lower resonance due to the central slot. The radiated power from these antennas received by a standard antenna is shown in the Fig.A.2(e). It is found that the radiation at both frequencies are linearly polarized along the $\pm Y$ axis (along the diagonal of the patch) where the resonance of an un-slotted patch is at 1.8GHz.

The measured co and cross-polarized radiation patterns along the XZ and YZ planes for all the antennas designed, at their corresponding resonance frequencies, are plotted in Fig.A.4. The patterns are broad as in the case of a conventional square patch antenna and offer a cross-polarization level better than -20dB.

References

1. R. Garg, P. Bhartia, I. Bahl and A. Ittipiboon, *Microstrip Antenna Design Handbook*, Artech House, 1995.
2. D. H. Schaubert, F. G. Farrar, A. Sindoris and S. T. Hayes. *Microstrip antennas with frequency agility and polarization diversity*. IEEE Trans. Antennas Propag., vol. 29, no. 1, pages 118-123, 1981.
3. J. S. Colburn, Y. Rahmat-Samii, M. A. Jensen and G. J. Pottie. *Evaluation of personal communications dual-antenna handset diversity performance*. IEEE Trans. Veh. Technol., vol. 47, no. 3, pages 737-746, 1998.
4. S. H. Hong, Y. S. Lee, M. S. Choi and Y. J. Yoon. *Polarization diversity with directional antennas for indoor environments*. Asia and Pacific Microwave Symposium (APMC), vol. 3, pages 781-784, 1999.
5. S. L. Karode and V. F. Fusco. *Dual polarized microstrip patch antenna using feed forward isolation enhancement for simultaneous transmit receive applications*. National Conf. on Ant. and Propag., IEE, no. 461, pages 49-52, 1999.
6. K. L. Wong. *Compact and broadband microstrip antenna*. John Wiley and Sons, Inc., 2002.
7. F. Yang and Y. R. Samii. *Patch antennas with switchable slots (PASS) in wireless communications: concepts, designs, and applications*. IEEE Ant. Propag. Mag., vol. 47, no. 2, pages 13-29, 2005.

8. C. Puente, J. Romeu, R. Pous and A. Cardama. *On the behavior of Sierpinski multiband fractal antenna*. IEEE Trans. Antennas Propag., vol. 46, no. 4, pages 517-524, 1998.
9. S. R. Best. *On the significance of self-similar fractal geometry in determining the multiband behavior of Sierpinski gasket antenna*. IEEE Trans. Antennas Propag., vol. 1, no. 1, pages 22-25, 2002.

Circular patch antenna with sector slot

A simple technique for achieving compact dual band microstrip antenna designs has been to load the radiating patch with a slot, which when appropriately designed can not only lower the fundamental resonant frequency of the antenna but also lead to a dual band operation. It is the meandering of the excited surface current paths in the radiating patch of the antenna that lowers its resonant frequency.

The meandering of the surface current paths can be achieved by loading several meandering slits at the non radiating edges of a rectangular patch [1] or at the boundary of a circular patch [2] or by loading slots inside the radiating patch [3]. The dual frequency operation is achieved when the slots perturb the fundamental resonant frequency of the patch exciting a new resonance mode. The resonance frequency of the new mode can be either lower [4,5] or higher [6] than the original dominant mode with either the same [4] or orthogonal polarization [7] and is strongly dependent on the slot dimensions.

In this section, a circular patch antenna loaded with a sector slot for dual band operation is presented. The lower resonance of the antenna is by virtue of the increase in the current path on the patch due to the slot while the higher resonance is similar to that of an un-slotted circular patch of same size. Since the introduction of the slot provides a lower resonance, an overall reduction in the patch area is also obtained.

The four different types of antennas designed in this section are, namely,

- Design 1: a microstrip fed circular microstrip antenna with sector slot,
- Design 2: a dual frequency dual polarized circular microstrip antenna with sector slot,

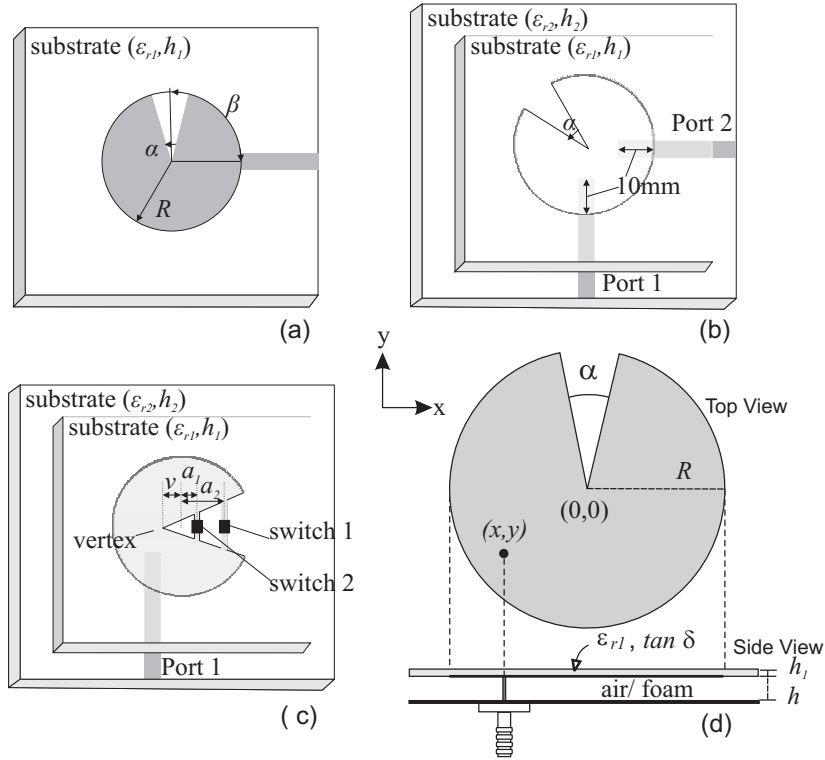


Fig. B.1: Geometry of the circular microstrip antenna designs with sector slot (a) Design 1, (b) Design 2, (c) Design 3, (d) Design 4

- Design 3: an electronically switchable circular microstrip antenna with sector-slot for multiple frequency operation,
- Design 4: a probe fed circular microstrip antenna with sector-slot with superstrate.

Geometry

Circular microstrip antennas are attractive as radiating elements due to their smaller area, as compared to rectangular patch antennas resonating at the same frequency. However, the high input impedance along the circumference restricts the direct use of microstrip feed to a circular patch. It has been reported that by perturbing the circular geometry via cutting a sector slot, a wide variation in the input impedance along the circumference of the patch is obtained [8]. Hence, the first design presented is a circular patch with sector

slot excited using a microstrip feed line on the circumference and is shown in Fig.B.1(a). The patch dimensions are $R=17.5\text{mm}$, $\alpha=20^\circ$ printed on FR4 glass epoxy substrate with $\epsilon_{r1}=4.36$ and $h_1=1.6\text{mm}$.

It is demonstrated that a circular patch with a sector slot exhibits dual resonances with orthogonal polarizations. This patch, when excited using a microstrip feed, can be operated at either of the resonant frequencies by switching the feed point at the periphery of the patch.

The two ports can also be simultaneously excited to have transmit/receive operations in the dual band. A good level of isolation between the ports is necessary for these antennas to eliminate cross talk. This is attained using electromagnetic feed geometry with two feed lines, each exciting one frequency. This is the second design presented as shown in Fig.B.1(b) where the 50Ω microstrip feed lines are printed on another substrate with $\epsilon_{r2}=4.36$ and $h_2=1.6\text{mm}$.

Due to the presence of the slot, the circular patch with sector slot operates at a much lower frequency compared to that of an un-slotted circular patch. In the third design shown in Fig.B.1(c), the slot is shunted at different points using PIN diodes. Depending upon the state of the PIN diodes (ON or OFF), the resonance of the antenna is found to be switching between three distinct frequencies. The dimensions of the patch are radius $R=16.5\text{mm}$, with a sector slot angle $\alpha=30^\circ$, with its vertex extended beyond the center of the patch by $v=2\text{mm}$. The patch is fed electromagnetically by a 50Ω microstrip line, both printed on same substrate used in the previous designs. The PIN diodes are placed across the slot, at $a_1=5\text{mm}$ and $a_2=10\text{mm}$ from the center of the patch. PIN diodes are integrated across the sector-slot through 100pF capacitors. The capacitors are used to isolate the DC bias circuit from RF. The DC bias is provided between the metal tab, in between the capacitors and diodes, and the rest of the patch.

In the fourth design, a single probe-fed circular patch antenna loaded with a sector slot along with a superstrate, as shown in Fig.B.1(d), having dual band operation is presented. The coordinates of the probe feed is suitably chosen for maximum impedance matching at both the resonances. A superstrate when employed not only protects the antenna from environmental hazards but lowers its resonance frequency further. The present design has

a coaxially fed conducting patch with air/foam as substrate and FR4 dielectric ($\epsilon_{r1}=4.36$, $h_1=1.6\text{mm}$ and $\tan\delta=0.02$) as radome. In this case, as copper cannot be deposited on air/foam, the patch was fabricated on FR4, inverted and supported by nylon spacers. The dimensions of the patch are radius $R=15.5\text{mm}$, with a sector slot angle $\alpha=20^\circ$, with the coaxial probe at (6, 6). The size of the ground plate and superstrate is $100\times 100\text{mm}^2$.

Simulations and Measurements

The simulated and measured return loss of the antennas designed, along with the isolation between the ports in the case of the dual port design, are plotted in Fig.B.2. The effect of the sector slot on the antenna radiating properties is studied by comparing the power received from the designed antennas and an un-slotted circular patch of the same size and is plotted in Fig.B.2. A standard horn antenna (at port 3) is used to receive the co-polarized power from the antennas placed at the same distance.

To have an insight on the polarization behavior of the antennas, the current distributions at the resonant frequencies of a circular patch with sector slot (design 1) are plotted in Fig.B.3, where the darker areas represents higher intensity. The Fig.B.3(b) shows that the higher resonance (at 2.48GHz) is the same as that of a circular patch of same size. But, the lower resonance shown in Fig.B.3(a)(at 1.81GHz) is a result of the perturbation in the current densities on the patch caused by the slot.

The co and cross-polarized antenna radiation patterns are also measured and plotted in Fig.B.4.

Results and Conclusion

The following are the results of the different compact circular microstrip patch antennas.

- Design 1 & 2: reported in *Publication no. 13*;

The return loss results of design 1, plotted in Fig.B.2(a), show that resonance frequencies of either 1.81GHz or 2.48GHz is excited in the

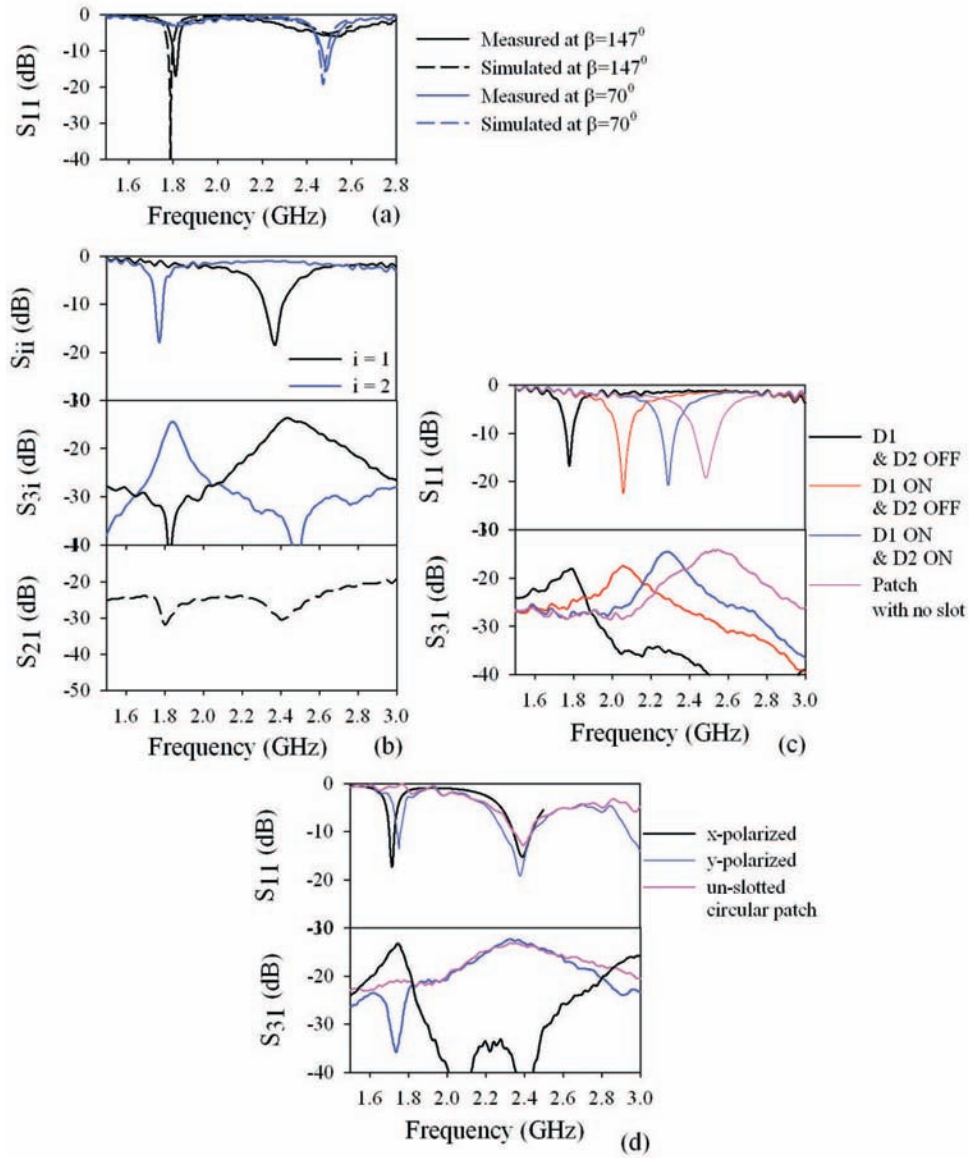


Fig. B.2: (a) Design 1: return loss S_{11} ; (b) Design 2: return loss S_{ii} for $i=1$ and 2 corresponding to ports 1 and 2, isolation between the ports (S_{21}) and the power received by a standard horn (S_{3i}); (c) Design 3: return loss S_{11} and the power received by a standard horn (S_{31}) for different switching states; and (d) Design 4: return loss S_{11} and the power received by a standard horn (S_{31})

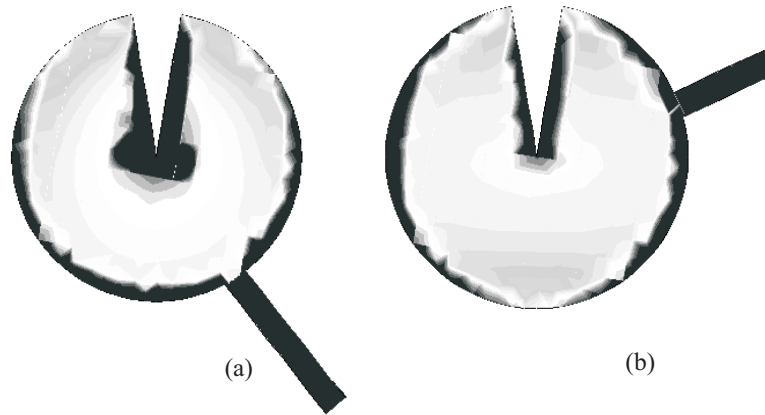


Fig. B.3: The simulated current distribution on the patch for design 1 at (a) 1.79GHz ($\beta=147^\circ$) and (b) 2.47GHz ($\beta=70^\circ$)

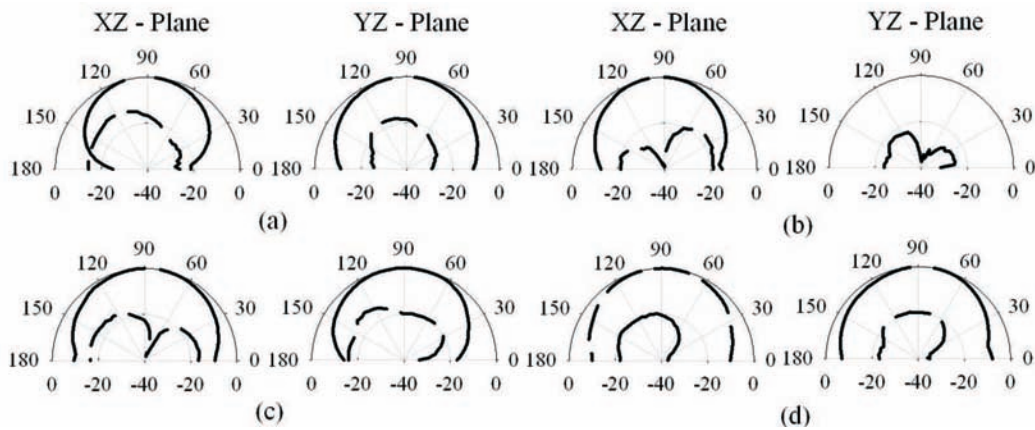


Fig. B.4: The measured radiation patterns of the antenna; Design 2 (a) at 1.83GHz, (b) at 2.43GHz; Design 4 (c) at 1.75GHz, (d) at 2.39GHz

microstrip-line-fed patch, depending on the feed position. The antenna exhibits a resonance at 2.48GHz when the microstrip feed position is at $\beta=70^\circ$. While, for $\beta=147^\circ$, the antenna resonates at 1.81GHz with an orthogonal polarization with respect to the previous feed position.

In design 2, the two resonances can be obtained simultaneously by exciting the antenna using two ports. The measured return loss and isolation between the ports, shown in Fig.B.2(b), shows that the antenna exhibits a resonance at 1.8GHz and 2.4GHz when excited at port 1 and port 2 respectively. It can be seen that the isolation between the ports is better

than 30dB.

The transmission characteristics of the dual port antenna in the two polarization planes are also shown in Fig.B.2(b). The relative gain of the proposed antenna at the two resonance frequencies are found to be comparable that of the circular patch antenna. As an added feature, this design provides an area reduction of 44% at the lower resonance when compared to an un-slotted circular patch operating at the same frequency.

- Design 3: reported in *Publication no. 14*;

It is observed, from the return loss plotted in Fig.B.2(c), that the antenna resonates at 1.78GHz, when both diodes are in OFF state. When diode 1 is in ON state, the resonance frequency is shifted to 2.065GHz. When both diodes are ON, the resonance frequency for the antenna is further shifted to 2.29GHz.

The transmission characteristics of the antenna (S_{31}), for different switch states, are also shown in Fig.B.2(c). It can be observed that the relative gains in all the cases are comparable with a simple circular patch antenna of the same radius.

Hence, a pair of PIN diodes, incorporated to shunt the slot, varies the length of the current path according to the diode states. The antenna switches between three distinct operating frequencies with same polarization for the different diode states.

- Design 4: reported in *Publication no. 15*;

The simulated and measured return loss of the proposed antenna, along with that of an un-slotted patch, are shown in Fig.B.2(d). The un-slotted circular patch antenna resonates almost at the same frequency as the higher resonance at 2.4GHz of the proposed antenna for small slot angles, α . The S_{31} measurements using a linearly polarized horn antenna indicated that the two resonances are orthogonally polarized.

The gain of the proposed antenna at the second resonance are comparable with that of the un-slotted circular patch antenna of the same radius while the gain at the first resonance is slightly lower.

Hence, a compact coaxially fed sector-slotted circular patch antenna with a superstrate for dual-frequency operation has been designed and experimentally verified. By virtue of the sector slot, when compared to an un-slotted circular patch with air as substrate, the proposed design has an advantage of 61% reduction in size along with dual frequency operation and protection from environmental hazards and mechanical strength due to the radome.

The co and cross-polarized radiation patterns, plotted in the XZ and YZ planes, at both the resonances for designs 2 & 4 are shown in Fig.B.4. In all the cases, the patterns are broad as in the case of a conventional circular patch and offer a cross-polarization level better than -18dB.

References

1. K. L. Wong and W. S. Chen. *Compact microstrip antenna with dual-frequency operation*. Electron. Lett., vol. 43, pages 646-647, 1997.
2. K. L. Wong, C. L. Tang and H. T. Chen. *Compact meandered circular microstrip antenna with a shorting pin*. Microw. Opt. Techno. Lett., vol. 42, pages 147-149, 2004.
3. F. Yang and Y. R. Samii. *Patch antennas with switchable slots (PASS) in wireless communications: concepts, designs, and applications*. IEEE Ant. Propag. Mag., vol. 47, no. 2, pages 13-29, 2005.
4. K. Y. Jan and K. L. Wong. *Single-feed dual-frequency circular microstrip antenna with an open-ring slot*. Microw. Opt. Techno. Lett., vol. 42, pages 157-160, 1999.
5. J. Costantine, K. Y. Kabalan, A. El-Hajj and M. Rammal. *New multi-band microstrip antenna design for wireless communications*. IEEE Ant. Propag. Mag., vol. 48, no. 6, pages 181-186, 2007.
6. K. P. Ray and D. D. Krishna. *Compact dual band suspended semi-circular microstrip antenna with half U-slot*. Microw. Opt. Techno. Lett., vol. 48, no. 10, pages 2021-2024, 2007.

7. K. S. Kim, T. Kim and J. Choi *Dual-frequency aperture coupled square patch antenna with double notches*. *Microw. Opt. Techno. Lett.*, vol. 24, pages 370-374, 2000.
8. S. Dey, C.K. Aanandan, P. Mohanan and K.G. Nair. *Modified circular patch antenna*. *Electron. Lett.*, vol. 29, pages 1126-1127, 1993.

Resume of the Author

EDUCATION

- March 2005 - present
Doctoral degree in Microwave Electronics
Department of Electronics, Cochin University of Science and Technology, Cochin, India
- June 2001 - December 2002
M. Tech (Masters in Technology) degree in Microwave Electronics
Department of Electronic Science, Delhi University South Campus, New Delhi, India.
- June 1999 - May 2001
M. Sc. (Masters in Science) degree in Electronics
Department of Electronic Science, Delhi University South Campus, New Delhi, India.
- June 1996 - May 1999
B. Sc. (Hons) (Bachelors in Science) degree in Electronics
Sri Venkateswara College, Delhi University South Campus, New Delhi, India.

AWARDS AND FELLOWSHIPS RECEIVED

- URSI Young Scientist Award(YSA) - August 2010
International Union of Radio Science (URSI) Commission B International Symposium on Electromagnetic Theory (EMT-S) held in Berlin, Germany, on August 16 - 19, 2010.
- DST WOS-A Project - November 2005
Awarded a project from the Dept. of Science and Technology (DST), Govt. of India, for a duration of 3 years for research in 'Design and Development of Multi-Band Fractal Antenna', under Women Scientist (WOS-A) 2004 Scheme, to be carried out as Principal Investigator (PI) at the Department of Electronics, Cochin University of Science and Technology, with a budget of 13.96 lakhs.
- Fellowships for attending EuMC - October 2007
Awarded student grant from The European Microwave Association and travel grants by different funding agencies under the Govt. of India (DST, CSIR and INSA) for presenting a research work at the European Microwave Conference (EuMC) at Munich, Germany in October 2007.

- JRF - March 2005
Junior Research Fellowship (JRF) from Cochin University of Science and Technology from March 2005-Nov 2005
- Gold Medal - June 2001
Awarded the Gold Medal for securing first position in University of Delhi in the M.Sc. program during the annual university convocation (2001).
- Endowment Scholarship - 1999
South Campus, Delhi University Scholarship during 1999 to 2001 for academic excellence at undergraduate level and during July 2002 to Dec 2003 for the M.Tech course.

EXPERIENCE

Research

- Project Associate with the Radar Division 1 at Society for Applied Microwave Electronics Engineering Research (SAMEER, IIT Campus, Bombay, India).
Feb 2003 - Dec 2003
- Project Trainee with the Communications Group at ISRO (ISAC), Bangalore, India as a part of the MTech curriculum.
July 2002 - Dec 2002
- Project Trainee at the National Physical Laboratory (NPL), New Delhi, India as a part of M.Sc. curriculum.
Jan 2001-June 2001

Teaching

- Lecturer (on contract) at the Department of Electronics, Cochin University of Science and Technology, Cochin, India.
Nov 2008 - present
- Lecturer at the Department of Electronics, Rajagiri College of Engineering and Technology, Cochin, India.
Dec 2003 - March 2005

Personal Details

Date of birth: 04.02.1979

Contact address: Department of Electronics,
Cochin University of Science and Technology, Thrikkakara,
Cochin-682022, India.

PUBLICATIONS

Journals - 14 Conferences - 13

1. **Deepti Das Krishna**, M. Gopikrishna, C. K. Aanandan, P. Mohanan, K. Vasudevan, “*Planar elliptical UWB antenna with band-notch characteristics*”, International Journal on Wireless & Optical Communications (IJWOC), World Scientific, vol. 4, pages 183-194, 2007.
2. **Deepti Das Krishna**, M. Gopikrishna, C. K. Aanandan, “*A CPW-fed triple band monopole antenna for WiMAX/WLAN applications*”, 38th European Microwave Conference (EuMC), Amsterdam, pages 897-900, 2008.
3. **Deepti Das Krishna**, M. Gopikrishna, C. K. Aanandan, “*A compact printed inverted cone antenna for UWB based applications*”, URSI International Symposium on Electromagnetic Theory (EMTS-2010), Berlin, pages 463-466, 2010.
4. R. Gayathri, T. U. Jesney, **Deepti Das Krishna**, M. Gopikrishna, C. K. Aanandan, “*Band-notched inverted-cone monopole antenna for compact UWB systems*”, Electronics Letters, Institution of Engineering Technology (IET), vol. 44, pages 1170-1171, 2008.
5. **Deepti Das Krishna**, M. Gopikrishna, C. K. Aanandan, P. Mohanan, K. Vasudevan, “*Compact wideband Koch fractal printed slot antenna*”, Microwaves Antennas & Propagation, Institution of Engineering Technology (IET), vol. 3(5), pages 782-789, 2009.
6. **Deepti Das Krishna**, M. Gopikrishna, C. K. Aanandan, P. Mohanan, K. Vasudevan, “*CPW-fed Koch fractal slot antenna for WLAN/WiMAX applications*”, IEEE Antennas and Wireless Propagation Letters (AWPL), vol. 7, pages 389-392, 2008.
7. **Deepti Das Krishna**, M. Gopikrishna, C. K. Aanandan, P. Mohanan, K. Vasudevan, “*Ultra-wideband slot antenna for wireless USB dongle applications*”, Electronics Letters, Institution of Engineering Technology (IET), vol. 44, pages 1057-1058, 2008.
8. **Deepti Das Krishna**, M. Gopikrishna, C. K. Aanandan, P. Mohanan, K. Vasudevan, “*Ultra-wideband slot antenna with band-notch characteristics for wireless USB dongle applications*”, Microwave and Optical Technology Letters, Wiley Interscience., vol. 51(6), pages 1500-1504, 2009.
9. **Deepti Das Krishna**, M. Gopikrishna, C. K. Aanandan, P. Mohanan, K. Vasudevan, “*Compact dual-polarized square microstrip antenna with*

- triangular slots for wireless communication*”, Electronics Letters, Institution of Engineering Technology (IET), vol. 42, pages 894-895, 2006.
10. **Deepti Das Krishna**, M. Gopikrishna, C. K. Aanandan, P. Mohanan, and K. Vasudevan, “*Square patch antenna with a bow-tie slot for dual port operation*”, International Conference on Microwaves, Antenna, Propagation and Remote Sensing (ICMARS), Jodhpur, pages 14-18, 2006.
 11. **Deepti Das Krishna**, M. Gopikrishna, C. K. Aanandan, P. Mohanan, and K. Vasudevan, “*Electronically switchable compact microstrip antenna with triangular slots for dual port operation*”, Proceedings on National Symposium on Antennas and Propagation (APSYM 2006), Cochin, pages 55-58, 2006.
 12. **Deepti Das Krishna**, Anupam R. Chandran and C. K. Aanandan, “*A Compact dual frequency antenna with Sierpinski-gasket based slots*”, 37th European Microwave Conference (EuMC) & 10th European Conference on Wireless Technology (ECWT), Munich, pages 1078-1080 & 320-322, 2007.
 13. **Deepti Das Krishna**, C. K. Aanandan, P. Mohanan, K. Vasudevan, “*Circular microstrip antenna with a sector slot for dual port operation*”, Microwave and Optical Technology Letters, Wiley Interscience, vol. 48, pages 505-508, 2006.
 14. **Deepti Das Krishna**, C. K. Aanandan, P. Mohanan, and K. Vasudevan, “*Electronically switchable circular microstrip antenna with sector-slot for multiple frequency operation*”, IEEE Antennas and Propagation Society International Symposium (IEEE APS), Albuquerque, pages 4277-4280, 2006.
 15. **Deepti Das Krishna**, M. Gopikrishna, C. K. Aanandan, P. Mohanan, K. Vasudevan, “*Compact dual Band slot loaded circular microstrip antenna with a superstrate*”, Progress in Electromagnetics Research (PIER), Electromagnetic Waves (EMW), vol. 83, pages 245-255, 2008.
 16. **Deepti Das Krishna**, M. Gopikrishna, C. K. Aanandan, “*A compact wideband Koch fractal printed slot antenna for WLAN applications*”, 5th IASTED International Conference on Antennas, Radar and Wave Propagation, Baltimore, Maryland, USA, pages 444-448, 2008.
 17. K. P. Ray, **Deepti Das Krishna**, “*Compact dual band suspended semi-circular microstrip antenna with half U-slot*”, Microwave and Optical Technology Letters, Wiley Interscience, vol. 48, pages 2021-2024, 2006.

18. M. Gopikrishna, **Deepti Das Krishna**, C. K. Aanandan, P. Mohanan, K. Vasudevan, “*Square monopole antenna for ultra wide band communication Applications*”, Journal of Electro-Magnetic Waves and Application (JEMWA), Electromagnetic Waves (EMW), vol. 21, pages 1525-1537, 2007.
19. M. Gopikrishna, **Deepti Das Krishna**, C. K. Aanandan, P. Mohanan, K. Vasudevan, “*A compact linear tapered slot antenna for UWB applications*”, Electronics Letters, Institution of Engineering Technology (IET), vol. 44, pages 1174-1175, 2008.
20. M. Gopikrishna, **Deepti Das Krishna**, C. K. Aanandan, P. Mohanan, K. Vasudevan, “*Design of a microstrip fed step slot antenna for UWB communication*”, Microwave and Optical Technology Letters, Wiley Interscience, vol. 51, pages 1126-1129, 2009.
21. M. Gopikrishna, **Deepti Das Krishna**, C. K. Aanandan, P. Mohanan, K. Vasudevan, “*Design of a compact semi-elliptic monopole slot antenna for UWB systems*”, Transactions on Antennas and Propagation, IEEE., vol. 57(3), pages 1834-1837, 2009.
22. **Deepti Das Krishna**, K. P. Ray, “*Semi-circular patch with half U-slot microstrip patch antenna for dual frequency operation*”, Asia Pacific Microwave Conference (APMC), New Delhi, 2006.
23. M. Gopikrishna, **Deepti Das Krishna**, C. K. Aanandan, “*A semi-elliptic slot antenna for UWB applications*”, 5th IASTED International Conference on Antennas, Radar, and Wave Propagation, Baltimore, Maryland, USA, pages 431-435, 2008.
24. M. Gopikrishna, **Deepti Das Krishna**, C. K. Aanandan, “*Band notched semi-elliptic slot antenna for UWB systems*”, 38th European Microwave Conference (EuMC), Amsterdam, pages 889-892, 2008.
25. M. Gopikrishna, **Deepti Das Krishna**, C. K. Aanandan, “*Design of a microstrip-fed stepped slot for UWB Communications*”, IEEE Antennas and Propagation Symposium (IEEE-APS), San Diego, pages 1098-1102, 2008.
26. M. Gopikrishna, **Deepti Das Krishna**, Anupam R. Chandran and C. K. Aanandan, “*5GHz WLAN band notched square monopole antenna for UWB systems*”, Proceedings on National Symposium on Antennas and Propagation (APSYM 2006), Cochin, pages 47-50, 2006.
27. M. Gopikrishna, **Deepti Das Krishna**, C. K. Aanandan, “*Design of a Compact Rectangular Strip Monopole Antenna for UWB Systems*”,

URSI International Symposium on Electromagnetic Theory EMTS-2010
Berlin, pages 467-470, 2010.

